Production of biodiesel and exopolysaccharides from *Scenedesmus abundans* cell factory in flat panel photobioreactor with autoflocculation harvesting strategy

A Thesis

Submitted for the Degree of

DOCTOR OF PHILOSOPHY

By

MAHESH R
Roll no: 166106015

Under the supervision of

Dr. Soumen Kumar Maiti

Associate Professor

Department of Biosciences and Bioengineering
Indian Institute of Technology Guwahati
Guwahati 781039, Assam, India

July 2023

INDIAN INSTITUTE OF TECHNOLOGY GUWAHATI

Department of Biosciences and Bioengineering

STATEMENT

I truly declare that the content described in this thesis is the result of experiment findings and investigations carried out by me under the supervision of Dr. Soumen Kumar Maiti in the Department of Biosciences and Bioengineering, Indian Institute of Technology Guwahati, Guwahati, Assam, India.

Acknowledgements have been made to other researchers for their described work and scientific observations of this work are also reported.

R. Mahesh.

Date: 05/07/2023 **Mahesh R**

INDIAN INSTITUTE OF TECHNOLOGY GUWAHATI

Department of Biosciences and Bioengineering

CERTIFICATE

It is certified that the work described in this thesis entitled, **"Production of biodiesel and exopolysaccharides from *Scenedesmus abundans* cell factory in flat panel photobioreactor with autoflocculation harvesting strategy"** by Mr. Mahesh R submitted for the partial fulfillment of Degree of Doctor of Philosophy is an authentic record of the results obtained from his research work carried out under my supervision in the Department of Biosciences and Bioengineering, Indian Institute of Technology Guwahati, Guwahati, Assam, India. The work described in this thesis has not submitted elsewhere for a degree.

Soumen Kr. Maiti

Dr. Soumen Kumar Maiti
Associate Professor
Supervisor
Department of Biosciences and Bioengineering
Indian Institute of Technology Guwahati
Guwahati 781039, Assam, India.

Acknowledgements

I wish to express sincere gratitude to my research supervisor, ***Dr. Soumen Kumar Maiti***, Department of Biosciences and Bioengineering who gave opportunity to pursue this research work with freedom to think and execute my plans in every experiment. I like to thank him for precious advice, guidance and consistent support throughout my research.

I owe gratitude to my doctoral committee members, ***Dr. Debasish Das***, ***Dr. Lalit Mohan Pandey*** and ***Dr. Priyadarshi Satpati*** for valuable suggestions that helped me to improve my thesis work.

My special thanks to ***Department of Biosciences and Bioengineering, Central Instrumentation Facility, IIT Guwahati*** and ***Mechanical workshop*** for providing necessary facilities in my research.

I would also like to thank ***IIT Guwahati*** and ***MHRD*** for providing financial assistance in my research.

My wholehearted thanks to lab in charges, ***Mr. Nurul, Mrs. Prarthana, Mr. Dipankar, Mr. Chandan*** and ***Mr. Niranjan*** during my research work.

It was pleasure to work with lab mates, ***Yashavanth, Suraj, Sahil, Meenakshi, Jitendra, Bhoomika, Pragati, Annu*** and ***Nitish*** for their help and kindness throughout my Ph.D. journey.

I thank specially to my senior, ***Dr. Venkateswara Rao Naira*** and my friends, ***Uttariya*** and ***Gaurav*** for being supportive in critical situations during my research work.

My special appreciation to ***my parents***, ***my twin brother*** for their blessings, love and understanding throughout my studies and extremely grateful to the ***Almighty God*** for all your blessings in my life.

Abstract

Fatty acid methyl ester (FAME, biodiesel) production from microalgae has been gaining momentum in order to mitigate current energy demand but still facing major challenges such as low biomass production in open pond cultivation systems, unsuccessful closed photobioreactor (PBR) design, inappropriate media balancing under natural sunlight, inefficient harvesting technology and unsuitable transesterification process. Moreover, in order to make biodiesel economically viable, there is a need to exploit other products concomitantly apart from biodiesel and reduce downstream processing costs. Exopolysaccharides (EPS) are one of the major valuable byproducts secreted by some microalgae directly into the media. Concomitant synthesis of intracellular and extracellular product fractions in microbial cell factories would be an excellent biorefinery outlook for the researchers to reduce overall cost of their production and yield profits. Major factors that influence oleaginous microalgae growth and lipid production under natural sunlight are photobioreactor design, adequate supply of macronutrients and micronutrients, availability of sunlight intensity, CO_2 supply, nitrogen starvation, mixing and mass transfer, process pH and culture temperature. Therefore, the algal biorefinery approach should focus on PBR design, media balancing for enrichment of multi-products, efficient harvesting technology for biomass recovery and desirable transesterification process for producing biodiesel. Arising from the above, the objectives of the study were formulated to develop process strategy for construction and characterization of medium scale flat panel PBR for producing biodiesel and exopolysaccharides from *S. abundans*. Accordingly, modulation of macronutrients and micronutrients were studied to enhance lipid content of *S. abundans* in single stage medium scale flat panel PBR under natural sunlight. Also, multi-objective

optimization of nutrients was performed in this study to enhance biodiesel, autosedimentation of *Scenedesmus abundans* and exopolysaccharides production in single stage medium scale flat panel PBR under diurnal natural sunlight. Finally, free lipase and immobilized lipase mediated direct transesterification optimized strategy was developed to enhance biodiesel from microalgal biomass in presence of methanol.

Parallel mini flat panel PBR and medium scale flat panel PBR were constructed for the cultivation of *S. abundans*. Customized unidirectional LED lighting system was developed to supply light energy to microalgae inside the laboratory. A high mass transfer efficient membrane sparger was designed and equipped at the bottom of flat panel PBR. The medium scale flat panel PBR produced overall mass transfer coefficient of CO_2 (K_{La,CO_2}) and mixing time (t_m) of 0.0125 s^{-1} and 8 sec respectively at 0.43 cm/s superficial gas velocity. Maximum biomass titer of 6.9 g/l was achieved at end of growth phase using optimized growth media in medium scale flat panel PBR at 2162 µE/m^2/s, 1 VVM indoor condition. The productions were 1.53 g/l (22% of DCW) FAME with productivity of 67 mg/l/ day and 236 mg/l EPS with yield of 37 mg/g biomass under nitrogen starvation. This microalgal strain have potential to produce multi-products (biodiesel, EPS) and also has the capability of natural autoflocculation.

Further to improve lipid production of *S. abundans*, the effect of macro and micronutrients were investigated. The optimized lipid media was formulated for enhancing lipid content in microalgae. Comparison of single stage and two stage strategies were also carried out in this study. The single stage produced 2.5 fold higher %FAME in DCW than two stage and economical as harvesting steps could be minimized. Biomass titer of 2.79 g/l with maximum FAME content of 46% was achieved using developed media in medium scale flat panel PBR under diurnal natural sunlight. FAME concentration, FAME productivity and

maximum EPS concentration of 1.28 g/l, 27 mg/l/day and 155 mg/l were obtained under sunlight study. Therefore, the exploitation of *S. abundans* as a co-producer of biodiesel and EPS under outdoor sunlight could be a feasible approach.

In addition to that, multi-objective optimization approach has been developed to increase the production of biodiesel, secretion of EPS and enhance autoflocculation (ASF) using *S. abundans* under diurnal light. For this study, Plackett-Burman design (PBD) was used for screening significant process variables. Diurnal simulated light intensity was generated from pulse width modulation (PWM) and OPTO22 control system that controls LED (light emitting diode) light intensity ranging from 0 to 2200 $\mu E/m^2/s$ (capable of mimicking sunlight intensities in laboratory). PBD determines urea, $CoCl_2.6H_2O$, $CuSO_4.5H_2O$ and $Na_2MoO_4.2H_2O$ as significant process variables in modified Chu-13 media that influences FAME content in dry biomass, FAME concentration, ASF and EPS concentration by *S. abundans.* The quadratic model equations of responses from RSM-CCD (response surface methodology-central composite design) enhance single objective at a time. Therefore, these model equations from RSM-CCD are used with composite desirability approach for formulating optimized multi-objective RSM media. The developed media increased the FAME production by 1.72 fold (70% in DCW), FAME titer by 2.3 fold (3.83 g/l), ASF by 1.08 fold (1.93) and EPS by 1.60 fold (462.50 mg/l) as compared to unoptimized media under diurnal LED light. The formulated media produced 55% of FAME content in dry biomass, 1.79 g/l FAME, ASF of 1.83 within 1 hr, 290 mg/l EPS under natural sunlight.

For this study, immobilised lipase mediated direct transesterification process was developed. Methanol was used as lipid extraction solvent, acyl acceptor and reaction medium. The optimized conditions for free lipase were 16:1 methanol to biomass mass ratio, lipase amount with respect to biomass (80%) with 50 mg/ml lipase concentration, 30 ºC

reaction temperature (room temperature) and works optimum without initial pH adjustments. Lipase loading of 10 mg/alginate bead (62.5 mg/ml enzyme concentration) produced highest FAME content in DCW (44%) among different enzyme loadings using calcium alginate entrapment method. Kinetic study reveals that transesterification efficiency increases with increase in reaction time for both optimized free lipase and immobilized lipase. Water behaves as a better storage medium as compared to buffers for immobilized lipase in reusability experiments. Lipase loading of 20 mg/alginate bead (125 mg/ml enzyme concentration) showed better reusability up to 5^{th} cycle.

As far as our knowledge is concerned, this is the first study of multi-objective optimization of nutrients to enhance FAME, autoflocculation and EPS concomitantly in *Scenedesmus abundans*. Also, very few studies have reported immobilized lipase mediated direct transesterification of algal biomass in presence of methanol to produce biodiesel. Hence, enhancement of biodiesel and EPS under sunlight without photoinhibition by natural autoflocculation in medium scale flat panel PBR paved way for biorefinery. Therefore, generation of multi-products by *S. abundans*, natural autoflocculation based biomass harvesting and lipase immobilization by entrapment method can make the process sustainable.

CONTENTS

Abbreviations / Notations

Term	Description
ASTM	American Society for Testing and Materials
ANOVA	Analysis of Variance
ASF	Autosedimentation Factor
BCF	Biomass Correlation Factor
CCD	Central Composite Design
CN	Cetane Number
CP	Cloud Point
CV	Coefficient of Variation
CoA	Coenzyme A
CFPP	Cold Filter Plugging Point
CI	Confidence Interval
R^2	Correlation coefficient
DU	Degree of Unsaturation
ρ	Density
DNA	Deoxyribonucleic acid
DO	Dissolved Oxygen Concentration
DCW	Dry Cell Weight
DEW	Dry Exopolysaccharide Weight
ER	Endoplasmic Reticulum
EPA	Environmental Protection Agency

EC number	Enzyme Commission number
EN	European Nation
EJ	Exajoules
EPS	Exopolysaccharide
FAME	Fatty Acid Methyl Ester
FID	Flame Ionization Detector
FP	Flash point
FTIR	Fourier Transform Infrared Spectroscopy
FFAs	Free Fatty Acids
GC	Gas Chromatography
GAP	Glyceraldehyde 3-Phosphate
HPLC	High Performance Liquid Chromatography
HHV	Higher Heating Value
HTL	Hydrothermal liquefaction
IEA	International Energy Agency
IV	Iodine Value
ν	Kinematic viscosity
LED	Light Emitting Diode
LCSF	Long Chain Saturation Factor
MN	Micronutrients Pool
t_m	Mixing time
MUFA	Mono Unsaturated Fatty Acid
NCL	National Chemical Laboratory

NCIM	National Collection of Industrial Microorganisms
NOAA	National Oceanic and Atmospheric Administration
ND	Not Determined
NM	Not Mentioned
OD	Optical Density
K_{La,CO_2}	Overall mass transfer coefficient of carbon dioxide
K_{La,O_2}	Overall mass transfer coefficient of oxygen
OSI	Oxidation Stability Index
PPM	Parts per million
3PG	3-Phosphoglycerate
PBR	Photobioreactor
PPFD	Photosynthetic Photon Flux Density
PBD	Plackett-Burman Design
PMMA	Polymethyl methacrylate
PTFE	Polytetrafluoroethylene
PUFA	Poly Unsaturated Fatty Acid
PU	Poly Urethane
PP	Pour Point
PXRD	Powder X-Ray Diffraction
PWM	Pulse Width Modulation
ROS	Reactive Oxygen Species
RSM	Response Surface Methodology
RPM	Rotations per minute

SV	Saponification Value
SFA	Saturated Fatty Acid
S/V	Surface area/Volume
SDGs	Sustainable Development Goals
TGA	Thermo Gravimetric Analysis
TAG	Triacylglycerol
UN	United Nations
VVM	Volume of air per Volume of liquid in photobioreactor per Minute

List of figures

List of tables

CHAPTER 1

Introduction

1.1. Background and rationale of the study

Energy is used in residential, commercial, industrial and transportation sector by human beings for their growth and development. It is believed that transportation sector is currently responsible for nearly 60% of world oil demand (Atabani et al., 2011). Majority of the energy supply is generated from burning of fossil-based non-renewable sources of energy such as oil, natural gas, coal (Shafiei & Salim, 2014). The current reserves of oil, natural gas and coal would be depleted completely within 50, 48.8 and 139 years according to current consumption rates and results in global energy crisis. Fig. 1.1A shows World energy consumption in 2020 (Looney & Dale, 2021). The burning of fossil fuels also resulted in rapid increase in the emissions of several greenhouse gases (mainly CO_2) that trap heat in atmosphere leading to global warming and climate change (EPA, 2020). The World's atmospheric CO_2 has increased from ~317 PPM (in 1960) to ~421 PPM at present (NOAA, 2022) (Fig 1.1B). As a result, the average global temperature on Earth has increased by 1.1 ºC since 1880. Global temperature is projected to warm about 1.5 ºC by 2050 and 2-4 ºC by 2100 (Collins et al., 2013). Therefore, much attention is paid on developing renewable source of energy such as hydroelectricity, solar (photo voltaic and thermal), wind, geothermal, tidal, lignocellulosic biomass since 1990s (IEA, 2019). The United Nations (UN) Rio+20 summit in Brazil in 2012 committed governments for implementing sustainable development goals (SDGs) that get accomplished by 2030 and integrate into the follow-up to the millennium development goals after their 2015 deadline. One of the sustainable development goal was to develop affordable and universal clean energy

(Griggs et al., 2013). Liquid biofuels such as bioethanol and fatty acid methyl ester (FAME, biodiesel) from biomass feedstock have emerged as transportation fuels with less emissions of CO_X and NO_X into the atmosphere. But, the current growth rate of liquid biofuels cannot meet the projected future energy consumption rates (IEA, 2019).

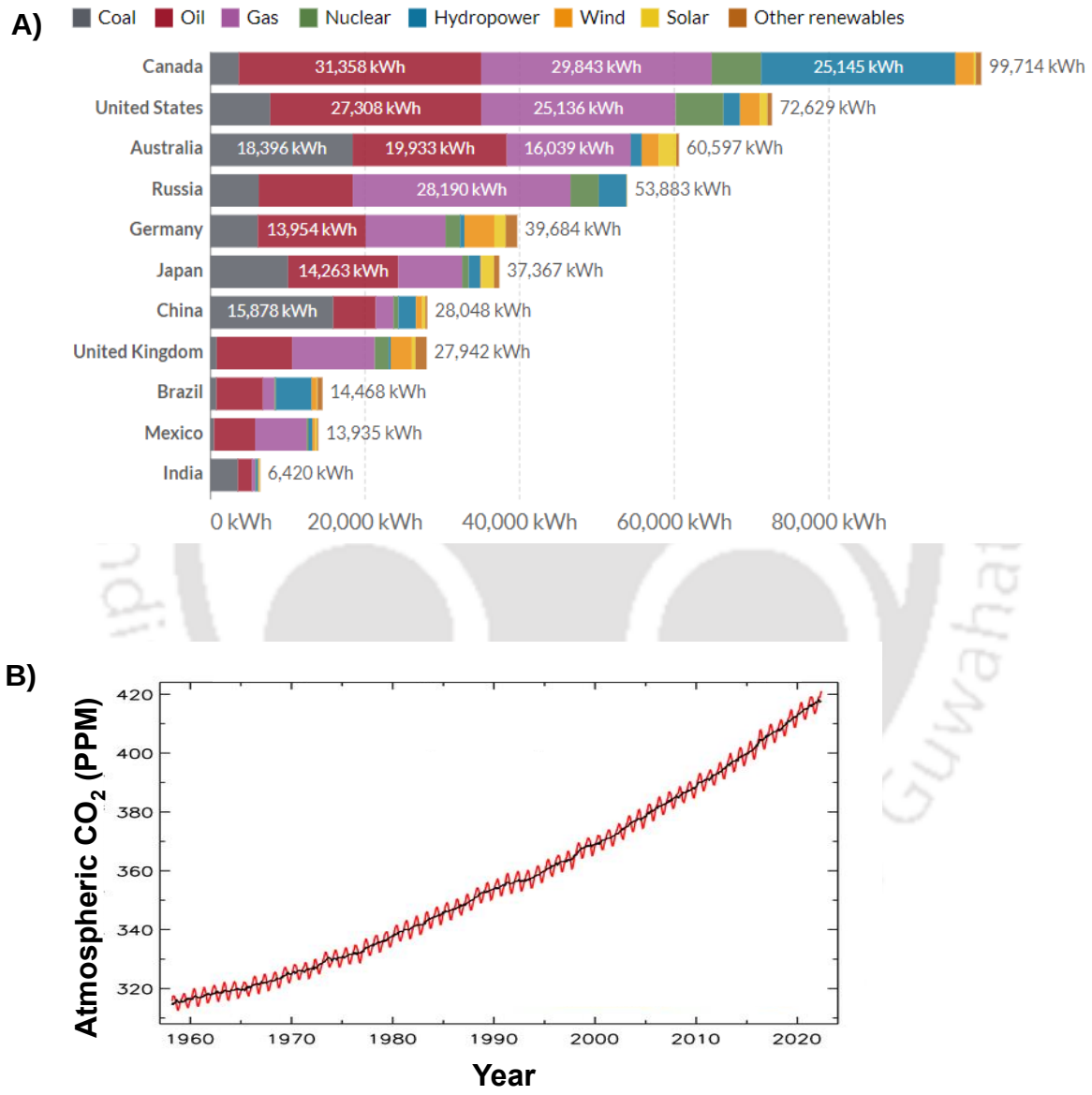

Fig. 1.1. Emergence of renewable energy. **A)** World energy consumption in 2020 (Looney & Dale, 2021) and **B)** CO_2 emissions caused due to burning of fossil fuels (NOAA, 2022).

Moreover, in order to make biodiesel production economically feasible, there is a need to exploit other products such as exopolysaccharides simultaneously via biorefinery approach.

Hence, the present research study focusses on enhancement in the production of biodiesel and exopolysaccharides. The FAME is produced from various oil crops/oleaginous biomass feedstock by direct transesterification (without extracting lipids) or two step transesterification (extracting lipids from biomass feedstock using methanol) followed by transesterification using methanol in presence of acid, alkali or enzyme (lipase) catalysts. Biodiesel has several advantages like better combustion, easier engine start-up, no sulphur, low CO_X and NO_X emissions, biodegradable, non-toxic, renewable as compared to conventional petrol and diesel (Knothe, 2012). Biofuels can be classified broadly into two types namely, primary and secondary biofuels. The primary biofuels also called as natural biofuels that are directly produced from firewood, plants, forest and animal waste. The secondary biofuels are directly produced from plants and microorganisms and can be further divided into three generations. The first generation of biofuels comprises production of ethanol from starch rich food crops such as wheat, barley, corn, potato, sugarcane or biodiesel from soybean, sunflower and animal fat. Whereas, the second generation of biofuels comprises production of bioethanol and biodiesel from several species of plants such as lignocellulosic biomass (straw, grass, wood), jatropha, cassava, miscanthus. The third generation of biofuels comprises the production of biodiesel from microalgae (Abdelaziz et al., 2013; Rodionova et al., 2017). Advantages and disadvantages of different generations of biofuels are shown in Table 1.1.

First and second-generation feedstocks influence the food chain and economy of the society (Singh et al., 2020). Microalgae, a third-generation feedstock are ubiquitous and have the ability to accumulate high lipid content (30-70%) (Udayan et al., 2022). Microalgae accumulate high neutral lipids and require less land areas as compared to conventional terrestrial oil crops such as soybean, sunflower, coconut, canola, palm, jatropha etc (Chisti, 2007). Fig. 1.2 shows the comparison of biodiesel feedstocks (Katiyar et al., 2017). Microalgae produces much higher oil yield (L/ha) as compared to other energy crops. Apart from that,

biodiesel from microalgae has already shown its great potential as their growth rate is very high (doubling time is less than a day) and lipid enriched microalgae can be used as commercial feedstock for biodiesel production (Cho & Park, 2018). Microalgae are the efficient photosynthetic organisms that grow under sunlight and CO_2 and thus help in mitigating CO_2 levels from the atmosphere. Fourth generation feedstock includes genetically modified organisms for the enhancement of biohydrogen production. Fourth generation feedstock comprises of biomass from second and third generations, after genetic modification (Sahay, 2021).

Table 1.1. Advantages and disadvantages of different generations of biofuels (Banerjee et al., 2019; Siddiki et al., 2022; Williams & Laurens, 2010).

Biofuel generation	Advantages	Disadvantages
First	Produces few pollutants than petro-diesel. Production facility could be well managed by farmers.	Can compete with agricultural lands and cause food crisis. Lower growth rates and seasonally varied outputs. Not sustainable for future generations.
Second	Requires less water, nutrition and able to grow in less fertile lands as compared to food crops. Waste valorization. Regular farming knowledge is sufficient to manage production facility.	Compete with arable lands leading to food crisis. Long periods of cultivation and seasonal variations in production outputs. Not sustainable for future generations.
Third	Higher growth rates and productivities. Sequester CO_2 in large amounts. Able to grow on non-arable lands, marine and waste water. Highly sustainable and huge scope for biorefinery.	High cost of production and lack of commercial feasibility. Efficient biomass cultivation systems, biomass to biodiesel conversion technologies are still in developing stage. Highly skilled labour is necessary for managing production.
Fourth	Able to grow on non-arable lands, brackish and saline water.	Environment friendly but release of genetically modified strains is a major concern. Technology in early development stages.

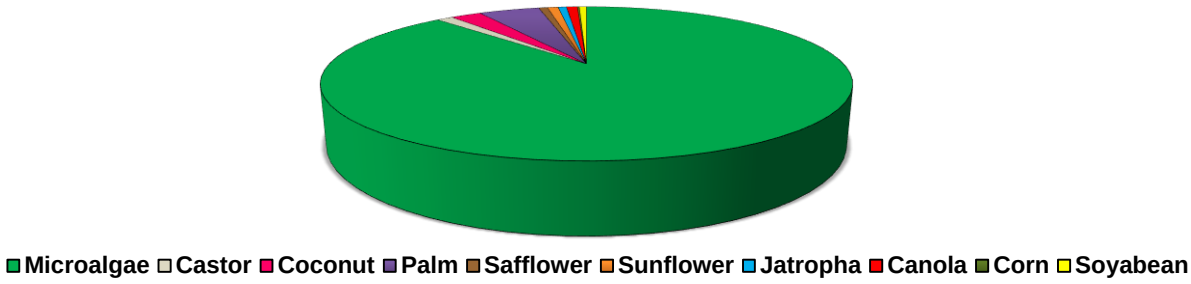

Fig. 1.2. Comparison of biodiesel feedstocks.

The oils from various feedstocks are processed to biodiesel by pyrolysis, dilution, micro-emulsification, and transesterification. Biodiesel produced from pyrolysis has a similar calorific value to diesel but has a lower cetane number. Micro-emulsification improves cetane number and viscosity but the biodiesel obtained is less stable from this process. In the dilution process, the usage of solvents such as ethanol results in a lowering of viscosity and density of biodiesel. The dilution process also results in incomplete burning and carbon deposition in engine cylinders. In transesterification, the separation of biodiesel is easier as low-density FAME stays at the top by leaving the glycerol-rich water layer at the lower phase. Among all the techniques of oil to diesel conversion, transesterification is the most economic and biodiesel produced by the direct transesterification of microalgae has similar properties to diesel (Singh et al., 2020). Hence, the present study was focused on enhancing the production of biodiesel and exopolysaccharides from *Scenedesmus abundans* photoautotrophically in single stage flat panel photobioreactor under diurnal natural sunlight. Also, immobilization of lipase enzyme by entrapment method was explored.

1.2. Problem statements

Artificial open ponds are most economical among wide variety of mass culturing systems for microalgae (Costa et al., 2019). But they require large land areas for microalgae cultivation and result in low biomass productivities due to less surface area/volume (S/V) ratio, contamination issues and water losses due to high evaporation rates. Therefore, closed PBR systems such as airlift, bubble column, horizontal tubular, vertical tubular, flat panel, etc., are made up of transparent acrylic (polymethyl methacrylate, also called as plexiglass) sheets of different sizes with perforated silicon rubber tubing or membrane sparger to facilitate mixing of algal cells and used for algal cultivation. Closed PBR systems allow maintenance of sterile culture with controlled parameters. Tubular and flat panel PBRs are the most commonly used closed systems for algal cultivation (Mahesh et al., 2019). The commerciality of biodiesel production from microalgae would be feasible with cost-effective PBR design for microalgae cultivation, process development and enrichment of multi-products under natural sunlight and using immobilized lipase for direct transesterification of algal biomass in presence of methanol to produce biodiesel.

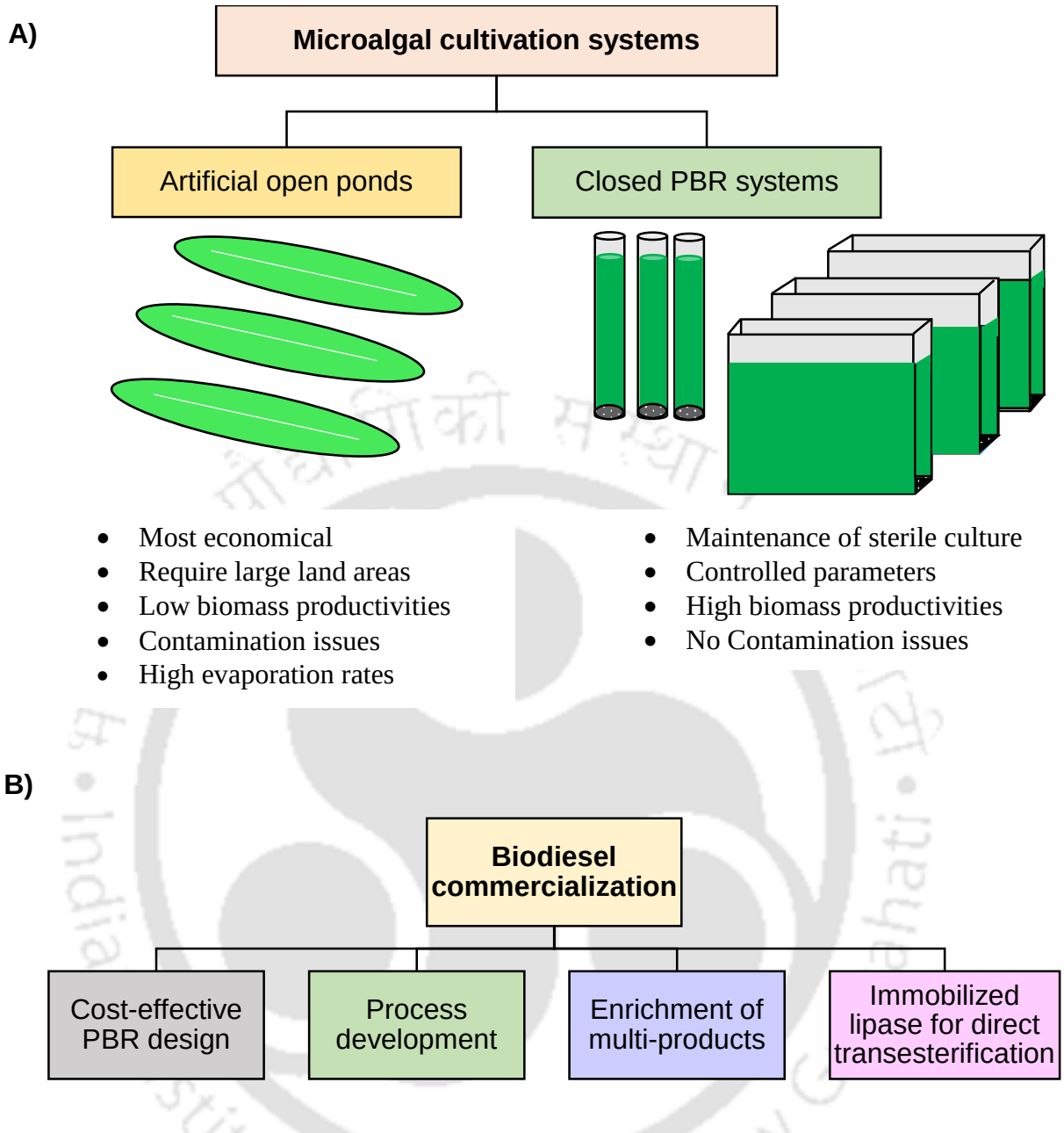

Fig. 1.3. Schematic diagram of **A)** problem statement and **B)** research hypotheses of this study.

1.2.1. Photobioreactor design

In order to overcome the inherent disadvantages of using open cultivation, numerous closed PBRs of various volumes and shapes have been designed. They offer better S/V ratios and higher biomass productivities as compared to open cultivation systems. The principle final goal of any PBR is a reduction in biomass production costs. This can be done by improving the design and shape of the PBR, controlling environmental parameters and favouring minimal

contamination risk. Although PBRs are widely used and have several advantages, still there are some major drawbacks that make them uneconomical for low cost end products. At higher operational volumes above 100 L, there is limited diffusion of light, which results in the inefficient growth of microalgae. A major concern is the development of microalgal biofilm on PBR surface, thus limiting light penetration. In addition, the initial investment, operational and maintenance cost of PBR is high, which eventually increases the biomass production cost (Acién et al., 2012). An efficient PBR design lies in the selection of suitable PBR, engineering of sparger for better mixing and mass transfer to minimize dark zones, less land area requirement, hydrodynamics and scale-up feasibility. Tubular PBRs are arranged horizontally, vertically, or helical coil of different sizes, usually having heights of 100 cm or less (Gupta et al., 2019). They yield high volumetric productivities but dissolved oxygen builds up, usually dark zones form at the center and larger optical path length decreases the light intensity. Flat panel PBRs can be arranged in straight or inclined position of different length, width, and height based on working volume requirement. They offer various advantages as compared to tubular PBRs such as large illumination surface area with high surface to volume ratio, smaller optical path length, lesser dark zones, low dissolved oxygen build-up etc (Mahesh et al., 2019). Therefore, flat panel PBR with cost effective mass transfer efficient sparger could be scalable and contribute to the commercialization of algal biofuels.

1.2.2. Process development criteria for multi-product synthesis

Apart from microalgae cultivation in PBRs, adequate supply of nutrients, nitrogen starvation, high light intensity, high CO_2, mixing and mass transfer, culture temperature and process pH support growth as well as trigger good neutral lipid in microalgae (Converti et al., 2009; Fernandes et al., 2014; Pal et al., 2011). Apart from intracellular products, algae can also secrete a range of extracellular products such as exopolysaccharides (EPS), exoenzymes, organic acids, extracellular phytohormones etc (Liu et al., 2016). EPS are one of the major

valuable byproducts secreted by specific microalgae directly into the media and they can be used in various applications as adhesives, detergents, textiles, cosmetics, pharmaceuticals (Raza et al., 2012). EPS can create binding of algal cells to one another forming flocs and enhance autoflocculation phenomena with specific metal ion combination (Salim et al., 2014). Higher autoflocculation rate enhances autosedimentation factor (ASF, ratio of bottom OD_{680} to top OD_{680} 1 hr) and also reduces the cost of drying of algal biomass. Microalgae harvesting operations include nearly 30% of the total biomass production cost (Schlesinger et al., 2012). A cheap harvesting technology such as autoflocculation would be employed, but this autoflocculation is a natural process and exhibited by some specific algae. The autoflocculation phenomena was observed because of the EPS produced by the cells that helps in the cell harvesting (Salim et al., 2014). Efficient algal harvesting technology such as autoflocculation is used after generation of intracellular and extracellular products. The difficulties in easy separation of value-added products without causing damage to the formation of other coproducts simultaneously in oleaginous microalgae is a major obstacle in biorefinery approach. Concomitant synthesis of high intracellular and extracellular product fractions in microbial cell factory would be an excellent biorefinery outlook for the researchers to reduce the upstream, downstream processing costs, overall cost of their production and yield profits (Naira et al., 2020). Thus, a process development criteria for multi-product synthesis could be feasible via microalgae biorefinery approach and efficient harvesting technology.

1.2.3. Enrichment of multi-products

Enhancement of multi-products from oleaginous microalgae are necessary to overcome the overall biodiesel production costs. Several studies stated the use of multi-objective optimization of nutrients to enhance desired products simultaneously. Aguirre and Bassi found biomass concentration of 1102.9 mg/l and lipid productivity/cellulose content in DCW ratio of 0.45 (mg lipid/l/day)(mg cellulose/mg biomass)$^{-1}$ for culture conditions of 3.77% (v/v) CO_2 in

air and 4.01 mM $NaNO_3$ in *Chlorella vulgaris* using overall desirability approach (Aguirre & Bassi, 2013). Fawzy reported that *A. gracilis* produced maximum biomass productivity, lipid content in DCW and lipid productivity (40.6 mg/l/day, 39.3% and 15.9 mg/l/day respectively) in RSM optimized media containing 1 g/l nitrogen, 0 g/l phosphorus and 1.36 M NaCl using desirability function approach (Fawzy, 2017). As per our knowledge, no studies have been performed using multi-response optimization to enhance FAME, ASF and EPS concomitantly in *Scenedesmus abundans*. Hence, multi-objective optimization of nutrients was performed in this study to enhance biodiesel, ASF and EPS from *S. abundans* photoautotrophically in single stage medium scale flat panel PBR under diurnal natural sunlight.

1.2.4. Lipase mediated transesterification for producing biodiesel

The use of alkaline catalysts (NaOH, KOH) is not desirable to produce FAMEs from biomass containing high free fatty acids (FFAs) because of soaps formation (Macías-Sánchez et al., 2015). On the other hand, acid (HCl, H_2SO_4) catalyzed biodiesel production from biomass containing high FFAs is very slow due to water formation (Canakci & Van Gerpen, 2001). Use of lipases as enzyme catalyst for transesterification process was studied to overcome the problems of chemical catalysts. However, if the free lipase enzyme mixes with the product or the solvent, it requires more downstream processing to separate them. The use of lipase immobilization by entrapment method protects the enzyme with the help of carrier (usually calcium alginate) and transesterification occurs by mass transfer of substrates through carrier. Apart from protection, lipase can be reused without significant loss of catalytic activity by immobilization method that in turn reduce operating cost for biodiesel production. Moreover, free alcohols such as excess methanol and glycerol produced, will stimulate dehydrogenases during the process and consequently inhibit the catalytic activity (Suali & Sarbatly, 2012). Therefore, precautions must be taken while adding the amount of solvents for transesterification reaction. Hence, free lipase and immobilized lipase mediated direct

transesterification of algal biomass in presence of methanol were performed in this study to produce biodiesel. The major research questions are how to design cost effective PBR for synthesis of multi-products from microalgae simultaneously, how to develop a process to enhance biodiesel from microalgae, feasibility of enrichment of multi-products and how to develop immobilized enzyme transesterification process for biodiesel production.

1.3. Objectives of the study

Based on the problem statements and current challenges for commercial microalgal biodiesel and exopolysaccharides production, following objectives were designed for sustainable biorefinery process. The core intention of the present study was to enhance the production of biodiesel and exopolysaccharides from *Scenedesmus abundans* cell factory in flat panel PBR. Free lipase, immobilized lipase mediated transesterification were studied to produce biodiesel from microalgal biomass. Therefore, the following objectives are formulated based upon the current bottlenecks in microalgal research.

I. Construction and characterization of medium scale flat panel PBR for producing biodiesel and exopolysaccharides from *S. abundans*.
II. Process design to enhance biodiesel in medium scale flat panel PBR under outdoor natural sunlight.
III. Multi-objective optimization of nutrients for enhancing biodiesel, autosedimentation factor and exopolysaccharides from *S. abundans* using composite desirability approach.
IV. Process development for immobilized enzyme based transesterification for biodiesel production from lipid enriched biomass of *S. abundans* by entrapment method.

1.4. Uniqueness of the study

The study highlights enhancement in the production of biodiesel and exopolysaccharides from *Scenedesmus abundans* cell factory in single stage medium scale flat panel photobioreactor under diurnal natural sunlight. Also, immobilized lipase mediated transesterification for producing biodiesel was explored.

- Medium scale flat panel PBR was constructed with high gas mass transfer, efficient neoprene rubber membrane sparger and less energy consumption for simultaneous production of biodiesel and EPS.
- *S. abundans* revealed its novelty by exhibiting no photoinhibition at 2162 μE/m^2/s high light intensity, capability of producing multi-products (biodiesel and EPS), cost effective natural autoflocculation based biomass harvesting and EPS purification can make the process sustainable.
- Single stage cultivation of *S. abundans* produced 2.5 fold higher FAME content than two stage and economical as harvesting steps could be minimized. Lipid enhancement in *S. abundans* using optimized lipid media under sunlight was proposed.
- Exploitation of *S. abundans* for enhancing the production of biodiesel and EPS using optimized multi-objective RSM media under sunlight could be a feasible approach.
- Lipase (steapsin) works optimum at room temperature without initial pH adjustments and could be reused without significant loss of catalytic activity after transesterification reaction by immobilizing lipase through entrapment method.

1.5. Organization of thesis

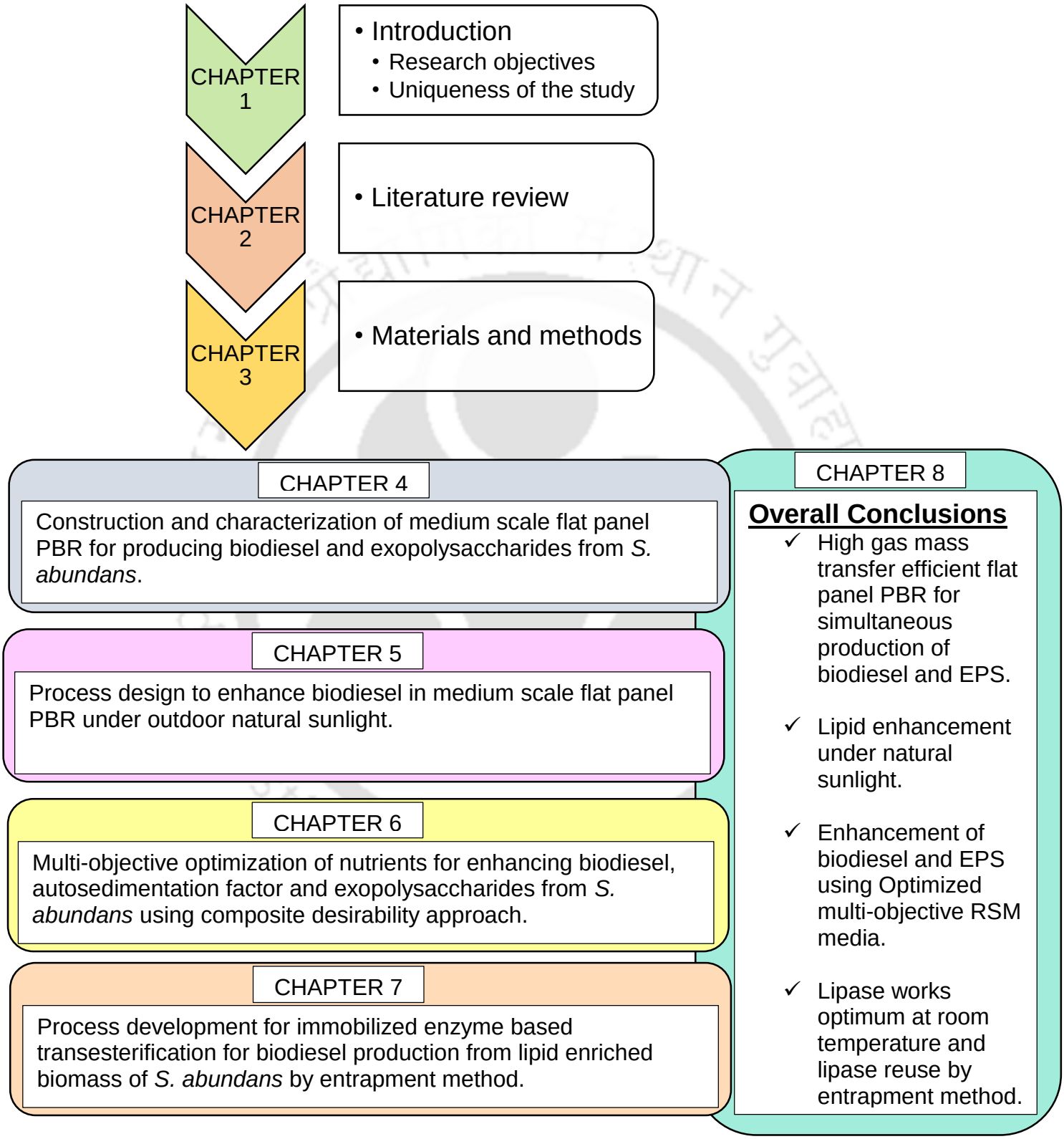

Fig. 1.4. Organization of thesis

Chapter 1 summarizes the background and motivation with highlighting problem statement (current bottlenecks of microalgal research), objectives of the study, uniqueness of the study, organization of thesis (Fig. 1.3) and experimental strategies followed to accomplish the project.

Chapter 2 broadly reviewed the recent scientific literature about the microalgae cultivation systems and criticized for the current engineering limitations that hinders the commerciality of microalgae biodiesel production. Emergence of renewable fuels, importance of exopolysaccharides, microalgae as biodiesel feedstock, an overview of microalgae growth parameters, triacylglycerol (TAG) metabolism in microalgae, special focus on nutrient regimes, lipid induction strategies were discussed in brief. A strong emphasis on efficient harvesting technology, enhancement of multi-product (biodiesel and EPS) from microalgae were also explained. Free lipase and immobilized lipase mediated transesterification in presence of methanol for producing biodiesel from microalgae were also discussed.

Chapter 3 focusses on materials and methodologies used for conducting experimental studies and analytical techniques to accomplish the formulated objectives.

Chapter 4 was detailed with the construction and characterization of medium scale flat panel PBR for producing biodiesel and exopolysaccharides from *S. abundans*.

Chapter 5 deals with the process design to enhance biodiesel in medium scale flat panel PBR under outdoor natural sunlight.

Chapter 6 details the multi-objective optimization of nutrients for enhancing biodiesel, autosedimentation factor and exopolysaccharides from *S. abundans* using composite desirability approach.

Chapter 7 outlines process development for immobilized enzyme based transesterification for biodiesel production from lipid enriched biomass of *S. abundans* by entrapment method.

Chapter 8 summarizes the overall conclusions drawn from all the studies conducted towards accomplishing the formulated objectives.

CHAPTER 2

Review of Literature

2.1. Biodiesel

Biodiesel (Greek, bio, life + diesel from Rudolf Diesel) is a diesel fuel derived from oils of plants, animals or microbes, usually composed of methyl esters of long-chain fatty acids. Therefore, it is also known as fatty acid methyl ester (FAME) (Demirbas, 2009). The chain length of the fatty acids, depends on source of the oil. Biodiesel is usually produced from the oil by chemical (acid, alkali) or enzymatic (lipase) transesterification, where the triglycerides in the oil are transesterified in presence of alcohol (usually short chain alcohol, methanol is preferred) to produce fatty acid methyl ester and glycerol. Biodiesel can be used in standard diesel engines, but is often blended as B5, B20 with conventional diesel (Scott et al., 2010). Microalgal biomass based biodiesel production has been gaining momentum in order to mitigate the rising of petroleum derived oil price, crisis of crude oil, global warming (Gavrilescu & Chisti, 2005). The biodiesel shows superiority over petrol and diesel in terms of renewability, sustainability, less toxicity, sulphur-free, better combustion, easier engine start-up and lesser greenhouse gases production (Aransiola et al., 2014). The produced biodiesel quality is assessed according to the ASTM D6751 or EN 14214 standards by using empirical equations such that it can be used directly in standard diesel engines or by blending with conventional diesel in 5% (B5) or 20% (B20) ratios (Demirbas, 2009).

2.1.1. Microalgae as superior feedstock for biodiesel production

As an alternative feedstock for biodiesel production, microalgae have the following advantages over conventional oil crops. They have simple structures with high photosynthetic

efficiency and short doubling time. They grow in all seasons, use less non arable lands and can be cultivated all year round. They sequester CO_2 in the air, efficiently remove nitrogen, phosphorus, heavy metals in wastewater and synthesize lipids in abundant amounts as compared to conventional oil crops which can be converted into biodiesel (Mata et al., 2010). For example, the CO_2 fixation efficiency of *Chlorella vulgaris* was up to 260 $mg.L^{-1}.h^{-1}$ in a membrane photobioreactor (Cheng et al., 2006). They may be cultivated on freshwater, saltwater lakes with eutrophication, oceans, marginal lands, deserts, etc. CO_2 utilization from thermal power plants by large-scale microalgae production facilities can reduce a great deal of greenhouse gas emissions and global warming. Microalgal biomass can be utilized in developing liquid and gaseous forms of biofuels such as bio-oil, bio-ethanol, biodiesel, bio-gas, bio-methane and bio-hydrogen. Bio-oil is produced by thermo-chemical conversion process in which biomass can be transformed into oil, carbon and gas at increased temperatures in the absence of oxygen. Pyrolysis and hydrothermal liquefaction are major types for bio-oil production. The process of pyrolysis mainly consists of three stages. In stage I, dehydration of algae sample is performed where water is released. In stage II, pyrolytic decomposition is performed. In stage III, char transformation and mineral matter decomposition are accomplished. Hydrothermal liquefaction process is carried out by exposing the algal biomass to high pressure (5–30 MPa) and high temperature (200–700 °C) under inert atmosphere (e.g. N_2 or He) or reducing gases (e.g. H_2 or CO) (Tian et al., 2014). Most of the microalgae carbohydrates are polysaccharides, like starch and cellulose. The complex multi-layered cell walls of microalgae contain high levels of polysaccharides that can be transformed into bio-ethanol via fermentation (Giordano & Wang, 2018). Biodiesel is produced by transesterification process in which raw lipids or triglycerides in presence of methanol gets converted into fatty acid methyl ester and glycerol using acid, alkali or enzymatic catalysts. The residues produced after biofuel production from microalgae could be used for biogas

production by anaerobic digestion. The anaerobic digestion process produces biogas that is composed of biomethane (CH_4) and carbon dioxide (CO_2) when microalgae consumes organic materials in absence of oxygen. Anaerobic digestion is divided in four different stages including hydrolysis, acidogenesis, acetogenesis and methanogenesis (Magdalena et al., 2018). Depending on the microalgae species, various high-value chemical compounds such as pigments, antioxidants, β-carotenes, polysaccharides, triglycerides, fatty acids, vitamins may be extracted via selective extractive techniques and largely used as bulk commodities in different industrial sectors (e.g. pharmaceuticals, cosmetics, nutraceuticals, functional foods, biofuels) (Barrow & Shahidi, 2007). In short, microalgae are a largely untapped sustainable biomass resource for renewable energy production.

2.2. Overview of microalgae

2.2.1. History and classification

Life was not existed on our Planet Earth due to volcanic eruptions, release of poisonous gases and high CO_2 levels in the atmosphere for billion of years ago. It was believed that phytoplanktons (algae, cyanobacteria) were the first life forms to step into mother Earth (Gualtieri & Barsanti, 2014). These unicellular photosynthetic organisms consumed high levels of CO_2 in presence of light and released O_2 in large amounts in the atmosphere. The released O_2 from these organisms resulted other life forms on our planet. Most of the conventional fossil fuels (coal, oil and natural gas) were formed from the dead remains of plants, animals and microbes (Bilanovic et al., 2009). The term ‘algae’ was coined by the father of classification, Carolus Linnaeus in the year 1753 which means sea weeds. Algae belong to thallophytes since they lack true roots, stems, leaves and does not contain differentiated tissues. Microalgae and macroalgae are the two major types of algae based on cellularity. Microalgae are unicellular algae that may either live singly or in colonies. Macroalgae/Seaweeds are multicellular algal species and can grow profusely at any time. The size of microalgae ranges between few µm to

few hundreds of µm whereas macroalgae can grow a length up to more than 80 m (Suganya et al., 2016). Algae can live predominantly in aquatic environments and can also occupy a variety of terrestrial habitats. According to conservative estimates, ~250,000 algal species exist in nature (Manoylov, 2014). Algae are photosynthetic organisms and require sunlight, CO_2 and water for their survival. They follow sexual, asexual modes of reproduction or both.

Anton van Leeuwenhoek (1674) observed unicellular algae under microscope. Carolus Linnaleus proposed 14 genera of algae. Out of 14 genera, 4 genera namely *Conferva, Ulva, Fucus* and *Chara* are considered as algae (Dahl, 1974). The descriptive classification of algae was proposed by W.H. Harvey (1836). He divided algae into four groups on the basis of thallus colour. Since then, many classifications have been proposed by algologists (phycologists) based on different characteristics like photosynthetic pigments (chlorophylls, carotenoids, phycobilins), biochemical nature of food reserve, cell wall composition, and flagella. West classified algae into four groups depending upon reproductive structures and presence or absence of flagella (West, 1916). A. Pascher also divided algae into eight divisions on the basis of phylogeny and interrelationships among various groups (Pascher, 1931). J. E. Tilden classified algae into five classes based on reserve food material, pigmentation and flagellation (Baweja & Sahoo, 2015). F.E. Fritsch (1935) classified algae into 11 classes as shown in Table 2.1. This classification was based on algal pigmentation, chemical nature of food reserve material, arrangement of flagella, presence or absence of organized nucleus and mode of reproduction (Fritsch, 1935).

Table 2.1. Classification of algae (Baweja & Sahoo, 2015; Fritsch, 1935).

Common name	Class	Order
Green algae	Chlorophyceae	Volvocales, Chlorococcales, Ulotrichales, Cladophorales, Chaetophorales, Charales, Oedogoniales, Conjugales, Siphonales
Yellow-green algae	Xanthophyceae	Heterochloridales, Heterococcales, Heterotrichales, Heterosiphonales
Orange algae	Chrysophyceae	Chrysomonadales, Chrysophaerales, Chrysotrichales
Diatoms/yellow or golden brown algae	Bacillariophyceae	Centrales, Pennales
Nearly brown algae	Cryptophyceae	Cryptomonadales, Cryptococcales
Dark yellow or brown algae	Dinophyceae	Desmomonadales, Thecatales, Dinophysiales, Dinoflagellata, Dinococcales, Dinotrichales
Bright green algae	Chloromonadineae	Chloromonadales
Euglenophyceae	Euglenophyceae	Divided into families – Euglenaceae, Astasiaceae, Peranemeceae
Brown algae	Phaeophyceae	Ectocarpales, Tilopteridales, Cutariales, Sporochnales, Desmarestiales, Laminariales, Sphacelariales, Dictyotales, Fucales
Red algae	Rhodophyceae	Bangiales, Nemalionales, Gelidiales, Cryptonemiales, Gigartinales, Rhodymeniales, Ceramiales
Blue green algae	Myxophyceae	Chroococcales, Chamaesiphonales, Pleurocapsales, Nostocales, Stigonematales

Scenedesmus abundans, a fresh water eukaryotic unicellular chlorophycean green microalgae have 2-4 celled colonies and are oval in shape with one or more lateral spines. The dimension of cells are 6-15 µm long and 2-7 µm broad with 3-8 µm long spines. Currently, there are 74 taxonomically accepted species of *Scenedesmus* (Guiry & GM, 2015). Hegewald

denotes *Acutodesmus*, *Desmodesmus* and *Scenedesmus* as three major categories. *Acutodesmus* is characterized as having acute cell poles. *Desmodesmus* and *Scenedesmus* have obtuse/truncated cell poles (differentiated by the presence or absence of cell spines respectively). Fossil records date *Scenedesmus* from 70 to 100 million years ago with *Desmodesmus* suspected to be the youngest of these three groups (Hegewald, 1997). *Scenedesmus* exist as unicells as well as coenobia of four or eight cells. Various coenobial architectures have been described, including linear, costulatoid, irregular, alternating, or dactylococcoid patterns (Lürling, 1999). *S. abundans* is oleaginous (lipid rich) high density microalgae and hence can be used as potential feedstock for biodiesel production. This candidate has the ability to coalesce (4 or 8 cells) under nutrient sufficient and nutrient deficient conditions by generating EPS around the cells.

2.2.2. TAG metabolism in algae

Microalgal cell cycle contains several consecutive procedures, including cell growth, DNA replication, nuclear division, and cellular division. Metabolism of both starch and lipid begins with an identical initial pool of molecules containing three carbons such as glyceraldehyde 3-phosphate (GAP) and 3- phosphoglycerate (3PG). Fig. 2.1 illustrates metabolic pathways that influence the accumulation of lipids by common C3 precursors (de Jaeger et al., 2014). As for autotrophic microalgae, light capture for photosynthesis is crucial for microalgal growth to accumulate energy reserves such as lipids. As a result, DNA replication and nuclear and cellular division in cell cycle can be completed through the utilization of the reserves to meet requirements of carbon and energy (Bišová & Zachleder, 2014). The lipid enrichment starts in the single stage when microalgal cell growth ceases due to light and nutrient limitation. Availability of adequate light intensity plays a crucial role in microalgal growth and neutral lipid enrichment. The lipid content of various microalgae species is shown in Table 2.2.

Wild type microalgal strains accumulate lipids under nutrient limited conditions resulting in the limitation of biomass productivities. Genetic engineering is a potential strategy to generate microalgal strains that accumulate lipids without growth impairment. Genetic modification was performed by adaptive laboratory evolution, random mutagenesis and direct genetic engineering. Adaptive laboratory evolution and physical mutagens such as UV light, gamma radiation and X-rays as well as chemical mutagens such as N′ -nitro-N-nitrosoguanidine and ethyl methanesulfonate have been applied on microalgae to generate random mutations. Efficient genetic engineering strategies such as advances in sequencing technology, development of fast, accurate and efficient DNA delivery systems and development of high throughput genome editing tools have become a crucial component for the generation of genetically improved microalgal strains (Muñoz et al., 2021). An *Escherichia coli* acetyl-CoA synthetase was overexpressed in the marine microalga *Schizochytrium* sp., resulting in 11.3% increase in fatty acids and 29.9% increase in biomass content, improved carbon utilization and reduced intracellular acetate concentration (Yan et al., 2013). Overexpression of acetyl-CoA synthetase in *C. reinhardtii* has increased intracellular acyl-CoA pools leading to 2.4-fold increase in TAG content when mutants were grown under nitrogen starvation conditions (Rengel et al., 2018). Genetic engineering of microalgae is difficult due to the barriers such as cell wall and cell membrane and often secreted extra polysaccharides (Mahesh et al., 2021). Sometimes, plasmids are lost from a population due to segregational loss, whereby a plasmid is lost by chance during cell division.

Table 2.2. Lipid content in the dry biomass of various species of microalgae.

Microalgae species	Medium type	Light intensity	Lipid content (% of dry cell weight)	Reference
Botryococcus braunii	BG-11	61 µE/m^2/s	30.2	(Ferreira et al., 2021)
Chlorella protothecoides	Proteose	200 µE/m^2/s	12.9	(Cheng et al., 2013)
Chlorella pyrenoidosa	BG-11	55 µE/m^2/s	8.5	(Yadavalli et al., 2020)
Chlorella vulgaris	BG-11	61 µE/m^2/s	21.9	(Ferreira et al., 2021)
Dunaliella parva	Johnson's	48.4 µE/m^2/s	39.1	(Fawzy & Alharthi, 2021)
Dunaliella tertiolecta	Sterilized f/2	100 µE/m^2/s	42	(Rizwan et al., 2017)
Euglena gracilis	Cramer-Myers	80 µE/m^2/s	28.4	(Chen et al., 2022)
Neochloris oleoabundans	Bold's Basal	3000 lux	35–54	(Tornabene et al., 1983)
Phaeodactylum tricornutum	Sterilized f/2	100 µE/m^2/s	53	(Yodsuwan et al., 2017)
Scenedesmus abundans	Modified Fogg's	40.5 µE/m^2/s	48	(Rai & Gupta, 2017)
Scenedesmus obliquus	BG-11	54 µE/m^2/s	47.6	(Anuradha et al., 2021)

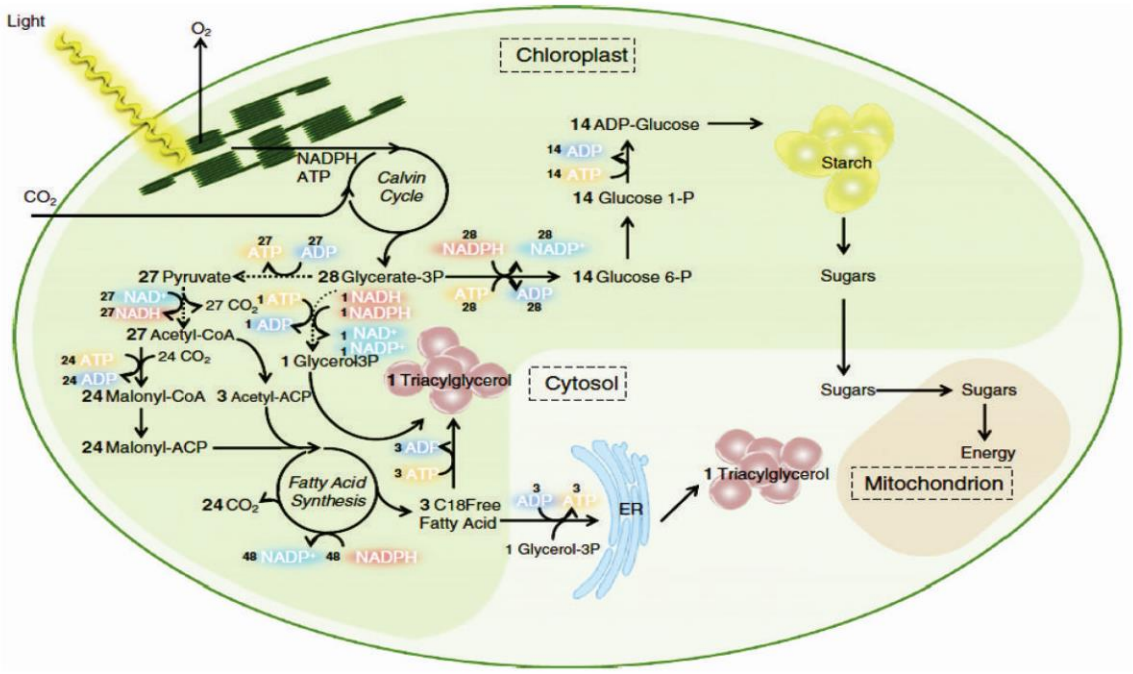

Fig. 2.1. Simplified triacylglycerol (TAG) metabolism in green microalgae. The dashed lines refer to the reactions that occur in the cytosol. The figure illustrates two possible pathways for TAG formation following the assumed route in the chloroplasts or over the endoplasmic reticulum (ER) membranes in the cytosol.

2.3. Factors influencing microalgae growth and lipid production

2.3.1. Microalgae cultivation and modes

The idea of cultivating algae in large quantity was conceived in 1952, at the Carnegie Institute of Washington. In 1960s, the Japanese experimented with outdoor culture in an 'open circulation system' by using shallow open pond in which the algal suspension was circulated via a series of moving pipes equipped with jets for the injection of fresh culture fluid. Later on, the Japan Nutrition Association developed a 20 m diameter pilot plant to investigate the industrial cultivation of algae further. Commercial production started in Japan, Europe, and Israel in late 1970s. During this period, algae cultures were commercially grown as healthy foods. As time went on, algal biomass production became important in the aquaculture, production of fine chemicals and health supplements.

Table 2.3. Major advantages and limitations of microalgae cultivation systems (Chisti, 2007; Doran, 1995; Posten, 2009; Ugwu et al., 2008).

Cultivation system	S/V ratio	Mixing	Gas exchange	Advantages	Limitations
Open ponds 	High	Paddle wheel	Poor, only achieved through surface aeration	Cost effective, simple and flexible design, beneficial for mass cultivation	Lower biomass productivity, susceptible to contamination, occupy large land space
Stirred tank PBR 	Low	Mechanical agitator	Injection through sparger	Good heat and mass transfer, good light dispersion, lower contamination issues, simple design, moderate biomass productivity	Low surface area to volume ratio, heating issues due to agitation, mechanical agitation require extra energy, expensive, not scalable
Vertical column PBR 	Low	Airlift/bubble	Open gas exchange at head space	High mass transfer, good mixing with low shear stress, higher biomass productivity, lower photoinhibition	Low surface area for illumination, dark zone formation, shading effect issues
Horizontal tubular PBR 	High	Recirculation via pumps	Injection into feed, dedicated degassing unit	High surface area to volume ratio, low hydrodynamic stress, low mutual shading effect, moderate biomass productivity	Dissolved oxygen build up, susceptible to photo inhibition, large space requirement
Flat panel PBR 	High	Airlift/bubble from bottoms or side	Open gas exchange at head space	High surface area to volume ratio, large surface areas for illumination, lesser optical path length, less dark zone formation, low oxygen buildup	frequent fouling and clean up issues

With advent of technology, the use of PBRs became more common. Currently, there are two widely practiced cultivation systems - open pond and closed PBRs. Microalgae can be cultivated in open pond system and closed PBR. Typically, the biomass productivities in PBRs are high as compared to open pond system due to its controlled environment. Moreover, the chance of contamination is very high in open pond. The major advantages and limitations of open ponds and closed PBRs are outlined in Table 2.3. Tubular PBRs and flat panel PBRs are most commonly used closed PBR systems. Algae can be cultivated in three modes, namely photoautotrophic, heterotrophic and mixotrophic. Photoautotrophic algal growth using CO_2 (from flue gases) is beneficial as CO_2 is cheaper than any other sugars and organic acids, and it is mostly obtained as a waste greenhouse gas emission from industries. Photoautotrophic cultivation of *Chlorella protothecoides* resulted in 12.9% lipid content in DCW at 200 $\mu E/m^2/s$ (Cheng et al., 2013). Heterotrophic mode of cultivation includes the utilization of organic carbon sources such as glucose, sucrose, glycerol and acetate by algae for their growth without light. In Heterotrophic cultivation, *Chlorella protothecoides* produced 46.1% lipid content in DCW from 5 L bioreactor (Li et al., 2007). Generally, heterotrophic cultivation of microalgae is performed in closed environments, e.g., stirred-tank bioreactors. In mixotrophic mode, both organic carbon sources and CO_2 are used for cultivating algae using a light source. Mixotrophic cultivation of *Chlorella protothecoides* produced maximum lipid content of 58.4% in DCW (Xiong et al., 2010). Mixotrophic mode of microalgal cultivation of *Chlorella protothecoides* produced highest lipid content in comparison to autotrophic and heterotrophic modes. This is because both organic carbon sources and CO_2 used in mixotrophic mode drive towards high lipid content in microalgae. Single stage microalgal cultivation is beneficial over two stage since harvesting steps can be minimized. As flat panel PBRs offer more advantages as compared to other cultivation systems, they are used in our present research study for cultivation of *S. abundans*.

2.3.2. Engineering of nutritional medium

Nutrient regimes play a crucial role in the cellular mechanism and biochemical composition of microalgal cells. Media is engineered with adequate supply of macronutrients and micronutrients. Nitrogen is essential for the synthesis of amino acids, proteins and photosynthetic pigments. Phosphorus is required for signal transduction, energy transfer and photosynthesis whereas magnesium is needed for cell growth. Sulfur is necessary for the synthesis of S-aminoacids and cell walls. Calcium plays a crucial role in signal transduction but the absence of calcium in the media triggers neutral lipid synthesis in some microalgae. Carbon is involved in the production of natural oils and the polymer of carbohydrates. Trace elements (Fe, Mn, Co, Zn, Cu, B, Mo) also have a profound impact on microalgal growth rate and lipid accumulation. Iron regulates gene expression and metabolism. Manganese accounts for the water oxidizing center of photosynthesis. CO_2 transport and fixation by carbonic anhydrase require Zinc/Cobalt. Copper is used for the functioning of cytochrome oxidase, a protein required in the respiratory electron transport chain. Boron plays a key role in the structure and stability of algal cell walls and molybdenum is responsible for nitrogen assimilation (Quigg, 2016; Sajjadi et al., 2018).

2.3.3. CO_2 levels, light wavelength and intensity

As carbon constitutes more than 50% of the algal biomass, it is crucial to supply sufficient carbon for the cultivation of microalgae (Show et al., 2017). Different organic and inorganic forms of carbon are utilized by microalgae depending on the nutrition mode. Organic carbon sources such as glucose, sucrose, glycerol and acetate could be effectively used by microalgae. But, there could be chance of contamination issues in using organic carbon. Inorganic carbon sources such as HCO_3^- and CO_3^{2-} are provided by either sodium bicarbonate or sodium carbonate. Sodium bicarbonate is available at low cost and has higher solubility. Moreover, it was shown that microalgae grow better with sodium bicarbonate as an inorganic

carbon source. In phototrophic cultivation of microalgae, carbon is supplied mainly in the form of CO_2 as inorganic carbon source. It is estimated that to generate 1 g of algal biomass, 1.7–1.8 g of CO_2, and for producing lipid-rich microalgae, up to 3 g CO_2 per g of biomass may be required (Morweiser et al., 2010). It should be noted that the metabolic efficiency and resulting microalgae composition of using CO_2 or carbonate/bicarbonate as carbon source could be different from species to species (Giordano et al., 2005). The low levels of CO_2 in ambient air are usually not sufficient to ensure high algal biomass productivity. While CO_2 concentrations of about 1–5% can often support maximal microalgal growth, laboratory cultures are often aerated with 5–15% CO_2 (Kusumaningtyas et al., 2017). Optimal growth of microalgae needs adequate amount of dissolved CO_2. In general, as the quantity of CO_2 increases to an optimal level, the growth of microalgae and production of lipids increase. Aeration of gas mixture with a high concentration of CO_2 can meet the requirement for CO_2. The amount of CO_2 in atmospheric air is not sufficient. Aeration with pure air resulted in a decrease in growth and lipid production of microalgae *Parachlorella kessleri* (Li et al., 2013). Limited amount of CO_2 available in cultures slows down the metabolism of microalgae causing reduced lipids (Gardner et al., 2013). To reduce costs, flue gas (rich in CO_2) can be introduced into microalgal culturing systems as a carbon source. However, high content of CO_2 will also affect the growth of microalgae. This is because unutilized CO_2 in culture will be converted to carbonic acid (H_2CO_3), reducing the pH value of the culture (Sibi et al., 2016). Therefore, optimal CO_2 levels are required for enhanced biomass and lipid production in microalgae.

Manipulation of light conditions, in terms of wavelength and intensity, is an important strategy to enhance biomass and lipid production in microalgae for biofuel production. Use of light-emitting diodes (LED), dyes and paints are amongst the current strategies for providing light of the desired wavelength and intensity to maximize the growth of microalgae (Ramanna et al., 2017; Singh et al., 2016). Exposure of microalgal cultures to blue (450–475 nm) and red

(630–675 nm) light is desirable as this allows maximum light absorption by chlorophyll pigments, and thus, enhances the performance of photosystems I and II (Choi et al., 2015).

Apart from wavelength, light intensity is another factor that can influence growth and lipid production in microalgae. For instance, high light (400 µE/m^2/s) induced more carbon allocation for lipid synthesis, resulting in the accumulation of neutral lipids and decreased carbohydrate content, in *Chlorella* sp. and *Monoraphidium* sp. (He et al., 2015). In parallel, there was a decrease in membrane lipids and photosynthetic efficiency (Fv/Fm), with increase in ROS scavenging enzymes in the two microalgae. Increase of light intensity from 250 to 400 µE/m^2/s was found to enhance total lipid and neutral lipid production in *Scenedesmus* sp. 11-1 (Liu et al., 2012a). Fluctuating high light intensities (990–1486 µE/m^2/s) enhanced accumulation of lipids, especially neutral lipids, of six oleaginous microalgae cultured under outdoor conditions (He et al., 2015). The neutral lipid accumulation was attributed to the conversion of glycolipids. However, lipid accumulation may not be enhanced in some microalgae when grown under high light intensity. For instance, the maximum TAG content of *T.obliquus* was not affected when light intensities were varied from 200–1500 µE/m^2/s (Breuer et al., 2013).

Adequate light intensity favours the overproduction of microalgal lipids (Hallenbeck et al., 2015). This might be because sufficient light intensity is beneficial to the storage of excess photoassimilates, which are further converted into chemical energy (Solovchenko et al., 2008). Microalga *Nannochloropsis* sp. experienced the accumulation of the highest amount of lipids (47% of DW) under the conditions with the highest light intensity (700 µE/m^2/s) (Pal et al., 2011). *C. sorokiniana, C. viscosa, C. emersonii, C. vulgaris, P. beijerinckii,* and *P. kessleri* CCALA255, NIES-2152, and NIES-2159 were able to increase the productivity of lipids under high light intensity of 600 µE/m^2/s (Takeshita et al., 2014). It has been seen that the lipid content of the microalgae *Scenedesmus abundans* kept on rising as the light intensity increased

from 3000 to 6000 lux (Mandotra et al., 2016). The highest lipid content of 32.77% was achieved, when the culture was under the light intensity of 6000 lux, followed by 27.10 and 21.20% in the culture with 5000 and 3000 lux intensity, respectively. Another study indicated that *Botryococcus* sp. had shown the highest lipid percentage (35.9%) at 6000 lux (Yeesang & Cheirsilp, 2011). However, highest lipid percentage (33.0%) of microalgae *N. oleoabundans* HK-129 was achieved at 14,800 lux intensity (Sun et al., 2014). Thus, different microalgal species have the highest lipid content at variable light intensities, since they indicate different efficiencies in light utilization. From this point of view, the ability to use light is microalgae-specific.

2.3.4. Effect of temperature and pH

The effect of temperature on microalgal growth and lipid production is similar to that of light intensity. Microalgal growth as well as lipid production exponentially increases to a certain extent as the temperature increases and reaches an optimal level. The optimal value of temperature where the highest biomass production is achieved varies from species to species (Sibi et al., 2016). Microalgae *C. vulgaris* accumulated maximum lipids at 25 °C, while the decrease of temperature resulted in an obvious decrease in the lipid content (Converti et al., 2009). The temperature of 20 °C was found to be the optimal temperature for microalgae *Scenedesmus* sp. to produce lipids (Xin et al., 2011). The lipid concentration of microalgae *S. obliquus* ranged from 18 to 40% of dry weight, when the temperature ranged from 20 to 27.5 °C (Vitova et al., 2015). As the temperature increased from 20 to 25°C, the lipid content of *N. oculata* simultaneously increased from 7.9 to 14.9% (Converti et al., 2009). In another study, the optimum temperature of *C. minutissima* was found to be 20°C, where lipid productivity was the highest (Cao et al., 2014). However, some reports under natural sunlight conditions suggest that the temperature control is not mandatory for some microalgal strains as it saves the cost of overall process (Fuentes-Grünewald et al., 2013). For this reason, the process design

of microalgal biomass production would be more feasible if the selected strain is tolerant to a wide range of temperatures.

Unlike temperature, the process pH monitoring and maintenance in algae culture is important for efficient CO_2 uptake by the cells. Day/night pH fluctuations driven by photosynthesis and respiration create an environment that exhibits changing pH ranges. CO_2 exists in three forms namely bicarbonate (HCO_3^-) at neutral pH and carbonate (CO_3^{2-}) at alkaline pH levels and dissolved CO_2 at acidic/neutral pH levels in the water (Scherholz & Curtis, 2013). However, most of the microalgal cells prefer dissolved CO_2 or HCO_3^- over the CO_3^{2-} species (Scherholz & Curtis, 2013). Therefore, the process pH of culture medium should be maintained in acidic or neutral pH conditions. Abu-Rezq et al. could maintain the pH of algae cultures in the pH range of 6.75–7.25 with CO_2 injections, while untreated cultures exhibited pH levels as high as pH 8.28 (Abu-Rezq et al., 1999). Moheimani found an optimum pH for biomass and lipid production of *Tetraselmis suecica* and *Chlorella* sp. of pH 7.5 and 7 respectively (Moheimani, 2013). pH may affect the lipid composition of *N. salina* (Griffiths & Harrison, 2009; Moheimani, 2013; Rodolfi et al., 2009). Lipid accumulation is maximized when *Nannochloropsis* cells are stressed by unfavorable conditions so that growth slows and energy is stored as lipids (Abu-Rezq et al., 1999; Wang et al., 2009).

2.3.5. Mixing and mass transfer

Efficient mixing prevents the settling of microalgal cells, minimizes the diffusion gradients (CO_2 + media components), strips out accumulated dissolved oxygen and most importantly aids movement of algal cells from light to dark zones (Kunjapur & Eldridge, 2010). Mixing could also improve biomass productivity by maximizing the solar energy capture leading to increase in specific light availability to algal cells (average light exposure per algal cell) (Wang et al., 2012). Mixing also helps in the improvement of lipid contents in microalgae that enhances biodiesel production. For example, Liu et al. investigated the effect of 400 µmol

photons/m^2/s light intensity in a column PBR with a diameter of 42 mm, effective volume of 0.6 l, and blowing air supplemented with CO_2 (2 %, v/v) at 25 °C using modified BG-11 media, in which the concentration of $NaNO_3$ was decreased to 4.41 mmol/l (1/4 of normal BG-11 media) on the growth and lipid production of *Scenedesmus* sp. 11-1 under N-limited condition for 12 days. *S.* sp. 11-1 culture was initially grown at the light intensity of 50 µmol photons/m^2/s for the first 2 days and then transferred to 400 µmol photons/m^2/s for 10 days. 3.88 g/l biomass titer with 32.9% neutral lipid content was achieved at the end of 12 days. The final neutral lipid yield and productivity were 1.28 g/l and 107 mg/l/day (Liu et al., 2012a).

The transportation of CO_2 for efficient absorption by the cells requires a sparger having high CO_2 mass transfer coefficient. The performance of sparger's mass transfer is usually measured in terms of overall mass transfer coefficients of O_2 (K_{La,O_2}) or CO_2 (K_{La,CO_2}) and mixing time (t_m). O_2 is sparged through metallic L-shaped sparger capable of generating big bubbles resulting in improper mixing of algal cells. However, agitation generated by electricity driven impellers generates small size bubbles for efficient mass transfer. But, the electrical energy required for running impeller would add extra cost for biodiesel production from microalgae. Therefore, the algal researchers developed sparging technology from air-lift type of reactors where mass transfer and mixing are driven by small or medium bubble size (Mirón et al., 2004; Ugwu et al., 2008). Different type of sparger designs (L-shaped, ring-shaped, perforated tubing, ceramic, compressed stainless steel, membrane and sintered disc) have been used by researchers in cultivation systems for mass production of algae (Contreras et al., 1998; Merchuk et al., 2000; Vega-Estrada et al., 2005). Despite of high CO_2 mass transfer coefficient, an ideal sparger should also be energy-efficient for aeration (minimize electricity requirement) for successful commercialization of microalgal biomass production.

2.3.6. Nutrient starvation

Variation in macronutrients such as nitrogen, phosphorus, and sulfur in culture media

will lead to alteration of macromolecular composition in microalgal cells. Under nutrient stress, lipid accumulation is favoured, and triacylglycerol is formed as the dominant ingredient (Sibi et al., 2016). Various studies have reported that most microalgal species can improve lipid accumulation and undergo transformation under nutrient stress (Li et al., 2014; Zhu et al., 2013). Nevertheless, as for some species, nutrient deficiency will not favour the accumulation of lipids. For instance, under nutrient deficiency the microalgae *Dunaliella salina* experienced lipid content decrease from 25% to 9% but carbohydrate increase from 16% to 56% (Alabi et al., 2009). Basic nutrient stresses, particularly the limitation of phosphorus and nitrogen in culture medium helps to induce the lipid contents of several microalgae such as, *Scenedesmus subspicatus*, *Scenedesmus* sp., *Spirulina platensis*, *Dunaliella tertiolecta*, *Neochloris oleoabundans*, *Chlorella vulgaris* (Brennan & Owende, 2010; Pal et al., 2011; Sharma et al., 2012; Widjaja et al., 2009). It is not unusual for algae to become nutrient-limited (i.e., nitrogen- and phosphorus-limited) in the natural environment (Harris, 2012). Nitrogen and phosphorus starvation shifts the lipid metabolism from membrane lipid synthesis to neutral lipid storage. This, in turn, increases the total lipid content of green algae (Hu, 2004). Calcium starvation leads to partial decrease in biomass yield and the lipid pool showed a profound rise. Limiting nutrient availability in terms of nitrogen, phosphorus, magnesium, sulphur and calcium starvation are most commonly used to induce lipid synthesis (Weldy & Huesemann, 2007; Zhila et al., 2005).

2.4. Exopolysaccharides

2.4.1. Production and applications of EPS

Exopolysaccharides are polymers of carbohydrates, proteins that are linked to each other in a linear or branched fashion with the aid of glycosidic linkages and their composition includes proteins, glycoproteins, or lipids, in addition to carbohydrates. Microorganisms such as bacteria, cyanobacteria, and green unicellular algae have the ability to produce

exopolysaccharides on the cell outer surface. Thus, in addition to biological necessity, EPS also possess numerous industrial and medicinal values in adhesives, detergents, textiles, cosmetics, wastewater treatment, brewing, and pharmaceuticals (Raza et al., 2012). Microalgae have a natural tendency to secrete EPS into the medium, thus making it easier to extract them (Gerbersdorf et al., 2009). In comparison to that in bacteria and fungi, the yield of EPS from microalgae is less. However, the composition of EPS is unique, presenting them as rare polymers with interesting properties, distinct from other polysaccharides.

Exopolysaccharides are used in food (e.g. jelly, candy, sauce and beverages), pharmaceuticals (e.g. capsule covering and antitumour drugs), textiles (e.g. printing and dyeing), cosmetics (e.g. body lotion and emulsifier), detergents, adhesives, wastewater treatment, bioremediation, bioflocculants and oil recovery (Liu et al., 2016). The exopolysaccharides from various algal groups like rhodophytes, cyanophytes chlorophytes and dinoflagellates have been widely reported to exhibit antibacterial, antiviral, antitumour, anticoagulant and antioxidant activities (Chen et al., 2010; Freire-Nordi et al., 2005). In a recent study, biodiesel (1.53 g/L) and exopolysaccharides (236 mg/L) were concomitantly produced via *Scenedesmus abundans* (Mahesh et al., 2019). These exopolysaccharides were composed of monosaccharides like glucose, galactose, arabinose and rhamnose.

2.4.2. Effect of stress conditions on EPS production

The production of EPSs, playing a structural and protective role in microbial biofilms, have been reported to be enhanced under stress conditions (Chakraborty et al., 2015; Rossi & De Philippis, 2015). Among the nutrient stresses provided to *Scenedesmus* sp. SB1, the nitrogen stress did not enhance EPS production (0.037 ± 0.012 mg/mL) when compared to that of normal BG-11 (0.051 ± 0.019 mg/mL). The acidic stress (pH 6) produced a 1.64 fold increase in the EPS production, 0.084 ± 0.037 mg/mL, than that in normal pH 6.8 ± 2 (0.051 ± 0.019 mg/mL). However, when the medium was set at a pH of 8, *Scenedesmus* sp. SB1

contributed 0.04 ± 0.013 mg/mL EPS only. On the other hand, when 1% NaCl was added to the medium, *Scenedesmus* sp. SB1 produced 0.086 ± 0.04 mg/mL of EPS, 1.68 fold higher than in normal BG-11. Likewise, 2 and 3% salinity stresses have also been found to increase EPS production, which is not as significant as 1% salinity stress (Angelaalincy et al., 2017). In another study, the maximum EPS production was 236 mg/l with a yield of 37 mg EPS/g biomass from *Scenedesmus abundans* at nitrogen starvation condition (Mahesh et al., 2019).

2.5. Downstream processing of microalgae for biodiesel production

2.5.1. Harvesting technologies

In succession to microalgal cultivation and lipid induction, harvesting of algal biomass is a solid-liquid operation in a top-down approach from algal growth to downstream applications. The unit operation accounts for nearly 30% of total biodiesel production cost along with a dewatering procedure (Schlesinger et al., 2012). The important factors that affect any harvesting technique include (a) nature of algal species (b) age of algal culture volume and (c) harvesting time. Challenges of microalgae harvesting arise due to small size of microalgal cells, the similarity of density of algal cells to that of growth medium and the negative surface charge on the algae. The separation of microalgae by centrifugation can have a harvesting energy requirement of 1 MJ kg^{-1} of dry biomass, greater than the energy cost of harvesting wood (0.7–0.9 MJ kg^{-1}) (Sawayama et al., 1999). After cultivation, algae are subjected to harvesting processes such as centrifugation, filtration (cake and ultrafiltration), sedimentation, flotation, flocculation (chemical, biological, magnetic, electro and autoflocculation) to separate the algal biomass and extracellular products. The leftover media after fractionation of the extracellular products can be recycled to the next batch with adequate nutrient resupplementation. The wet/dried algal biomass after harvesting is extracted and fractionated into platforms of lipids, carbohydrates and proteins via various downstream processing techniques. Table 2.4 shows the comparison of microalgal harvesting methods.

Table 2.4. Comparison of microalgal harvesting methods (Grima et al., 2003; Mohn, 1988; Shen et al., 2009).

Microalgal harvesting method	Advantages	Disadvantages
Centrifugation	Can handle most algal types with rapid efficient cell harvesting	High capital and operational costs
Filtration	Wide variety of filter and membrane types available	Highly dependent on algal species, best suited for large algal cells, clogging or fouling issues
Ultrafiltration	Can handle delicate cells	High capital and operational costs
Sedimentation	Low cost, potential for use as a first stage to reduce energy input and cost of subsequent stages	Algal species specific, best suited to dense non-motile cells, separation can be slow, low final concentration
Chemical flocculation	Wide range of flocculants available with low price	Removal of chemical flocculants, causes chemical contamination
Autoflocculation	Natural process exhibited by some specific algae	Algal species specific
Flotation	Can be more rapid than sedimentation, possibility to combine with gaseous transfer	Algal species specific, high capital and operational cost

Flocculation can occur naturally in certain microalgae by a process known as autoflocculation. Microalgae may flocculate in response to environmental stress such as changes in nitrogen, pH and dissolved oxygen (Schenk et al., 2008; Uduman et al., 2010). Autoflocculation is exhibited by some specific microalgae species and process can be slow (Schenk et al., 2008). Flocculation can be induced by chemicals, both inorganic and organic, or by microorganisms. The type of flocculants used for harvesting may be algae species-specific. Recovery and recycling of the flocculants could be problematic (Grima et al., 2003; Mohn, 1988; Oswald, 1988; Shen et al., 2009). The shape, size and composition of flocs can be very diverse depending on microalgal species and flocculant (Jago et al., 2007). An ideal flocculant should be inexpensive, nontoxic and effective in low concentrations. It should also preferably be derived from non fossil fuel sources, be sustainable and renewable (Grima et al.,

2003). Mahesh et al. observed that *Scenedesmus abundans* settles down to 0.025 m with OD_{680} of 41.8 within 3 min from initial height of 0.23 m (initial OD_{680} = 5.2) corresponding to almost 90% cell recovery without adding any flocculants (Mahesh et al., 2019). EPS with specific metal ion combination was responsible for autoflocculation phenomena in *S. abundans*. Moorthy et al. also studied the same strain of *Scenedesmus abundans* sedimentation by flocculation strategy (Moorthy et al., 2017). In their study, with initial biomass concentration of 0.55 g/l, the flocculation efficiency was 45% in 12 h (total settling time was 26.5 h) without adding any flocculants.

2.5.2. Biodiesel production and quality assessment

2.5.2.1. Cell disruption and conversion of lipids to biodiesel

The lipid enriched biomass after harvesting was freeze dried/dried in oven at 70 ºC for 24 hrs and subjected to cell disruption technologies. Depending on the cell wall rigidness of microalgae and products of interest, the cell disruption technology has to be decided (Günerken et al., 2015). Broadly, the cell disruption methods are divided into two categories, namely mechanical and non-mechanical methods. The mechanical type of cell disruption requires energy in the form of shear force, wave energy, current and heat. The methods such as bead milling and high pressure homogenization can be categorized under shear-force based cell disruption. Bead milling breaks the algal cells by creating compressive and shear forces applied through fast-moving solid beads (Günerken et al., 2015). In high-pressure homogenization, the cells are pressed through a small orifice where cell lysis is promoted by turbulence, shear stress and cavitation mechanisms. The wave energy based cell disruption techniques include ultrasonication, microwaves and pulsed electric field treatment (Günerken et al., 2015). In ultrasonication, the cells are lysed due to shock waves generated by bursting of microbubbles caused by cavitation effect. During microwaves treatment, the algal cell walls are disrupted due to high heating in short time which damages the pectin and cellulose structures of algal

cell wall. In the pulsed electric field treatment, the cell disrupts due to an electric potential that generates across the cell wall. With regard to heat based cell disruption, steam explosion and hydrothermal liquefaction (HTL) were explored recently. In steam explosion, the wet/dry biomass is subjected to temperatures in the range of 180–240 °C and pressures of 1–3.5 MPa. A sudden depressurizing explodes the algal cells to release lipids, soluble sugars and solid residues (Cheng et al., 2015). Hydrothermal liquefaction is a thermochemical treatment that converts biomass feedstock directly into bio-oil (bio-crude). In the HTL process, the algal biomass are exposed to high pressure (5–30 MPa) and high temperature (200–700 °C) under inert atmosphere (e.g. N_2 or He) or reducing gases (e.g. H_2 or CO) (Tian et al., 2014). The use of ultra-sonication, microwaves, steam explosion and hydrothermal liquefaction methods are very efficient in extracting lipids from algal biomass, but they cannot be used for large-scale applications due to their very high energy demands (Hidalgo et al., 2013).

Therefore, the non-mechanical cell disruption methods are used as they use less energy as compared to mechanical methods and include chemical and biological techniques. In chemical methods, chemicals like antibiotics, ionic liquids, special nanoparticles, chelating agents, chaotropes, detergents, solvents, supercritical liquids, hypochlorites, acids and alkali are used (Günerken et al., 2015; Lee et al., 2017). The biological cell disruption techniques uses enzymes such as cellulases, lipases, lysozymes, pectinases and proteases for lysing rigid algal cell wall containing cellulose, membrane lipids and proteins (Wu et al., 2017). The most common methods for cell disruption are using chemical solvents such as methanol that acts as lipid extracting solvent. Transesterification process is carried out after extracting lipids/triglycerides in the presence of alcohol (methanol/ethanol) and catalyst, either chemical or enzymatic catalyst to accelerate the reaction and produce biodiesel as shown in Fig. 2.2. There are two different methods of transesterification namely two step transesterification (lipid extraction via solvent followed by transesterification) and direct transesterification of algal

biomass to produce biodiesel. Direct transesterification have advantages such as less lipid loss during extraction process, less time consuming and higher yield of crude biodiesel over two step transesterication (Ehimen et al., 2010).

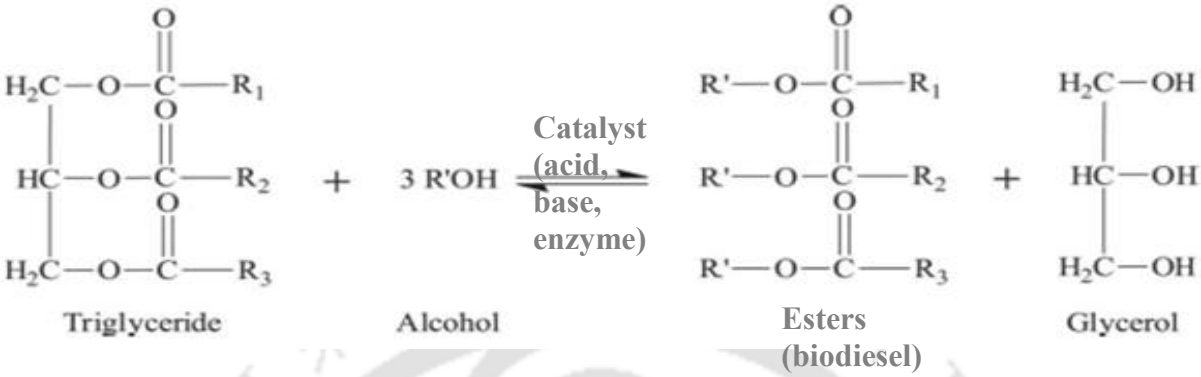

Fig. 2.2. Transesterification reaction for the production of biodiesel extracted from triglycerides of microalgal biomass.

Biodiesel production from microalgae lipids has been performed using both acid and alkaline homogeneous catalysis (Nagle & Lemke, 1990; Vijayaraghavan & Hemanathan, 2009). However, due to the high free fatty acid (FFA) content in microalgae lipids, alkaline catalysts are not suitable for biodiesel production (Ehimen et al., 2010; Miao & Wu, 2006). The use of acid catalysts produced higher biodiesel conversion yield from microalgae lipids compared to alkaline catalysts under the same reaction conditions (Nagle & Lemke, 1990).

Lipases (triacylglycerol acylhydrolases, EC number 3.1.1.3) are important biocatalysts for biodiesel production from microalgae because of their excellent biochemical, physiological properties and biodegradability nature as compared to conventional acid and base catalysts (Gupta et al., 2004). Lipase catalyzed biodiesel production was first reported by Mittelbach (Yücel et al., 2012). Advantages of lipase in biodiesel production are high efficiency in converting free fatty acids to methyl esters, specific reaction, less energy consumption, mild reaction conditions, low temperature, and reduces the formation of side products and wastes (Abdulla & Ravindra, 2013). *Burkholderia cepacia* lipase, *Candida antarctica* lipase, *Thermomyces lanuginous* lipase are most widely used bacterial, yeast and fungal lipases respectively for biodiesel production (Ranganathan et al., 2008; Tan et al., 2010). There are

several factors affecting enzymatic transesterification process namely pH, concentration of substrates, temperature, activity of the enzyme and spacing between the enzyme molecules and the substrate. Each enzyme works best at their optimum condition and varies depending on its origin. The specialities of enzyme are non-toxic, reusable, and sometimes, it can be reused till 10^{th} cycle by enzyme immobilization (cost of enzyme would be compensated by immobilizing enzyme). Commonly, lipases will be immobilized in four methods such as adsorption, covalent binding, entrapment and cross-linking as shown in Fig. 2.3 (Tan et al., 2010).

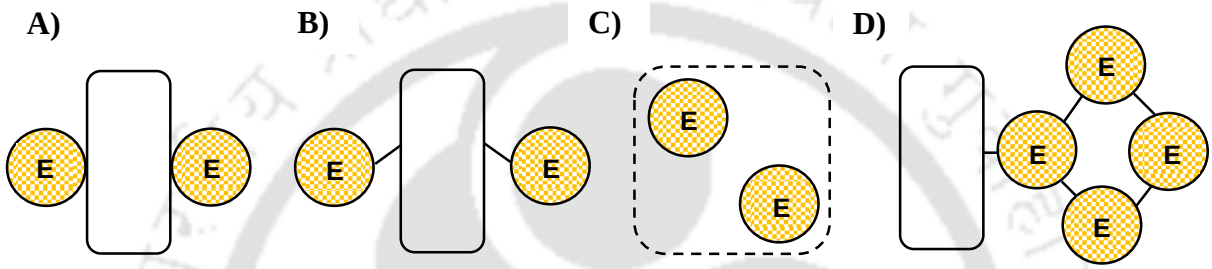

Fig. 2.3. Schematic diagram of enzyme immobilization methods. **A)** Adsorption, **B)** Covalent binding, **C)** Entrapment and **D)** Cross-linking (E denotes enzyme).

Adsorption is the attachment of lipase enzyme on the surface of the carrier by weak forces such as Van der Waals, hydrophobic interactions or dispersion forces (Tan et al., 2010). Adsorption is the most widely used method because the process is easy and can be operated at low cost under mild conditions without major activity loss. Large scale industries use adsorption method to immobilize *C. artarctica* lipase on acrylic resin which is known by its commercial name Novozyme 435 and *Candida* sp. 99–125 lipase immobilized on cheap textile membrane. Biodiesel yield can reach between 90% and 97% by adsorption method in cotton seed and microalgae respectively (Royon et al., 2007; Singh et al., 2014). Major disadvantages of adsorption method are weak interaction between lipase and the carrier could make the immobilized lipase sensitive to pH, ionic strength and temperature etc. The adsorption capacity is small and the protein might be stripped off from the carrier (Tan et al., 2010; Yücel et al., 2012).

Another approach to immobilize lipase is covalent binding in which the covalent bonds are formed between the aldehyde groups of surface and active amino acid residues on the surface of the enzyme (Yücel et al., 2012). The strong interactions between lipase and the support would not result in enzyme leaching during the catalytic process. A variety of supports have been used such as inorganic materials, natural polymers (agarose, chitin and chitosan), synthetic polymers (hydrophobic polypeptides, nylon fibers) and Eupergits (made by copolymerization of N,N´-methylenebismethacrylamide, glycidyl methacrylate, allyl glycidyl ether and methacrylamide) for immobilization of lipases by covalent bonding (Bhushan et al., 2008; Knezevic et al., 2006). Lipase from *Thermomyces lanuginosus* was immobilized by covalent attachment onto polyglutaraldehyde activated styrene-divinylbenzene copolymer, which was used to catalyze methanolysis of canola oil for biodiesel synthesis. Under the optimized conditions, the maximum biodiesel yield was 97% at 50 °C in 24 hr reaction. The immobilized enzyme retained its activity during 10 repeated batch reactions (Dizge et al., 2009a; Dizge et al., 2009b). Limitations of covalent binding method are laborious preparation of immobilized enzyme causing lipase to lose its activity. Some coupling reagents are toxic (Tan et al., 2010; Yücel et al., 2012).

Cross-linking is another method for immobilization which is defined as the interaction of a three dimensional network within enzyme, coupling reagent, and carrier (Yücel et al., 2012). Lipase from *B. cepacia* was immobilized on modified attapulgite with the optimized conditions as follows: 10 g jatropha oil, 2.4 g methanol being added at 3 hr intervals, 7 wt% water, 10 wt% immobilized lipase, 35 °C reaction temperature and 24 hr reaction time. The maximum biodiesel yield reached 94% after 24 hr under these reaction conditions. After 10 times of lipase reuse, the biodiesel yield was around 89% that corresponds to 94% obtained in the first batch (You et al., 2013). Major drawbacks of this immobilization method are intense cross-linking conditions and mechanical strength of the immobilized lipase is low (Tan et al.,

2010; Yücel et al., 2012). Table 2.5 shows the comparison of different methods of enzyme immobilization.

Table 2.5. Comparison of enzyme immobilization methods (Tan et al., 2010; Yücel et al., 2012).

Immobilization Method	Advantages	Disadvantages
Adsorption	Lipase works at mild conditions, method is easy and low cost investment, regenerated carrier could be used several times	Weak interaction between lipase and the carrier could make the immobilized lipase sensitive to pH, ionic strength and temperature etc, adsorption capacity is small and protein might get stripped off from the carrier
Covalent binding	Thermal and operational stable enzyme	The laborious preparation of immobilized enzyme might cause lipase to lose its activity and some coupling reagents are toxic
Cross-linking	Lipase is stable due to strong interaction between lipase and carrier	The cross-linking conditions are intense and mechanical strength of the immobilized lipase is low
Entrapment	The conditions are moderate and applicable to a wide range of carrier and lipases, method is fast, cheap and easy	The lipase is only effective for low molecular weight substrates because it has the mass transfer restriction during the catalytic process

Entrapment method is based on capturing the lipase within a polymer network that retains the enzyme but allows the substrate and products to pass through. It can also be defined as mixing an enzyme with a polymer solution and then cross-linking the polymer to form a lattice structure that captures the enzyme (Yücel et al., 2012). *P. cepacia* was entrapped in hydrophobic sol–gel and immobilized lipase could catalyze biodiesel production of 67% with soybean oil as feedstock. Lipase immobilization by entrapment is applicable to wide range of carriers as well as lipases and this method is fast, cheap and easy. The mass transfer restriction during the catalytic process is only disadvantage of this method and it can be reduced by optimizing the process variables and conditions (Tan et al., 2010; Yücel et al., 2012).

2.5.2.2. Assessment of biodiesel quality

The biodiesel quality was determined by assessing saponification value (SV), iodine value (IV), cetane number (CN), degree of unsaturation (DU), long chain saturation factor (LCSF), cold filter plugging point (CFPP), cloud point (CP), pour point (PP), oxidation stability index (OSI), higher heating value (HHV), kinematic viscosity (ν), density (ρ) and flash point (FP). The biodiesel properties of any biomass feedstock should be close/comply with standard values of American society of testing and materials (ASTM) or European Nation (EN) for considering good quality biodiesel and feasibility of using biodiesel in automobiles. The comparison of biodiesel properties of some microalgae species and diesel with ASTM D6751 and EN 14214 biodiesel standards was shown in Table 2.6.

Table 2.6. Comparison of biodiesel properties of some microalgae and diesel with ASTM D6751 and EN 14214 biodiesel standards (Brennan & Owende, 2010; Islam et al., 2013).

Biodiesel property	**ASTM D6751**	**EN 14213/ EN 14214**	***N. oculata***	***Extubocellulus* sp.**	***Biddulphia* sp.**	**Diesel**
SV (mg KOH g^{-1} oil)	ND	ND	203	209	210	ND
IV (g I_2 100 g^{-1} oil)	ND	≤ 120	81	65	88	ND
CN	≥ 47	≥ 51	55	57.8	52.5	51
DU	ND	ND	69	69	67	ND
LCSF	ND	ND	3.7	3	2.7	ND
CFPP (ºC)	ND	≤5 (summer) ≤-20 (winter)	-4.8	-7	-7.9	ND
HHV (MJ Kg^{-1})	ND	≥ 35	39.8	40.1	40	45.9
ν (mm^2 s^{-1}, 40 ºC)	1.9 – 6	3.5 – 5	4.2	3.92	3.71	1.2 – 3.5
ρ (kg m^{-3}, 15 ºC)	ND	860 – 900	880	890	890	830 – 840

The properties of biodiesel are highly influenced by the fatty acid profile of the algae. The saponification value (SV) is the measure of milligrams of KOH required to saponify one gram of oil. The SV is inversely proportional to the molecular mass of fatty acids. The main aim of calculating SV is to calculate the CN of the biodiesel (Mandotra et al., 2014).

Iodine value (IV) is used to determine the unsaturation of biodiesel oil that is expressed as number of grams of iodine required to iodize 100 gram of oil. Higher the double bond in the

fatty acid chain, higher the IV for that oil. The higher the degree of unsaturation, the higher is the NOx emissions in combustion (Knothe et al., 2006). Higher IV of the biodiesel oil may result in the polymerization of glycerides and deposition of lubricant in the engine (Francisco et al., 2010).

Cetane number (CN) is a dimensionless indicator that characterizes ignition quality of fuels for compression ignition engines and it is highly influenced by fatty acid profile. High cetane value is the indicator of better combustion, low nitrous oxide (NO_x) emission, less occurrence of knocking and easier start-up of engine (Arias-Peñaranda et al., 2013; Knothe, 2012). Diesel fuel with large quantities of saturated and monounsaturated FAMEs have high value of CN.

Degree of unsaturation (DU) is sum of the masses of monounsaturated and polyunsaturated acid that influence the oxidative stability of biodiesel (Francisco et al., 2010). Presence of large quantities of polyunsaturated (more than one double bond) FAME negatively affects the oxidative stability of the biodiesel due to the fact that they contain reactive sites which are susceptible for free radical attack.

Long chain saturation factor (LCSF) is also an important biodiesel property that determines the behavior of biodiesel at lower temperatures (Mondal et al., 2019). Biodiesel can be characterized by its flow properties at colder temperatures i.e., applicability in winters and colder regions. The cold flow properties can be expressed as CFPP, CP and PP. Cold filter plugging point (CFPP) is the lowest temperature at which 20 ml of fuel passes through a filter within 60 s by applying a vacuum of 2 kPa. The CFPP test employs rapid cooling conditions. For this reason, CFPP does not reflect the actual limit of the fuel's operability temperature. (Barabás & Todoruţ, 2011). The cloud point (CP) is the temperature at which crystals first start to form in the fuel. The cloud point is reached when the temperature of the biodiesel is low enough to cause wax crystals to precipitate. Initially, cooling temperatures cause the formation

of the solid wax crystal nuclei that are submicron in scale and invisible to the human eye. Further decrease of temperature causes these crystals to grow. The temperature at which crystals become visible (the crystal's diameter ≥ 0.5 μm) is defined as the cloud point because the crystals form a cloudy suspension. Below the CP, these crystals might plug filters or drop to the bottom of a storage tank (Barabás & Todoruţ, 2011). The pour point (PP) is the temperature at which the fuel contains so many agglomerated crystals that it is essentially a gel and will no longer flow. This occurs if the temperature of the biodiesel drops below CP, when the microcrystals merge and form large clusters, which may disrupt the flow of the biodiesel through the pipes of the engine's fuel system (Barabás & Todoruţ, 2011).

Biodiesel quality can be affected by oxidation during storage (in contact with air) and characterized by the oxidative stability of biodiesel. Biodiesel oxidation can occur during storage while awaiting distribution or within the vehicle fuel system itself. The heating value at constant volume of a fuel (containing elements carbon, hydrogen, oxygen, nitrogen and sulfur) is the quantity of heat liberated when a unit quantity of the fuel is burned in oxygen in an enclosure of constant volume, the products of combustion being gaseous carbon dioxide, nitrogen, sulfur dioxide, and water, with the initial temperature of the fuel and the oxygen and the final temperature of the products at 25°C (Barabás & Todoruţ, 2011). Due to high oxygen content, biodiesel has lower mass energy values than petroleum diesel. As the fatty acid carbon chain increases (for a constant unsaturation level), the mass fraction of oxygen decreases, so the heating value increases (Hoekman et al., 2012; Ramírez-Verduzco et al., 2012). The kinematic viscosity (ν) of biodiesel depends on the source of biodiesel production, whose value must be low for better engine operations. If the viscosity is higher than the standard limits of biodiesel, engine deposits can occur. Fuel density (ρ) is the mass of unit volume, measured in a vacuum. Since density is strongly influenced by temperature, the biodiesel quality standards state the determination of density at 15 °C. If the density of biodiesel is inappropriate, the

particulate matter emissions are released as white smoke due to incomplete combustion (Ismail & Ali, 2015). The flash point (FP) is the minimum temperature calculated to a barometric pressure of 101.3 kPa at which the fuel will ignite (flash) on application of an ignition source under specified conditions. It is used to classify fuels for transport, storage and distribution according to hazard level. Higher FP values make fuels safer with regard to storage, fuel handling and transportation (Barabás & Todoruţ, 2011).

CHAPTER 3

Materials and methods

3.1. Experimental microalgal strain

Scenedesmus abundans NCIM 2897, a fresh water eukaryotic unicellular oleaganious green microalgae was used in this study. The microalgal strain was purchased from National Collection of Industrial Microorganisms (NCIM), National Chemical Laboratory (NCL), Pune, India. This species is capable of producing 70% lipid content in DCW under nutrient starvation and has the ability to coalesce (4 or 8 cells) due to EPS with specific metal ions. The biodiesel quantification by gas chromatography revealed abundance of methyl esters of palmitate (C16:0), oleate (C18:1) and linoleate (C18:2 cis and trans) as compared to other FAME that proves the potential of *S. abundans* towards good quality biodiesel based on ASTM and EN standards (Mahesh et al., 2019). The microscopic image of *S. abundans* was taken in an inverted microscope (specifications: appendices, Table A2) is depicted below (Fig. 3.1).

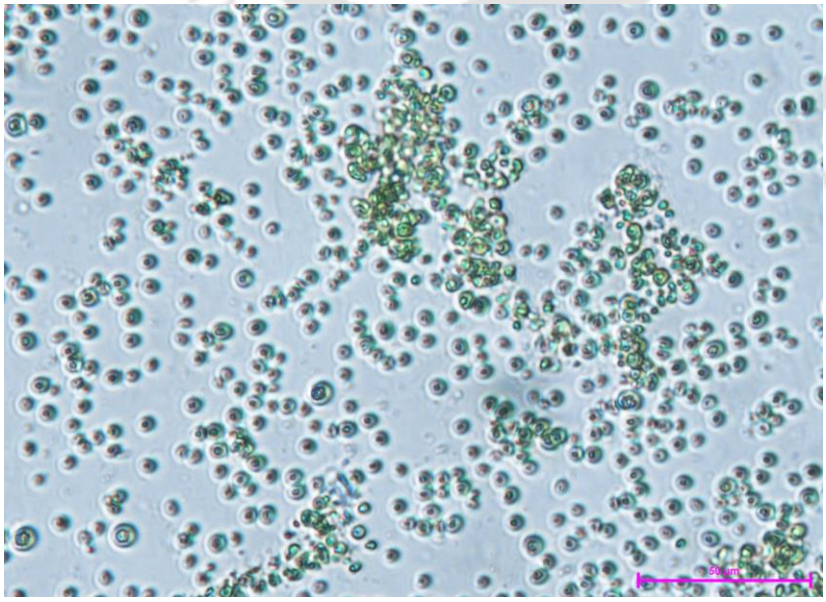

Fig. 3.1. Microscopic image of *Scenedesmus abundans* NCIM 2897.

3.2. Culture medium and maintenance

The algal inoculum was maintained in modified Chu-13 media (pH 7.5 ± 0.1) (Mahesh et al., 2019). The composition of the modified Chu-13 media used for inoculum is shown in Table 3.1. The inoculum for all experiments were prepared in 500 ml reagent bottle with perforated silicone rubber tubing as sparger autotrophically (Fig. 3.2). The experimental conditions for inoculum preparation were: 50 W cool white LED used as light source with photoperiod of 14 hr light:10 hr dark cycle at 405 µE/m^2/s light intensity, 0.5 l/min air flow rate was maintained throughout to attain 1 VVM and 2% (v/v) CO_2 was sparged during light period. These experimental conditions were not optimized but used for microalgal inoculum cultivation as suggested by researchers in their studies. Liu et al. reported that increasing light intensity from 250 to 400 µE/m^2/s enhances total lipid and neutral lipid production in *Scenedesmus* sp. 11-1 (Liu et al., 2012a). Zhao et al. stated that 2% CO_2 was the optimal concentration for cell growth and lipid accumulation in *Scenedesmus quadricauda* (Zhao et al., 2012). Researchers suggest that temperature control is not mandatory for some microalgal strains as it saves the cost of overall process under natural sunlight (Fuentes-Grünewald et al., 2013). Al-Shatri et al. reported that pH was not controlled for the growth of *Scenedesmus dimorphus* and variation in the pH of culture depends on the nature of metabolites secreted in response to the nutrients in the media (Al-Shatri et al., 2014). Aeration conditions of 1.2 VVM was found optimal for the cultivation of *Chlorella vulgaris* in airlift photobioreactor (Madhubalaji et al., 2020). The active mid log phase culture (5 days old) was used for all experimental studies.

Table 3.1. Modified Chu-13 media composition for inoculum.

Media component	Concentration (mg/l)
Urea	500
K_2HPO_4	80
$MgSO_4.7H_2O$	200
$CaCl_2.2H_2O$	107
Ferric citrate	20
Citric acid	100
$CoCl_2.2H_2O$	0.02
$ZnSO_4.7H_2O$	0.44
$CuSO_4.5H_2O$	0.16
$Na_2MoO_4.2H_2O$	0.084
H_3BO_3	5.72
$MnCl_2.4H_2O$	3.62

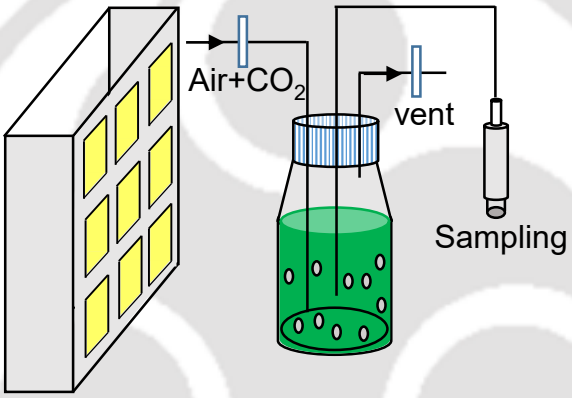

Fig. 3.2. Transparent bottle equipped with perforated tubing for inoculum preparation.

3.3. Preparation of buffers for storing lipase-calcium alginate beads

3.3.1. Preparation of 50 mM Tris-HCl buffer

Weigh 3.94 g Tris-HCl and add it in 500 ml reagent bottle. Add 400 ml distilled water in 500 ml reagent bottle and dissolve. Set the pH of solution to 7 ± 0.2 using 8 N NaOH. Make up the final volume to 500 ml using distilled water. Sterilization of 50 mM Tris-HCl buffer was carried out in autoclave at 121 ºC, 15 psi for 20 minutes and stored at 4 ºC after cooling down.

3.3.2. Preparation of 50 mM sodium phosphate buffer

Stocks of $Na_2HPO_4.2H_2O$ (1.424 g/40 ml) and $NaH_2PO_4.H_2O$ (1.104 g/40 ml) were prepared. For preparing 40 ml of 0.2 M sodium phosphate buffer, add 30.8 ml of

$Na_2HPO_4.2H_2O$ and 9.2 ml of $NaH_2PO_4.H_2O$ in 50 ml centrifuge tube. Further for preparing 100 ml of 0.05 M sodium phosphate buffer, dilute 0.2 M sodium phosphate buffer to 0.05 M by adding water (25 ml of 0.2 M sodium phosphate buffer was mixed with 75 ml of water). Set the pH of 50 mM sodium phosphate buffer to 7 ± 0.2. Sterilization of 50 mM sodium phosphate buffer was carried out in autoclave at 121 ºC, 15 psi for 20 minutes and stored at 4 ºC after cooling down.

3.3.3. Preparation of 50 mM citrate buffer

For preparing 200 ml of 50 mM citrate buffer, 100 ml of 0.1 M citrate buffer was initially prepared. Citrate buffer (100 ml of 0.1M) was prepared by adding 2.427 g of sodium citrate dihydrate and 0.3358 g of citric acid. Add distilled water until the volume is 100 ml. For preparing 200 ml of 50 mM citrate buffer, dilute 0.1 M citrate buffer to 0.05 M by adding water (100 ml of 0.1 M citrate buffer was mixed with 100 ml of water). Set the pH of 50 mM citrate buffer to 7 ± 0.2 using 8N NaOH. Sterilization of 50 mM citrate buffer was carried out in autoclave at 121 ºC, 15 psi for 20 minutes and stored at 4 ºC after cooling down.

3.4. Analytical techniques

3.4.1. Quantification of dry cell weight, specific growth rate, overall biomass and FAME productivity, biomass yield

The DCW of *S. abundans* was measured by centrifuging cells at 10000 RPM for 10 min and then cells are dried at hot air oven (70 ºC) for 24 hrs. Optical density at 680 nm (OD_{680}) of microalgal cells was measured by a visible spectrophotometer (specifications: appendices, Table A2). Biomass correlation factor (BCF) was calculated at regular intervals by dividing measured DCW with measured OD_{680}. DCW was also estimated by multiplying measured OD_{680} and BCF. BCF varies depending upon nutrient concentrations present in the media during culture period. The specific growth rate, overall biomass and FAME productivity, biomass yield were estimated from the following equations (3.1) – (3.4).

$$Specific\ growth\ rate, \mu = \frac{ln\left(\frac{X_2}{X_1}\right)}{t_2 - t_1} \quad (3.1)$$

$$Overall\ biomass\ productivity, P_{biomass} = \frac{X_f - X_i}{t_f - t_i} \quad (3.2)$$

$$Overall\ FAME\ productivity, P_{FAME} = \frac{FAME_f - FAME_i}{t_f - t_i} \quad (3.3)$$

$$Biomass\ yield, Y_{x/s} = \frac{X_{t2} - X_{t1}}{S_{t1} - S_{t2}} \quad (3.4)$$

Where, X_2 and X_1 are biomass titers at time t_2 and t_1 respectively. X_f is final biomass titer at the end of growth phase at time t_f and X_i is initial biomass titer at time t_i. $FAME_f$ is final FAME titer at time t_f and $FAME_i$ is initial FAME titer at time t_i X_{t2} and X_{t1} are biomass concentrations at substrate concentrations S_{t2} and S_{t1} respectively.

3.4.2. Estimation of chlorophyll-a and carotenoid concentration

Microalgal culture of 1 ml of OD_{680} 0.1 – 0.7 was collected in 2 ml amber centrifuge tube and centrifuged at 10000 RPM for 10 minutes. The supernatant was discarded after centrifugation without disturbing the pellet. The cell pellet was mixed thoroughly with 1.5 ml methanol for cell lysis and kept in waterbath at 45 °C for 30 minutes and allow them to cool until they reach room temperature. Algal samples were centrifuged at 10000 RPM for 10 minutes and absorbances of the clear supernatant at 480 nm, 652 nm, 665 nm, 680 nm was measured keeping methanol as blank by visible spectrophotometer. $A_{480}, A_{652}, A_{665}$ and A_{680} were multiplied by the dilution factor to obtain final $A_{480}, A_{652}, A_{665}$ and A_{680}. Chlorophyll-a (Chl-a), and photoprotective carotenoids were determined by the following equations (3.5) and (3.6) (Pruvost et al., 2011; Strickland & Parsons, 1968).

$$[Chl - a]\left(\frac{mg}{l}\right) = 16.5169A'_{665} - 8.0962\ A'_{652} \quad (3.5)$$

$$[Carotenoid]\left(\frac{mg}{l}\right) = 4A'_{480} \quad (3.6)$$

Absorbencies at 480, 652 and 665 nm were corrected for turbidity as $A'_{652} = A_{652} - A_{680}$, $A'_{665} = A_{665} - A_{680}$ and $A'_{480} = A_{480} - A_{680}$

3.4.3. Estimation of extracellular urea concentration

Microalgal culture was collected using 10 ml pipette at regular time intervals in 2 ml centrifuge tube and samples were centrifuged at 10000 RPM for 10 minutes to obtain clear supernatant. The concentration of urea in the supernatant was estimated using diacetyl monoxime method using standard urea in urea free media (Rosenthal, 1955). Under strong acidic conditions, urea reacts with diacetyl monoxime to form a yellow condensed product, which is intensified to red colour in the presence of ferric ions and thiosemicarbazide (stabilise the colour). The coloured product formed was measured spectrophotometrically at 540 nm.

Reagents preparation for urea estimation

Stock acid reagent A

Dissolve 0.2 g $FeCl_3.6H_2O$ in 6 ml of distilled water. Add 4 ml H_3PO_4 and mix well. Store in a brown bottle at room temperature. Stable for 6 months.

Mixed acid reagent B

Add slowly 100 ml of concentrated H_2SO_4 to 400 ml distilled water in 1 litre conical flask kept in an ice cold waterbath. Mix well and add 0.3 ml of stock acid reagent A. Mix and store in a brown bottle at room temperature. Stable for 6 months.

Stock colour reagent C

Dissolve 1 g diacetyl monoxime in distilled water and make up the volume to 50 ml in a volumetric flask. Store in a brown bottle at room temperature. Stable for 6 months.

Stock colour reagent D

Dissolve 0.25 g thiosemicarbazide in distilled water and make up the volume to 50 ml in a volumetric flask. Store in a brown bottle at room temperature. Stable for 6 months.

Mixed colour reagent E

Mix 35 ml of stock colour reagent C with 35 ml of stock colour reagent D and make up the volume to 500 ml with distilled water. Store in a brown bottle at room temperature. Stable

for 6 months.

Reagent F

The reagent F was prepared fresh at the time of analysis by mixing double-distilled water, mixed acid reagent B and mixed colour reagent E in the ratio 1:1:1.

Urea standard, sample preparation and analysis

Standard urea concentrations (50 mg/l and 100 mg/l) were prepared and urea free media was used as blank. The urea samples to be analysed were diluted with urea free media such that diluted urea concentrations fall in the range of 0 to 100 mg/l urea. 100 µl of sample was mixed thoroughly with 3 ml of reagent F in the test tube and kept in 100 °C water bath for 15 minutes. Remove the tubes from water bath and cool for 5 min. Set the spectrophotometer to zero with blank at 540 nm and measure the absorbance of urea standard and samples. Graph was plotted by keeping standard urea concentration along y axes and measured OD_{540} along x axes. Slope was calculated from graph and multiplied with dilution factor and OD_{540} of the urea sample to obtain urea concentration.

3.4.4. Estimation of extracellular K_2HPO_4 concentration

Microalgal culture was collected using 10 ml pipette at regular time intervals in 2 ml centrifuge tube and samples were centrifuged at 10000 RPM for 10 minutes to obtain clear supernatant. The concentration of K_2HPO_4 in the supernatant was estimated using ascorbic acid method (John, 1970). In this method, ammonium molybdate and potassium antimonyl tartrate react in acidic medium with phosphate to form a heteropoly acid - phosphomolybdic acid that is reduced to molybdenum blue by ascorbic acid. The coloured product formed was measured spectrophotometrically at 880 nm.

Reagents preparation for K_2HPO_4 estimation

5 N H_2SO_4

Dilute 70 ml concentrated H_2SO_4 to 500 ml with distilled water.

Potassium antimonyl tartrate solution

Dissolve 1.3715 g $K(SbO)C_4H_4O_6.1/2\ H_2O$ in 400 ml distilled water in a 500 ml volumetric flask and dilute to volume. Store in a glass stoppered bottle.

Ammonium molybdate solution

Dissolve 20 g $(NH_4)_6Mo_7O_{24}.4\ H_2O$ in 500 ml distilled water. Store in a glass stoppered bottle.

Ascorbic acid (0.1 M)

Ascorbic acid (0.1 M) was prepared freshly by dissolving 1.76 g ascorbic acid in 100 ml distilled water. The ascorbic acid solution was stable for 1 week at 4 °C.

Combined reagent

The combined reagent was prepared by mixing 5 N H_2SO_4, potassium antimonyl tartrate solution, ammonium molybdate solution, 0.1 M ascorbic acid in the ratio 10:1:3:6. The combined reagent was stable for 4 hours.

Phosphate standard, sample preparation and analysis

Standard K_2HPO_4 concentrations (2 mg/l and 4 mg/l) were prepared and K_2HPO_4 free media was used as blank. The K_2HPO_4 samples to be analysed were diluted with K_2HPO_4 free media such that diluted K_2HPO_4 concentrations fall in the range of 0 to 4 mg/l K_2HPO_4. 160 µL of combined reagent was mixed thoroughly with 1 ml of sample. Incubate for 10 min. Set the spectrophotometer to zero with blank at 880 nm and measure the absorbance of K_2HPO_4 standard and samples. Graph was plotted by keeping standard K_2HPO_4 concentration along y axes and measured OD_{880} along x axes. Slope was calculated from graph and multiplied with dilution factor and OD_{880} of the K_2HPO_4 sample to obtain K_2HPO_4 concentration.

3.4.5. Autoflocculation efficiency study in medium scale flat panel photobioreactor

Autoflocculation efficiency of algal cells was measured in medium scale PBR by stopping the aeration and sample of settled cells has been taken for measuring the optical

density at different time. Height of the settled cells and clear liquid have also been measured to determine the biomass recovery using the following equation (3.7).

$$Recovery_{set}\ (t) = \frac{H_{set}\ (t) \times A_{reactor} \times OD_{set,680}\ (t) \times f}{H\ (t_0) \times A_{reactor} \times OD_{set,680}\ (t_0) \times f}$$

$$= \frac{H_{set}\ (t) \times OD_{set,680}\ (t)}{H\ (t_0) \times OD_{set,680}\ (t_0)} \quad (3.7)$$

where, $OD_{set,680}\ (t)$ is the optical density at 680 nm of settled cells at time t, $OD_{set,680}\ (t_0)$ is the initial optical density at 680 nm of the culture before starting autoflocculation, $H_{set}\ (t)$ is the height of the settled cells at time t, $H\ (t_0)$ is the initial culture liquid height before starting autoflocculation (0.23 m), $A_{reactor}$ is cross sectional area of the PBR and f is the factor for conversion of OD_{680} to biomass concentration.

3.4.6. Autosedimentation factor, autoflocculation rate and autoflocculation efficiency analysis of *S. abundans*

Autosedimentation factor was found by collecting 10 ml microalgal sample in 15 ml centrifuge tube using 10 ml pipette. OD_{680} of culture before autoflocculation was measured. After 1 hr, 1 ml clear liquid was collected from top, middle portion of centrifuge tube gently without disturbing the culture at the bottom. OD_{680} and clear liquid volume of top, middle layer was measured and volume of settled cells was also noted. Bottom OD_{680} and autosedimentation factor was calculated after knowing OD_{680} before autoflocculation, top and middle OD_{680} after autoflocculation by the following equations (3.8) and (3.9).

$$OD_{bot,680}\ (t) = \frac{OD_{680}\ (t_o) * V\ (t_o) - OD_{top,680}\ (t) * V_{top}\ (t) - OD_{mid,680}\ (t) * V_{mid}\ (t)}{V_{bot}\ (t)} \quad (3.8)$$

$$ASF = \frac{OD_{bot,680}\ (t) * (V_{top}\ (t) + V_{mid}\ (t))}{OD_{top,680}\ (t) * V_{top}\ (t) + OD_{mid,680}\ (t) * V_{mid}\ (t)} \quad (3.9)$$

Where, $OD_{bot,680}\ (t)$, $OD_{mid,680}\ (t)$ and $OD_{top,680}\ (t)$ are optical densities at 680 nm of culture at bottom, middle and top portion at time t respectively. $V_{top}\ (t)$, $V_{mid}\ (t)$ and $V_{bot}\ (t)$ are culture volume of top, middle and bottom portion at time t respectively. $OD_{680}\ (t_o)$ and $V\ (t_o)$

are initial optical density at 680 nm of culture and starting culture volume respectively.

Autoflocculation rate was monitored by collecting 30 ml microalgal sample in 50 ml centrifuge tube using 10 ml pipette. Clear liquid of 1 ml was collected from top, middle portion from centrifuge tube gently after 1, 3, 6, 12, 24, 30 hr without disturbing culture at the bottom. OD_{680} and clear liquid volume of top, middle layer was measured and volume of settled cells was also noted. Bottom OD_{680} was calculated after knowing OD_{680} before autoflocculation, top and middle OD_{680} after autoflocculation by equation (3.8). Autoflocculation efficiency (%) was also calculated from equation (3.10).

$$\%\ Autoflocculation\ efficiency\ (t) = \frac{OD_{bot,680}\ (t) * V_{bot}\ (t)}{OD_{680}\ (t_o) * V\ (t_o)} * 100 \qquad (3.10)$$

Where, $OD_{bot,680}\ (t)$ and $V_{bot}\ (t)$ are optical density at 680 nm of culture at bottom and culture volume of bottom portion at time t respectively. $OD_{680}\ (t_o)$ and $V\ (t_o)$ are initial optical density at 680 nm of culture and starting culture volume respectively.

3.4.7. Quantification of cell free exopolysaccharides collected after autoflocculation

For quantification of cell free EPS, 30 ml microalgal culture from medium scale PBR was collected in 50 ml centrifuge tube using 10 ml pipette. The collected culture was kept undisturbed for a day at room temperature and *S. abundans* started settling slowly. The settling of cells is caused due to EPS that can create binding of algal cells to one another forming flocs and enhance autoflocculation phenomena with specific metal ion combination. When whole algal culture settles completely at the bottom, 10 ml clear liquid (cell free EPS) was collected in fresh 15 ml centrifuge tube. The collected cell free EPS was centrifuged at 10000 RPM for 10 minutes and dried at hot air oven (70 ºC) for 24 hrs. The cell free dried EPS was estimated by measuring the initial and final weights of 15 ml centrifuge tube. The EPS attached to cell surface was also measured by heating the cells in a water bath at 45 °C for 20 min for detaching the EPS from cell surface, followed by centrifugation at 10000 RPM for 10 min. Attached EPS quantification was done by measuring the initial and final weight of centrifuge tube.

3.4.8. Characterization of exopolysaccharides

Protein content in EPS. The total protein content of EPS was examined using BSA as standard. 20 µl EPS sample, 300 µl of bradford reagent and 680 µl of water were mixed in 2 ml centrifuge tube and incubated at room temperature for 5 min. The coloured product was measured spectrophotometrically at 595 nm.

Monosaccharide composition analysis of EPS by HPLC. The EPS (10 mg) was pretreated with 1 ml of 4% H_2SO_4 at 121 °C for 30 min, centrifuged at 10000 RPM for 10 min (Sebastião et al., 2013) and supernatant was injected in HPLC (specifications: appendices, Table A2) having Aminex HPX 87H column (specifications: appendices, Table A2). 5 mM H_2SO_4 was used as mobile phase (flowrate of 0.6 ml/min) and column oven temperature of 50 °C. Glucose, arabinose, xylose, ribose, fructose, mannose, raffinose, maltose, rhamnose, galactose, glucuronic acid and polygalacturonic acid were used as standard.

Fourier transform infrared spectroscopy (FTIR) analysis. The FTIR (specifications: appendices, Table A2) was used for detection of functional groups present in EPS (4000–500 cm^{-1} wave number range, 4 cm^{-1} of spectral resolution and 128 scans). The FTIR spectra of exopolysaccharides, standard sugars and uronic acids were analysed.

Powder X-ray diffraction (PXRD) analysis. The X ray diffractometer (specifications: appendices, Table A2) was used for analysis of XRD spectra of exopolysaccharides. The XRD spectra of exopolysaccharides was obtained using Copper K-α radiation wavelength (λ) of 1.54 Å.

Thermogravimetry (TGA). DSC/TGA analyser (specifications: appendices, Table A2) was used for the TGA analysis of EPS. 10 mg of EPS was used for the analysis.

3.4.9. Software used

Design–Expert®, trial version 7.0.0 (specifications: appendices, Table A2) was used to obtain the analysis of variance and regression analysis from experimental data.

3.4.10. Monitoring of culture pH and temperature

pH electrode (specifications: appendices, Table A2) and thermometer (specifications: appendices, Table A2) were inserted on the top of medium scale PBR for online monitoring of culture pH indicated by pH controller (specifications: appendices, Table A2) and culture temperature respectively. pH data was stored online using OPTO22 control system (specifications: appendices, Table A2) and culture temperature readings were noted daily at regular intervals as indicated by thermometer.

3.4.11. Zeta potential quantification

Zetasizer (specifications: appendices, Table A2) was used to determine the charge (zeta potential) of EPS and its binding to cells through charge neutralization mechanism. Microalgal culture of 30 ml was collected in 50 ml centrifuge tube using 10 ml pipette. Microalgal sample was collected in 5 ml centrifuge tube. After autoflocculation, spent media and autoflocculated biomass were also collected respectively in separate 5 ml centrifuge tubes. Zeta potential was measured for samples before autoflocculation, spent media and autoflocculated biomass with equilibration time of 30 seconds and 20 processed runs in Omega cuvette (specifications: appendices, Table A2).

3.4.12. FAME quantity and quality assessment

Direct transesterification of microalgal biomass was performed to produce FAMEs. 30 mg of oven dried biomass was taken in 5 ml centrifuge tube and lysed with 1 ml of 2% (v/v) NaOH in methanol at 90 ºC in a shaking water bath at 150 RPM for 20 minutes. Then, 1 ml of 5% (v/v) H_2SO_4 in methanol was added and followed same incubation conditions as mentioned previously (Mahesh et al., 2019; Naira et al., 2019). Deionized water and hexane of equal volume (1 ml each) were added to cooled transesterified reaction mixture to produce FAME in the hexane layer. The hexane layer was washed twice with water to remove aqueous impurities and filtered through a 0.2 µm filter. Purified FAMEs of 1 µl in hexane was injected in CP-Sil

8CB column (specifications: appendices, Table A2) by gas chromatography (GC) equipped with FID detector (specifications: appendices, Table A2) using 10 µl GC syringe (specifications: appendices, Table A2). "Supelco 37 component FAME mix" (specifications: appendices, Table A2) was used as FAME standard. Helium at a constant flow rate of 1.5 ml/min was used as carrier gas with split ratio 1:50. The oven temperature of GC was programmed as follows: 60 °C for 5 min holding, followed by ramping at the rate of 5 °C min^{-1} till 280 °C and then 15 min holding. The injector and detector temperature was set at 250 °C and 280 °C respectively (Mahesh et al., 2019; Naira et al., 2019).

The biodiesel quality was analysed by estimating saponification value (SV), iodine value (IV), cetane number (CN), degree of unsaturation (DU) (Francisco et al., 2010), long chain saturation factor (LCSF), cold filter plugging point (CFPP) (Ramos et al., 2009), cloud point (CP), pour point (PP) (Sarin et al., 2009), oxidation stability index (OSI) (Park et al., 2008), higher heating value (HHV), kinematic viscosity (ν), density (ρ) (Saxena et al., 2013) and flash point (FP) (Naira et al., 2019) by using empirical equations (3.11) – (3.23).

$$SV = \sum \left[\frac{(560 \times F_i)}{M_i}\right] \quad (3.11)$$

$$IV = \sum \left[\frac{(254 \times F_i \times D_i)}{M_i}\right] \quad (3.12)$$

$$CN = \left[46.3 + \left(\frac{5458}{SV}\right)\right] - (0.225 \times IV) \quad (3.13)$$

$$DU = \sum MUFA + [2 \times \sum PUFA] \quad (3.14)$$

$$LCSF = 0.1 \times F_{C16:0} + 0.5 \times F_{C18:0} + 1 \times F_{C20:0} + 1.5 \times F_{C22:0} + 2 \times F_{C24:0} \quad (3.15)$$

$$CFPP = 3.1417 \times LCSF - 16.477 \quad (3.16)$$

$$CP = 0.526 \times F_{C16:0} - 4.992 \quad (3.17)$$

$$PP = 0.571 \times F_{C16:0} - 12.24 \quad (3.18)$$

$$OSI = \left(\frac{117.9295}{(F_{C18:2} + F_{C18:3})}\right) + 2.5905 \quad (3.19)$$

$$HHV(MJ.Kg^{-1}) = \sum \left[\frac{(F_i \times \delta_i)}{100}\right] \quad (3.20)$$

$$\delta_i = 46.19 - \frac{1794}{M_i} - 0.21 \times D_i$$

$$\nu(mm^2.s^{-1}) = e^{\sum\left[\frac{(F_i \times \ln(\nu_i))}{100}\right]} \quad (3.21)$$

$$\ln(\nu_i) = -12.503 - (0.178 \times D_i) + 2.496 \times \ln M_i$$

$$\rho\ (g.cm^{-3}) = \sum\left[\frac{(\rho_i \times F_i)}{100}\right] \quad (3.22)$$

$$\rho_i = 0.8463 + \frac{4.9}{M_i} + 0.0118 \times D_i$$

$$FP = 23.362 \times \sum\left[\frac{(N_i \times F_i)}{100}\right] + 4.854 \times \sum\left[\frac{(D_i \times F_i)}{100}\right] \quad (3.23)$$

Where, F_i is percentage of each FAME in total FAME, M_i is molecular weight of corresponding FAME, D_i is number of double bonds in each FAME, N_i is the number of carbon atoms in individual FAME, MUFA and PUFA are mono unsaturated and poly unsaturated fatty acids in wt% respectively.

3.4.13. Calculation of transesterification efficiency

Transesterification efficiency was calculated from the following equation (3.24)

$$\%Transesterification\ efficiency = \frac{FAME_{produced}}{biomass_{used}} * 100 \quad (3.24)$$

Where $FAME_{produced}$ is mg of FAME produced after transesterification of biomass. $biomass_{used}$ is mg of biomass used for transesterification reaction.

CHAPTER 4

Construction and characterization of medium scale flat panel PBR for producing biodiesel and exopolysaccharides from *S. abundans*

4.1. Background and uniqueness of the study

Flat panel PBRs exhibit higher biomass productivities due to larger surface to volume ratio, lesser optical path length and low oxygen build up (Brennan & Owende, 2010). However, a cost-effective and highly efficient mass transfer component, i.e., sparging system is essential in these PBRs. Conventional spargers (L-sparger) in stirred tank bioreactors are efficient when mechanical agitators/impellers are operating. These spargers usually produce air bubbles that are bigger in size and later they break up into smaller bubbles due to contact with impeller blades. Baffles in the stirred tank reactors also helps in better mixing. However, the issue with stirred tank reactor is energy/electricity consumption for the mechanically driven agitation. Thus, large scale cultivation of microalgae using stirred tank bioreactor is not economically feasible due to requirement of high electrical energy for operating the impeller. Also, the impeller blades can cause shear stress to microalgal cells leading to its death. Therefore, flat panel PBRs have been developed with low cost spargers (perforated tubing, membrane type). The sparger was equipped at bottom of the PBRs to mimic bubble driven flat panel PBR. The bubble force generated from sparger help in mixing of algal cells without settling. In this work, a low cost, scalable and efficient bubble driven medium scale flat panel PBR was constructed with black neoprene rubber membrane sparger equipped at the bottom of the reactor. If 1000x version of medium scale flat panel PBR (considering length, width and height of photobioreactor as 100x, 2x and 5x respectively) with the current neoprene membrane sparger

would have constructed for scale-up, there would be mixing issues in the top of the PBR due to less water column pressure. Also, bubble coalescence occurs in which two or more gas bubbles in the liquid medium coalesce to form a single larger bubble in upscaled version of reactor. These large bubbles in the liquid medium of reactor would result in inefficient mixing of algae. If we try to increase the width of photobioreactor, availability of specific light intensity would be less per algal cell and height of the photobioreactor would be increased to some extent. Scale-up issues and complications could be restricted by increasing the length of photobioreactor instead of increasing the height and width. If we increase the length of photobioreactor, proportionally we have to increase the size and number of holes of neoprene membrane sparger. In line with the medium scale PBR, a customized unidirectional LED lighting system was developed to perform photoautotrophic experiments (with light energy as the sole energy source to microalgae) in the laboratory.

Biodiesel production process from microalgae includes the following steps; microalgal cultivation, lipid enrichment, dewatering, drying and direct transesterification of lipid enriched biomass through catalytic or enzymatic process to get fatty acid methyl ester (FAME). However, commercialization of biodiesel production from microalgae is still facing problems due to high production costs (Wu et al., 2012). Moreover, in order to make the biodiesel production process from microalgae economically viable, we have to exploit for other products concomitantly apart from biodiesel. Exopolysaccharides (EPS) are one of those product secreted by specific microalgae and they can be used in various applications as adhesives, detergents, textiles, cosmetics, pharmaceuticals (Raza et al., 2012). Microalgae harvesting operations accounts for 30% of the total biomass production cost (Schlesinger et al., 2012). There is a need to look for efficient microalgae harvesting strategy such as autoflocculation. It has been seen that specific microalgae can secrete EPS responsible for cell to cell attachments due to glycoproteins present in EPS and thus coalesce of cells and autoflocculation phenomena

was observed (Salim et al., 2013). The EPS with specific metal ion combination can create a partial or complete binding with microalgal cells. With a partial binding, the unbinding part of EPS can bind to other microalgal cells, therefore the network of EPS and microalgal cells created the floc thus enabling the downstream process become easy (Salim et al., 2014).

In this work, we have studied the possibility for concomitant production of biodiesel and exopolysaccharides using microalgae, *Scenedesmus abundans*. Here we have used parallel mini flat panel photobioreactor and medium scale flat panel photobioreactor constructed by Mahesh et al. for microalgae cultivation (Mahesh et al., 2019). Customized unidirectional LED lighting systems designed by Mahesh et al. was also used for this study (Mahesh et al., 2019). A media has been formulated for growth of microalgae. Biomass recovery and EPS separation by natural autoflocculation has also been studied to reduce the cost of production.

4.2. Experimental set up of PBR and lighting system

4.2.1. Construction of parallel mini and medium scale flat panel photobioreactor

Light capturing surface of the photobioreactors (PBRs) have been made using 10 mm thicker transparent acrylic (polymethyl methacrylate, PMMA, also called plexiglass) sheet (specifications: appendices, Table A2). The height of parallel mini scale flat panel PBR was 0.076 m and volume of each mini flat panel PBR was 100 ml. The light path length (W, width of the photobioreactor) was chosen as 0.025 m and length of the each photobioreactor was 0.05 m. The inner measurement of medium scale single flat panel photobioreactor was 0.025 m × 0.3 m × 0.3 m (W × H × L), resulting in a culture chamber volume of 2.36 l. Fig. 4.1 illustrates the overviews of both the photobioreactors culture vessel frames assembly.

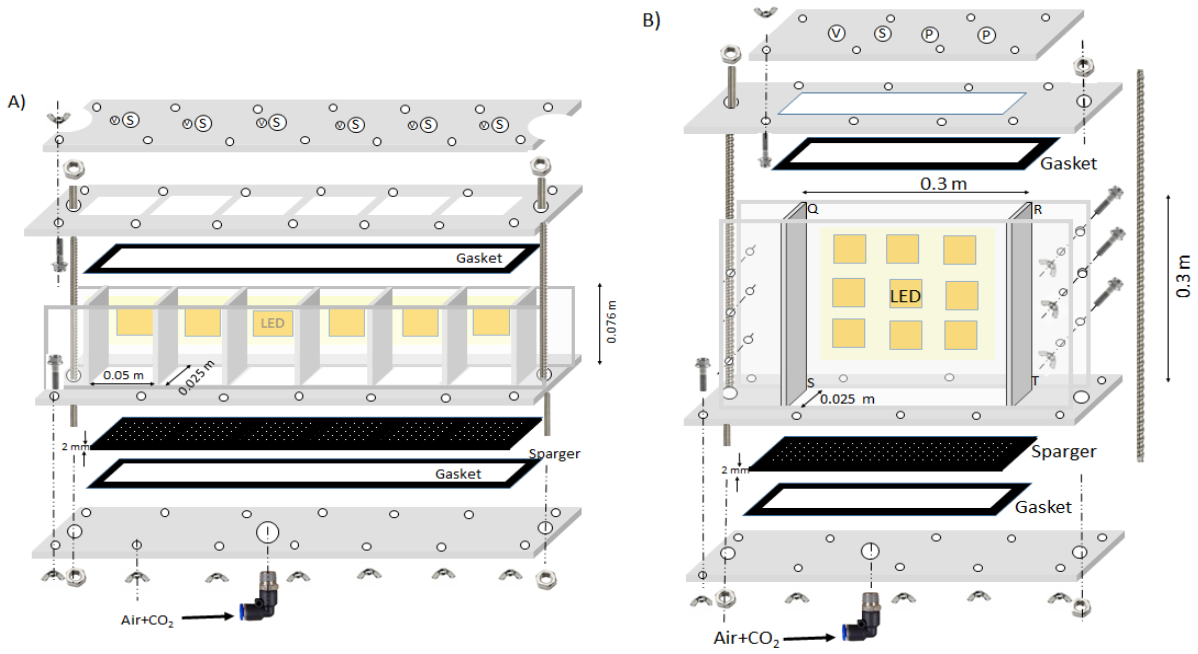

Fig. 4.1. Schematic diagram of flat panel photobioreactors (PBRs) for cultivation of microalgae. **A)** parallel mini PBR and **B)** medium scale PBR.

At bottom of the PBRs, a customized low cost membrane sparger was equipped to mimic bubble driven flat panel PBR. The membrane sparger was designed using a black neoprene rubber sheet (thickness: 2 mm), made porous gently by 30 gauge fine needle at an equidistance of 0.0085 m resulting in 24,600 number/m^2. Mixture of air and CO_2 (2 bar pressure) was sparged through the rubber sparger from the bottom of reactors to achieve bubble-driven agitation. The bubble size can be controlled by the inlet pressure of the gas mixture. The front and back plexiglass sheets were held together by bolts (specifications: appendices, Table A2). A flat rubber gasket of 2 mm thickness was placed in between neoprene rubber sparger and bottom plate to prevent the gas leakage. The culture vessel consisted of openings for sensors, sampling ports and gas exhaust.

4.2.2. Customized unidirectional LED lighting systems

LED (cool white) panel (6 × 100 W, 6500 K color temperature) and LED (cool white) panel (9 × 100 W, 6500 K color temperature) were installed perpendicular to surface (one side) of parallel mini reactors and medium scale reactor respectively (Fig. 4.1). Aluminium heat

sinks combined with CPU fans reduce the heat generated from LEDs. Light intensity can be controlled from 0 to 2200 µE/m^2/s using constant current source regulator (specifications: appendices, Table A2). Light (lux) was measured using a lux meter (specifications: appendices, Table A2) and was converted to µE/m^2/s using the factor of "74 lux = 1 µE/m^2/s PPFD" (Photosynthetic Photon Flux Density) for LED (Apogee Instruments, Inc. USA).

4.3. Experimental studies

4.3.1. Determination of overall mass transfer coefficient of oxygen (K_{La,O_2}) and carbon dioxide (K_{La,CO_2}) of the medium scale flat panel photobioreactor

The overall mass transfer coefficient of O_2 from gas bubble to liquid (K_{La,O_2}) was determined using "cell free dynamic method" procedure considering time lag constant (τ_p) of the dissolved oxygen probe (specifications: appendices, Table A2) for medium scale flat panel PBR. The probe response profile was modelled as a first order function for determining the time lag constant in the following equation (4.1) (Philichi & Stenstrom, 1989).

$$\frac{dO_{2,mp}}{dt} = \frac{O_2 - O_{2,mp}}{\tau_p} \tag{4.1}$$

The linear expression of this equation; $\ln\frac{O_2 - O_{2,mp}}{O_2 - O_{2,mp_0}} = \frac{-1}{\tau_p}$ was used to determine the τ_p by step change of the dissolved oxygen concentration (DO). Where, $O_{2,mp}$ is the measured DO by the probe (probe reading), O_2 is the actual DO. O_{2,mp_0} is the initial measured value of DO by the probe and τ_p is the time lag constant of the probe. To determine the τ_p of the dissolved oxygen probe (DO probe), two closed vessels (full of water) having negligible gas head space to minimize gas escaping from water to head space were used. Air-nitrogen gas mixture was sparged for some time to get low DO in first vessel (R_1) as shown in Fig. 4.2A. Similarly, only air was sparged to get higher DO in second vessel, then stopped sparging and closed the vessel (R_2) (Fig. 4.2A). The DO probe was kept for long time in first vessel (low DO) for probe equilibration. Then the equilibrated DO probe was quickly transferred to the second vessel

water having high DO (vessel was kept at airtight condition) and kept for long time (Fig. 4.2A).

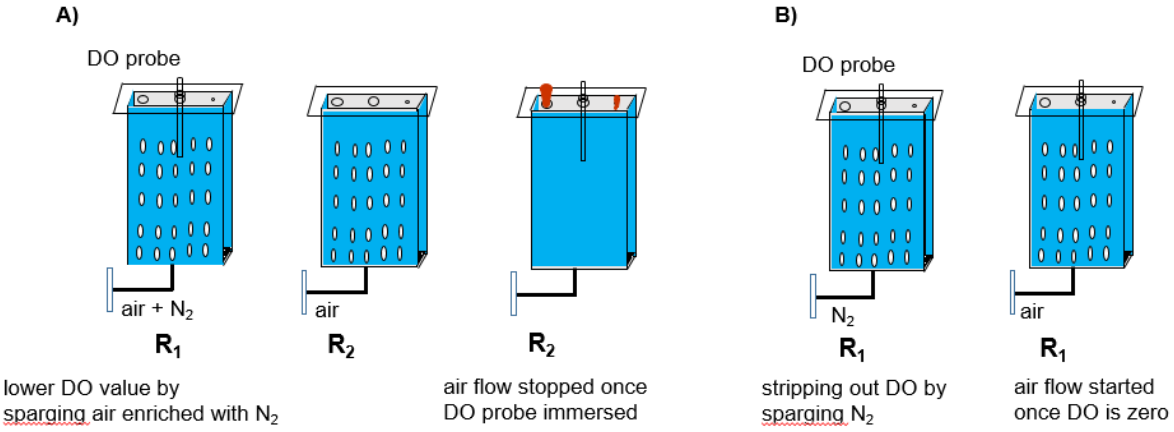

Fig. 4.2. Experimental set up for determination of τ_p and K_{La,O_2}. **A)** τ_p estimation and **B)** K_{La,O_2} estimation.

The response of the probe ($O_{2,mp}$) in second vessel after transferring the probe from first vessel was tabulated and used to calculate τ_p by plotting $\ln\frac{O_2-O_{2,mp}}{O_2-O_{2,mp_0}}$ vs t. After keeping the probe in second vessel for long time probe become equilibrated with actual DO level of the second vessel (O_2) and that time $O_{2,mp}$ value indicated as the O_2. Two separate experiments have been performed for average τ_p determination. K_{La,O_2} of the PBR was estimated in cell free media by degassing method assuming the liquid phase was well mixed considering probe response time (τ_p) determined above. To measure K_{La,O_2} using this method, the DO probe equipped PBR was sparged at fixed rate to get constant dissolved oxygen. Then the air flow was stopped and dissolved oxygen was stripped out from media by sparging nitrogen. The dissolved oxygen concentration falls down to very low value using this deoxygenation and stripping process. Then, the nitrogen sparging was stopped and media was aerated by sparging air at constant rate (Fig. 4.2B). The reading of the probe after aeration was tabulated and used to calculate K_{La,O_2} using the Equation (4.2).

$$\frac{dO_2}{dt} = K_{La,O_2}\,(O_2^* - O_2) \qquad (4.2)$$

The combination of Equations (4.1) and (4.2) gives the following expression (Equation

(4.3)) and value of K_{La,O_2} can be determined according to that expression knowing τ_p value from linear expression of Equation (4.1) using nonlinear regression (Garcia-Ochoa & Gomez, 2009).

$$\frac{O_2^* - O_{2,mp}}{O_2^* - O_{2,mp_0}} = \frac{\tau_p}{1 - \tau_p K_{La,O_2}} \left[\frac{1}{\tau_p} e^{-K_{La,O_2} t} - K_{La,O_2} e^{-\frac{1}{\tau_p}}\right] \quad (4.3)$$

K_{La,O_2} of medium scale PBR (2 l volume) was calculated at three different superficial velocity of air varying from 0.215 cm/s (0.5 VVM, volume of air/volume of liquid in photobioreactor/min, 1 l/min) to 0.86 cm/s (2 VVM, 4 l/min). Two separate experiments were conducted for each VVM air sparging for K_{La,O_2} determination. The overall mass transfer coefficient of CO_2 in liquid can be calculated using Graham's Law $\left(D_{CO_2} = D_{O_2} \times \sqrt{\frac{M_{O_2}}{M_{CO_2}}}\right)$ which relates the diffusivity (D) to molar mass (M) and Higbie model $\left(K_{La,CO_2} = K_{La,O_2} \times \sqrt{\frac{D_{CO_2}}{D_{O_2}}}\right)$ knowing the overall mass transfer coefficient of O_2 (K_{La,O_2}) in liquid and the molar mass of CO_2 (M_{CO_2} = 44 g/mol) and O_2 (M_{O_2} = 32 g/mol) (Ndiaye et al., 2018). By combining of Graham's Law and Higbie model, $K_{La,CO_2} = K_{La,O_2}\left(\frac{M_{O_2}}{M_{CO_2}}\right)^{1/4}$. Therefore, the mass transfer coefficient of O_2 can give the idea of the mass transfer coefficient of CO_2 in the algal PBR.

4.3.2. Determination of mixing time (t_m) of the medium scale flat panel photobioreactor

The mixing time is defined as the time required for a bolus of a tracer material to be dispersed throughout the photobioreactor to a certain degree. In this study, mixing times at several superficial gas velocities (0.215 cm/s to 0.86 cm/s) were determined by pH tracer (Zhang et al., 2014). Here degree of dispersion considered as 95% of total concentration difference. So t_m calculated as time required to reach the pH value to $pH_\infty + 0.05\,(pH_\infty - pH_0)$ after a pulse addition of acid. Here pH_∞ is the ultimate stable pH

and pH_0 is the initial pH just before injection of acid tracer.

Time constant of pH probe was calculated before finding t_m. A step change approach has been used to get pH probe lag. After pH probe calibration, it was inserted into 50 ml falcon tube containing buffer of 7 in room temperature and was allowed to equilibrate with the pH of the buffer of 7. Then, the pH probe was quickly transferred to an another 50 ml falcon tube containing buffer of pH 4 and the response of the pH probe after transferring the probe into second buffer (pH :4) was tabulated. To fit the response profile, the following first order model was used (Zhang et al., 2014).

$$pH = pH_0 + \Delta pH\left(1 - e^{\frac{a-t}{\tau_1}}\right) \tag{4.4}$$

Where, a is the probe delay time, τ_1 probe time constant, ΔpH (pH step change) = $pH_{stable} - pH_0$ and pH_0 is the initial pH. The first order model does not fit adequately, particularly for the slow phase. Then the following second order model was applied to fit the pH probe response (Zhang et al., 2014).

$$pH = pH_0 + \Delta pH\left[A_1\left(1 - e^{\frac{a-t}{\tau_1}}\right) + A_2\left(1 - e^{\frac{a-t}{\tau_2}}\right)\right] \tag{4.5}$$

Where, τ_1 probe time constant for quick response phase, τ_2 probe time constant for slow response phase and $A_1 + A_2 = 1$ (amplitude). After calculating the time constant of pH probe, mixing time (t_m) of the medium scale flat panel photobioreactor was found by pH tracer experiment (Fig. 4.3).

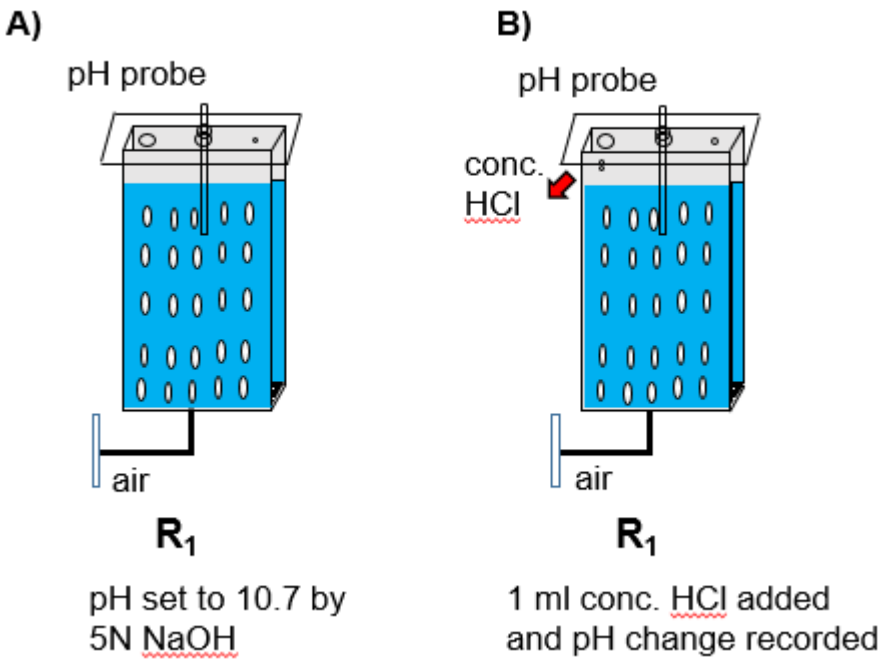

Fig. 4.3. Experimental set up for determination of t_m. **A)** Restoration of pH to 10.7 by 5N NaOH and **B)** Injection of 1 ml bolus conc. HCl as tracer.

The photobioreactor liquid (cell free) was adjusted to pH 10.7 by addition of required amount of 5 N NaOH (Fig. 4.3A). A 1 ml bolus of concentrated HCl as the tracer was injected in the liquid at a distance of 12.7 cm from pH electrode (specifications: appendices, Table A2) and at 2.54 cm from the surface of the liquid (Fig. 4.3B). The pH electrode was positioned at the centre of the photobioreactor and 7.6 cm from the surface of the liquid. The change of pH was tabulated in every second. After each experiment, 5 N NaOH was added to restore the pH to its starting point. Mixing time (t_m) was calculated at three different superficial velocity of air varying from 0.215 cm/s (0.5 VVM, 1 l/min) to 0.86 cm/s (2 VVM, 4 l/min) in triplicate.

4.3.3. Experiments in parallel mini flat panel photobioreactor

The experiments for selecting the nitrogen source and the concentration of nitrogen, K_2HPO_4, $MgSO_4$, $CaCl_2$ and micronutrients for growth were conducted in parallel mini flat panel PBR. One variable at a time was varied for all these experiments. For nitrogen source variation experiment, $NaNO_3$, urea, NH_4Cl, $(NH_4)_2SO_4$ and KNO_3 were considered with nitrogen (N) concentration of 44.16 mg/l in media mentioned in inoculum preparation (Refer

Section 3.2). For urea concentration variation experiments urea was varied from 0 to 5.3 g/l and for phosphate concentration variation experiment K_2HPO_4 was varied from 0.01 to 2 g/l with optimum urea concentration. For $MgSO_4$ and $CaCl_2$ optimization experiments $MgSO_4.7H_2O$ was varied from 0 to 5 g/l and $CaCl_2.2H_2O$ was varied from 0 to 5 g/l. For micronutrient optimization, it was varied from 0.005 to 5% of 1000X micronutrient solution. 1000X micronutrient solution: ($CoCl_2.2H_2O$ − 0.02 g/l, $ZnSO_4.7H_2O$ − 0.44 g/l, $CuSO_4.5H_2O$ − 0.16 g/l, $Na_2MoO_4.2H_2O$ − 0.084 g/l, H_3BO_3 − 5.72 g/l, $MnCl_2.4H_2O$ − 3.62 g/l). A fixed light intensity of 405 µE/m^2/s was used for all the above experiments.

For light intensity variation, it was varied from 81 to 2162 µE/m^2/s in parallel mini flat panel PBR to study the effect of light intensity on the growth of microalgae. The pH of media was set to 7.5 after adding nutrient concentrations in all the experiments. Other experimental conditions were: photoperiod – 14 hr light:10 hr dark cycle, air flow rate (1 VVM) with 2% (v/v) CO_2 in air (pressure 2 bar) through 50 mm 0.2 µm PTFE filters (specifications: appendices, Table A2) from the bottom of reactor, initial biomass concentration − 0.11 g/l for all experiments. In all the experiments, CO_2 flow was stopped during night periods for cell respiration and air flow kept constant to ensure mixing of algal cells without any settling. The microalgal sample was collected in triplicate from each photobioreactor and dry cell weight (DCW) was measured. To maintain the height of culture liquid due to evaporation loss, water was added before starting and ending of light period.

4.3.4. Experiments in medium scale flat panel photobioreactor

The nutrient concentrations that gave best growth in nutrient concentration variation experiments in parallel mini PBR was used as optimal growth media in medium scale (2.36 l) flat panel PBR. The biomass was grown autotrophically in batch with a working culture volume of 2 l. Constant high light intensity of 2162 µE/m^2/s was used to study the microalgae growth, chlorophyll – a and carotenoid synthesis, urea and phosphate utilization, lipid and EPS

production on the basis of light intensity variation experiment. The minimum and maximum culture temperature in indoor conditions were recorded as 24 °C (at night) and 46.5 °C (light period) during experiment. Experiment was performed in single stage for growth as well as lipid induction. The lipid induction phase started once the urea gets depleted in the media and culture reached the stationary phase. The biomass, lipid and EPS were measured at respective time intervals under nitrogen starvation. Other experimental conditions were same as followed in parallel mini flat panel PBR.

4.4. Results and Discussion

4.4.1. Overall mass transfer coefficient of the medium scale flat panel PBR

The lag time constant (τ_p) of O_2 probe has been estimated as 39 sec by plotting $\ln \frac{O_2 - O_{2,mp}}{O_2 - O_{2,mp_0}}$ vs t (Fig. 4.4B) of the experimental data (Fig. 4.4A) generated by exposing the probe to a step change of the dissolved O_2 concentration described in **Section 4.3.1**. The overall volumetric mass transfer coefficient of O_2 (K_{La,O_2}) of the medium scale flat panel photobioreactor with working volume of 2 l has been determined by nonlinear regression of the Equation (4.3) using the experimental data (Fig. 4.4C) generated a step change of O_2 percentage in the sparging gas stream as described in **Section 4.3.1**. The prediction and experimental data was well matched (Fig. 4.4D). The overall volumetric mass transfer coefficient of CO_2 (K_{La,CO_2}) was determined using Graham's law and Higbie model described in **Section 4.3.1** by knowing the K_{La,O_2}.

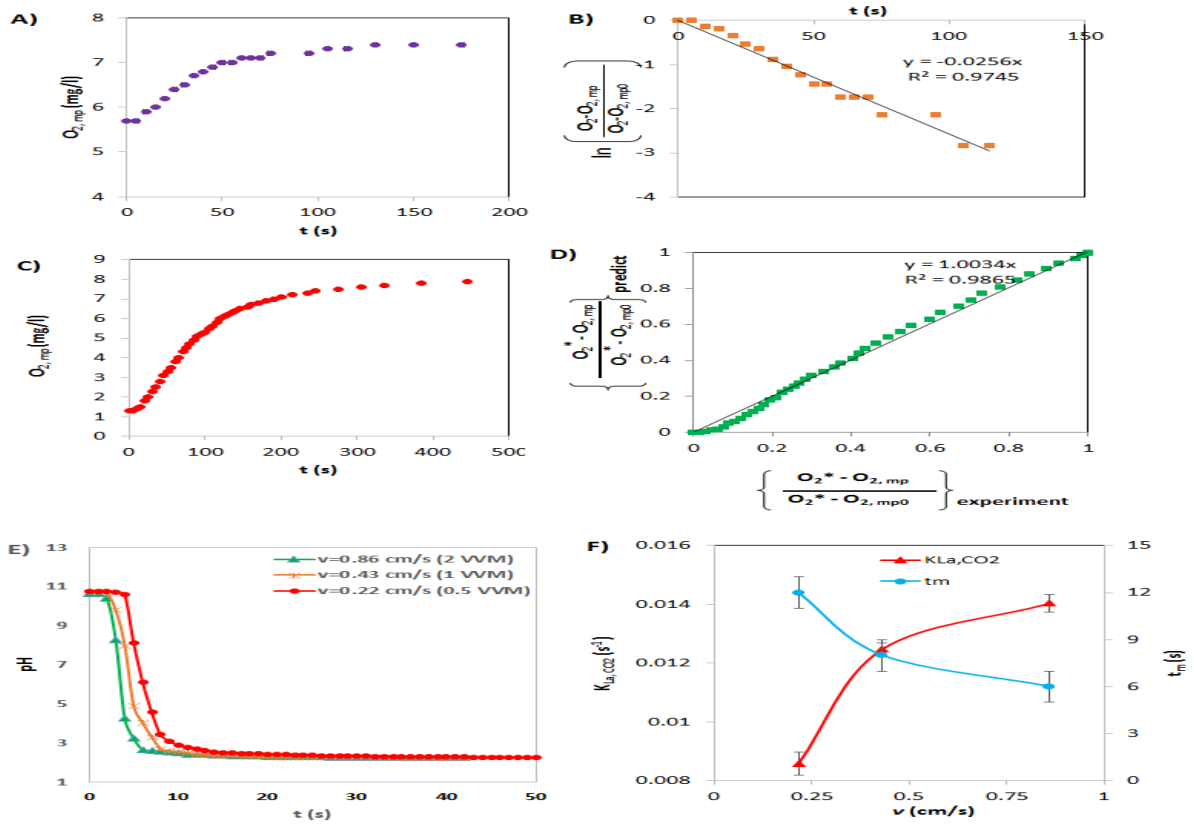

Fig. 4.4. Determination of carbon dioxide mass transfer coefficient (K_{La,CO_2}) and mixing time (t_m). **A)** and **B)** Determination of dissolved oxygen probe lag time constant (τ_p), **C)** and **D)** Determination of K_{La,O_2} using probe lag time constant, **E)** Response time profile of pH probe in a step change study and **F)** K_{La,CO_2} and t_m at different superficial gas velocity.

The K_{La,CO_2} of the medium scale flat panel photobioreactor (working volume of 2 l) has been determined as 0.0125 ± 0.0002 s^{-1} (45 hr^{-1}) at 0.43 cm/s superficial gas velocity (1 VVM, 2 l/min air flow rate). The K_{La,CO_2} was decreased to 0.0086 ± 0.0004 s^{-1} at lower superficial velocity of 0.215 cm/s (0.5 VVM, 1 l/min) (Fig. 4.4F). At higher superficial gas velocity of 0.86 cm/s (at 2 VVM, 4 l/min) the K_{La,CO_2} was not increased significantly (0.0141 ± 0.0003 s^{-1}) (Fig. 4.4F). At higher superficial gas velocity (0.86 cm/s) though the gas holdup increased in the PBR, the size of the bubble generated by rubber sheet sparger system (needle pinhole size increased at high pressure) was also increased and mutually there was not significant increment of overall mass transfer coefficient. The size changes of bubble can be visualized by naked eye.

The overall mass transfer coefficient achieved in the PBR developed in current study without mechanical agitator was comparable to available PBRs. Grima et al determined the CO_2 mass transfer coefficient for a stirrer tank algae photobioreactor at different agitator speeds and it was 0.003 s^{-1} at 150 RPM and 0.011 s^{-1} at 300 RPM (Grima et al., 1993). The PBR cannot be operated at very high RPM though the K_{La,CO_2} was increased with increase of RPM in their study as algae is very much shear sensitive. The low value of K_{La,CO_2} in their PBR may be due to high bubble diameter (~1.8 mm) generated through normal perforated sparger used in their study. In an another study, Ndiaye et al. developed two airlift photobioreactors with central aeration and two lateral baffles which allow liquid recirculation and studied for gas mass transfer in the context of airlift photobioreactor scale-up. The K_{La,CO_2} was 0.005 s^{-1} for laboratory scale (0.87 l) and 0.0014 s^{-1} for pilot scale (87 l) photobioreactors at 0.4 cm/s superficial gas velocity which are very low as compared to that of K_{La,CO_2} (0.0125 s^{-1}) observed in current study at 0.43 cm/s superficial gas velocity (Ndiaye et al., 2018). The low value of K_{La,CO_2} may be due to the large diameter of bubble (3 mm) in both the reactors generated by the installed sparger in that study. Carvalho and Malcata have determined the K_{La,CO_2} of two hollow fiber photobioreactors (HFPR) having microporous polypropylene membranes and polysulfone membrane to cultivate microalgae *Nannochloropsis* sp. (Carvalho & Malcata, 2001). The K_{La,CO_2} were 0.00025 s^{-1} for the polypropylene membrane and 0.00022 s^{-1} for the polysulfone membrane which was higher than the K_{La,CO_2} (0.00011 s^{-1}) achieved by traditional plain bubbling studied by same researchers also for comparison. But the K_{La,CO_2} achieved in their study are much lesser than the value achieved in current study. This may be due to low transmembrane pressure in the HFPR and large bubble size in conventional bubbling.

4.4.2. Mixing time (t_m) of the medium scale flat panel PBR

The time constant of pH probe was found by step change approach. The Fig. 4.5A shows there are two response phase; quick response and slow response in the change of pH profile. The first order model does not fit adequately, particularly for the slow phase (Fig. 4.5B). The second order model was well fitted to the response (Fig. 4.5C). There was almost no delay time; $a = 0$; The fitted parameter values are; $\tau_1 = 0.9\ s$ and $\tau_2 = 22\ s$. The quick response time constant is very less (less than 1 s). The time constant for quick response phase of the pH probe is ~1 sec and therefore not included in mixing time calculation.

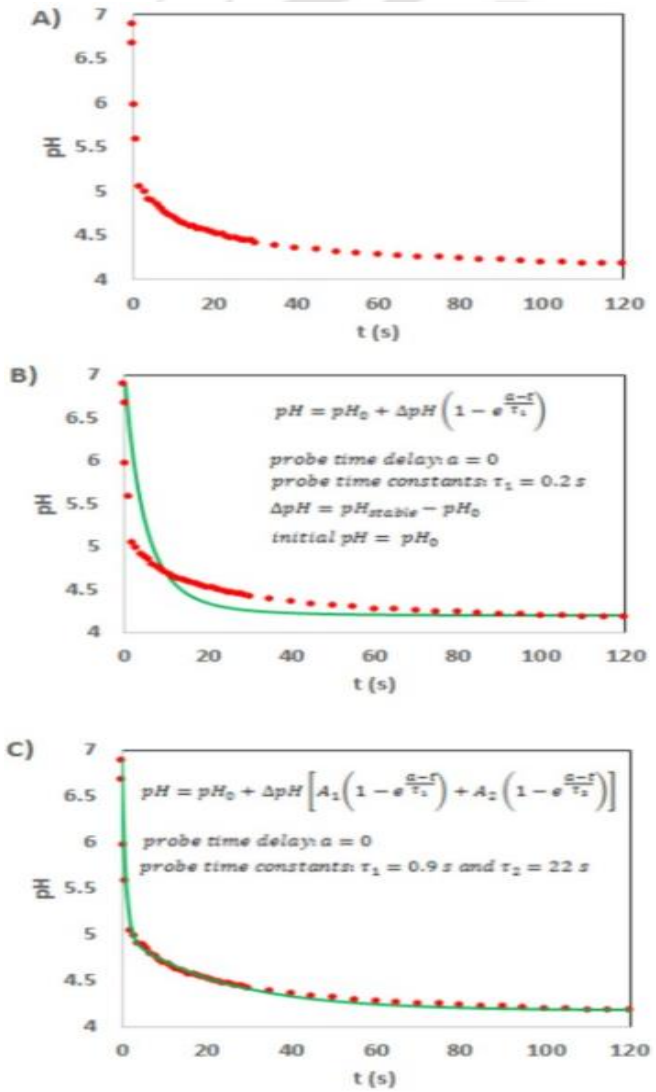

Fig. 4.5. Determination of time constant of pH probe. **A)** Quick response and slow response of pH, **B)** First order model of pH probe response and **C)** Second order model of pH probe response.

Mixing time (t_m) has also been calculated at different superficial gas velocity using acid tracer in current study (Fig. 4.4E). Mixing time was 8 sec for 0.43 cm/s superficial gas velocity and decreases with the increase of superficial gas velocity (Fig. 4.4F). It can be observed that the mixing time (t_m) is significantly lower, but it is not negligible, compared to the mass transfer time scale $\left(\frac{1}{K_{La,O_2}}\right)$ as $\frac{1}{K_{La,O_2}} = 8.96\, t_m$ for the 0.215 cm/s superficial gas velocity, $\frac{1}{K_{La,O_2}} = 9.26\, t_m$ for the 0.43 cm/s superficial gas velocity and $\frac{1}{K_{La,O_2}} = 10.96\, t_m$ for the 0.86 cm/s superficial gas velocity. The t_m was 18 s for 0.87 l and 78 s for 87 l photobioreactor at 0.4 cm/s superficial gas velocity in the airlift photobioreactor developed by Ndiaye et al. used for scale-up studied (Ndiaye et al., 2018). Large diameter bubble (3 mm) generated by sparging system used in their study resulted in low rising velocity of bubble probably the reason for high mixing time.

4.4.3. Effect of nutrients on the growth of *S. abundans*

In nitrogen source variation experiment, all nitrogen sources produced almost same biomass titer of 1.7 g/l at 144 hr with 405 µE/m^2/s (Fig. 4.6A). Urea has been chosen as nitrogen source for *Scenedesmus* growth for further study as it is cheap and has high nitrogen content (~47% N in urea). It was observed that biomass growth was limited at low concentration or absence of urea in media and growth was inhibited at high concentration of urea (5300 mg/l) (Fig. 4.6B). Highest biomass titer of 1.73 g/l was achieved at 2500 mg/l of urea and therefore chosen for further study. Similarly, limitation and inhibition concentrations of K_2HPO_4 for biomass growth were observed at 10 mg/l and 2000 mg/l respectively (Fig. 4.6C). Same concentration of biomass (1.7 g/l) were achieved with K_2HPO_4 concentrations of 100, 500 and 1000 mg/l with 405 µE/m^2/s light intensity. K_2HPO_4 concentration of 1000 mg/l was chosen to minimize the frequency of its feeding at high light intensity and chosen for next experiments. Optimal $MgSO_4.7H_2O$ concentration was 1500 mg/l and contributed to highest biomass titer

of 1.95 g/l at 96 hr (Fig. 4.6D) and chosen for next study. Low concentrations (0–200 mg/l) of $MgSO_4.7H_2O$ limiting the biomass growth and inhibition was shown at 5000 mg/l. The highest biomass titer of 3.95 g/l was achieved with $CaCl_2.2H_2O$ of 1000 mg/l at 144 hr (Fig. 4.6E) and used for subsequent experiments. 0.1% of 1000X micronutrient solution ($CoCl_2.2H_2O$ − 0.02 mg/l, H_3BO_3 − 5.72 mg/l, $MnCl_2.4H_2O$ − 3.62 mg/l, $ZnSO_4.7H_2O$ − 0.44 mg/l, $CuSO_4.5H_2O$ − 0.16 mg/l, $Na_2MoO_4.2H_2O$ − 0.084 mg/l) contributed to highest biomass titer of 3.95 g/l (Fig. 4.6F). 5% of 1000X micronutrient solution was shown as inhibition concentration. The optimum medium composition; 2500 mg/l urea, 1000 mg/l K_2HPO_4, 1500 mg/l $MgSO_4.7H_2O$, 1000 mg/l $CaCl_2.2H_2O$ and 0.1% micronutrient solution was chosen for further study.

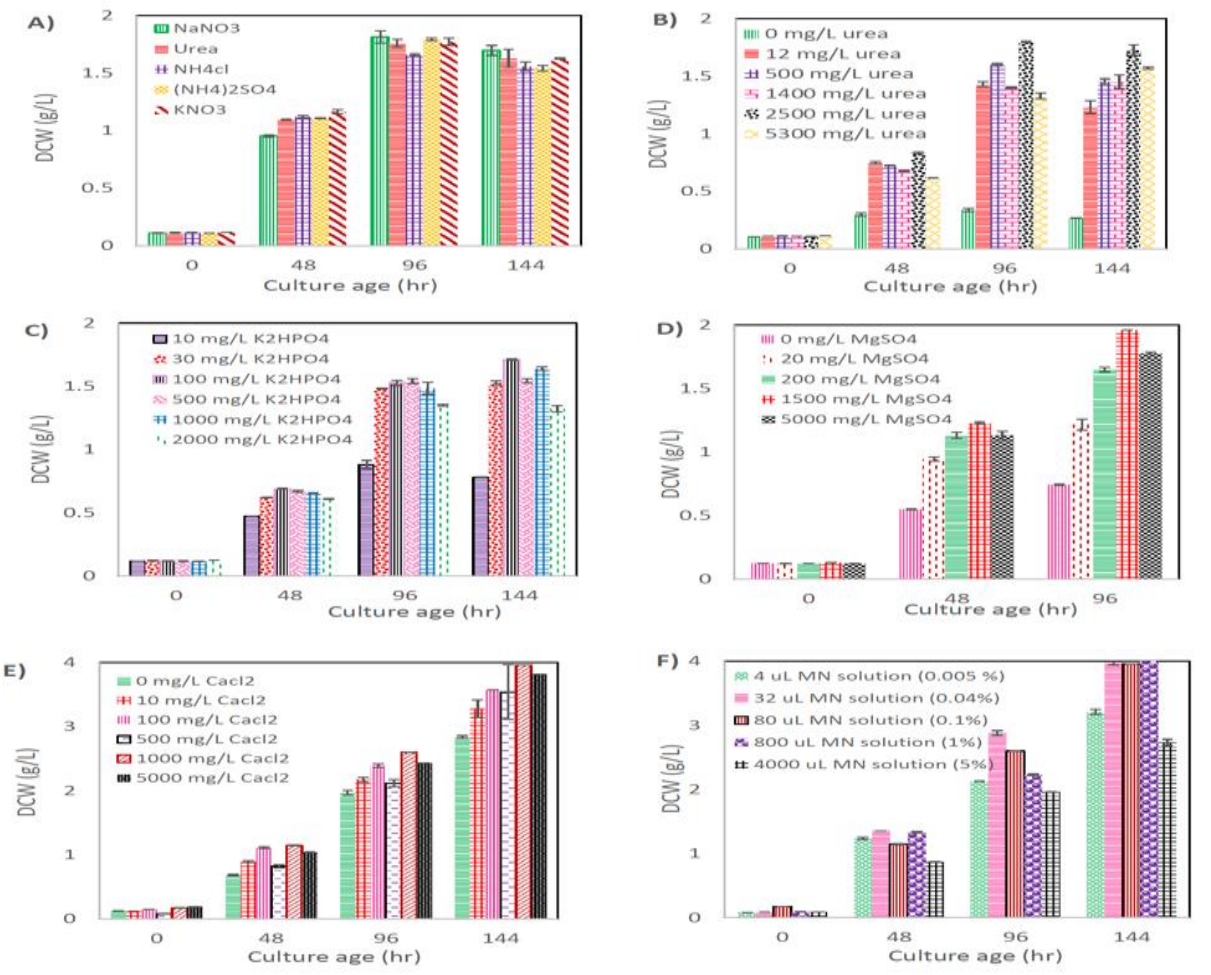

Fig. 4.6. Biomass growth at different nitrogen sources and different concentration of nutrient under 405 µE/m^2/s light intensity in parallel mini PBR. Biomass growth at different **A)** nitrogen sources. Initial nitrogen (N) concentration was 44 mg/l ($NaNO_3$: 269 mg/l, urea: 95 mg/l, NH_4Cl: 169 mg/l, $(NH_4)_2SO_4$: 208 mg/l and KNO_3: 320 mg/l), initial concentration of **B)** urea, **C)** K_2HPO_4, **D)** $MgSO_4$, **E)** $CaCl_2$ and **F)** micronutrient solution.

4.4.4. Biomass growth and chlorophyll-a production at different light intensity

To check the light limitation and photoinhibition on microalgae growth, a set of experiments with different light intensity (81, 405, 878, 2162 µE/m^2/s) were conducted in small scale parallel mini PBR with media composition that gave highest biomass growth from nutrient variation experiments. The 2162 µE/m^2/s light intensity was chosen based on the highest sun light availability at noon time in Guwahati region. Low biomass growth due to limitation of light intensity was observed at 81 µE/m^2/s (Fig. 4.7A). Light intensity of 2162 µE/m^2/s gave highest specific growth rate of 1.6 day^{-1} at initial stage (upto 48 hr) as compared to other light intensities which clearly shows that there is no photoinhibition in the range of 2100 µE/m^2/s light on growth of *Scenedesmus abundans* (Fig. 4.7B). The overall specific growth rate was also highest (0.7 day^{-1}) at 2162 µE/m^2/s among all other light intensities. The specific growth rate decreases upon time because of less light available to the cells caused due to dense biomass.

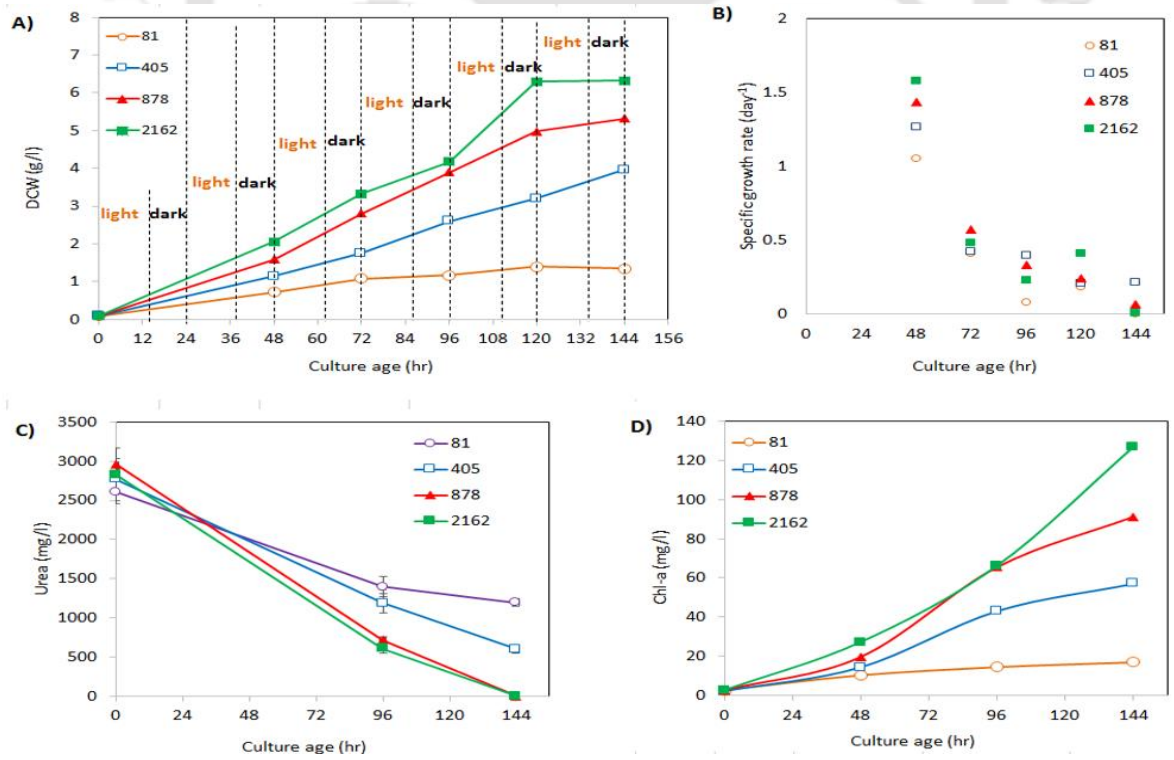

Fig. 4.7. Biomass growth at different light intensity (81–2162 µE/m^2/s) in parallel mini PBR. **A)** dry cell weight (DCW), **B)** specific growth rate, **C)** urea consumption and **D)** Chl-a synthesis.

Despite of sufficient nutrients availability in the media, stationary phase was achieved at 144 hr because of light limitation. The 2162 µE/m^2/s gave highest biomass titer of 6.3 g/l whereas 81 µE/m^2/s gave lowest biomass titer of 1.34 g/l after 6 days (Fig. 4.7A). The chlorophyll-a concentration was also higher in 2162 µE/m^2/s as the sufficient photon flux density is available per cell resulting in high photosynthetic activity (Fig. 4.7D). The urea utilization rate was also higher at high light and consumed totally at 144 hr (Fig. 4.7C).

4.4.5. Simultaneous production of lipid and EPS in medium scale flat panel PBR under high light intensity

Highest biomass concentration of 6.4 g/l was achieved at 2162 µE/m^2/s at the end of growth phase from light intensity variation experiments in parallel mini PBR. An experiment was conducted in 2 l working culture volume (medium scale) flat panel photobioreactor under 2162 µE/m^2/s light intensity for concomitant production of lipid and EPS using optimized growth media developed in small scale parallel mini PBR. Biomass growth, chlorophyll-a and carotenoid synthesis, urea and K_2HPO_4 utilization have also been studied. Highest specific growth rate of 4.2 day^{-1} was achieved at the end of 1st day light period where overall specific growth rate was 0.7 day^{-1} in the growth phase (upto 134 hr). Overall biomass titer of 6.9 g/l and biomass productivity of 1.2 g/l/day were attained at the end of growth phase (134 hr) (Fig. 4.8A). After growth period, biomass loss has been observed for almost two days at nitrogen limiting period and then total biomass concentration started to increase at nitrogen starvation condition (Fig. 4.8A). This biomass increment may be due to accumulation of triacylglycerol (TAG) in cell. Note that the biomass growth ceased at 134 hr though the urea and phosphate were present in culture media indicating the light limitation. The chlorophyll-a and carotenoid concentrations were increased in growth phase and reached to 80 mg/l and 20 mg/l respectively in nitrogen sufficient condition (Fig. 4.8C). The level of chlorophyll-a and carotenoid did not increase at high rate in nitrogen deprive condition as seen in the growth phase.

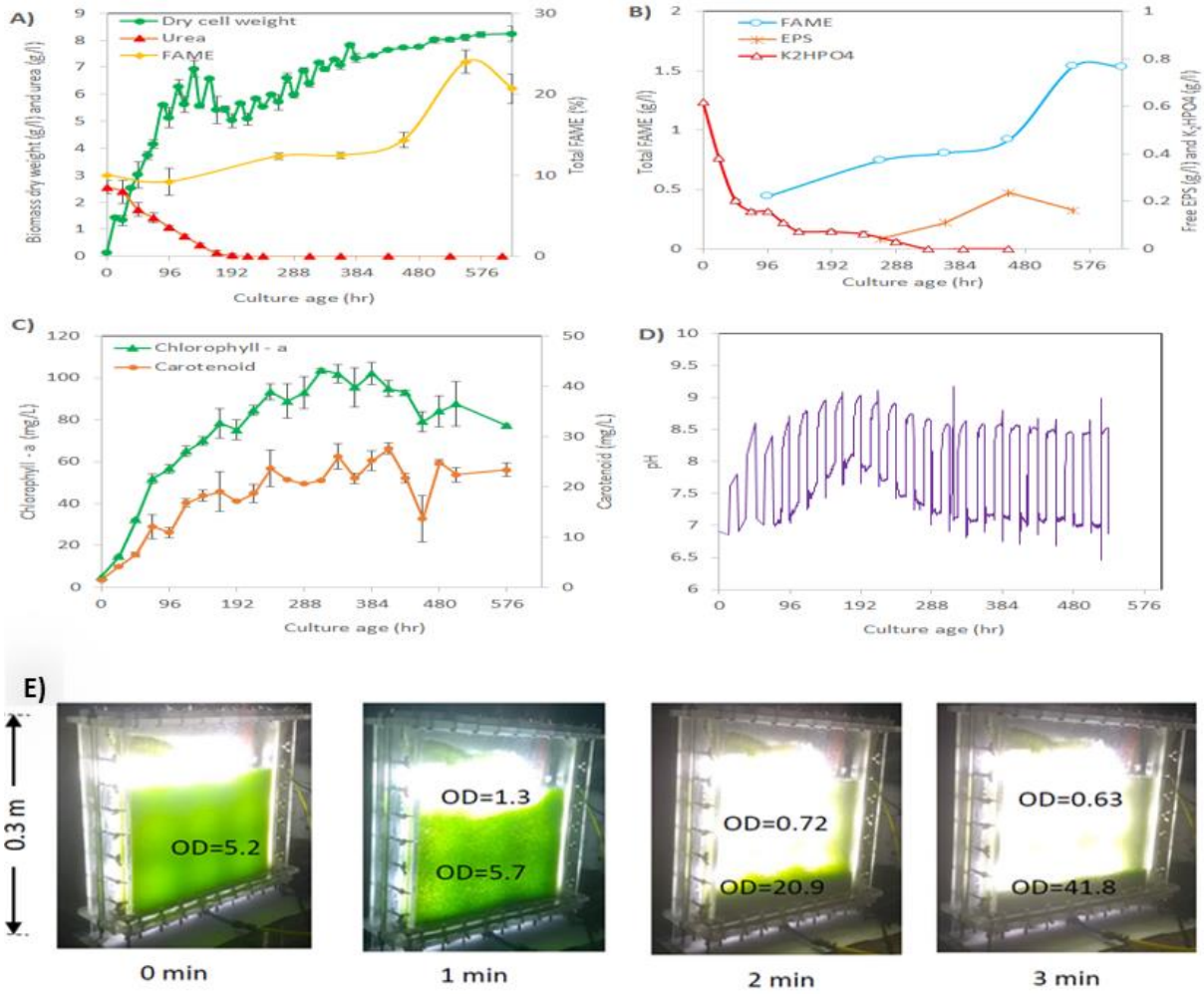

Fig. 4.8. Biomass growth in medium scale PBR. **A)** Dry cell weight (DCW), urea consumption and FAME content, **B)** phosphate consumption, FAME and EPS production, **C)** Chl-a and carotenoid synthesis, **D)** pH of the culture and **E)** Autoflocculation.

It has been observed that urea and extracellular phosphate were consumed completely at the end of 192th hr and 336th hr respectively (Fig. 4.8A and 4.8B). Overall biomass yield with respect to urea and phosphate were 3.2 g biomass/g urea and 12.5 g biomass/g K_2HPO_4 respectively at the end of growth phase (134 hr). The lipid accumulation started slowly at nitrogen limiting condition and the maximum FAME content (22%) with a concentration of 1.53 g/l FAME was achieved after 15 days of nitrogen deprivation. The overall FAME productivity of 67 mg/l/day was achieved in this study. The FAME content (22%) in *Scenedesmus abundans* obtained in this study is double than that of the FAME content (10–13%) already reported using *S. abundans* isolated from Dal lake, India (Mandotra et al., 2014).

Note that the cultivation photobioreactor and sparging system were different in their study. Their *S. abundans* was grown in a 20 l indigenous photobioreactor made up of high density polyethylene (40 cm height and 26 cm diameter) using silicon tube air sparging system under the indirect sun light at an approximate light intensity of 150 µE/m^2/s at a temperature of 28 °C ± 2 °C with KNO_3 as nitrogen source. Low light and large diameter of the photobioreactor could be the reason for less FAME content in their study. In an another study of lipid production by *Scenedesmus abundans* UTEX 1358, the biomass productivity was 16.9 mg/l/day and lipid productivity was 3.55 mg/l/ day (highest lipid content 21%) under low light using optimal nitrogen source i.e., ammonium nitrate (González-Garcinuño et al., 2014). In their study, *S. abundans* was grown in 500 ml Erlenmeyer shake flask with agitation of 125 RPM under light intensity of 60 µE/m^2/s (light/ dark periods 10:14 hr) at 20 °C. The low production rate in their study may be due to limitation of light and CO_2. In the current study, it was observed that the quantity of attached EPS was very low (only 5% of free EPS) indicates the high rate of detachment of EPS from cell surface which decrease the downstream processing cost of EPS production. The maximum EPS production was 236 mg/l with a yield of 37 mg EPS/g biomass at nitrogen starvation condition. In a different study, Angelaalincy et al. achieved maximum 48 mg/l EPS using *Scenedesmus sp*. SB1 at $NaNO_3$ stress condition through media optimization via Plackett–Burman Design and response surface methodology (RSM) (Angelaalincy et al., 2017). Note that, the EPS produced in their study was attached EPS which can increase the cost of downstream processing of EPS purification. In the current study, the culture pH profile depicted in Fig. 4.8D showed the rise in pH in growth phase and slight decline in nitrogen starvation condition.

4.4.6. Autoflocculation of *Scenedesmus abundans*

Autoflocculation study was carried out during the experiment of simultaneous production of lipid and EPS described above. Once the biomass optical density (OD_{680}) reached

to 5.2 (dry cell weight concentration of around 1.5 g/l), natural autoflocculation efficiency has been measured without adding any extra flocculants at room temperature. The autoflocculation started immediately after stopping the sparging of gas mixture (Fig. 4.8E). The biomass settled down to height of 0.05 m with OD_{680} of 20.9 from initial height of 0.23 m (initial OD_{680} = 5.2) within 2 min. It has been observed that it settles down to 0.025 m with OD_{680} of 41.8 within 3 min corresponding to almost 90% cell recovery. The autoflocculation efficiency has also been checked at higher biomass density (data not shown). Moorthy et al. also studied the same strain of *Scenedesmus abundans* sedimentation by flocculation strategy (Moorthy et al., 2017). In their study, with initial biomass concentration of 0.55 g/l, the flocculation efficiency was 45% in 12 hr (total settling time was 26.5 hr) without adding any flocculants and with addition of chitosan and bentonite clay flocculants the efficiency was increased to 78% in 12 hr (total settling time was 15 hr). This low flocculation efficiency and high settling time may be due to the less production of EPS which can act as natural flocculant. *Scenedesmus abundans* proved its ability of natural autoflocculation which can reduce the downstream processing cost for biomass harvesting and EPS production.

4.4.7. Assessment of biodiesel quality

The FAME content of *Scenedesmus abundans* grown under 2162 µE/m^2/s was shown in Fig. 4.8A. The percentage of each FAME in total FAME, % SFA (saturated fatty acid), % MUFA, % PUFA composition were listed in Table 4.1. FAME quantified by gas chromatography shows the abundance of palmitate (C16:0), oleate (C18:1) and linoleate (C18:2) fatty acid methyl esters as compared to other FAME and thus representing a potential use of the strain for good quality biodiesel production. The DU, SV, IV, CN, LCSF, CFPP, OSI, CP and PP values of biodiesel obtained for 552 hr microalgal culture were also given in Table 4.1. The minimum value of CN and the maximum value of IV according to European biodiesel standard (EN 14214) are 51 and 120 g I_2 100 g^{-1} fat respectively (Demirbas, 2009).

The properties of biodiesel such as cetane number (CN), degree of unsaturation (DU), saponification value (SV), iodine value (IV), long chain saturation factor (SV), cold filter plugging point (CFPP), cloud point (CP), pour point (PP), oxidation stability index (OSI) were close to the European biodiesel standards (EN 14214, EN 14112) which proves the feasibility of using biodiesel from *Scenedesmus abundans* in automobiles (Knothe, 2006).

Table 4.1. Biodiesel quantity and quality analysis of 552 hr microalgal culture at 2162 µE/m^2/s.

FAME	**%FAME in DCW**	**%FAME in total FAME**
C12:0	0.05	0.23
C14:0	0.16	0.72
C15:0	0.11	0.52
C15:1	0.09	0.42
C16:0	5.73	26.06
C16:1 cis	0.17	0.78
C16:1 tr	1.82	8.29
C16:2 cis	0.72	3.28
C16:2 tr	0.06	0.28
C16:3 cis	0.08	0.38
C16:3 tr	0.08	0.36
C17:0	0.26	1.19
C17:1	0.09	0.42
C17:2 cis	0.05	0.22
C17:2 tr	0.07	0.33
C18:0	0.93	4.21
C18:1 cis	3.34	15.21
C18:2 cis	6.54	29.58
C18:2 tr	1.61	7.33
C18:3	0.04	0.18
SFA	7.24	32.93
MUFA	5.51	25.12
PUFA	9.25	41.94
FAME	22.00	100.00
Biodiesel property	**Value**	**Unit**
DU	109.00	–
SV	188.95	mg KOH g^{-1} oil
IV	91.54	g I_2 100 g^{-1} oil
CN	54.58	–
LCSF	4.71	–
CFPP	−1.68	°C
CP	8.72	°C
PP	2.64	°C
OSI	5.77	hrs

4.4.8. Characterization of EPS

Presence of 10% (w/w) of protein in EPS was confirmed using Bradford method. The functional groups present in arabinose, rhamnose, galactose, glucose and glucuronic acid are identical with the functional groups present in the EPS confirmed by FTIR which proves that these sugars and acid are present in EPS (Fig. 4.9A). The information about the functional groups present in sugars, glucuronic acid and EPS produced in this study with the wavenumber range (cm^{-1}) was given in Table 4.2. From HPLC analysis of EPS, it can be concluded that arabinose, rhamnose, galactose, glucose and glucuronic acid are present in EPS by comparing their retention time with the retention time of EPS (Fig. 4.9B). The results obtained by FTIR are similar to the results obtained through HPLC, thus confirming the presence of sugars and acids in the polysaccharide. The crystallinity of the EPS from *Scenedesmus abundans* was examined by the PXRD technique. The sharp thin peaks of EPS observed in XRD indicates its crystallinity nature (Fig. 4.9C).

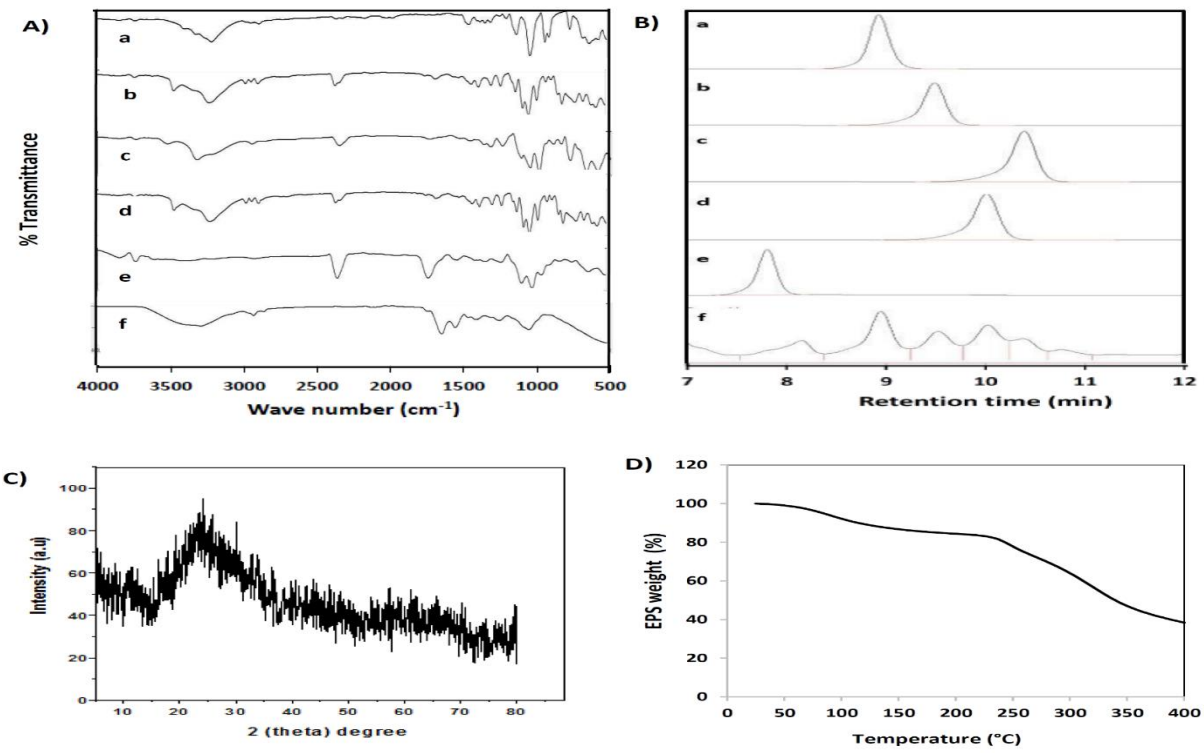

Fig. 4.9. EPS characterization. **A)** FTIR, **B)** HPLC, **C)** PXRD and **D)** TGA analysis. For Fig. **A** and **B**, **a:** glucose, **b:** galactose, **c:** arabinose, **d:** rhamnose, **e:** glucuronic acid and **f:** EPS produced in this study.

Table 4.2. FTIR Spectra of EPS of *S. abundans* (current study) and standard sugars and uronic acid (Coates, 2000; Silverstein & Bassler, 1962).

Component	Wave number (cm^{-1})	Assignment	Intensity
Scenedesmus abundans EPS (current study)	3400	O-H stretch (H-bonded)	strong
	3275	O-H stretch	strong
	2960	C-H stretch	medium
	2920	C-H stretch	medium
	2850	C-H stretch	weak
	2349	O-H stretch	weak
	2100	C≡C stretch	weak
	1725	C=O stretch (acid)	strong
	1640	C=C stretch	strong
	1540	N-H bending	strong
	1455	C-H bending	medium
	1403	C-H bending	medium
	1242	C-N stretch	medium
	1040	C-O stretch	strong
Glucose	3220	O-H stretch	strong
	2980	$C-H_2$ stretch	medium
	2885	C-H stretch	medium
	1450	C-H bending	weak
	1030	C-O stretch	strong
Galactose	3462	O-H stretch (H-bonded)	strong
	3225	O-H stretch	strong
	2980	$C-H_2$ stretch	medium
	2885	C-H stretch	medium
	2350	O-H stretch	weak
	1030	C-O stretch	Strong
Arabinose	3525	O-H stretch (H-bonded)	medium
	3320	O-H stretch	strong
	2948	C-H stretch	medium
	2350	O-H stretch	strong
	1240	C-O stretch	strong
	1048	C-O stretch	strong
Rhamnose	3461	O-H stretch (H-bonded)	strong
	3222	O-H stretch	strong
	2980	$C-H_2$ stretch	medium
	2885	C-H stretch	medium
	2351	O-H stretch	medium
	1428	C-H bending	medium
	1222	C-O stretch	strong
	1030	C-O stretch	strong
Glucuronic acid	2360	O-H stretch	medium
	1725	C=O stretch (acid)	medium
	1060	C-O stretch	strong

The crystallinity of EPS is also one of the reasons indicating its less degradability over wide range of temperatures which was proven by thermogravimetry (TGA) (Fig. 4.9D). The thermal stability of EPS was evaluated by TGA analyser to enable the polysaccharide in various applications. TGA gives the percent weight loss of the compound against time. From the Fig. 4.9D, it was confirmed that the weight loss in the EPS from *Scenedesmus abundans* is a three-step process in which 7% mass loss is detected in the first phase at 25–100 °C due to moisture removal, 10% loss is detected in the second phase at 100–225 °C and 45% loss is detected at 225–400 °C in the third phase, implying the use of this polymer in high temperature.

4.5. Conclusions

Parallel mini and medium scale flat panel PBR were constructed for the cultivation of microalgae *S. abundans*. A high mass transfer efficient membrane sparger was designed and equipped at the bottom to mimic bubble driven flat panel PBR. The medium scale flat panel PBR produced K_{La,CO_2} and t_m of 0.0125 s^{-1} and 8 sec respectively at 0.43 cm/s superficial gas velocity. Maximum biomass titer of 6.9 g/l was achieved at end of growth phase using optimized growth media. The productions were 1.53 g/l (22% of DCW) FAME with productivity of 67 mg/l/ day and 236 mg/l EPS with yield of 37 mg/g biomass under nitrogen starvation. Capability of producing multiproducts by this strain, and cost effective natural autoflocculation based biomass harvesting and EPS purification can make the process sustainable.

CHAPTER 5

Process design to enhance biodiesel in medium scale flat panel PBR under outdoor natural sunlight

5.1. Background and uniqueness of the study

Adequate supply of macronutrients and micronutrients are essential for enhancing growth and lipid synthesis in algal cells. A few studies have investigated the combined effects of metal ions for improving biomass and lipid productivities of *Scenedesmus abundans*. Also, the study of effect of micronutrient levels on lipid content in microalgae especially in *Scenedesmus abundans* is very sparse. This chapter not only focuses on the effect of individual nutrients influencing microalgal physiology, but also studied the combined effect of micronutrient interactions. Many researchers have focused on different cultivation strategy to improve the lipid productivity. It has been shown that two stage cultivation system can improve the lipid productivity by increasing cell amount for many microalgae due to separation of lipid accumulation phase from microalgae growth phase. Note that, typically there is a trade-off between these two phases as the nutrient composition responsible for high growth of microalgae can decrease the lipid accumulation and vice-versa. But in two stage strategy, an extra step between these two phases is required where cell is harvested after high growth and re-suspended in a nutrient limiting media for promoting lipid thereby increasing the overall process cost. Single stage strategy can improve the lipid content in microalgae but it sacrifices the cell concentration. The comparison of single and two stage cultivation strategy for lipid accumulation in *Scenedesmus* sp. was not explored extensively so far. Simultaneous production of multiproduct by microbial cell factories can make the bioprocess economically viable (Naira

et al., 2020). Apart from intracellular neutral lipid, *Scenedesmus* sp. can secrete extracellular polymeric substances such as exopolysaccharides (EPS) under artificial LED lighting system (Mahesh et al., 2019; Salim et al., 2014). Also this EPS creates a partial or complete binding of algal cells due to glycoproteins that are responsible for cell to cell attachments forming flocs giving rise to autoflocculation phenomena thereby decreases the cell harvesting cost (Mahesh et al., 2019; Salim et al., 2014). Though production capability of EPS and autoflocculation efficiency of *Scenedesmus* sp. have been explored for the cultivation system under LED light but these are not investigated earlier under outdoor natural sunlight.

In the present work, we have studied the effect of both macro and micronutrients mainly boron and manganese on growth and lipid accumulation in *Scenedesmus abundans*. Comparative study of single stage and two stage processes for growth and lipid induction in *Scenedesmus abundans* have also been carried out. The effect of natural outdoor sunlight on EPS production capability and autoflocculation efficiency have been investigated in current study.

5.2. Test tube PBRs with LED lighting system

Transparent test tube photobioreactors were made using 1 mm thicker borosil test tubes (18 mm outer diameter, 16 mm inner diameter and 150 mm height) with a total capacity of 27 ml (Fig. 5.1A). The test tube caps were drilled such that 8 mm diameter PU pipe enters into the test tube. A mixture of air and CO_2 (2 bar pressure) was sparged through PU pipe from the top of the test tube PBRs via 50 mm 0.2 µm PTFE filters (specifications: appendices, Table A2). A small hole has been made in the test tube cap that acts as a vent. Parallel mini flat panel PBR (Fig. 5.1B), medium-scale flat panel PBR (Fig. 5.1C) and customized unidirectional LED lighting systems were used as designed by Mahesh et al (Mahesh et al., 2019). The light path length of mini flat panel and medium scale flat panel PBR was 25.4 mm. Constant current source regulator controls the light intensity of LED ranging from 0 to 2200 µE/m^2/s.

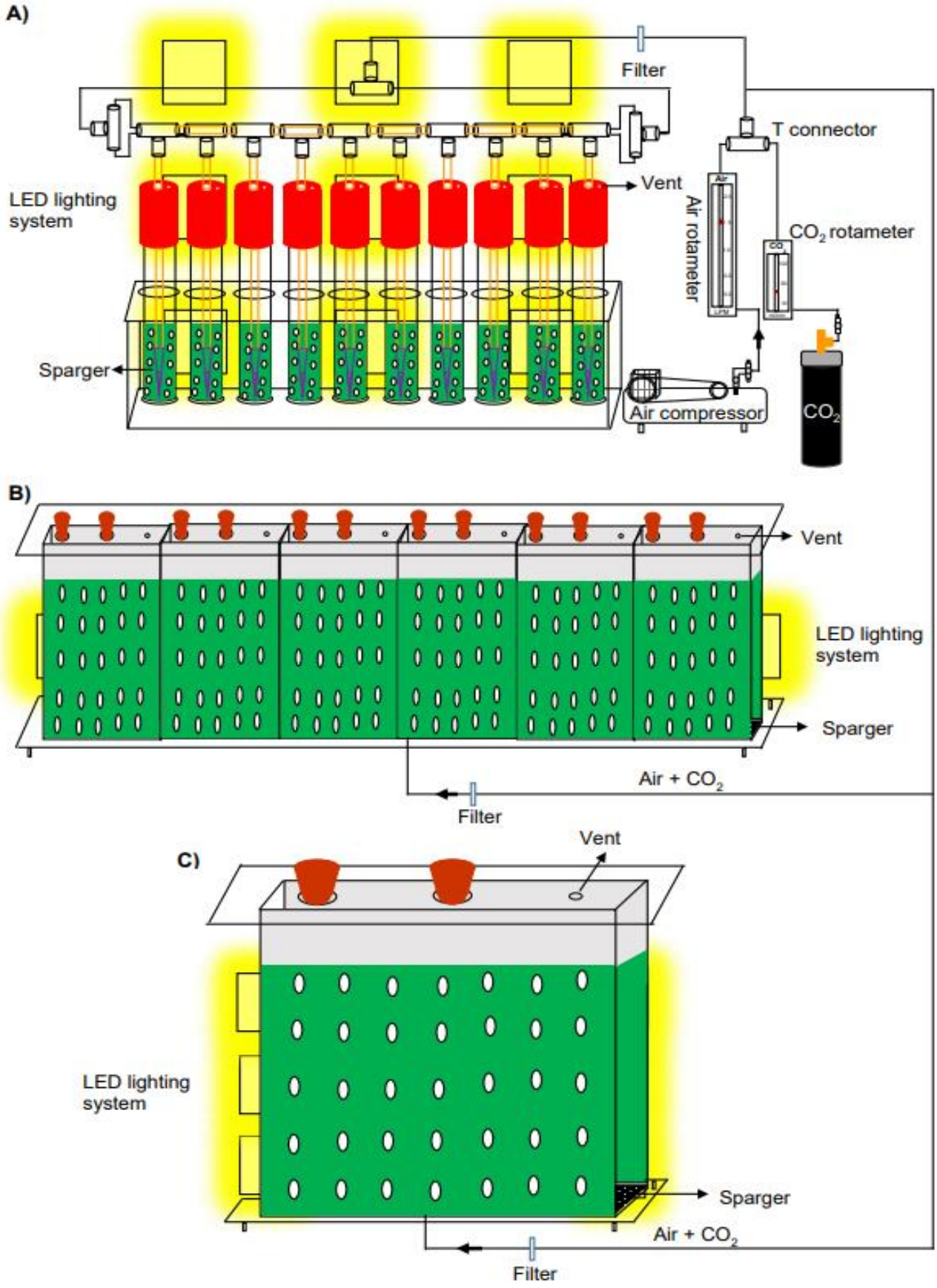

Fig. 5.1. Schematic diagram of photobioreactors for microalgae cultivation. **A)** test tube PBR, **B)** parallel mini flat panel PBR and **C)** medium scale flat panel PBR.

Diurnal natural sunlight intensities from dawn to dusk and incident LED light intensities on the surface of the reactor (in lux) was measured using a lux meter (specifications: appendices, Table A2). Light (in lux) was converted to PPFD (Photosynthetic Photon Flux Density) in $\mu E/m^2/s$ by dividing with the conversion factor of 54 and 74 for diurnal natural sunlight and cool white LED respectively (Apogee Instruments, Inc. USA). The Color temperature of diurnal natural sunlight and cool white LED are 5000 K and 6500 K. Light intensities were constant in all indoor experiments.

5.3. Experimental design for high FAME production from *Scenedesmus abundans*

5.3.1. Experiments in medium scale flat panel PBR and parallel mini flat panel PBR

Medium scale flat panel PBR and parallel mini flat panel PBR were used preliminary to study the effect of nutrients in single stage. The modified Chu-13 media composition used in this experiment was as follows: 2500 mg/l urea, 35 mg/l K_2HPO_4, 75 mg/l $MgSO_4.7H_2O$, 20 mg/l $CaCl_2.2H_2O$, 20 mg/l ferric citrate, 100 mg/l citric acid, 0.04% of 1000 X micronutrient. 1000 X micronutrient - ($CoCl_2.2H_2O$ − 0.02 g/l, H_3BO_3 − 5.72 g/l, $MnCl_2.4H_2O$ − 3.62 g/l, $ZnSO_4.7H_2O$ − 0.44 g/l, $CuSO_4.5H_2O$ − 0.16 g/l, $Na_2MoO_4.2H_2O$ − 0.084 g/l). These nutrient concentrations of the media were chosen so that all nutrients would be almost utilized by microalgae at stationary phase. The experimental conditions for medium scale flat panel PBR were as follows: 100 W cool white LED with photoperiod of 14 hr light:10 hr dark cycle, 2162 $\mu E/m^2/s$ light intensity, 2 l/min air flow rate with 2% (v/v) CO_2 from bottom of the reactor, working volume – 2 l. Initial biomass concentration of 0.11 g/l was used for all autotrophic batch experiments and algal samples were collected in triplicates for dry cell weight (DCW) and FAME measurement. The whole algal culture was collected from medium scale flat panel PBR at 153 hr and transferred to parallel mini flat panel PBR without performing centrifugation once urea was almost consumed. The different nutrient combinations added in parallel mini flat panel PBR were as follows: 0 mg/l urea, 80 mg/l K_2HPO_4, 200 mg/l $MgSO_4.7H_2O$, 107

mg/l $CaCl_2.2H_2O$, 0.1% of 1000 X micronutrient was used as control. K_2HPO_4 concentrations of 0 mg/l and 1000 mg/l was used keeping other nutrients same as control. Similarly, 0 mg/l $MgSO_4.7H_2O$, 1500 mg/l $MgSO_4.7H_2O$ and 0 mg/l $CaCl_2.2H_2O$, 1000 mg/l $CaCl_2.2H_2O$ was used to find the effect of $MgSO_4$ and $CaCl_2$. For micronutrient, 0% and 0.2% of 1000 X micronutrient was added to determine the effect of micronutrients for microalgal lipid production. The experimental conditions in parallel mini flat panel PBR were as follows: 50 W cool white LED with photoperiod of 14 hr light:10 hr dark cycle, 878 µE/m^2/s light intensity, 1 VVM air flow rate with 2% (v/v) CO_2 from bottom of the reactor and working volume – 80 ml was used in each parallel mini flat panel PBR chamber. Water was added before and after light period to reduce the evaporation losses due to bubble driven agitation. CO_2 was not sparged during dark period but air flow remained undisturbed throughout batch to prevent settling of algal cells and for cell respiration in all experiments.

5.3.2. Experiments in test tube PBR

5.3.2.1. Macronutrient variation

Macronutrient concentration variation (urea, K_2HPO_4, $MgSO_4.7H_2O$, $CaCl_2.2H_2O$) was performed using single stage strategy in test tube PBR for lipid production. Modified Chu-13 media was used as control media as follows: 500 mg/l urea, 80 mg/l K_2HPO_4, 200 mg/l $MgSO_4.7H_2O$, 107 mg/l $CaCl_2.2H_2O$, 20 mg/l ferric citrate, 100 mg/l citric acid, 0.1% of 1000X H_3BO_3 (5.72 mg/l), 0.1% of 1000X $MnCl_2.4H_2O$ (3.62 mg/l) and 0.1% of 1000X other micronutrients pool (MN). 1000X other micronutrients pool - ($CoCl_2.2H_2O$ − 0.02 g/l, $ZnSO_4.7H_2O$ − 0.44 g/l, $CuSO_4.5H_2O$ − 0.16 g/l, $Na_2MoO_4.2H_2O$ − 0.084 g/l). Nutrients were varied one at a time for all the experiments while other nutrients were same as mentioned in the control media. Urea was varied from 0 to 2.5 g/l and K_2HPO_4 was varied from 0 to 1 g/l. $MgSO_4.7H_2O$ was varied from 0 to 1.5 g/l and $CaCl_2.2H_2O$ was varied from 0 to 1 g/l. Macronutrients such as citric acid and ferric citrate are present in fewer quantities in control

media and used as such without any modification. The experimental conditions in test tube PBR for nutrient variation experiments were as follows: 100 W cool white LED used as light source, photoperiod – 14 hr light:10 hr dark cycle, light intensity 1081 µE/m^2/s, sparging: 2% (v/v) CO_2 in air and 15 ml working volume. The average light intensity of 1081 µE/m^2/s was chosen based on sunlight intensities measured from dawn to dusk in the summer season in the Guwahati, India. The appropriate sample volume was collected in triplicates at every 48 hr interval for OD_{680} measurement. Algal culture of 5 ml was collected on the 20th day from the start of the experiment to find the DCW and FAME of the sample.

5.3.2.2. Micronutrient variation and interaction

H_3BO_3, $MnCl_2.4H_2O$ and other micronutrients pool (MN, $CoCl_2.2H_2O$, $ZnSO_4.7H_2O$, $CuSO_4.5H_2O$, $Na_2MoO_4.2H_2O$) were varied one at a time for all the experiments while other macronutrients kept constant in test tube PBR. H_3BO_3 and $MnCl_2.4H_2O$ were varied from 0 to 1% of 1000X H_3BO_3 (5.72 g/l) and 0 to 1 % of 1000X $MnCl_2.4H_2O$ (3.62 g/l) respectively. For other micronutrients pool, it was varied from 0 to 1% of 1000X stock ($CoCl_2.2H_2O$: 0.02 g/l, $ZnSO_4.7H_2O$: 0.44 g/l, $CuSO_4.5H_2O$: 0.16 g/l, $Na_2MoO_4.2H_2O$: 0.084 g/l). Micronutrients H_3BO_3 and $MnCl_2.4H_2O$ were varied independently as they are present in high quantities as micronutrients in modified Chu-13 media (57% H_3BO_3 and 36% $MnCl_2.4H_2O$ out of all micronutrients). For further improvement in lipid production, micronutrient interaction experiments was also performed in a single stage test tube PBR with the macronutrients level that gave the highest FAME concentration in macronutrient variation experiments. The experimental conditions were same as those performed in the macronutrient concentration variation experiment. For micronutrient interaction study experiments, full factorial design was performed in test tube PBR with three levels of H_3BO_3, $MnCl_2.4H_2O$ and other micronutrients pool each resulting 27 experiments. The levels have been chosen based on one at a time experiments. The sample collection procedure for OD_{680}, DCW and FAME analysis was same

as mentioned in macronutrient variation experiments.

5.3.3. Experiments in parallel mini flat panel PBR using selected media

Based on two objectives; i) FAME titer (g/l) and ii) FAME increment from 10 days to 20 days in micronutrient interaction study in test tube PBR, few media combinations have been selected and cultured for longer period of time in parallel mini flat panel PBR (expecting more FAME production). In this experiment, FAME was quantified for 10, 20, 30, 36, and 40 days. The experimental conditions in parallel mini flat panel PBR were as follows: 100 W cool white LED used as light source, photoperiod – 14 hr light:10 hr dark cycle, light intensity 1081 $\mu E/m^2/s$, 1 VVM air flow rate with 2% (v/v) CO_2, 80 ml working volume was used in each mini flat panel PBR chamber. Appropriate sample volume was collected in triplicates at every 48 hr interval for OD_{680} measurement, chlorophyll-a and carotenoid of the sample. Algal culture of 12 ml was collected after 10, 20, 30, 36 and 40 days from the start of the experiment to find the DCW and FAME of the sample.

5.3.4. Experiments in medium scale flat panel PBR using single stage and two stage strategy with optimal media

Optimized lipid media that produced highest FAME content and FAME production from selective micronutrient interactions in parallel mini flat panel PBR was used in single stage medium scale flat panel PBR. Optimized growth media proposed by Mahesh et al. was used in another medium scale flat panel PBR (Mahesh et al., 2019). Once the algal cells in the growth media reaches the stationary phase due to light limitation, the algal culture was collected and centrifuged at 3000 RPM for 5 minutes for a two stage experiment (Naira et al., 2019). In two stage, the concentrated algal biomass was resuspended in optimized lipid media without urea. The experimental conditions used in medium scale flat panel PBR (single stage and two stage) were as follows: 100 W cool white LED used as light source, photoperiod – 14 hr light:10 hr dark cycle, light intensity 1081 $\mu E/m^2/s$, 2 lpm air flow rate with 2% (v/v) CO_2,

2 l working volume. Appropriate sample volume was collected in triplicates at every 24 hr for OD_{680} measurement, chlorophyll-a and carotenoid of the sample. The samples were collected in triplicates at regular intervals for DCW measurement, FAME, free dry exopolysaccharide weight (DEW) and autoflocculation efficiency estimation.

5.3.5. Experiments in parallel mini flat panel PBR under high light intensity using two stage strategy

High cell density culture was obtained using optimized growth media and then it was centrifuged at 3000 RPM for 5 minutes and suspended as 0.5, 1.5, 5 g/l in optimized growth media without urea and optimized lipid media without urea in parallel mini flat panel PBR to find the effect of light intensity in varying biomass concentrations. Centrifugation speed was kept low (3000 RPM) to minimize shear stress. The experimental conditions were as follows: 50 W cool white LED used as light source, photoperiod – 14 hr light:10 hr dark cycle, light intensity 2162 $\mu E/m^2/s$, 1 VVM air flow rate with 2% (v/v) CO_2, 80 ml working volume was used in each parallel mini flat panel PBR. The algal samples were collected in triplicates at respective time intervals for DCW measurement and FAME quantification.

5.3.6. Experiments in medium scale flat panel PBR with optimum media under outdoor natural sunlight using single stage strategy

Optimized lipid media was used in single stage medium scale flat panel PBR under outdoor natural sunlight in the month of November - December 2020 at 26°11′03″ N (latitude) and 91°44′44″ E (longitude) in the Guwahati region, India. Sun generally rises at 5:45 am and sets at 4:30 pm in the Guwahati region during November - December 2020. Sunlight intensities (in $\mu E/m^2/s$) and culture temperature (°C) were taken every 30 minutes from dawn to dusk during the experiment. Process pH readings were monitored online by the OPTO22 control system. The experimental conditions were diurnal natural sunlight intensities from dawn to dusk, 2 lpm air flow rate with 2% (v/v) CO_2, 2 l working volume was used in medium scale

flat panel PBR. Appropriate sample volume was collected in triplicates every 12 hr for OD_{680} measurement. Chlorophyll-a and carotenoid of the sample were estimated every 24 hr. Samples were collected in triplicates at respective time intervals for DCW measurement, FAME, free DEW, autoflocculation rate and autoflocculation efficiency estimation.

5.3.7. Experiments in medium scale flat panel PBR with optimum media under high light intensity using single stage strategy

Optimized lipid media produced high FAME content in DCW under outdoor natural sunlight in all the experiments. Hence, this media was further explored for FAME and EPS production in single stage at high light intensity (2162 µE/m^2/s) as this microalgal strain showed no photoinhibition in the range of 2100 µE/m^2/s (Mahesh et al., 2019). The experimental conditions were as follows: 100 W cool white LED used as light source, photoperiod – 14 hr light:10 hr dark cycle, light intensity 2162 µE/m^2/s, 2 lpm air flow rate with 2% (v/v) CO_2, 2 l working volume was used in medium-scale flat panel PBR. Appropriate sample volume was collected in triplicates every 24 hr to find OD_{680}, chlorophyll-a, and carotenoid in the sample. Samples were collected in triplicates at respective time intervals for DCW measurement, FAME, free DEW and autoflocculation efficiency estimation.

5.4. Results and Discussion

5.4.1. Nutrient effect in single stage on FAME production

Minimal composition of nutrients in medium scale PBR resulted dry cell weight of 2.06 g/l at stationary phase (48 hr). Stationary phase was achieved just after 2 days due to less amount of nutrients availability in the media other than urea. Urea was almost consumed at the end of 144 hr (Fig 5.2A). The highest specific growth rate 3.16 day^{-1} was observed at the end of 1st day light period (14 hr) and decreases with culture age due to low nutrient levels and less light intensity available to the cells (Fig. 5.2A).

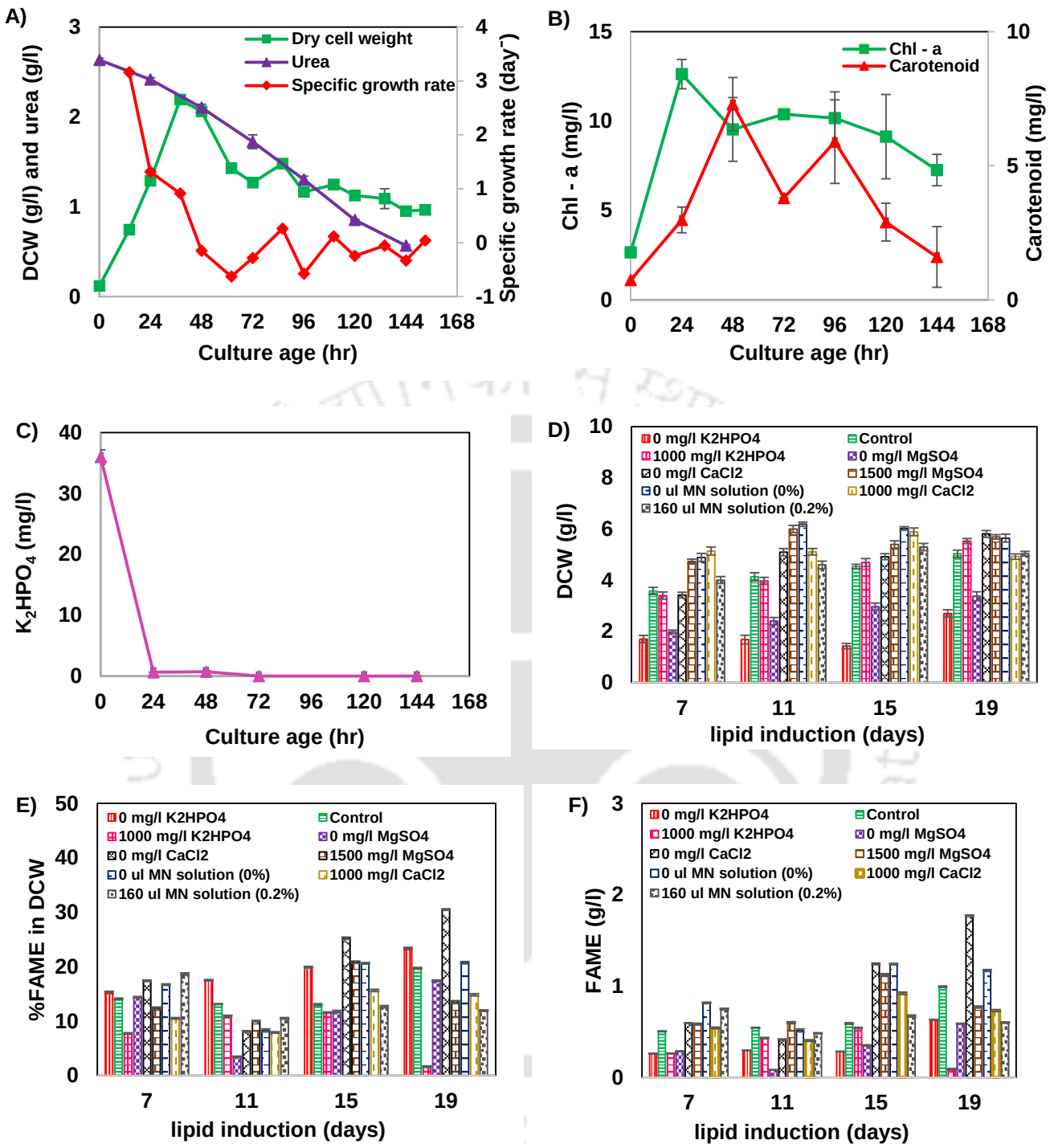

Fig. 5.2. Biomass growth in medium scale PBR and effect of nutrients in single stage parallel mini PBR for FAME production. **A)** DCW, urea and specific growth rate, **B)** Chl-a and carotenoid synthesis, **C)** K_2HPO_4 utilization, **D)** DCW profile, **E)** %FAME profile and **F)** FAME profile.

The maximum chlorophyll-a and carotenoid concentrations were 12.62 mg/l and 7.3 mg/l at 24 hr and 48 hr respectively (Fig. 5.2B). The chlorophyll-a and carotenoid levels were decreased in this study indicating the absence of sufficient amount of nutrients for microalgal

growth. Previous study by Mahesh et al. reported chlorophyll-a and carotenoid concentrations of 80 mg/l and 20 mg/l respectively using optimised growth media with same culture conditions in medium scale PBR (Mahesh et al., 2019). Extracellular K_2HPO_4 was totally consumed at 72 hr (Fig. 5.2C). Overall biomass yield with respect to urea and K_2HPO_4 were 3.67 g biomass/g urea and 55.17 g biomass/g K_2HPO_4 respectively at the end of growth phase (48 hr). DCW of 1.27 g/l with 15.6% FAME and 0.19 g/l FAME titer was achieved at 72 hr (data not shown). DCW of 5.8 g/l with maximum FAME content (30.5%) and 1.77 g/l FAME was obtained among studying the effect of nutrients in single stage in parallel mini flat panel PBR after 19 days of lipid induction when 0 mg/l $CaCl_2.2H_2O$ was used (Fig. 5.2D, 5.2E and 5.2F). Esakkimuthu et al. studied the effect of calcium on growth rate and lipid accumulation in *Scenedesmus obliquus* using Bold Basal medium under 100 µmol photons/m^2/s at 25 °C. They reported that there is only slight reduction in growth and 47.5% of lipid content (280% higher than the control conditions) in DCW in absence of Ca (II) (Esakkimuthu et al., 2016). K_2HPO_4 (0 mg/l) resulted in less DCW (2.7 g/l) whereas 1000 mg/l K_2HPO_4 resulted in less FAME (1.6%). Less DCW (3.37 g/l) was observed when 0 mg/l $MgSO_4$ was used (Fig. 5.2D, 5.2E and 5.2F).

5.4.2. Effect of macronutrients on lipid accumulation in *S. abundans*

Experiments of concentration variation of macronutrient (urea, K_2HPO_4, $MgSO_4.7H_2O$, $CaCl_2.2H_2O$) were performed in test tube PBR to find the effect of macronutrients on microalgae growth and lipid accumulation. At very low concentration of nutrients, less biomass growth was observed except $CaCl_2$ (Fig. 5.3). Growth inhibition has also been seen in the case of high K_2HPO_4 and $MgSO_4$ (Fig. 5.3B and 5.3C). Both FAME concentration and % of FAME in dry cell weight (DCW) are negligible in case of a very low concentration of urea (Fig. 5.3E). But at a higher titer of urea, the accumulation of FAME is 39% and FAME titer is 1.33 g/l at 20 days, though the accumulation started after exhaustion of urea (data not shown).

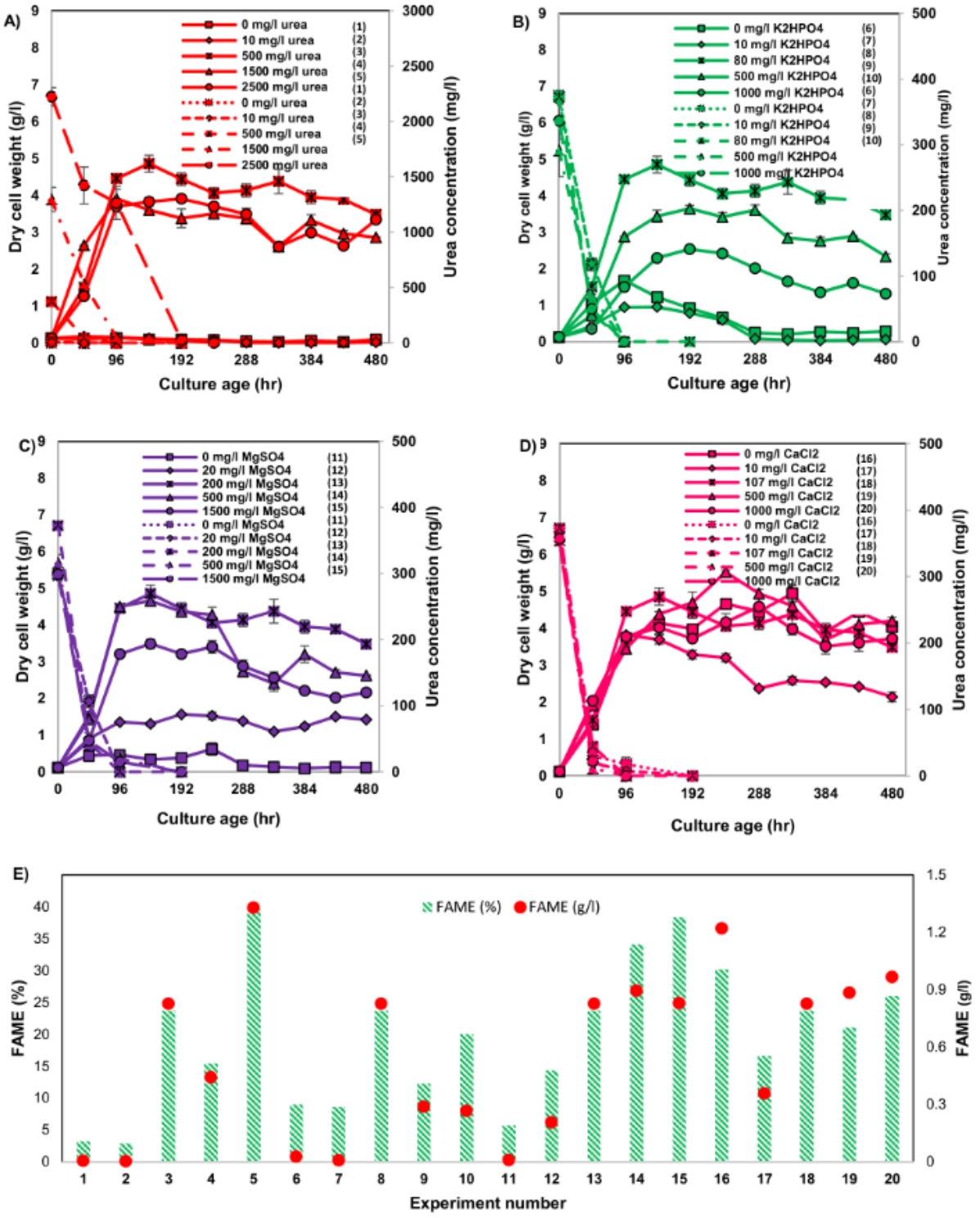

Fig. 5.3. Biomass growth, urea utilization and FAME profile of macronutrients in test tube PBR. **A)** urea, **B)** K_2HPO_4, **C)** $MgSO_4$, **D)** $CaCl_2$ and **E)** FAME profile of macronutrients at 20 days.

Even though the FAME accumulation is very high (32%) at the K_2HPO_4 limiting condition, FAME concentration (g/l) is very low due to less biomass growth at 20 days (Fig. 5.3B and Fig. 5.3E). Production of FAME was highest at 80 mg/l K_2HPO_4 (Fig. 5.3E). High

$MgSO_4$ can favor for high FAME content but the FAME concentration was not improved at high level of $MgSO_4$ due to growth inhibition (Fig 5.3C and and 5.3E). This significant rise in the percentage accumulation of lipid at high $MgSO_4$ concentration could be due to the fact that Mg ions help in activating acetyl-CoA carboxylase, catalyzing the first step of fatty acid biosynthesis (Nelson et al., 2008). Also, the chloroplast pyruvate dehydrogenase complex requires Mg ions for providing acetyl-CoA and NADH for fatty acid synthesis (Camp & Randall, 1985). $MgSO_4$ of 200 mg/l has been considered as optimum level based on the FAME titer (Fig. 5.3E). The limiting condition of $CaCl_2$ can improve both % of FAME as well as the titer (g/l) of FAME. $CaCl_2$ free media produces 1.2 g/l of FAME with 30% FAME content at 20 days (Fig. 5.3E). In previous study, it has also been shown that lipid accumulation in *Scenedesmus obliquus* in the N11 medium was highest (303.3 mg/l) at 18 days at calcium starvation condition (Gorain et al., 2013). Urea was almost consumed by the cells at the end of 96^{th} hr in all the macronutrient variation experiments except 1500 mg/l urea and 2500 mg/l urea (Fig. 5.3). It was observed that 1500 mg/l urea and 2500 mg/l urea were consumed completely at the end of 192 hr and 240 hr respectively (Fig. 5.3A). From the current study, it is clear that less urea, K_2HPO_4 and $MgSO_4$ concentrations resulted in less FAME whereas $CaCl_2$ free media resulted in high FAME. The optimum macronutrient composition (2500 mg/l urea, 80 mg/l K_2HPO_4, 200 mg/l $MgSO_4.7H_2O$, 0 mg/l $CaCl_2.2H_2O$) with varying concentration levels of micronutrient, H_3BO_3 and $MnCl_2$ were used for performing interaction experiments to further investigate their effect on microalgal FAME production.

5.4.3. Role of Boron, Manganese and other micronutrients on FAME production

Like macronutrients, some micronutrients can also affect microalgae growth and lipid accumulation. Micronutrients such as H_3BO_3 (1000 X), $MnCl_2.4H_2O$ (1000 X) and other micronutrients pool (MN, stock: $CoCl_2.2H_2O$: 1000 X, $ZnSO_4.7H_2O$: 1000 X, $CuSO_4.5H_2O$: 1000 X, $Na_2MoO_4.2H_2O$: 1000 X) have been chosen to check the effect on FAME production.

H_3BO_3 and $MnCl_2.4H_2O$ micronutrients have been chosen separately as they are present in high quantities in modified Chu-13 media. To check the effect of micronutrients, one at a time variation experiments were carried out. $MnCl_2$ and other micronutrient pool-free media produces very less biomass whereas growth limitation was not observed in H_3BO_3 free media (Fig. 5.4A, 5.4B and 5.4C). Though growth inhibition was observed at higher concentration of other micronutrients pool, but FAME titer was increased to 0.9 g/l at 10 days (Fig 5.4A and 5.4D). Similarly, growth was also hampered at higher concentration of $MnCl_2$, H_3BO_3 (Fig. 5.4B and 5.4C). The optimum level of H_3BO_3 and $MnCl_2$ is 0.5% for both the nutrient (Fig. 5.4D). Rocha et al. suggested that the addition of trace elements improves neutral lipid storage in *Scenedesmus* spp (Rocha et al., 2019).

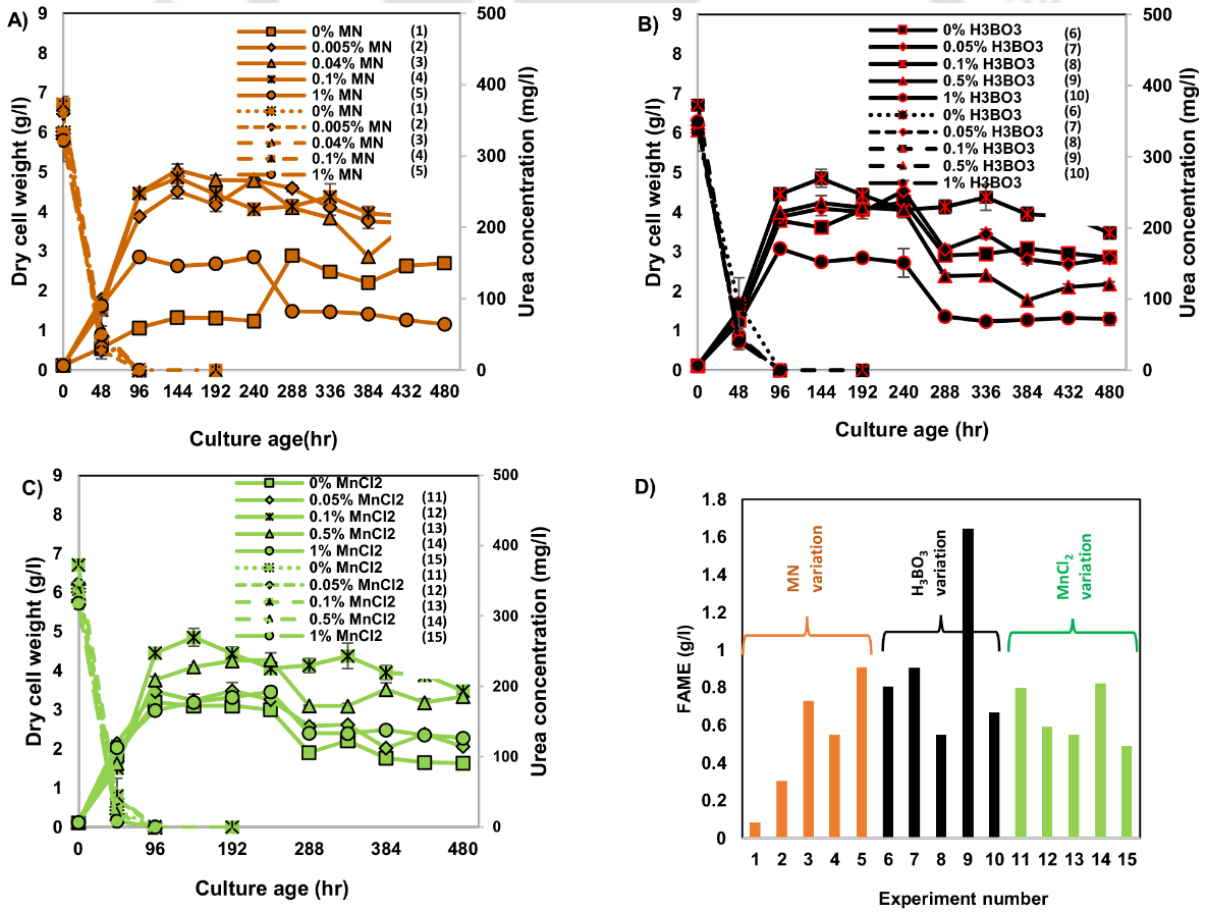

Fig. 5.4. Biomass growth, urea utilization and FAME profile of micronutrients in test tube PBR. **A)** micronutrients pool, **B)** H_3BO_3, **C)** $MnCl_2$ and **D)** FAME profile of micronutrients at 10 days.

For further improvement in lipid production, micronutrient interaction experiments was carried out with boron where H_3BO_3 was varied from 0.25 % (v/v) to 0.75 % (v/v) and for manganese, $MnCl_2.4H_2O$ was varied from 0.2 % (v/v) to 0.8 % (v/v) of stock solutions. Other micronutrients pool was varied from 0.5 % (v/v) to 1.5 % (v/v). To check the interaction, experiments with all possible combinations of different concentrations of H_3BO_3, $MnCl_2.4H_2O$ and other micronutrients pool were carried out with optimum levels of macronutrients (Refer **Section 5.4.2** for optimum levels of macronutrient).

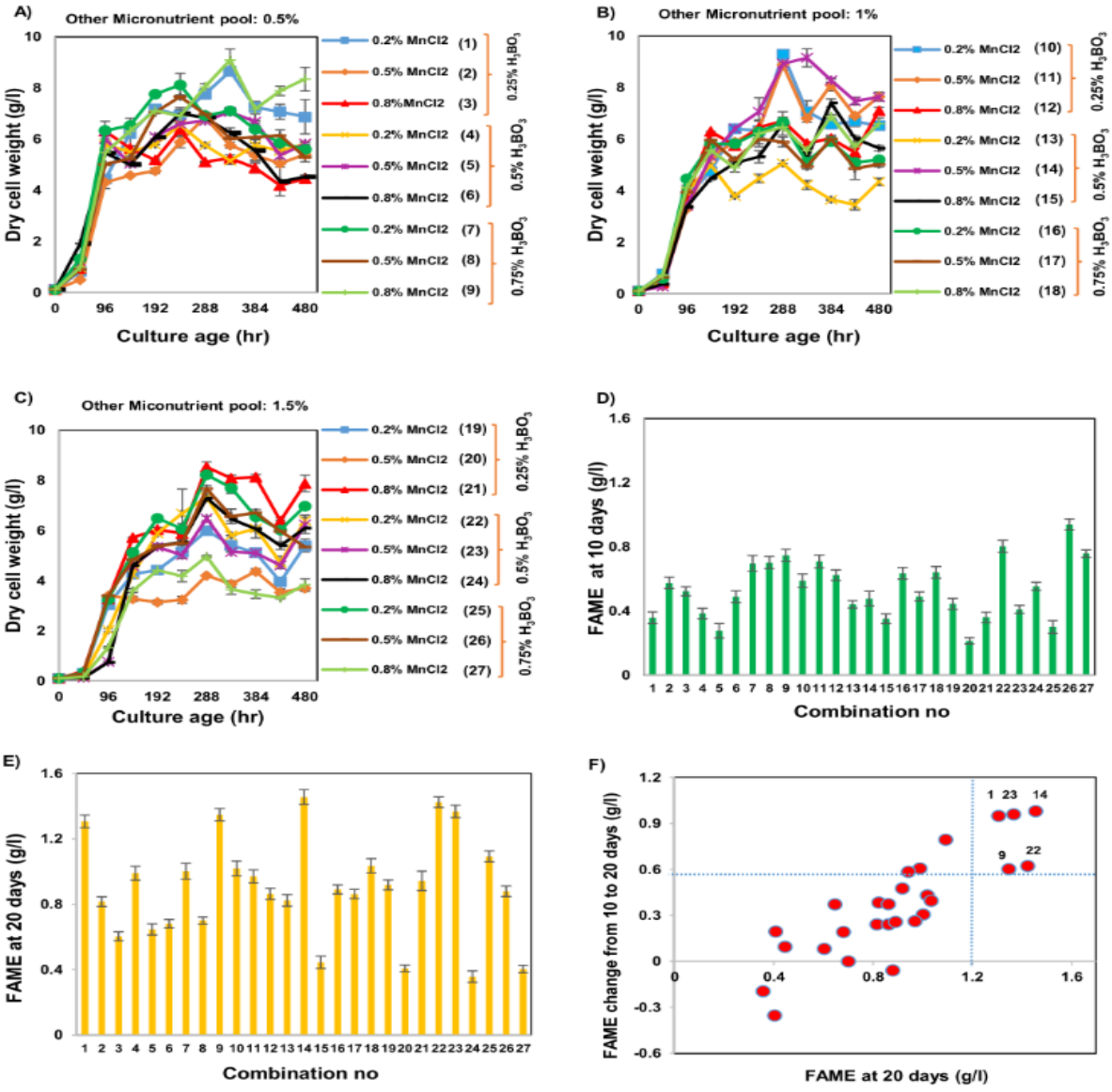

Fig. 5.5. DCW and FAME profile of micronutrient interaction. DCW of **A)** 0.5% MN, **B)** 1% MN, **C)** 1.5% MN with different H_3BO_3 and $MnCl_2$, FAME at **D)** 10 days, **E)** 20 days of MN interaction, **F)** FAME change from 10 to 20 days.

Some of the interaction experiment combinations can produce more than 8 g/l of dry biomass (DCW) (Fig. 5.5A) and several interaction experiment combinations have more than 7 g/l of biomass production (Fig. 5.5A, 5.5B and 5.5C). This could be due to the presence of higher concentrations of micronutrients with a high amount of urea in the media. The maximum production of FAME was 1.45 g/l with 0.5% boron, 0.5% manganese and 1% other micronutrients pool which is higher than the production in macronutrient variation experiments (Fig 5.5E). It has been noted that a significant amount of FAME has been increased in several combinations from 10 days to 20 days old culture (Fig. 5.5D and 5.5E). Based on FAME concentration (>1.2 g/l) and FAME increment (>0.6 g/l), several combinations have been selected for further improvement assuming the chances of more increment in a longer period (Fig. 5.5F).

5.4.4. Selective micronutrient interactions for FAME production in parallel mini flat panel PBR

Five selected combinations based on concentration of FAME and improvement of FAME concentration from 10 to 20 days in test tube PBR were considered and cultivated for longer period to find the best nutrient recipe in parallel mini PBR. Parallel mini PBR (light path length: 25.4 mm) were used instead of test tube PBRs (light path length: 16 mm) for this study because finally 2 l flat panel PBR with the same light path length will be used for the scale-up study. The stationary phase was observed at 192 hr in all combinations. Increment in biomass concentration was observed in a later stage due to the accumulation of lipid. The highest DCW of 4.7 g/l was achieved at 576 hr in media combination with 1% micronutrient pool, 0.5% H_3BO_3, 0.5% $MnCl_2$ whereas low biomass titer was observed when a lower concentration of H_3BO_3 (0.25%) was used (Fig. 5.6A). The maximum biomass concentration in this reactor was lesser than test tube PBR as the light path length is higher in parallel mini flat panel PBR than that of test tube PBR.

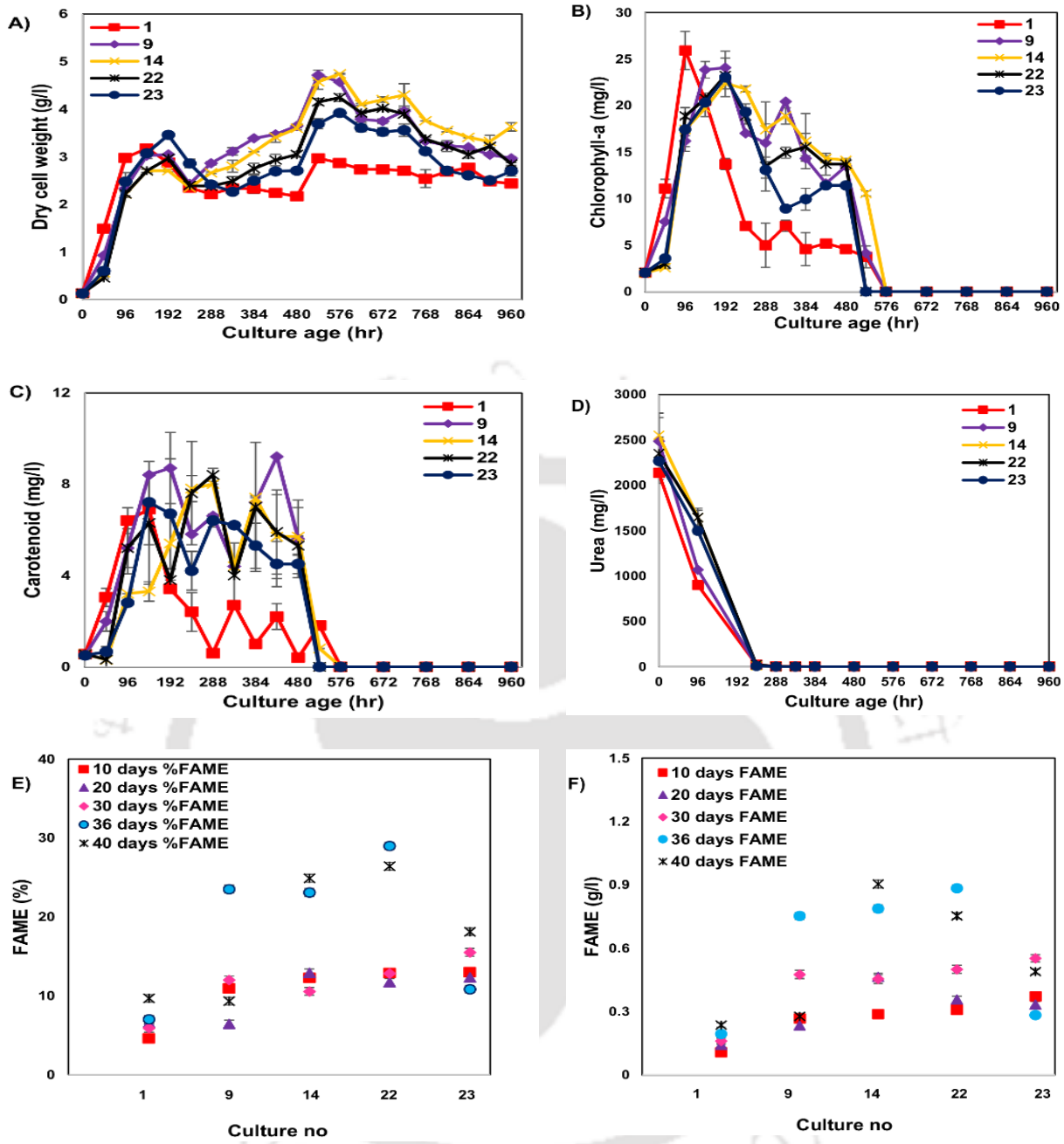

Fig. 5.6. Biomass growth, urea utilization and FAME profile of selective micronutrient interactions in parallel mini PBR. **A)** DCW profile, **B)** Chlorophyll–a profile, **C)** Carotenoid profile, **D)** Urea utilization profile, **E)** FAME content in DCW and **F)** FAME profile. The culture number were same as Fig. 5.5.

The chlorophyll-a and carotenoid concentrations reached a maximum at the end of 192 hr and then starts decreasing and finally became zero for all the experiments (Fig. 5.6B and 5.6C). Urea concentration decreases gradually and became zero at 240 hr (Fig. 5.6D). The nutrient combination with 1.5% micronutrient pool, 0.5% H_3BO_3 and 0.2% $MnCl_2$ (combination 22) produce the highest FAME (~30%) and 0.9 g/l FAME at 36 days among all

other experiments (Fig. 5.6E and 5.6F) and therefore this media was used as optimized lipid media. Note that media having combination 14 also produced 0.9 g/l FAME with 25% of FAME at 40 days.

5.4.5. Production of FAME and EPS using single stage and two stage strategies in medium scale flat panel PBR

To check the production capability, experiments was performed autotrophically with optimized lipid media (22nd combination in **Section 5.4.3** and **Section 5.4.4**: 2500 mg/l urea, 80 mg/l K_2HPO_4, 200 mg/l $MgSO_4.7H_2O$, 0 mg/l $CaCl_2.2H_2O$, 20 mg/l ferric citrate, 100 mg/l citric acid, 0.5 % of 1000X H_3BO_3, 0.2 % of 1000X $MnCl_2.4H_2O$ and 1.5 % of 1000X other micronutrients pool) in 2 l medium-scale flat panel PBR. A two stage experiment (optimized growth media followed by nitrogen deprived optimized lipid media) was also carried out in medium scale PBR. A maximum DCW of 4.25 g/l at 768 hr and 8.7 g/l at 720 hr were observed in single stage and two stage respectively (Fig. 5.7A). Overall biomass productivity of 0.48 g/l/day was observed at the end of the growth phase (120 hr) in a single stage. Maximum chlorophyll-a and carotenoid concentrations were 37 mg/l and 10 mg/l in a single stage at the end of 96 hr respectively. Similarly, the highest chlorophyll-a and carotenoid concentrations were 97 mg/l and 33 mg/l in two stage at the end of 216 hr respectively (Fig. 5.7B and 5.7C). Urea was consumed completely and became zero at 264 hr in single stage (Fig. 5.7D). Overall biomass yield with respect to urea was 2.0 g biomass/g urea in growth phase (120 hr) in single stage whereas in the two stage, overall biomass yield with respect to urea was 3.15 g biomass/g urea in growth phase before transferring in urea free media (216 hr). K_2HPO_4 was consumed at 96th hr with biomass yield of 39.82 g biomass/g K_2HPO_4 in single stage whereas in two stage, K_2HPO_4 was exhausted at 72 hr with biomass yield of 10.65 g biomass/g K_2HPO_4. FAME concentration of 1.16 g/l FAME with 32% FAME content in microalgae was achieved at the end of 864 hr (Fig. 5.7E). The overall FAME productivity was 32 mg/l/day.

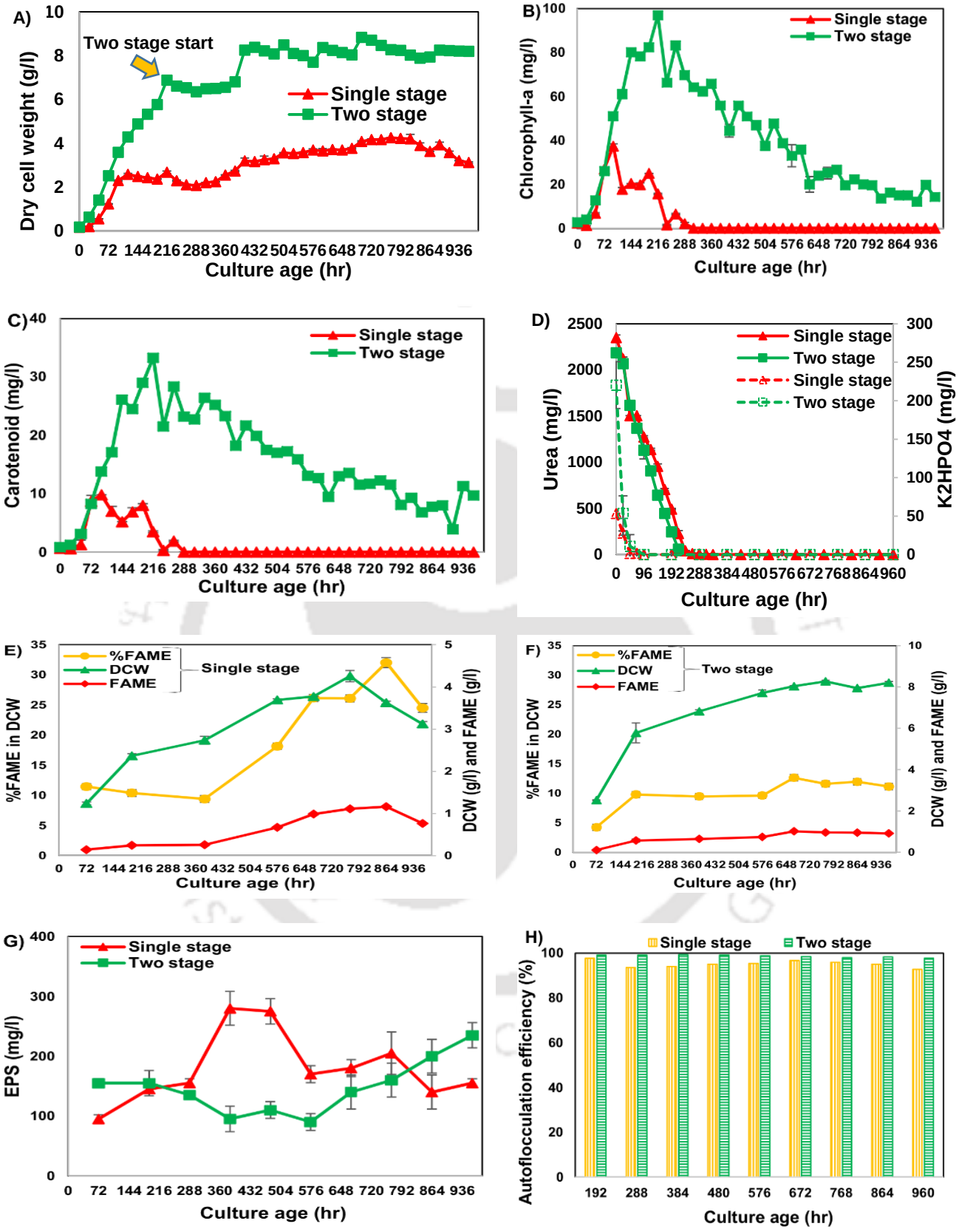

Fig. 5.7. Biomass growth, FAME and EPS profile of single stage and two stage strategies in medium scale PBR. **A)** DCW, **B)** Chlorophyll–a, **C)** Carotenoid, **D)** Urea and K_2HPO_4 profile, **E)** DCW and FAME profile of single stage, **F)** DCW and FAME profile of two stage, **G)** EPS profile and **H)** Autoflocculation efficiency.

DCW of 8.03 g/l with the highest %FAME (12.61%) and 1.01 g/l FAME were obtained at the end of 672 hr in two stage studies (Fig. 5.7F). The FAME content using single stage strategy was 2.5 fold higher than that of the FAME content in the two stage. This is because the nutrient concentrations and environmental conditions in the culture media in single stage collectively contribute towards lipid enrichment. Maximum EPS titer of 280 mg/l was obtained with a yield of 102 mg EPS/g biomass at the end of 384 hr in single stage where the highest EPS concentration of 235 mg/l was achieved at the end of 960 hr in two stage (Fig. 5.7G). Autoflocculation efficiency of 98-99% was observed at different culture age for both single and two stage cultivation system (Fig. 5.7H). Similarly, Yeh and Chang reported that the two stage starvation strategy did not work well in improving lipid production of *C. vulgaris* ESP-31 (Yeh & Chang, 2011).

5.4.6. FAME analysis of varying biomass concentration with high light intensity and media interaction using two stage

To find the effect of light intensity in varying biomass concentrations in two stage, experiments were performed with varying biomass concentration (0.5 g/l, 1.5 g/l, 5 g/l) in nitrogen deprived optimized growth media (MG) and nitrogen deprived optimized lipid media (ML) at 2162 µE/m^2/s light intensity. FAME content in DCW was found to be 6.47% before varying biomass concentrations (data not shown). Biomass concentrations (0.5 g/l, 1.5 g/l and 5 g/l) in MG media produced FAME content (16.44%, 16.65%, 20.97%) at 35 days of lipid induction (Fig. 5.8B). The biomass concentrations 0.5 g/l, 1.5 g/l, 5 g/l using MG media decreased to 0.1 g/l, 0.54 g/l and 1.68 g/l (Fig. 5.8A). This may be due to 1 g/l K_2HPO_4, 1.5 g/l $MgSO_4.7H_2O$ and 1 g/l $CaCl_2.2H_2O$ in the media causing substrate inhibition. The %FAME in DCW increases with decrease in DCW from 10 to 35 days of lipid induction due to adequate light availability. The same biomass concentrations 0.5 g/l, 1.5 g/l, 5 g/l biomass concentrations in ML media contributed to maximum FAME content (16.05%, 20.83%, 18.38%) (Fig. 5.8B).

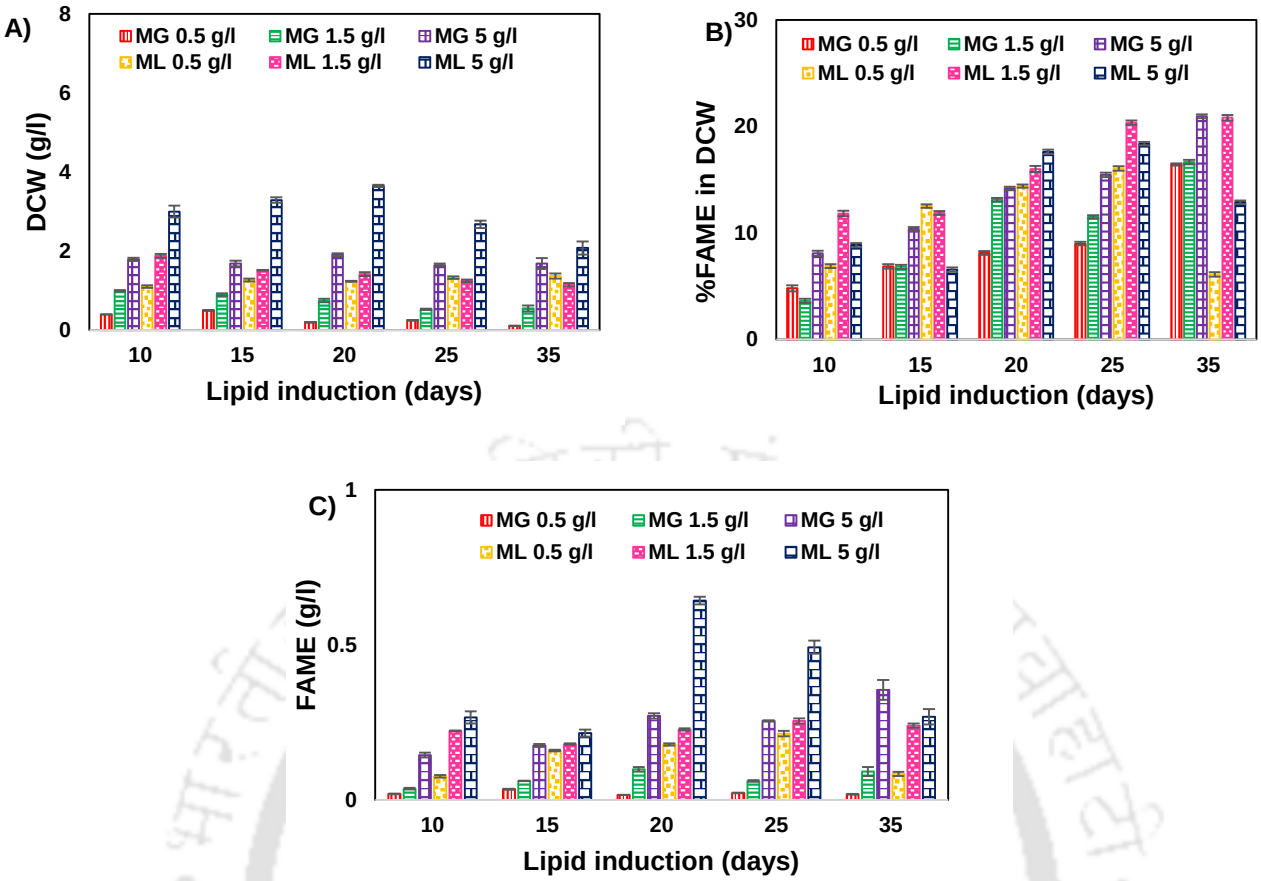

Fig. 5.8. Biomass growth and FAME profile of two stage strategy in parallel mini PBR at 2162 µE/m^2/s. **A)** DCW profile, **B)** FAME content in DCW profile and **C)** FAME profile of varying biomass concentration.

Biomass concentration (0.5 g/l) increased to 1.36 g/l whereas 1.5 g/l and 5 g/l biomass concentrations decreased to 1.14 g/l and 2.07 g/l respectively using ML media (Fig. 5.8A). FAME content in DCW in two stage depicted just a marginal rise as FAME content before nitrogen starvation was 6.47%. Moreover, these two stage experiments produced less FAME content in DCW as well as FAME concentration when compared to single stage even at 2162 µE/m^2/s (Fig. 5.8B and 5.8C).

5.4.7. Production of FAME and EPS using optimum media in medium scale flat panel PBR under diurnal natural sunlight using single stage

To check the lipid and EPS production capability and autoflocculation efficiency at outdoor condition, *S. abundans* was cultivated with optimized lipid media in medium scale PBR using single stage strategy. Sunlight intensities and culture temperature from dawn to

dusk are noted during the cultivation period (Fig. 5.9A). A biomass titer of 2.95 g/l with overall biomass productivity of 0.31 g/l/day was achieved at the end of the growth phase (216 hr) (Fig. 5.9B). The overall specific growth rate was found to be 0.36 day^{-1} at the end of the growth phase (Fig. 5.9B). A maximum DCW of 3.36 g/l was achieved at the end of 936 hr. Maximum chlorophyll-a and carotenoid concentrations were 44 mg/l and 14 mg/l (Fig. 5.9C). Urea was exhausted completely at 432 hr with biomass yield of 0.88 g biomass/g urea (Fig. 5.9B). Extracellular K_2HPO_4 was utilized rapidly and consumed completely at 48 hr with biomass yield of 12.62 g biomass/g K_2HPO_4 (Fig. 5.9E). A maximum EPS concentration of 155 mg/l was observed at 816 hr (Fig. 5.9E). Biomass titer of 2.8 g/l with 46% FAME content in DCW and 1.28 g/l FAME were achieved after 28 days of nitrogen starvation with FAME productivity of 27 mg/l/day (Fig. 5.9D). In Comparison to indoor study at 1081 µE/m^2/s artificial LED light (Refer **Section 5.4.5**), outdoor cultivation produced higher FAME content (%) and FAME titer (g/l) with marginal decrease in FAME productivity (mg/l/day) using *S. abundans* (Fig. 5.7E and 5.9D). Chen et al. studied outdoor cultivation of *Chlorella vulgaris* ESP-31 in 50 l vertical tubular type photobioreactor for lipid production. In their study, 44% lipid content and 0.7 g/l lipid concentration with lipid productivity of 26 mg/l/day were achieved (Chen et al., 2014). In another study, 0.95 g/l DCW of *Chlorella* sp.1 with 20% lipid was achieved using optimized BG-11 media in a bubble column photobioreactor under sunlight. The biomass productivity, lipid concentration and lipid productivity obtained in their study were 53 mg/l/day, 190 mg/l and 10 mg/l/day respectively (Sharma et al., 2016). The present study reported 1.28 g/l of FAME with 27 mg/l/day of FAME productivity which is higher than the above mentioned studies. In the current study, the process pH profile depicted in Fig. 5.9F showed a rise in pH in the growth phase and a decrease in nitrogen starvation condition. Autoflocculation was monitored and cells settled with a high autoflocculation efficiency where 322.8 OD_{680} was achieved from initial OD_{680} of 11.3 after 30 hrs (data not shown).

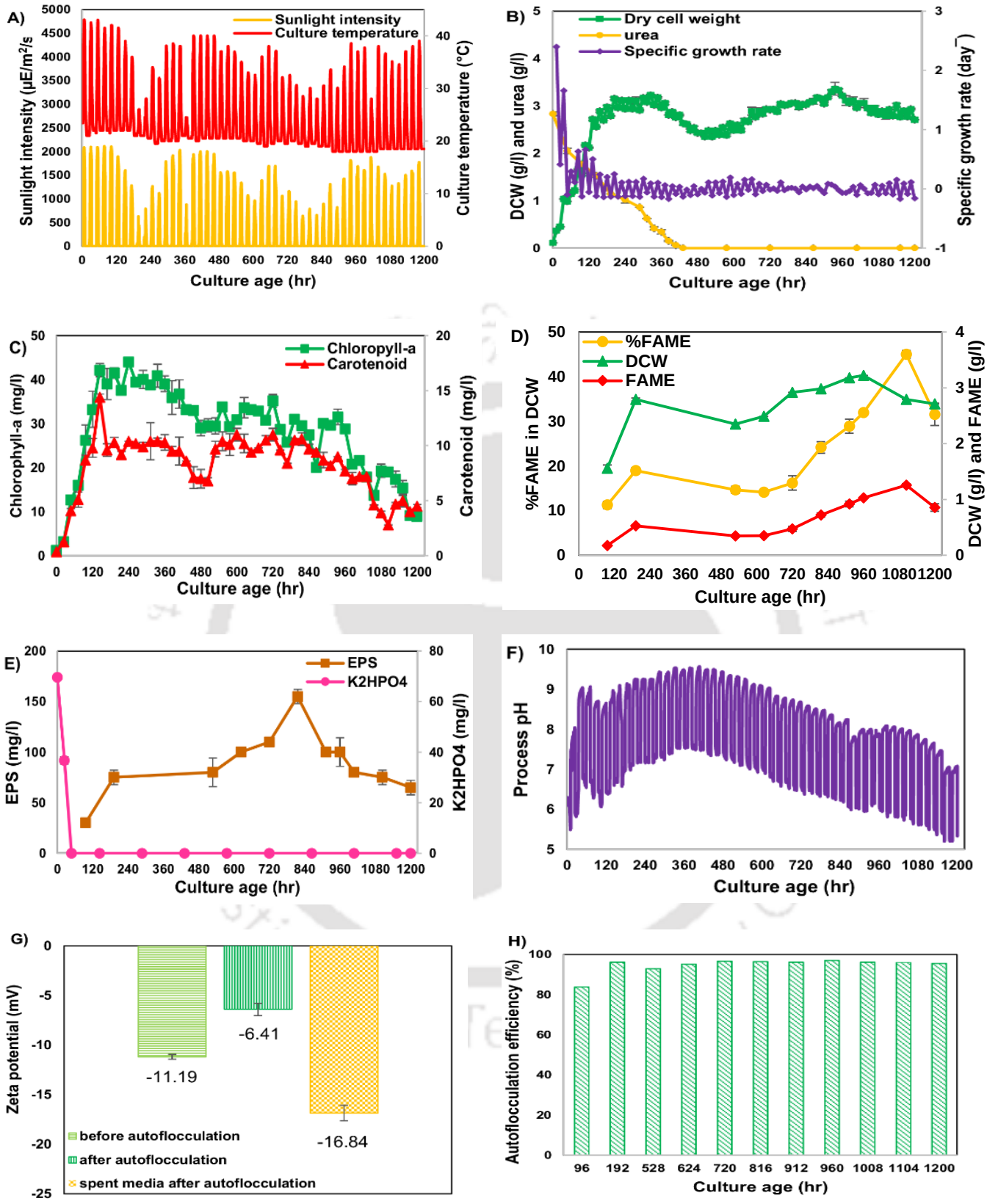

Fig. 5.9. Biomass growth, FAME and EPS profile in medium scale PBR under outdoor natural sunlight. **A)** Sunlight intensity, culture temperature, **B)** DCW, urea utilization, specific growth rate **C)** Chlorophyll-a and carotenoid synthesis, **D)** DCW, FAME content in DCW, FAME, **E)** EPS and K_2HPO_4 profile, **F)** Process pH, **G)** Zeta potential, **H)** Autoflocculation efficiency.

Note that there was no difference in % FAME for biomass without autoflocculation and autoflocculated biomass after 30 hrs. Autoflocculation efficiency of 84-97 % was achieved at different culture age (Fig. 5.9H). Thus, the natural autoflocculation of *S. abundans* make the biodiesel production economical by lowering the harvesting cost. EPS was responsible for natural autoflocculation confirmed from zeta potential without pH adjustments (Fig. 5.9G). pH of microalgal culture sample in 5 ml centrifuge tube before autoflocculation was 6.5. A significant reduction in zeta potential to a value of -6.41 mV for autoflocculated biomass as compared to biomass before autoflocculation (-11.19 mV) and spent media after autoflocculation (-16.84 mV) indicates charge neutralization that contributes to natural autoflocculating ability of *S. abundans* (Fig. 5.9G). This suggests that free EPS produced by *S. abundans* binds to algal cells creating flocs and giving rise to natural autoflocculation. The glycoproteins present in free EPS are patched to microalgal cell surfaces through a charge neutralization mechanism. Salim et al. studied that autoflocculation of *E. texensis* is due to the EPS containing glycoproteins patched to the cell surface (Salim et al., 2014).

5.4.8. Production of FAME and EPS using optimum media in medium scale flat panel PBR under high light intensity using single stage

To check the production capability of FAME, EPS and autoflocculation efficiency, experiment was performed with optimized lipid media in medium scale PBR at 2162 $\mu E/m^2/s$ in single stage. A biomass titer of 2.41 g/l with overall biomass productivity of 0.57 g/l/day was achieved at growth phase (96 hr) under high light (Fig. 5.10A). The overall specific growth rate was found to be 0.75 day^{-1} at the end of the growth phase (96 hr). The highest DCW of 4.37 g/l was observed at 696 hr. Maximum chlorophyll-a and carotenoid concentrations were 33 mg/l and 11 mg/l (Fig. 5.10B). A previous study by Mahesh et al. reported chlorophyll-a and carotenoid concentrations of 80 mg/l and 20 mg/l respectively using optimized growth media with the same culture conditions in medium scale PBR (Mahesh et al., 2019).

Table 5.1. Comparison of biomass, FAME and EPS by *S. abundans* in single stage and two stage at different light intensities[a].

Stage/light intensity	Growth (days)	Nitrogen starvation (days)	Biomass (growth phase) (g/l)	Biomass productivity (growth phase) (g/l/day)	Biomass (g/l) with max.%FAME	Maximum FAME content (% of DCW)	FAME (g/l)	Overall FAME productivity (mg/l/day)	Maximum EPS (mg/l)	Overall EPS productivity (mg/l/day)	EPS yield (mg/g biomass)
Single stage[b] at 1081 µE/m^2/s (medium scale PBR)	5	25	2.58 ± 0.04	0.48 ± 0.007	3.62 ± 0.03	32 ± 0.84	1.16 ± 0.019	32 ± 0.53	280 ± 28	17.5 ± 1.76	102 ± 6.9
Single stage[b] at diurnal natural sunlight (medium scale PBR)	9	28	2.95 ± 0.01	0.31 ± 0.001	2.79 ± 0.00	46 ± 0.84	1.28 ± 0.02	27 ± 0.51	155 ± 7	4.5 ± 0.2	52 ± 2.37
Single stage[b] at 2162 µE/m^2/s (medium scale PBR)	4	21	2.41 ± 0.01	0.57 ± 0.004	3.47 ± 0.05	58 ± 0.49	2.01 ± 0.01	61 ± 0.47	160 ± 0	6 ± 0	39 ± 1.22
Two stage[c] at 1081 µE/m^2/s (medium scale PBR)	9	19	6.87 ± 0.05	0.74 ± 0.005	8.03 ± 0.02	12.61 ± 0.54	1.01 ± 0.04	36 ± 1.43	235 ± 21	6 ± 0.53	29 ± 2.81
Two stage[c] at 2162 µE/m^2/s (5 g/l biomass in parallel mini PBR)	NM	25	NM	NM	2.67 ± 0.09	18.38 ± 0.16	0.49 ± 0.02	20 ± 0.85	ND	ND	ND

NM: not mentioned; ND: not determined

a) Experimental data were presented as mean ± standard deviation of duplicate experiments and triplicate samples.

b) Optimized lipid media was used in single stage (nitrogen starvation naturally occurred without transferring to another medium).

c) Optimized growth media was used for growth followed by optimized lipid media without urea in two stage.

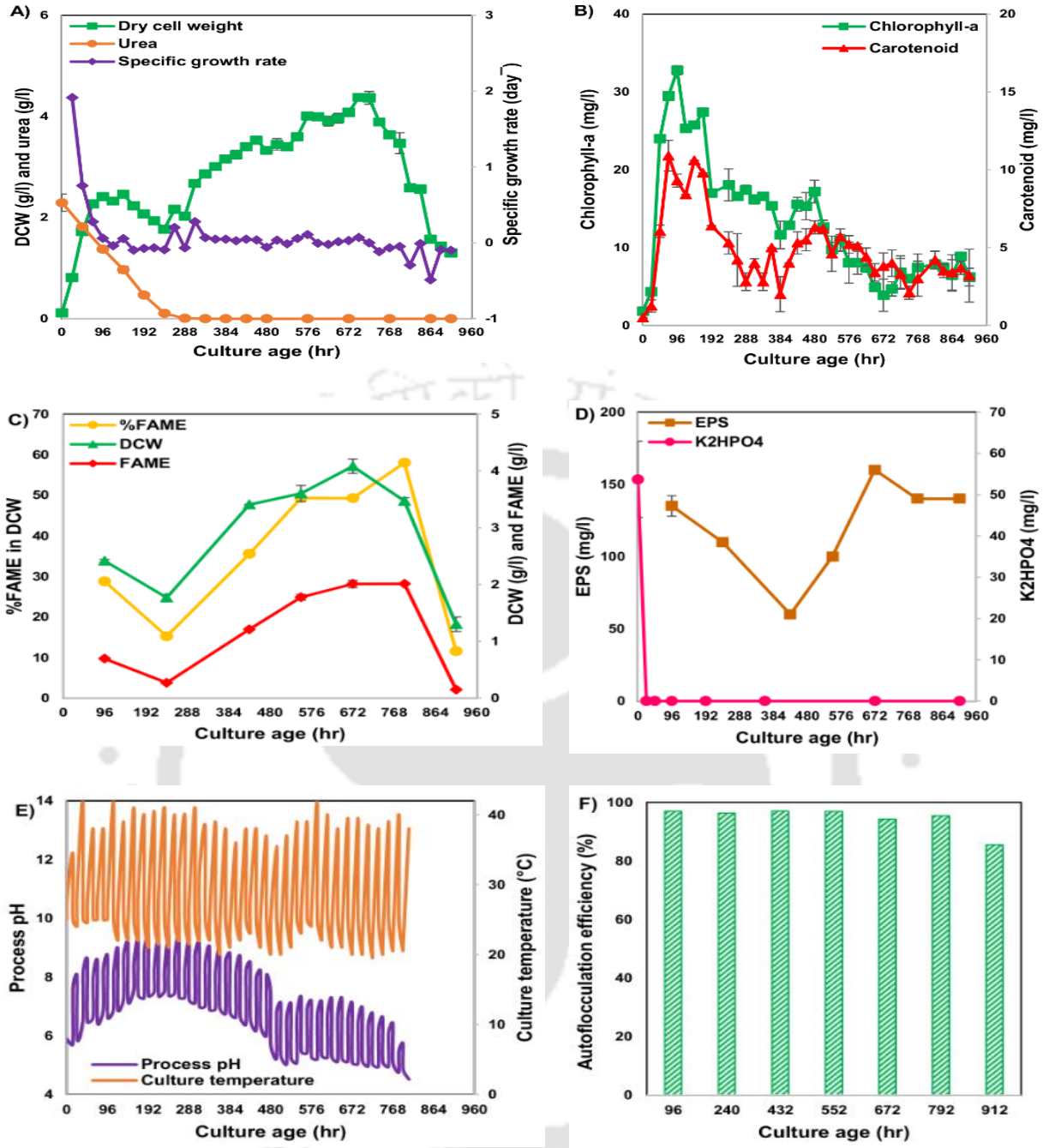

Fig. 5.10. Biomass growth, FAME and EPS profile in medium scale PBR at 2162 µE/m^2/s. **A)** DCW profile, urea utilization, specific growth rate, **B)** Chlorophyll-a and carotenoid synthesis, **C)** DCW, FAME content in DCW, FAME, **D)** EPS and K_2HPO_4 profile, **E)** Process pH, culture temperature, **F)** Autoflocculation efficiency.

Urea was consumed completely at 288 hr (Fig. 5.10A). Overall biomass yield with respect to urea was 0.83 g biomass/g urea. K_2HPO_4 was consumed at the end of 24 hr (Fig. 5.10D) and the overall biomass yield with respect to K_2HPO_4 was 12.87 g biomass/g K_2HPO_4. A maximum EPS concentration of 160 mg/l was observed at the end of 672 hr (Fig. 5.10D).

Table 5.1 shows the comparison of biomass, FAME and EPS production by *S. abundans* in single stage and two stage at different light intensities as well as diurnal natural sunlight. DCW of 3.47 g/l with the highest %FAME (58%) and 2.01 g/l FAME were achieved at 792 hr under high light (Fig. 5.10C, Table 5.1). The overall FAME productivity was 61 mg/l/day. Doubling the light intensity from 1081 µE/m^2/s to 2162 µE/m^2/s in single stage almost doubled the FAME content in DCW from 32% to 58% in the medium scale PBR (Fig 5.7E and Fig 5.10C). The %FAME in DCW and FAME titer achieved in this study was 2.63 fold and 1.31 fold higher than that of the previous study with the same experimental conditions reported by Mahesh et al (Mahesh et al., 2019). Liu et al. cultivated *Scenedesmus* sp. 11-1 and reported 3.88 g/l biomass titer with 32.9% neutral lipid content was achieved at the end of 12 days. The final neutral lipid yield and productivity were 1.28 g/l and 107 mg/l/day (Liu et al., 2012b). Note that the cultivation photobioreactor (column PBR) and sparging system were different in their study. Low light and large diameter of the column photobioreactor could be the reason for less neutral lipid content in their study. In another study of lipid production by an indigenous microalga *Scenedesmus obliquus* CNW-N, the lipid content in DCW increased from 11.48% to 22.4% at the end of 9 days where the biomass productivity and lipid productivity were 626.6 mg/l/day and 140.4 mg/l/ day respectively (Ho et al., 2012). In the present study, triggering lipid content in microalgae by low nutrient levels hinders biomass growth to a certain extent. Optimized lipid media would be responsible for lipid production at high light intensity (2162 µE/m^2/s). Therefore, it is concluded that lipid content in microalgae increases by the synergistic effect of nutrient levels, specific light availability per cell due to high light intensity and environmental conditions (process pH and culture temperature) in the culture media. The process pH and culture temperature profile depicted in Fig. 5.10E showed a rise at the end of the growth phase (96 hr). Process pH decreased during nitrogen deprivation. Autoflocculation efficiency of 94-97% was achieved at different culture age except at 912 hr (Fig. 5.10F).

5.4.9. Assessment of biodiesel quality from *S. abundans*

Biodiesel quality was measured for the highest %FAME content in DCW samples for the single stage cultivation with 1081 µE/m^2/s (864 hr), and diurnal natural sunlight (1104 hr) and 2162 µE/m^2/s (792 hr) in medium scale PBR. The percentage of each FAME in DCW, each FAME in total FAME, % SFA (saturated fatty acid), % MUFA (monounsaturated fatty acid), and % PUFA (polyunsaturated fatty acid) composition were listed in Table 5.2. FAME quantification by gas chromatography revealed the abundance of methyl esters of palmitate and linoleate (trans and cis) as compared to other FAME proving the capability of this strain for good quality biodiesel production. Methyl esters of C_{16} and C_{18} fatty acids constitute 98% of total FAME. The SV, IV, CN, DU, LCSF, CFPP, CP, PP, OSI, HHV, Density, Kinematic viscosity and FP values of biodiesel were also listed in Table 5.2. These values were close to ASTM D6751-12 and EN 14214 standards which indicates the feasibility of using the biodiesel produced by *S. abundans* in automobiles (Knothe, 2012). This renewable energy crop *S. abundans* despite synthesizing high oil yield in less land as compared to other conventional oil crops, it has also proved its nature in terms of biodiesel quality. Cetane number is an important biodiesel property that is highly influenced by SFA and MUFA profiles and increases with the length of the fatty acid chain. A high cetane value indicates better combustion, low nitrous oxide (NO_x) emissions into the atmosphere and easier engine start-up. The CN values of methyl esters of sunflower oil and soybean oil were 49 and 45 respectively (Shereena & Thangaraj, 2009). The CN values from *S. abundans* obtained in the current study were 48.81 ± 0.04, 44.82 ± 0.06 and 45.28 ± 0.08 at 1081 µE/m^2/s, diurnal natural sunlight and 2162 µE/m^2/s respectively in single stage medium scale PBR.

Table 5.2. Biodiesel composition and properties of *S. abundans* in single stage medium scale PBR at 1081 µE/m^2/s (864 hr), Diurnal natural sunlight (1104 hr) and 2162 µE/m^2/s (792 hr).

FAME	1081 µE/m^2/s		Diurnal natural sunlight		2162 µE/m^2/s	
	%FAME in DCW	%FAME in total FAME	%FAME in DCW	%FAME in total FAME	%FAME in DCW	%FAME in total FAME
C12:0	0.04	0.11	0.07	0.16	0.04	0.07
C14:0	0.14	0.45	0.12	0.26	0.09	0.15
C15:0	-	-	0.10	0.22	0.07	0.12
C15:1	0.08	0.24	0.08	0.17	0.06	0.10
C16:0	9.50	30.23	8.03	17.61	11.12	19.29
C16:1 cis	-	-	0.48	1.05	0.57	0.99
C16:1 trans	0.42	1.35	4.15	9.10	3.28	5.69
C16:2 cis	0.71	2.27	1.01	2.22	0.67	1.17
C16:2 trans	0.28	0.91	0.08	0.16	0.04	0.07
C16:3 cis	0.06	0.19	0.05	0.12	0.03	0.06
C16:3 trans	-	-	0.07	0.16	0.05	0.08
C17:0	0.22	0.68	0.34	0.75	0.33	0.57
C17:1	0.22	0.68	0.47	1.05	0.37	0.64
C17:2 cis	0.03	0.10	0.55	1.20	0.07	0.12
C17:2 trans	0.05	0.16	0.28	0.62	0.23	0.41
C18:0	0.88	2.82	0.68	1.49	1.19	2.07
C18:2 cis	12.81	40.77	8.28	18.16	12.99	22.52
C18:2 trans	5.93	18.87	20.20	44.30	26.35	45.69
C18:3	0.01	0.06	0.55	1.20	0.09	0.17
C20:0	0.02	0.06	-	-	0.01	0.02
C20:1	0.01	0.05	-	-	-	-
∑ C16-C18	30.60	97.47	43.58	95.57	56.38	97.8
SFA	10.80	34.35	9.34	20.49	12.85	22.29
MUFA	0.73	2.32	5.18	11.37	4.28	7.42
PUFA	19.88	63.33	31.07	68.14	40.52	70.29
FAME	31.41	100.00	45.59	100.00	57.65	100.00

Biodiesel property	***value***	***value***	***value***
SV	196.55 ± 0.01 mg KOH g^{-1} oil	196.15 ± 0.01 mg KOH g^{-1} oil	195.17 ± 0.02 mg KOH g^{-1} oil
IV	112.25 ± 0.25 g I_2 100 g^{-1} oil	130.2 ± 0.27 g I_2 100 g^{-1} oil	128.81 ± 0.24 g I_2 100 g^{-1} oil
CN	48.81 ± 0.04	44.82 ± 0.06	45.28 ± 0.08
DU	128.95 ± 0.10	147.64 ± 0.14	147.99 ± 0.09
LCSF	4.49 ± 0.01	2.50 ± 0.01	2.98 ± 0.02
CFPP	-2.35 ± 0.02 °C	-8.59 ± 0.04 °C	-7.10 ± 0.03 °C
CP	10.90 ± 0.03 °C	4.27 ± 0.05 °C	5.15 ± 0.04 °C
PP	5.02 ± 0.04 °C	-2.18 ± 0.05 °C	-1.22 ± 0.04 °C
OSI	4.56 ± 0.01 hrs	4.44 ± 0.01 hrs	4.31 ± 0.01 hrs
HHV	39.62 ± 0.01 MJ Kg^{-1}	39.59 ± 0.01 MJ Kg^{-1}	39.62 ± 0.01 MJ Kg^{-1}
ρ (at 15 °C)	878 ± 0.01 kg m^{-3}	881 ± 0.00 kg m^{-3}	880 ± 0.00 kg m^{-3}
v (at 40 °C)	3.96± 0.02 mm^2 s^{-1}	3.84 ± 0.01 mm^2 s^{-1}	3.89 ± 0.01 mm^2 s^{-1}
FP	432.75 ± 0.02 °C	435.31 ± 0.01 °C	437.51 ± 0.02 °C

ASTM D6751-12 standard, SV < 500, CN ≥ 47, OSI ≥ 3

EN 14214 standard IV ≤ 120, HHV ≥ 35, 860 ≤ ρ ≤ 900, 3.5 ≤ v ≤ 5.0, FP ≥ 120, CP and PP - location and season dependent, CFPP - ≤ +5 (summer) or ≤ -20 (winter)

5.5. Conclusions

Test tube PBRs are used to find the effect of macro and micronutrients on microalgal growth and lipid production using single stage strategy. The optimized lipid media was formulated for enhancing lipid content in microalgae. The single stage produced 2.5 fold higher %FAME in DCW than two stage and economical harvesting steps could be minimized. Biomass titer of 2.79 g/l with maximum FAME content of 46% was achieved using developed media under outdoor natural sunlight. FAME productivity and maximum EPS concentration 27 mg/l/day and 155 mg/l were obtained under sunlight study. *S. abundans* could be a potential candidate for simultaneous production of biodiesel and exopolysaccharides by natural autoflocculation. Therefore, the exploitation of *S. abundans* as a co-producer of biodiesel and EPS under sunlight could be a feasible approach.

CHAPTER 6

Multi-objective optimization of nutrients for enhancing biodiesel, autosedimentation factor and exopolysaccharides from *S. abundans* using composite desirability approach

6.1. Background and uniqueness of the study

Earth receives around 1.9×10^6 EJ of energy from Sun in visible light each year and only a fraction of this light energy is used for harnessing algal biomass via photosynthesis (Moheimani & Parlevliet, 2013). Growth rate and chemical composition of microalgae can be altered by using specific nutrient levels, proper environmental conditions based on process requirements, media balancing to yield large amount of desired products (Juneja et al., 2013). Medium optimization was generally performed by two different methods viz. traditional method (one factor at a time/empirical) and statistical methods. The traditional empirical method is ineffective, time consuming and lacks to produce collective interaction effect between process variables. Statistical methods include Plackett-Burman design, response surface methodology and regression analysis. The PBD design was used to determine the significant process variables affecting responses. RSM was used for studying interactions between process variables. But, RSM approach was only used for optimization of several process variables for enhancing individual response viz. FAME, ASF, EPS and other value-added products. As per our knowledge, no studies have been performed using multi-response optimization to enhance FAME, ASF and EPS concomitantly in *Scenedesmus abundans*.

Hence, the present study focussed on multi-objective optimization of nutrients for enhanced production of biodiesel i.e., fatty acid methyl ester (FAME), autosedimentation factor

and exopolysaccharides via *Scenedesmus abundans*. Here, we have customized test tube photobioreactors for performing PBD, RSM and multi-objective optimization experiments under diurnal simulated sunlight. An optimized multi-objective RSM media has been formulated and used in medium scale flat panel photobioreactor under diurnal natural sunlight and diurnal simulated sunlight. Biomass growth, FAME profile, autosedimentation factor analysis, EPS production, autoflocculation rate and autoflocculation efficiency for cell recovery have also been determined to reduce the cost of production.

6.2. Test tube photobioreactors with customized LED lighting system

Transparent test tube photobioreactors were customized using 1 mm thicker borosil test tubes (25 mm outer diameter, 23 mm inner diameter and 150 mm height) with total capacity of 55 ml and 6 mm polyurethane (PU) pipes (outer diameter 8 mm, inner diameter 6 mm) (Fig. 6.1A). Pipette tips (1000 µl and 200 µl) were attached at the bottom of the PU pipe and act as sparger. Mixture of air and CO_2 (2 bar pressure) was sparged from the top of the PBRs via 50 mm 0.2 µm PTFE filters (specifications: appendices, Table A2). Medium scale flat panel PBR (path length 25.4 mm) and customized unidirectional LED lighting systems were used as designed by Mahesh et al (Mahesh et al., 2019). Lux meter (specifications: appendices, Table A2) was used to measure diurnal natural sunlight as well as diurnal simulated sunlight intensities. Diurnal simulated light intensity was generated from pulse width modulation (PWM) (specifications: appendices, Table A2) and OPTO22 control system (specifications: appendices, Table A2) that controls LED light intensity ranging from 0 to 2200 µE/m^2/s (capable of mimicking sunlight intensities in laboratory). Light intensities (in lux) were converted to PPFD (photosynthetic photon flux density) in µE/m^2/s by dividing with the conversion factor of 54 and 74 for diurnal natural sunlight and cool white LED respectively (Apogee Instruments, Inc. USA). Color temperature of diurnal natural sunlight and cool white LED are 5000 K and 6500 K respectively.

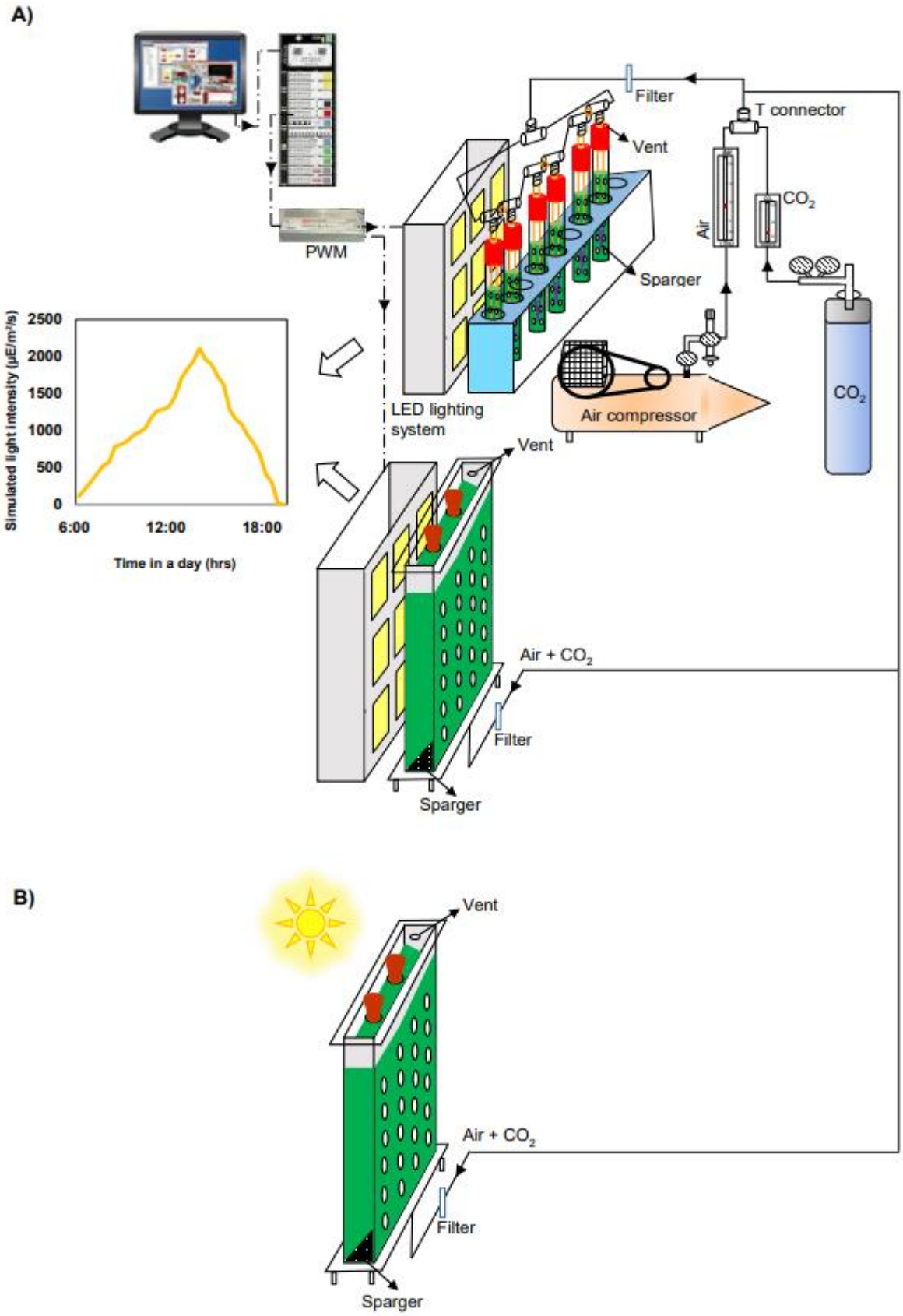

Fig. 6.1. Schematic diagram of photobioreactors for cultivation of microalgae. **A)** test tube PBR and medium scale flat panel PBR at diurnal simulated sunlight, **B)** medium scale flat panel PBR under diurnal natural sunlight.

6.3. Experimental design of multi-objective optimization for production of biodiesel and exopolysaccharides with high autosedimentation factor

6.3.1. Plackett-Burman experimental design based screening for significant process variables

Statistical techniques of experimental design were used to determine the significant nutrients affecting responses viz. %FAME in DCW (%), FAME concentration (g/l), ASF (ratio of bottom OD_{680} to top OD_{680} 1 hr) and EPS concentration (mg/l) of *S. abundans* by PBD. The PBD is a two factorial design that identifies critical nutrient parameters required for elevating responses by screening n variables in n+1 experiments (Plackett & Burman, 1946). The general form of PBD technique is based on the first-order polynomial model as mentioned in equation (6.1).

$$Y = \beta_0 + \sum \beta_i x_i \quad (6.1)$$

Where, Y is the response, β_0 is the model intercept, β_i is the linear coefficient and x_i is the level of the independent variable. The control composition of the modified Chu-13 media used was as follows: 500 mg/l urea, 80 mg/l K_2HPO_4, 200 mg/l $MgSO_4.7H_2O$, 107 mg/l $CaCl_2.2H_2O$, 100 mg/l citric acid, 20 mg/l ferric citrate, 0.0286 mg/l $CoCl_2.6H_2O$, 0.44 mg/l $ZnSO_4.7H_2O$, 0.16 mg/l $CuSO_4.5H_2O$, 0.084 mg/l $Na_2MoO_4.2H_2O$, 5.72 mg/l H_3BO_3, 3.62 mg/l $MnCl_2.4H_2O$. All the media components in modified Chu-13 media were considered as process variables where each process variables was varied over 2 levels. Lower (–1) and higher limit (+1) of process variables were given in Table 6.1 and they were chosen based on previous nutrient variation experiments for growth and lipid analysis. Table 6.2 shows Plackett-Burman experimental design and results. Initial biomass concentration of 0.11 g/l was used for all experiments that were done in single stage batch autotrophically and algal samples were collected in triplicates. The experimental conditions in test tube PBRs were as follows: 100 W cool white LED used as light source, photoperiod – 12 hr diurnal light:12 hr dark cycle, diurnal

simulated light intensity generated from PWM connected to OPTO22 controller, sparging: 2% (v/v) CO_2 in air and 35 ml working volume. Water was added before and after light period to reduce the evaporation losses due to bubble driven agitation in all experiments. CO_2 flow was stopped during dark period but air flow was undisturbed throughout batch to prevent settling of algal cells and for cell respiration in all experiments. In the present study, the process variables significant at 95% confidence level ($p \leq 0.05$) were considered to have significant effect on responses and thus used for further optimization by RSM.

Table 6.1. Lower and higher limits of process variables for Plackett-Burman Design.

Process variable	Coded symbol	lower limit (-1) mg/l	higher limit (+1) mg/l
Urea	A	100	2500
K_2HPO_4	B	30	1000
$MgSO_4.7H_2O$	C	75	1500
$CaCl_2.2H_2O$	D	0	1000
Citric acid	E	20	500
Ferric citrate	F	5	100
$CoCl_2.6H_2O$	G	0.012	0.286
$ZnSO_4.7H_2O$	H	0.176	4.4
$CuSO_4.5H_2O$	J	0.064	1.6
$Na_2MoO_4.2H_2O$	K	0.0336	0.84
H_3BO_3	L	2.288	57.2
$MnCl_2.4H_2O$	M	1.448	36.2

Table 6.2. Plackett-Burman experimental design and range of process variables with observed response values (720 hr).

Run	A	B	C	D	E	F	G	H	J	K	L	M	FAME content in DCW (%wt.)	FAME conc. (g/l)	ASF	EPS conc. (mg/l)
1	-1	-1	-1	1	1	-1	1	1	-1	-1	1	1	0.81 ± 0.45	0.002 ± 0.001	21.52 ± 0.66	50 ± 7
2	-1	1	-1	1	-1	-1	-1	-1	1	1	-1	1	45.83 ± 0.78	0.788 ± 0.03	135.47 ± 0.88	150 ± 4
3	1	-1	1	-1	-1	-1	-1	1	1	-1	1	1	20.37 ± 0.76	0.782 ± 0.02	14.81 ± 0.55	262.5 ± 14
4	1	-1	-1	-1	-1	1	1	-1	1	1	-1	-1	14.35 ± 0.80	0.375 ± 0.02	54.54 ± 0.23	187.5 ± 7
5	-1	-1	1	1	1	1	-1	1	-1	1	-1	-1	6.70 ± 0.42	0.111 ± 0.01	2.48 ± 0.62	425 ± 14
6	1	1	-1	1	-1	1	-1	-1	-1	-1	1	1	3.47 ± 0.45	0.011 ± 0.02	14.41 ± 0.52	137.5 ± 7
7	1	1	1	1	-1	1	-1	1	-1	-1	-1	-1	4.84 ± 0.52	0.436 ± 0.03	1.14 ± 0.29	225 ± 7
8	-1	-1	-1	-1	1	1	-1	1	1	-1	-1	1	3.17 ± 0.48	0.025 ± 0.005	15.52 ± 0.36	200 ± 7
9	-1	1	-1	-1	-1	-1	1	1	-1	1	1	-1	17.14 ± 0.75	0.205 ± 0.01	38.56 ± 0.75	100 ± 7
10	1	1	1	-1	1	-1	1	-1	-1	-1	-1	1	21.24 ± 0.73	0.683 ± 0.03	6.01 ± 0.79	50 ± 4
11	-1	-1	1	1	-1	1	1	-1	-1	1	1	1	2.75 ± 0.41	0.022 ± 0.005	4.70 ± 0.35	100 ± 4
12	1	-1	1	-1	1	-1	-1	-1	-1	1	1	-1	11.04 ± 0.79	0.044 ± 0.01	18.73 ± 0.32	50 ± 7
13	1	-1	-1	1	1	1	1	-1	1	-1	1	-1	10.37 ± 0.77	0.157 ± 0.02	54.81 ± 0.59	100 ± 7
14	1	1	-1	-1	1	1	1	1	-1	1	-1	1	21.07 ± 0.72	0.353 ± 0.02	29.27 ± 0.34	125 ± 4
15	1	-1	1	1	-1	-1	1	1	1	1	-1	1	25.66 ± 0.74	0.795 ± 0.04	14.46 ± 0.39	150 ± 7
16	1	1	-1	1	1	-1	-1	1	1	1	1	-1	13.98 ± 0.78	0.156 ± 0.01	28.07 ± 0.62	112.5 ± 4
17	-1	1	1	-1	1	1	-1	-1	1	1	1	1	8.06 ± 0.45	0.069 ± 0.005	82.46 ± 0.55	112.5 ± 7
18	-1	1	1	1	1	-1	1	-1	1	-1	-1	-1	0.69 ± 0.43	0.005 ± 0.001	44.24 ± 0.56	62.5 ± 4
19	-1	1	1	-1	-1	1	1	1	1	-1	1	-1	1.06 ± 0.47	0.005 ± 0.001	7.57 ± 0.45	112.5 ± 4
20	-1	-1	-1	-1	-1	-1	-1	-1	-1	-1	-1	-1	4.89 ± 0.49	0.034 ± 0.005	10.70 ± 0.42	162.5 ± 7

6.3.2. Response surface methodology

The levels of the significant parameters and the interaction effects between various media components that influence the responses significantly were analysed by central composite methodology. The total number of experiments to be performed in central composite design was calculated by using equation (6.2).

$$N = 2^k + 2k + c \quad (6.2)$$

Where, N is total number of experimental runs. k is number of significant process variables. c is number of center points. In this study, the experiment design was a five level four factor consisting of 30 experiment trials containing 8 axial points ($\pm\alpha$ from the center point), 16 factorial points (±1 from the center point) and 6 replicates (at the center). Table 6.3 shows the levels of significant process variables viz. urea (100–2500 mg/l), $CoCl_2.6H_2O$ (0.01–0.28 mg/l), $CuSO_4.5H_2O$ (0.06–1.60 mg/l) and $Na_2MoO_4.2H_2O$ (0.03–0.84 mg/l). The value of α was calculated by using equation (6.3).

$$\alpha = 2^{k/4} \quad (6.3)$$

Where, k is the number of significant process variables. Therefore, the value of α is equal to $2^{4/4} = 2$.

Table 6.3. The levels of variables for central composite design.

Significant process Variable	Coded symbol	levels				
		-α	-1	0	+1	+α
Urea (mg/l)	X_1	100	700	1300	1900	2500
$CoCl_2.6H_2O$ (mg/l)	X_2	0.01	0.08	0.15	0.21	0.28
$CuSO_4.5H_2O$ (mg/l)	X_3	0.06	0.45	0.83	1.22	1.60
$Na_2MoO_4.2H_2O$ (mg/l)	X_4	0.03	0.24	0.44	0.64	0.84

For statistical calculations, the relation between coded and actual values are described in the following equation (6.4).

$$X_i = \frac{A_i - A_0}{\Delta A} \quad (6.4)$$

Where, X_i is the coded value of variable. A_i is the actual value of variable. A_0 is the actual value of A_i at the center point and A is the step change of variable. The responses were analysed by using a second order polynomial equation and experimental data was fitted by multiple regression procedure. The mathematical relationship of the response (Y) to the significant independent process variables viz. X_1, X_2, X_3 and X_4 is given in the following quadratic polynomial equation (6.5).

$$Y = \beta_0 + \beta_1 X_1 + \beta_2 X_2 + \beta_3 X_3 + \beta_4 X_4 + \beta_{12} X_1 X_2 + \beta_{13} X_1 X_3 + \beta_{14} X_1 X_4 + \beta_{23} X_2 X_3 + \beta_{24} X_2 X_4 + \beta_{34} X_3 X_4 + \beta_{11} X_1^2 + \beta_{22} X_2^2 + \beta_{33} X_3^2 + \beta_{44} X_4^2 \quad (6.5)$$

Where, Y is the predicted response. X_1, X_2, X_3 and X_4 are significant independent process variables. β_1, β_2, β_3 and β_4 are linear regression coefficients. β_{12}, β_{13}, β_{14}, β_{23}, β_{24} and β_{34} are interactive regression coefficients. β_{11}, β_{22}, β_{33}, β_{44} are quadratic regression coefficients. β_0 is the model intercept. The experimental conditions in test tube PBRs were same as followed in Plackett-Burman design.

6.3.3. Multi-response optimization

There were four responses (%FAME in DCW, FAME concentration, ASF and EPS concentration) considered for this study. Therefore, multi-response optimization by desirability function approach was used to enhance responses of *S. abundans*. This approach changes multi-objective problem to a single objective problem by formulating a special objective function called as composite desirability function (D). The individual desirability function (d_i) for an objective function to be maximized can be written in a general form as mentioned in the following equations (6.6) – (6.8).

$$d_i = 0\,, \quad Y_i \leq Low_i \quad (6.6)$$

$$d_i = \left(\frac{Y_i - Low_i}{High_i - Low_i}\right)^{r_i}, \; Low_i < Y_i < High_i \quad (6.7)$$

$$d_i = 1, \quad Y_i \geq High_i \quad (6.8)$$

Where, Y_i represents response. Low_i represents lower limit of the response. $High_i$ represents

upper limit of the response. r_i represents weight or significance level. In the present study, quadratic equations of responses %FAME in DCW (Y_1(%wt.)), FAME concentration (Y_2(g/l)), ASF (Y_3) and EPS concentration (Y_4(mg/l)) resulted from ANOVA (analysis of variance) of RSM was used in equations (6.6) – (6.8). Weights of 1, 2, 3, 4 and 5 (1 – lowest priority, 5 – highest priority) was used on weight scale of 1 to 5. Once the individual d_i values are determined from equations (6.6) – (6.8), they are combined into composite desirability function (D) which is calculated as the geometric mean of the d_i values as shown in the following equation (6.9).

$$D = (d_1 \times d_2 \times \dots d_k)^{1/k} \quad (6.9)$$

Where, $0 \leq D \leq 1$. k denotes the number of responses (Derringer & Suich, 1980). In the present study, desirability approach was used by assigning 1, 2, 3, 4 and 5 significance levels for four responses giving rise to 625 combinations (5^4). The experimental conditions were same as followed in Plackett-Burman design.

6.3.4. Experiments in medium scale photobioreactor using optimum media under diurnal natural sunlight

Optimized multi-objective RSM media was used in single stage medium scale flat panel PBR under diurnal natural sunlight in the month of August - September 2021 at 26°11′03″ N (latitude) and 91°44′44″ E (longitude) in Guwahati, India. Sun generally rises at 5:00 am and sets at 6:00 pm in Guwahati during August - September 2021. Sunlight intensities (in µE/m^2/s) and culture temperature (°C) were measured at every 1 hr from dawn to dusk using lux meter and thermometer respectively during experiment. Process pH readings were monitored online by OPTO22 control system. Sunlight intensity (in lux) was converted to µE/m^2/s by dividing with conversion factor of 54 (1 µE/m^2/s = 54 lux). The experimental conditions were diurnal natural sunlight intensities from dawn to dusk, 2 lpm air flow rate with 2% (v/v) CO_2, 2 l working volume was used in medium scale flat panel PBR. Appropriate sample volume was

collected in triplicates at every 12 hr to find OD_{680}. Chlorophyll-a and carotenoid of the sample were estimated at every 24 hr. Samples were collected in triplicates at respective time intervals for DCW measurement, FAME, free dry exopolysaccharide weight (DEW), autosedimentation factor, autoflocculation rate, autoflocculation efficiency estimation. Water was added in dawn and dusk to reduce evaporation losses due to bubble driven agitation.

6.3.5. Experiments in medium scale photobioreactor using optimum media under diurnal simulated sunlight

Optimized multi-objective RSM media was also used in single stage medium scale flat panel PBR under diurnal simulated sunlight. The experimental conditions were as follows: 100 W cool white LED used as light source, photoperiod – 12 hr diurnal light:12 hr dark cycle, diurnal simulated light intensity generated from PWM connected to OPTO22 controller, 2 lpm air flow rate with 2% (v/v) CO_2, 2 l working volume was used in medium scale flat panel PBR. Appropriate sample volume was collected in triplicates at every 24 hr to find OD_{680}. Chlorophyll-a and carotenoid of the sample were estimated at every 24 hr. Samples were collected in triplicates at respective time intervals for DCW measurement, FAME, free DEW, autosedimentation factor, autoflocculation rate, autoflocculation efficiency estimation.

6.4. Results and Discussion

6.4.1. Statistical optimization of media components for enhancing the production of FAME, autosedimentation factor and EPS using PBD

The screening of important nutrients in modified Chu-13 media affecting responses viz. %FAME in DCW, FAME concentration, ASF and EPS concentration of *S. abundans* was investigated by PBD using Design Expert software. The PBD experimental results of responses at 720 hr was shown in Table 6.2. The PBD experiment produced highest %FAME in DCW of 46%, 0.79 g/l FAME, ASF of 135.47 and 425 mg/l EPS from all experiments (Table 6.2). $Na_2MoO_4.2H_2O$ (coded symbol K) was found to have significant positive effect (+ 9.57) on

%FAME in DCW of *S. abundans* with p = 0.05 whereas urea (coded symbol A) was found to have significant positive effect (+ 0.25) on FAME concentration with p < 0.05 (95% CI) (Fig. 6.2A and 6.2B).

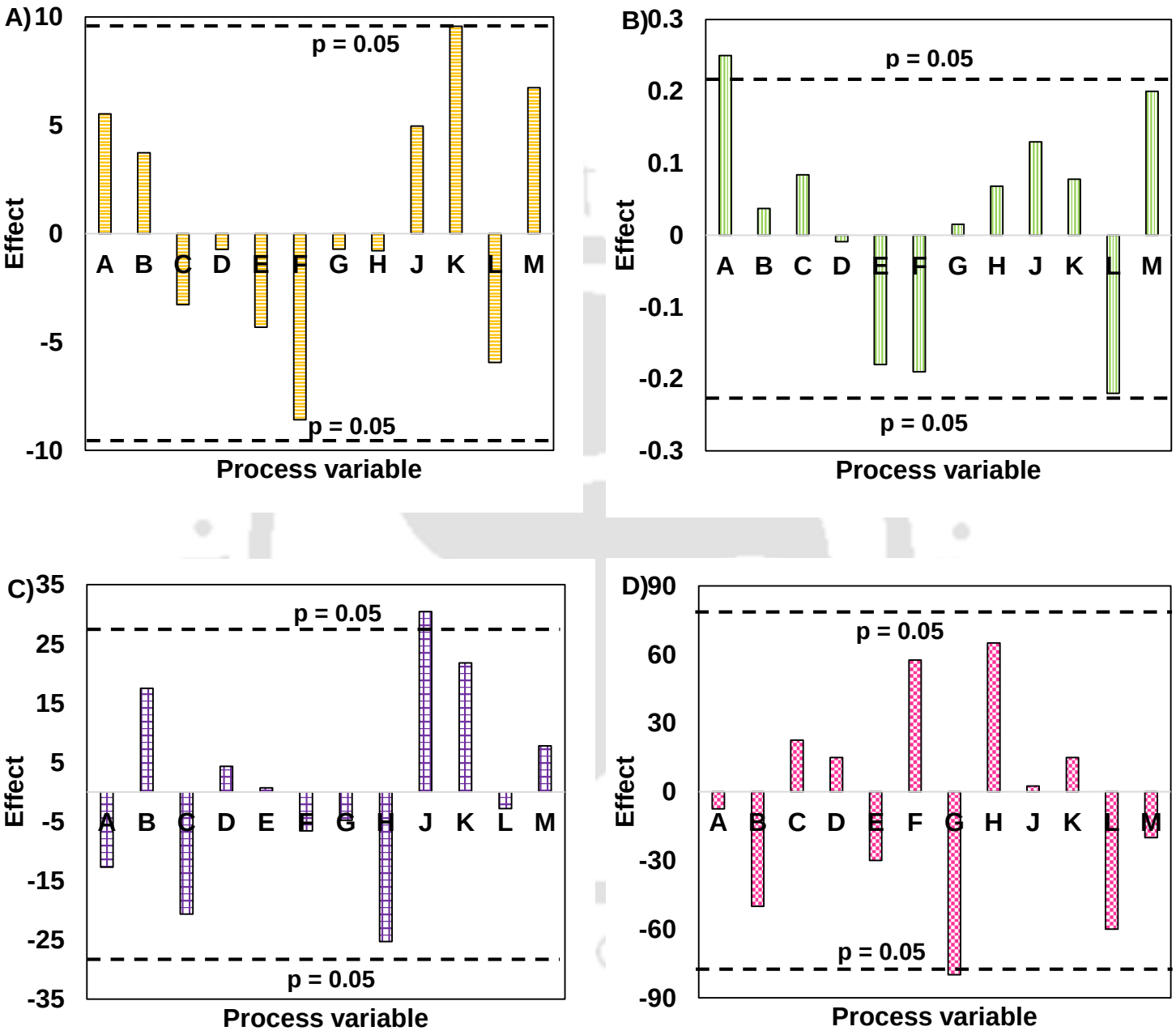

Fig. 6.2. Positive and negative effects of process variables on responses from PBD analysis. Positive and negative effects on **A)** FAME content in DCW, **B)** FAME concentration, **C)** Autosedimentation factor and **D)** EPS concentration.

Dou et al. identified that six-times increase of Mo^{+6} concentration in modified *F*/2 media increases the lipid content of *Nannochloropsis oculata* (Dou et al., 2013). This may be due to the presence of high concentration of molybdenum drives the synthesis of stress protein in microalgae to promote lipid accumulation (Mandal et al., 2019). These results conclude that $Na_2MoO_4.2H_2O$ have significant positive impact on FAME content as observed in our current study. In another study, Yang et al. have identified $NaNO_3$ as significant process variable with positive effect for promoting lipid production in *Scenedesmus* sp. by Plackett-Burman design (Yang et al., 2014). This was in agreement with our study as urea had significant positive effect on FAME production. $CuSO_4.5H_2O$ (coded symbol J) had significant positive effect (+ 30.44) on ASF of *S. abundans* with $p < 0.05$ (95% CI) (Fig. 6.2C). The presence of EPS with Cu^{+2} metal salts in media can interfere with the negative charge on surface of microalgal cells and thus facilitates the autosedimentation in *S. abundans* by charge neutralization. The presence of cationic and anionic functional groups on EPS can efficiently accumulate copper metal ions (Yin et al., 2019). The adsorption capability of Cu^{+2} metal ions by EPS helps in partial or complete binding of algal cells forming flocs and enhance autoflocculation. $CoCl_2.6H_2O$ (coded symbol G) had significant negative effect (- 80) on EPS concentration with $p < 0.05$ (95% CI) (Fig. 6.2D). *Nostoc linckia*, a fresh water cyanobacterium showed increased production of EPS when exposed to moderate Co^{+2} metal ion concentration (40 mg/l) (Mona & Kaushik, 2015). Therefore, process variables (urea, $CoCl_2.6H_2O$, $CuSO_4.5H_2O$ and $Na_2MoO_4.2H_2O$) which have 95% CI with significant effect were used in response surface methodology.

6.4.2. RSM – CCD based production of FAME, autosedimentation factor and EPS in *S. abundans*

Further optimization of significant process variables (urea, $CoCl_2.6H_2O$, $CuSO_4.5H_2O$ and $Na_2MoO_4.2H_2O$) resulted from PBD analysis were used in RSM – CCD approach to

maximize responses. Highest %FAME in DCW (63%) was observed in expt 22 (30 days) and highest FAME concentration (4.03 g/l) was observed in expt 2 (30 days) whereas lowest %FAME in DCW (4%) and FAME concentration (0.04 g/l) was observed in expt 23 (Fig. 6.3A). Interestingly, highest EPS concentration of 625 mg/l was observed in expt 23 whereas lowest EPS concentration of 125 mg/l was found in expt 10 (Fig. 6.3B). Autosedimentation factor lies in the range of 1.46 to 9.90 for all RSM experiments (Fig. 6.3B). It is also evident from Pareto analysis of RSM, only FAME concentration increases with increase in %FAME in DCW for some experiments. Other responses are following contradictory relationship to each other (when one of the response increases, other response decreases) (Fig. 6.3 (C, D, E, F, G and H)). The RSM – CCD approach produced quadratic polynomial equations (expressed in terms of coded value) viz. %FAME in DCW ($Y_1(\%wt.)$), FAME ($Y_2(g/l)$), ASF (Y_3) and EPS ($Y_4(g/l)$) as the functions of four independent process variables-urea (X_1), $CoCl_2.6H_2O$ (X_2), $CuSO_4.5H_2O$ (X_3) and $Na_2MoO_4.2H_2O$ (X_4) was as follows:

$$\%FAME\ in\ DCW\ (Y_1(\%wt.) = 39.90 - 4.87X_1 + 0.35X_2 - 1.38X_3 + 0.37X_4 - 1.13X_1X_2 - 3.26X_1X_3 - 1.21X_1X_4 - 2.42X_2X_3 + 8.98X_2X_4 + 2.39X_3X_4 - 6.96X_1^2 - 0.27X_2^2 + 0.52X_3^2 + 3.57X_4^2 \quad (6.10)$$

$$FAME\ (Y_2(g/l)) = 1.65 - 0.37X_1 - 0.17X_2 - 0.10X_3 + 8.742e\text{-}003X_4 + 0.24X_1X_2 - 0.25X_1X_3 - 0.066X_1X_4 - 0.29X_2X_3 + 0.38X_2X_4 - 0.018X_3X_4 - 0.25X_1^2 + 0.049X_2^2 + 0.089X_3^2 + 0.16X_4^2 \quad (6.11)$$

$$ASF\ (Y_3) = 5.73 + 0.47X_1 - 0.54X_2 - 0.97X_3 - 0.077X_4 - 0.23X_1X_2 - 0.16X_1X_3 - 8.459e\text{-}003X_1X_4 - 0.14X_2X_3 - 0.24X_2X_4 - 0.13X_3X_4 - 0.61X_1^2 - 0.78X_2^2 + 0.33X_3^2 - 0.18X_4^2 \quad (6.12)$$

$$EPS\ (Y_4(g/l)) = 256.25 + 12.50X_1 + 17.71X_2 + 25.00X_3 - 25.00X_4 - 15.63X_1X_2 + 48.44X_1X_3 + 17.19X_1X_4 + 28.13X_2X_3 + 0.000X_2X_4 + 1.56X_3X_4 + 40.36X_1^2 + 15.36X_2^2 - 15.89X_3^2 + 9.11X_4^2 \quad (6.13)$$

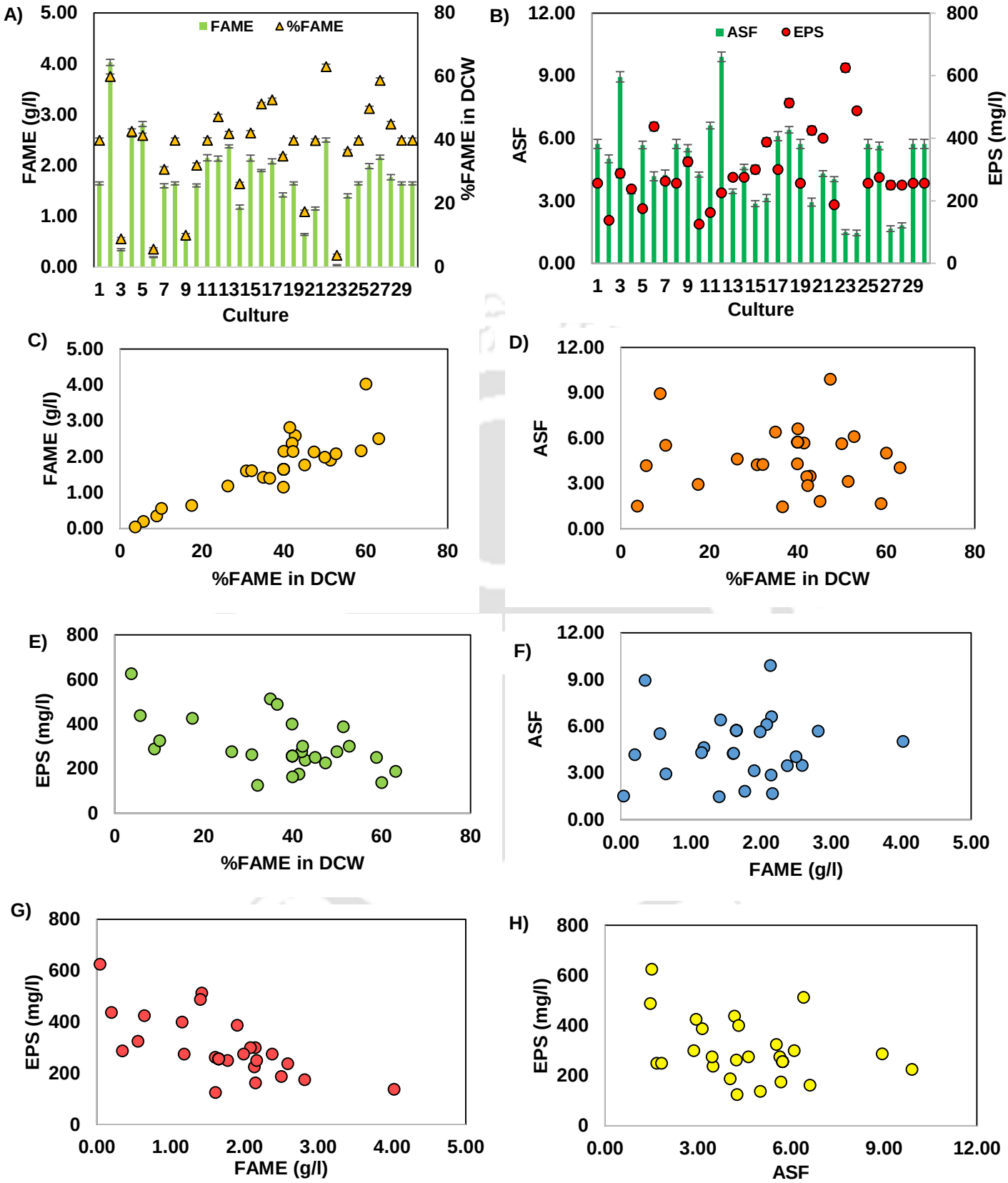

Fig. 6.3. A) FAME profile, **B)** ASF and EPS profile of RSM-CCD experimental runs at 720 hr, Pareto analysis of RSM-CCD at 720 hr of **C)** FAME and FAME content in DCW, **D)** ASF and FAME content in DCW, **E)** EPS and FAME content in DCW, **F)** ASF and FAME, **G)** EPS and FAME, **H)** EPS and ASF.

The complete CCD matrix with observed and predicted response values (720 hr) are presented in Table 6.4. The statistical testing of the quadratic regression equation models was performed using ANOVA (Table 6.5). The model F values of 1.77, 2.07, 1.60 and 0.84 are observed for %FAME in DCW, FAME, ASF and EPS respectively (Table 6.5). The CV (coefficient of variation) and R^2 (correlation coefficient) values are also presented in Table 6.5. The results showed that X_1, X_2X_4 and X_1^2 are significant model term for %FAME in DCW whereas X_1, X_2X_3, X_2X_4 and X_1^2 are significant model term for FAME concentration with $p \leq 0.1$ for both responses (90% CI). For autosedimentation factor, X_3, X_1^2 and X_2^2 are found to be significant model terms whereas X_1^2 is significant model term for EPS concentration with 90% CI for both responses (Table 6.5). Yang et al. reported that optimized soil extract medium containing 3.07 g/l $NaHCO_3$, 15.49 mg/l $NaH_2PO_4.2H_2O$ and 803.21 mg/l $NaNO_3$ produced 304.02 mg/l lipid in *Scenedesmus* sp. using response surface methodology (Yang et al., 2014). The less lipid concentration in their study was due to absence of CO_2 and light limitation. In an another study, Angelaalincy et al. used optimized BG 11 media and reported maximum EPS of 48 mg/l by *Scenedesmus* sp. SB1 through response surface methodology (Angelaalincy et al., 2017). Wingender et al. reported Cu^{+2} adsorption on carboxyl, phosphoryl, amide, amino and hydroxyl functional groups present in EPS molecules (Wingender et al., 1999). Therefore, it is reasonable to judge that EPS with specific concentrations of metal ions have the ability to enhance autoflocculation phenomena in microalgae giving rise to high ASF values. Therefore, it can be concluded that the mathematical models can be utilized for optimization of independent variables (urea, $CoCl_2.6H_2O$, $CuSO_4.5H_2O$ and $Na_2MoO_4.2H_2O$) and predicting responses. But, quadratic equations (6.10) – (6.13) resulted after RSM analysis from Design Expert software enhance single objective at a time. Therefore, RSM combinations based on desirability approach was performed to enhance all the responses.

Table 6.4. Central composite design matrix with observed and predicted response values (720 hr).

Run	Significant process variable				FAME content in DCW (%wt)		FAME (g/l)		ASF		EPS (mg/l)	
	X_1 (mg/l)	X_2 (mg/l)	X_3 (mg/l)	X_4 (mg/l)	Observed value	Predicted value	Observed value	Predicted Value	Observed value	Predicted value	Observed value	Predicted value
1[a]	1300	0.15	0.83	0.44	39.90 ± 0.74	39.90	1.65 ± 0.03	1.65	5.73 ± 0.22	5.73	256.25 ± 7	256.25
2	700	0.08	1.22	0.24	60.00 ± 0.78	49.46	4.03 ± 0.06	3.22	5.01 ± 0.19	3.62	137.50 ± 4	248.44
3	1900	0.08	0.45	0.64	8.89 ± 0.42	22.69	0.34 ± 0.02	0.91	8.94 ± 0.25	7.00	287.50 ± 14	260.94
4	700	0.08	0.45	0.64	42.75 ± 0.76	26.08	2.59 ± 0.03	1.76	3.48 ± 0.15	5.29	237.50 ± 7	267.19
5	700	0.08	1.22	0.64	41.39 ± 0.73	39.46	2.81 ± 0.05	2.58	5.68 ± 0.18	3.70	175.00 ± 4	167.19
6	1900	0.21	1.22	0.24	5.69 ± 0.41	13.55	0.20 ± 0.01	0.47	4.18 ± 0.21	3.38	437.50 ± 14	427.60
7	1300	0.01	0.83	0.44	30.79 ± 0.77	38.13	1.60 ± 0.04	2.18	4.23 ± 0.24	3.71	262.50 ± 4	282.29
8[a]	1300	0.15	0.83	0.44	39.90 ± 0.74	39.90	1.65 ± 0.03	1.65	5.73 ± 0.22	5.73	256.25 ± 7	256.25
9	2500	0.15	0.83	0.44	10.08 ± 0.45	2.34	0.56 ± 0.02	0.00	5.53 ± 0.17	4.24	325.00 ± 14	442.71
10	1900	0.21	0.45	0.24	32.07 ± 0.72	32.43	1.61 ± 0.03	1.71	4.26 ± 0.12	5.66	125.00 ± 4	227.60
11	700	0.21	0.45	0.64	39.95 ± 0.74	51.83	2.15 ± 0.06	2.27	6.61 ± 0.16	4.46	162.50 ± 4	277.60
12	1300	0.15	0.06	0.44	47.31 ± 0.79	44.73	2.13 ± 0.05	2.21	9.90 ± 0.23	8.97	225.00 ± 7	142.71
13	700	0.08	0.45	0.24	41.97 ± 0.75	45.65	2.38 ± 0.03	2.33	3.46 ± 0.11	4.70	275.00 ± 7	354.69
14	1300	0.15	1.60	0.44	26.27 ± 0.44	39.23	1.18 ± 0.04	1.79	4.62 ± 0.13	5.11	275.00 ± 7	242.71
15	1900	0.21	0.45	0.64	42.20 ± 0.71	43.92	2.14 ± 0.06	2.39	2.86 ± 0.14	5.27	300.00 ± 14	208.85
16	1900	0.08	1.22	0.24	51.34 ± 0.46	37.90	1.90 ± 0.02	1.65	3.14 ± 0.17	4.71	387.50 ± 14	367.19
17	1900	0.08	0.45	0.24	52.68 ± 0.49	47.11	2.08 ± 0.05	1.74	6.10 ± 0.22	6.45	300.00 ± 7	279.69
18	1300	0.15	0.83	0.03	34.92 ± 0.48	53.45	1.42 ± 0.04	2.29	6.41 ± 0.15	5.15	512.50 ± 14	342.71
19[a]	1300	0.15	0.83	0.44	39.90 ± 0.74	39.90	1.65 ± 0.03	1.65	5.73 ± 0.22	5.73	256.25 ± 7	256.25
20	1900	0.08	1.22	0.64	17.44 ± 0.43	23.05	0.64 ± 0.02	0.74	2.93 ± 0.19	4.76	425.00 ± 14	354.69
21	1900	0.21	1.22	0.64	39.85 ± 0.47	34.61	1.15 ± 0.03	1.07	4.31 ± 0.14	2.49	400.00 ± 4	415.10
22	1300	0.15	0.83	0.84	63.09 ± 0.75	54.94	2.50 ± 0.04	2.32	4.04 ± 0.12	4.85	187.50 ± 7	242.71
23	100	0.15	0.83	0.44	3.69 ± 0.41	21.81	0.04 ± 0.01	1.37	1.51 ± 0.11	2.34	625.00 ± 14	392.71
24	1300	0.28	0.83	0.44	36.49 ± 0.45	39.53	1.40 ± 0.04	1.51	1.46 ± 0.13	1.55	487.50 ± 4	353.13
25[a]	1300	0.15	0.83	0.44	39.90 ± 0.74	39.90	1.65 ± 0.03	1.65	5.73 ± 0.22	5.73	256.25 ± 7	256.25
26	700	0.21	0.45	0.24	49.92 ± 0.72	35.49	1.99 ± 0.05	1.33	5.63 ± 0.18	4.82	275.00 ± 4	365.10
27	700	0.21	1.22	0.64	58.79 ± 0.76	55.54	2.16 ± 0.04	1.95	1.67 ± 0.14	2.33	250.00 ± 14	290.10
28	700	0.21	1.22	0.24	45.00 ± 0.78	29.63	1.77 ± 0.05	1.08	1.82 ± 0.12	3.19	250.00 ± 7	371.35
29[a]	1300	0.15	0.83	0.44	39.90 ± 0.74	39.90	1.65 ± 0.03	1.65	5.73 ± 0.22	5.73	256.25 ± 7	256.25
30[a]	1300	0.15	0.83	0.44	39.90 ± 0.74	39.90	1.65 ± 0.03	1.65	5.73 ± 0.22	5.73	256.25 ± 7	256.25

[a]Experiments performed at the central value. The observed values of responses are represented as mean value ± standard deviation.

Table 6.5. ANOVA for response surface quadratic models of FAME content in DCW, FAME, autosedimentation factor and EPS (720 hr).

Source	FAME content in DCW (%wt)[a]			FAME concentration (g/l)[b]			Autosedimentation factor[c]			EPS concentration (mg/l)[d]		
	SS	F value	p value	SS	F value	p value	SS	F value	p value	SS	F value	p value
Model	4245.23	1.77	0.1414	12.94	2.07	0.0879	68.33	1.60	0.1869	1.629e+005	0.84	0.6291
X_1	568.72	3.33	0.0882	3.21	7.16	0.0173	5.41	1.78	0.2021	3750.00	0.27	0.6114
X_2	2.95	0.017	0.8973	0.67	1.49	0.2408	6.99	2.30	0.1503	7526.04	0.54	0.4736
X_3	45.40	0.27	0.6138	0.26	0.59	0.4547	22.39	7.36	0.0160	15000.00	1.08	0.3158
X_4	3.32	0.019	0.8910	1.834e-003	4.097e-003	0.9498	0.14	0.047	0.8313	15000.00	1.08	0.3158
X_1X_2	20.45	0.12	0.7342	0.93	2.09	0.1692	0.81	0.27	0.6125	3906.25	0.28	0.6041
X_1X_3	169.72	0.99	0.3349	0.98	2.19	0.1595	0.43	0.14	0.7136	37539.06	2.70	0.1214
X_1X_4	23.50	0.14	0.7160	0.070	0.16	0.6981	1.145e-003	3.765e-004	0.9848	4726.56	0.34	0.5688
X_2X_3	93.56	0.55	0.4709	1.32	2.96	0.1061	0.29	0.097	0.7600	12656.25	0.91	0.3555
X_2X_4	1289.35	7.54	0.0150	2.28	5.10	0.0392	0.89	0.29	0.5965	0.000	0.000	1.0000
X_3X_4	91.63	0.54	0.4754	5.381e-003	0.012	0.9141	0.25	0.083	0.7770	39.06	2.805e-003	0.9585
X_1^2	1326.89	7.76	0.0138	1.73	3.88	0.0678	10.17	3.34	0.0874	44689.36	3.21	0.0934
X_2^2	1.95	0.011	0.9164	0.067	0.15	0.7039	16.51	5.43	0.0342	6475.07	0.46	0.5057
X_3^2	7.44	0.044	0.8375	0.22	0.48	0.4982	2.95	0.97	0.3402	6921.50	0.50	0.4916
X_4^2	350.49	2.05	0.1727	0.74	1.65	0.2183	0.91	0.30	0.5918	2278.65	0.16	0.6916
Residual	2564.48			6.71			45.61			2.089e+005		
Lack of fit	2564.48			6.71			45.61			2.089e+005		
Pure error	0.000			0.000			0.000			0.000		

[a]CV = 34.96%; R^2 = 0.6234.

[b]CV = 39.62%; R^2 = 0.6585.

[c]CV = 36.80%; R^2 = 0.5997.

[d]CV = 39.95%; R^2 = 0.4381.

6.4.3. Experimental verification of multi-objective optimization of media components to maximize FAME, autosedimentation factor and EPS using desirability approach

The aim of the present study was to maximize FAME content in DCW, FAME production, autosedimentation factor and EPS production by using the composite desirability function approach. Two combinations satisfied the predicted cut off value of responses (%FAME in DCW > 60%, FAME concentration > 3 g/l, autosedimentation factor > 3, EPS concentration > 325 mg/l) Therefore, two experiments were performed with the respective concentrations of significant process variables as shown in Table 6.6. The dry cell weight profile of 2 experimental runs was shown in Fig. 6.4A. Highest DCW of 5.43 g/l was observed in 1st experimental run whereas expt 2 produced DCW of 5.18 g/l at 720 hr (Fig. 6.4A). The FAME profile, ASF and EPS profile of 2 experimental runs at 720 hr was depicted in Fig. 6.4B, 6.4C and Table 6.6. Table 6.6 shows the multi-objective optimization of process variables with observed and predicted values at 720 hr. Maximum FAME content in DCW (70%), FAME (3.83 g/l), ASF (1.93) and EPS (462.50 mg/l) was observed in 1st experimental run. Expt 2 produces FAME content in DCW (49%), FAME (2.55 g/l), ASF (1.74) and EPS (362.50 mg/l). Despite of ASF being low, other responses have increased tremendously in experimental run 1. Multi-objective optimization of process variables may not enhance all the observed (actual) responses. The experimental combination that favours most of the responses viz. %FAME in DCW, FAME concentration, EPS concentration could be chosen as optimized multi-objective RSM media. Therefore, experimental run 1 in Table 6.6 was considered as optimized nutrient combination because FAME content in DCW, FAME and EPS concentration increased to great extent with a marginal increase in autosedimentation factor. The maximum predicted response values for optimized nutrient combination were 61.92% FAME content in DCW, 3.71 g/l FAME, ASF of 3.10, 332.30 mg/l EPS at the optimum level of 659.63 mg/l urea, 0.08 mg/l $CoCl_2.6H_2O$, 1.17 mg/l $CuSO_4.5H_2O$ and 0.03 mg/l $Na_2MoO_4.2H_2O$.

Table 6.6. Multi-objective optimization of process variables with observed and predicted values (720 hr).

Run	Significance (r_i)				Process variables				%FAME in DCW (%)		FAME conc. (g/l)		ASF		EPS conc. (mg/l)	
	%FAME	FAME (g/l)	ASF	EPS (mg/l)	X_1 (mg/l)	X_2 (mg/l)	X_3 (mg/l)	X_4 (mg/l)	Observed value[a]	Predicted value	Observed value[a]	Predicted value	Observed value[a]	Predicted value	Observed value[a]	Predicted value
1	1	5	2	5	659.63	0.08	1.17	0.03	70.43 ± 0.76	61.92	3.83 ± 0.04	3.71	1.93 ± 0.11	3.10	462.50 ± 14	332.30
2	1	3	4	5	1299.98	0.10	1.17	0.03	49.38 ± 0.78	61.02	2.55 ± 0.04	3.01	1.74 ± 0.15	4.58	362.50 ± 14	328.08

[a]All observed values of responses are represented as mean value ± standard deviation.

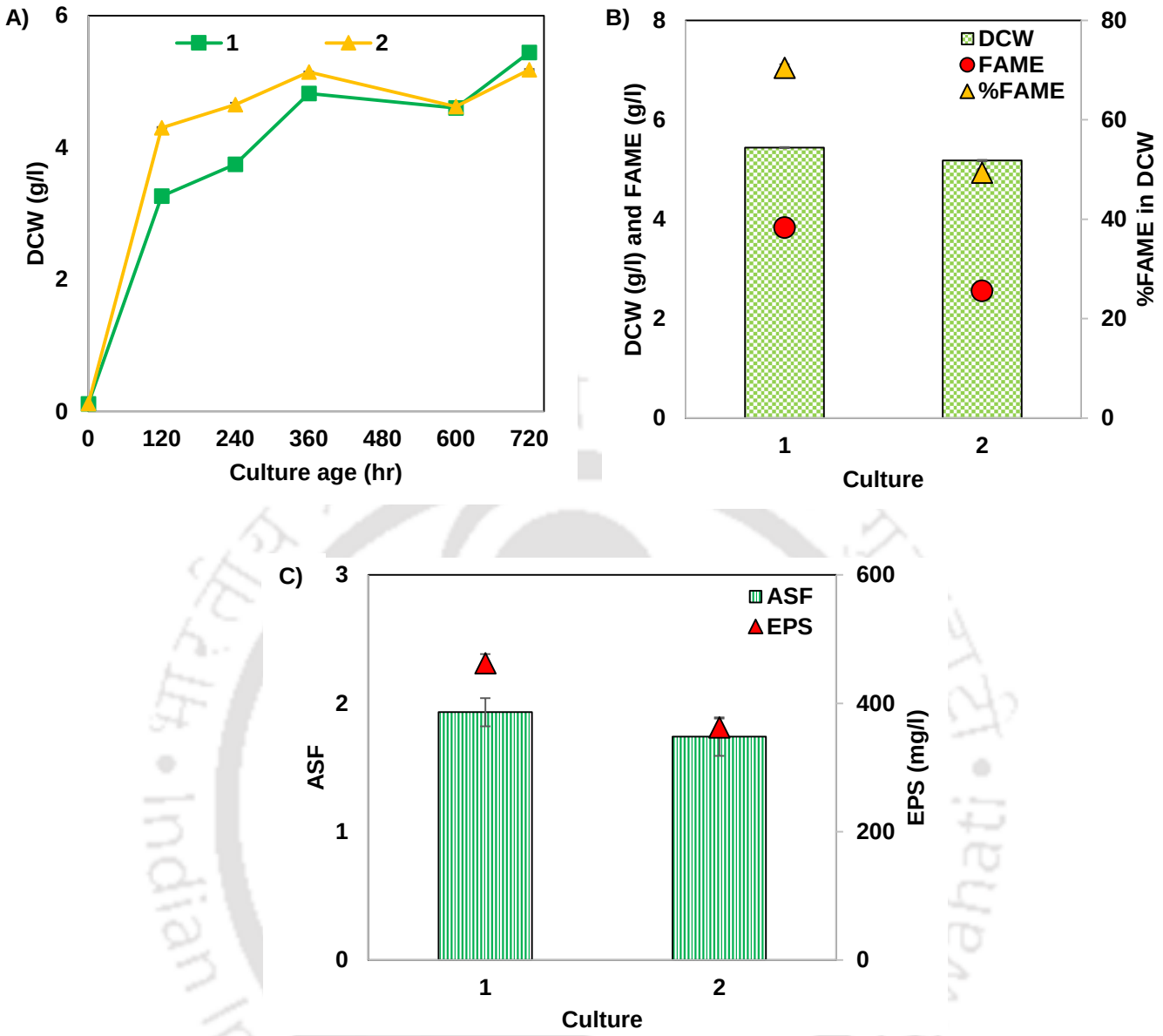

Fig. 6.4. Multi-objective optimization of process variables in test tube PBR. **A)** Dry cell weight profile of experimental runs. **B)** Dry cell weight and FAME profile, **C)** ASF and EPS profile of experimental runs at 720 hr.

Hussain et al. reported that *Botryococcus braunii* produced 40% lipid content in DCW and 64 mg/l/day biomass productivity in 10 l glass jars using modified Chu-13 media by Pareto frontier and two-objective optimization (Hussain et al., 2020). They used CO_2 enriched air (2.5% v/v CO_2) at a rate of 200 ml/min and rotary agitation of 92 RPM with 170 µE/m^2/s light intensity. The lipid content in their study would have improved by using high light intensity. In another study, Anuradha et al. reported 47.66% lipid content in DCW and 1275.8 mg/l/day biomass productivity in *Scenedesmus obliquus* by desirability function approach (Anuradha et

al., 2021). The combined effect of optimized media constituents with observed values of responses in the current study was as follows: 70% FAME (1.72 fold), 3.83 g/l FAME (2.30 fold), ASF of 1.93 (1.08 fold) and 462.50 mg/l EPS (1.60 fold) as compared to unoptimized media (control) (Table 6.7). The nutrient combination with 659.63 mg/l urea, 0.08 mg/l $CoCl_2.6H_2O$, 1.17 mg/l $CuSO_4.5H_2O$ and 0.03 mg/l $Na_2MoO_4.2H_2O$ (experimental run 1) produces highest FAME (70%), 3.83 g/l FAME, ASF of 1.93 and 462.50 mg/l EPS at 720 hr (Fig. 6.4B and 6.4C) and therefore this media was used as optimized multi-objective RSM media in larger PBR.

6.4.4. Simultaneous production of FAME, autosedimentation factor and EPS using optimized media under diurnal natural sunlight

Experiment was performed with optimized multi-objective RSM media in medium scale PBR under diurnal natural sunlight in single stage. Sunlight intensities and weather temperature readings from dawn to dusk were noted and since sunlight is diurnal by nature, it has broad range (0 – 2000 $\mu E/m^2/s$) of continuous light intensity variations from dawn to dusk (Fig. 6.5A). Sunny, cloudy and rainy days were responsible for variation in sunlight intensities and weather temperature apart from diurnal nature during light period of experiment. The process pH and culture temperature profile were also recorded (Fig. 6.5B). The process pH profile shown in Fig. 6.5B depicts that there is rise in pH in growth phase. The process pH decreases during nitrogen starvation period. Culture temperature variation was due to varying sunlight intensities and algal metabolism. Biomass titer, overall biomass productivity and overall specific growth rate of 1.72 g/l, 0.32 g/l/day, 0.52 day^{-1} were achieved at the end of growth phase (120 hr). The highest specific growth rate of 2.24 day^{-1} was observed at the end of 1^{st} day light period and decreases with culture age due to light limitation (Fig. 6.5C). Maximum dry cell of weight of 4.30 g/l was observed at 564 hr. Maximum chlorophyll-a and carotenoid concentrations were 31 mg/l (96 hr) and 6.8 mg/l (96 hr) respectively (Fig. 6.5D).

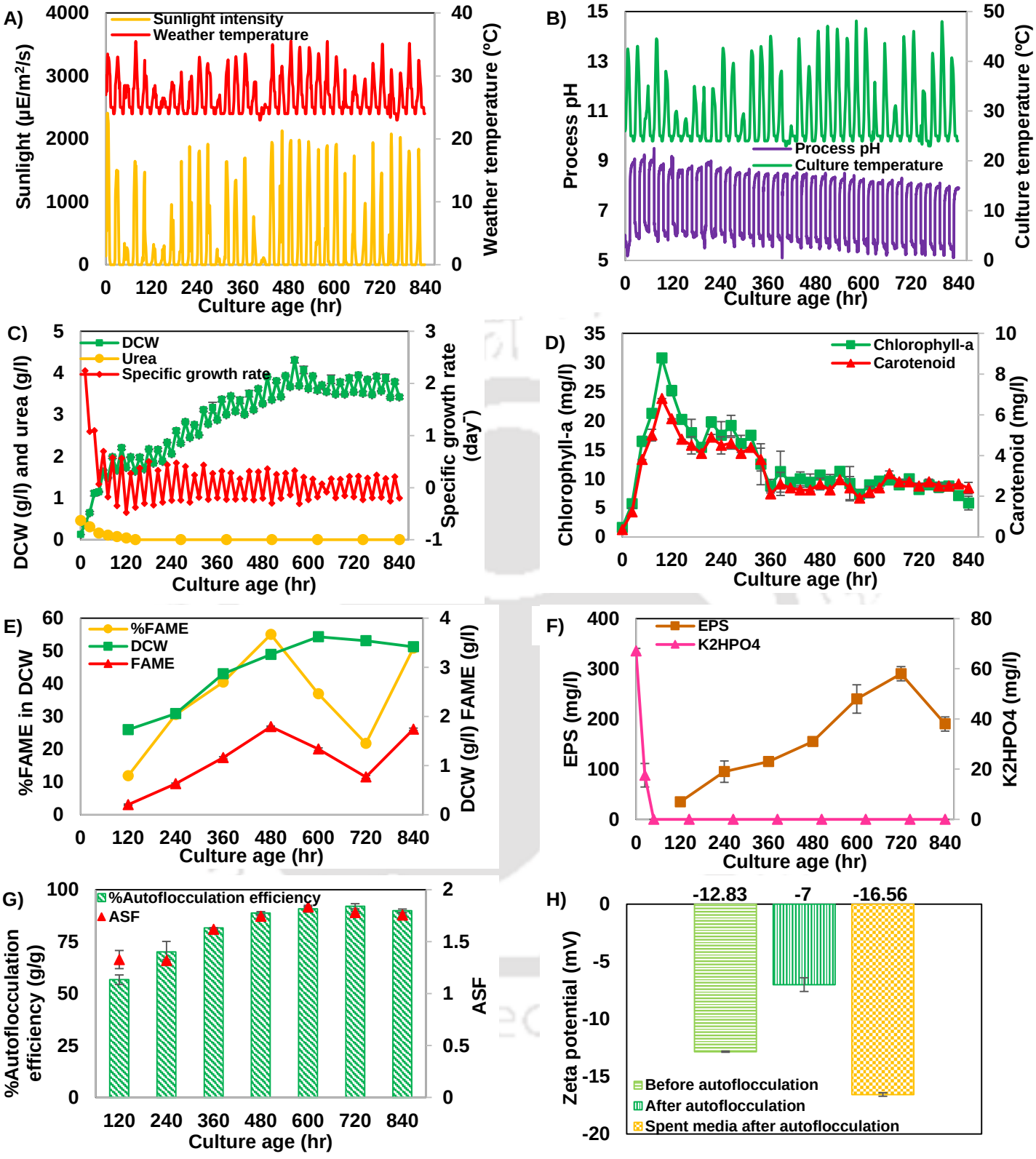

Fig. 6.5. Biomass growth under diurnal natural sunlight in medium scale PBR. **A)** Sunlight intensity and weather temperature, **B)** Process pH and culture temperature, **C)** Dry cell weight, urea utilization and specific growth rate, **D)** Chlorophyll-a and carotenoid synthesis, **E)** Dry cell weight, FAME content in DCW, FAME concentration, **F)** EPS and K_2HPO_4 profile, **G)** autosedimentation factor and autoflocculation efficiency and **H)** Zeta potential.

The chlorophyll-a and carotenoid concentration decreases when triacylglycerols gets accumulated in high amounts within algal cells. Urea was completely consumed by the algal cells at 144 hr and overall biomass yield with respect to urea was 3.27 g biomass/g urea (Fig. 6.5C). Extracellular K_2HPO_4 also became zero at 48 hr and overall biomass yield with respect to K_2HPO_4 was found to be 15.29 g biomass/g K_2HPO_4 (Fig. 6.5F). Biomass titer of 3.26 g/l with 55% FAME content was obtained at 480 hr (Fig. 6.5E). The maximum FAME concentration and overall FAME productivity were 1.79 g/l and 90 mg/l/day respectively. Maximum EPS concentration of 290 mg/l was achieved at 720 hr in the current study (Fig. 6.5F). Overall EPS productivity and overall EPS yield with respect to biomass were 10 mg/l/day and 82 mg EPS/g biomass at 720 hr respectively. The optimized nutrient levels, adequate light intensity from sunlight and environmental conditions (process pH and culture temperature) in the media would be synergistically responsible for high FAME and EPS production from *S. abundans*. Maximum autosedimentation factor of 1.83 was observed at 600 hr. Maximum autoflocculation efficiency of 92% was obtained at 720 hr (Fig. 6.5G). As per our knowledge, this was the first study to report optimized multi-objective RSM media to enhance FAME, EPS and ASF simultaneously in *S. abundans* under diurnal natural sunlight. EPS with specific metal ion combination contributes to autoflocculation phenomena that is confirmed from zeta potential analysis without pH adjustments. pH of microalgal culture sample in 5 ml centrifuge tube at 720 hr before autoflocculation was 7.64. A significant reduction in zeta potential value (-7 mV) was noted for after autoflocculation sample as compared to before autoflocculation (-12.83 mV) and spent media after autoflocculation (-16.56 mV) samples at 720 hr (Fig. 6.5H). This significant reduction in zeta potential may be occurred due to the positive charges present in EPS with specific metal ions adhere to negative charges present in surface of microalgal cells through charge neutralization mechanism that contributes for natural autoflocculating capacity of *S. abundans*. Salim et al. stated that

glycoproteins present in EPS patched to the cell surface and responsible for autoflocculation phenomena in *Ettlia texensis* (Salim et al., 2014). Autoflocculation rate with bottom OD_{680} was monitored for microalgal sample collected at 720 hr in the current study and cells settled in quick time from 20.4 OD_{680} (0 hr) to 278.8 OD_{680} (30 hr) (See Fig. A1 in **Section 3**, Appendices). This natural autoflocculation ability of *S. abundans* decreases the costs involved in algal harvesting. The production cost of biodiesel from algae depends on the yield of algal biomass from the culture system, lipid content in microalgae, the scale of production systems and cost of recovering biodiesel from algal biomass. Chisti estimated the production cost of algae oil from a photobioreactor with an annual production capacity of 10,000 tons per year. Assuming the oil content of algae to be 30%, Chisti determined production cost of $2.80/l of algal oil. This estimation did not include costs of converting algae oil to biodiesel, or the distribution or marketing cost for biodiesel and taxes (Chisti, 2007). In the current study, 55% of FAME content (almost doubled as compared to Chisti assumption) was achieved under diurnal natural sunlight in constructed flat panel PBR, natural autoflocculation of *S. abundans* due to EPS with specific metal ion combination, coproduction of EPS in enhanced amounts could estimate to half of the production cost determined by Chisti.

6.4.5. Simultaneous production of FAME, autosedimentation factor and EPS using optimized media under diurnal simulated sunlight

Experiment was also performed with optimized multi-objective RSM media in medium scale PBR under diurnal simulated sunlight in single stage. The process pH and culture temperature profile were also recorded. As the culture temperature was not controlled, the resulted temperature was due to varying light intensities and algal metabolism during experiment (Fig. 6.6A). The process pH profile shown in Fig. 6.6B depicts that there is rise in pH in growth phase. The process pH decreases during nitrogen starvation period. Biomass titer, overall biomass productivity and overall specific growth rate of 3.32 g/l, 0.53 g/l/day, 0.55 day^{-}

^{1} were achieved at the end of growth phase (144 hr). The highest specific growth rate of 2.46 day^{-1} was observed at 24 hr. The specific growth rate decreases with culture age and became zero at stationary phase (144 hr) (Fig. 6.6C). Dry cell weight increases after growth phase due to accumulation of neutral lipids in *S. abundans* during nitrogen starvation (Fig. 6.6C). Maximum dry cell of weight of 6.25 g/l was observed at 696 hr. Maximum chlorophyll-a and carotenoid concentrations were found to be 24.5 mg/l (72 hr) and 6.1 mg/l (72 hr) respectively (Fig. 6.6D). Chlorophyll-a and carotenoid concentrations decreased drastically and colour of microalgal cells turned from green to greenish yellow during the mid-phase of nitrogen starvation period. This clearly indicates the shift of metabolic pathway from growth to lipid induction. Urea was completely consumed by the algal cells at 72 hr and overall biomass yield with respect to urea was 4.98 g biomass/g urea (Fig. 6.6C). Extracellular K_2HPO_4 also became zero at 24 hr and overall biomass yield with respect to K_2HPO_4 was found to be 19.2 g biomass/g K_2HPO_4 (Fig. 6.6F). The comparison of biomass, FAME, ASF and EPS production by *S. abundans* grown in medium scale PBR at diurnal natural sunlight and diurnal simulated sunlight was given in Table 6.7. Biomass titer of 5.40 g/l with 68% FAME content was obtained at 480 hr (Fig. 6.6E, Table 6.7). The maximum FAME concentration and overall FAME productivity were 3.69 g/l and 185 mg/l/day respectively.

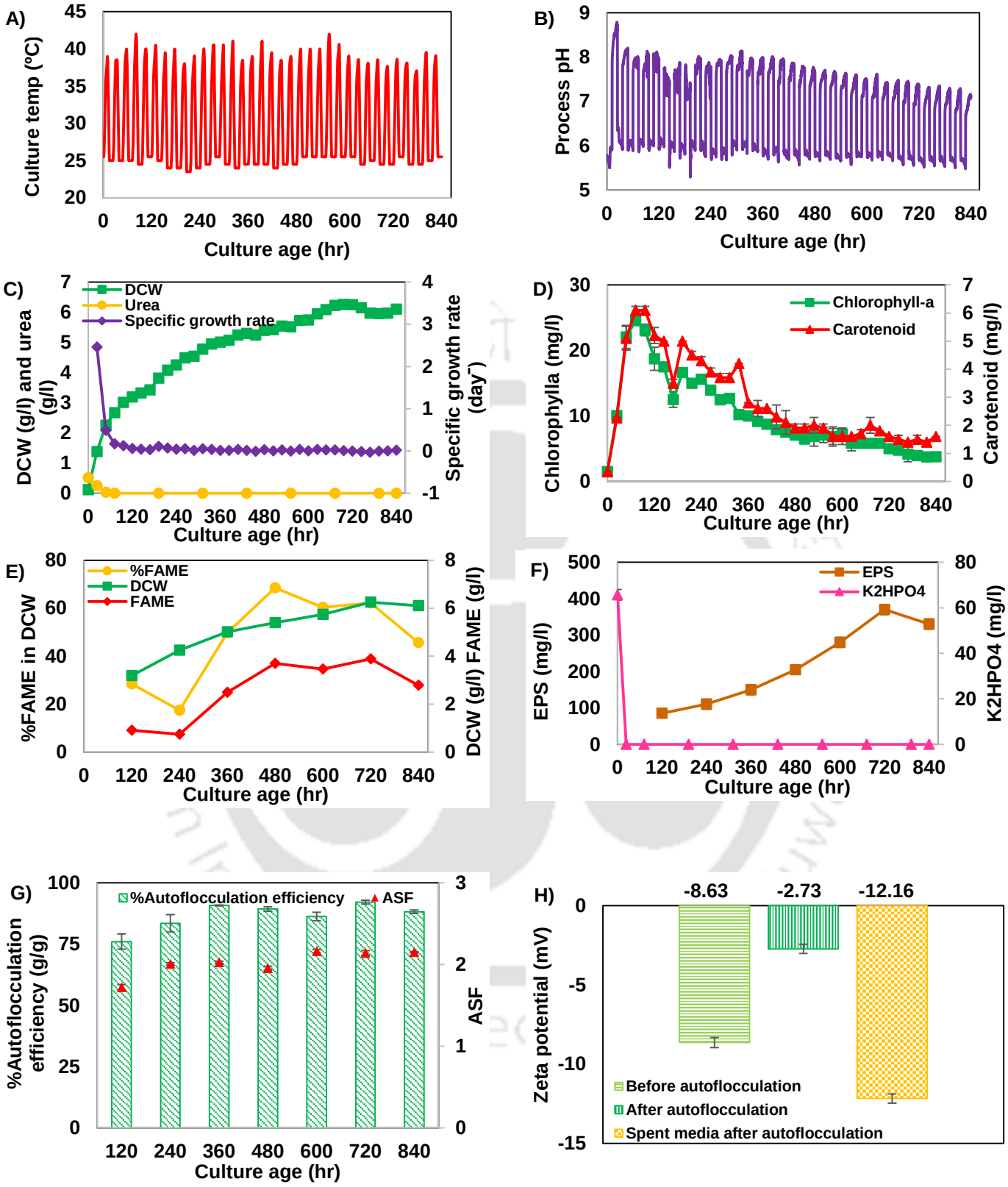

Fig. 6.6. Biomass growth at diurnal simulated sunlight in medium scale PBR. **A)** Culture temperature, **B)** Process pH, **C)** Dry cell weight, urea utilization and specific growth rate, **D)** Chlorophyll-a and carotenoid synthesis, **E)** Dry cell weight, FAME content in DCW, FAME concentration, **F)** EPS and K_2HPO_4 profile, **G)** autosedimentation factor and autoflocculation efficiency and **H)** Zeta potential.

Fawzy reported that *A. gracilis* produced maximum biomass productivity, lipid content in DCW and lipid productivity (40.6 mg/l/day, 39.3% and 15.9 mg/l/day respectively) in RSM optimized media containing 1 g/l nitrogen, 0 g/l phosphorus and 1.36 M NaCl using desirability function approach (Fawzy, 2017). In their study, they used 300 ml Erlenmeyer flask under constant illumination of 48.4 μmole/m^2/s and cultures were gassed with sterile air provided by air pump at 25 °C. The biomass productivity, lipid content in DCW and lipid productivity in their study would have enhanced by using high light intensity and air enriched with CO_2. In another study, Fawzy and Alharthi reported biomass productivity, lipid content in DCW and lipid productivity (48.59 mg/l/day, 39.08% and 19.91 mg/l/day respectively) in *Dunaliella Parva* by Derringer desirability function approach (Fawzy & Alharthi, 2021). Aguirre and Bassi found biomass concentration of 1102.9 mg/l and lipid productivity/cellulose content in DCW ratio of 0.45 (mg lipid/l/day)(mg cellulose/mg biomass)$^{-1}$ for culture conditions of 3.77% (v/v) CO_2 in air and 4.01 mM $NaNO_3$ in *Chlorella vulgaris* using overall desirability approach (Aguirre & Bassi, 2013). Less biomass concentration and less lipid productivity/cellulose content in DCW ratio resulted in their study was due to light intensity limitation. Maximum EPS concentration of 370 mg/l was achieved at 720 hr in the current study (Fig. 6.6F). Overall EPS productivity and overall EPS yield with respect to biomass were 12 mg/l/day and 59 mg EPS/g biomass at 720 hr respectively. Maximum autosedimentation factor of 2.16 was observed at 600 hr. Maximum autoflocculation efficiency of 92% was obtained at 720 hr (Fig. 6.6G). The zeta potential values of -8.63 mV, -2.73 mV and -12.16 mV were observed for before autoflocculation, after autoflocculation and spent media after autoflocculation of *S. abundans* at 720 hr (Fig. 6.6H). pH of microalgal culture sample in 5 ml centrifuge tube at 720 hr before autoflocculation was 6.72. The decrease in zeta potential value (-2.73 mV) for sample after autoflocculation depicts that EPS with specific metal ion combination was responsible for autoflocculation through charge neutralization

mechanism. Autoflocculation rate was monitored for the sample collected at 720 hr and microalgal cells started to settle in quick time from 31.6 OD_{680} (0 hr) to 434.2 OD_{680} (30 hr) without adding any flocculants (See Fig. A2 in **Section 3**, Appendices). The autoflocculating capacity of *S. abundans* eradicates the costs involved in harvesting process to great extent. The spent media after autoflocculation of biomass and extraction of EPS can be used for next batch after recycling of nutrients. Note that the autoflocculation is a natural process and it is exhibited by some specific algae. The high FAME and EPS production with the ability of natural autoflocculation by *S. abundans* would definitely be used as sustainable and commercial biorefinery feedstock.

Table 6.7. Comparison of combined effect of optimized medium constituents on the response (FAME content in DCW, FAME concentration, autosedimentation factor and EPS concentration).

Conditions	Process variables				Observed values of responses			
	Urea (mg/l)	$CoCl_2.6H_2O$ (mg/l)	$CuSO_4.5H_2O$ (mg/l)	$Na_2MoO_4.2H_2O$ (mg/l)	FAME content in DCW (%)[a]	FAME conc. (g/l)[a]	ASF[a]	EPS conc. (mg/l)[a]
Unoptimized modified Chu-13 media in test tube PBR	500.00	0.028	0.16	0.084	40.91 ± 0.72	1.66 ± 0.02	1.78 ± 0.13	287.50 ± 7
Optimized multi-objective RSM media in test tube PBR at diurnal simulated sunlight	659.63	0.08	1.17	0.03	70.43 ± 0.76	3.83 ± 0.04	1.93 ± 0.11	462.50 ± 14
Optimized multi-objective RSM media in medium scale PBR under diurnal natural sunlight	659.63	0.08	1.17	0.03	55.03 ± 0.43	1.79 ± 0.01	1.83 ± 0.01	290.00 ± 14
Optimized multi-objective RSM media in medium scale PBR at diurnal simulated sunlight	659.63	0.08	1.17	0.03	68.49 ± 0.46	3.69 ± 0.02	2.16 ± 0.01	370.00 ± 14

[a]All observed values of responses are represented as mean value ± standard deviation.

6.4.6. Evaluation of biodiesel quality from *S. abundans*

Biodiesel quality was calculated for highest %FAME content in DCW samples for the single stage cultivation under diurnal natural sunlight (480 hr) and diurnal simulated sunlight (480 hr) in medium scale PBR. The percentage of each FAME in DCW, each FAME in total FAME, % SFA (saturated fatty acid), % MUFA (mono unsaturated fatty acid), % PUFA (poly unsaturated fatty acid) composition were given in Table 6.8. FAME quantification by gas chromatography revealed abundance of methyl esters of palmitate, linoleate (trans and cis) as compared to other FAME that proves the potential of *S. abundans* towards good quality biodiesel. Methyl esters of C_{16} and C_{18} fatty acids constitute 98% of total FAME. The SV, IV, CN, DU, LCSF, CFPP, CP, PP, OSI, HHV, Density, Kinematic viscosity and FP values of biodiesel were also given in Table 6.8. These values were close to ASTM D6751-12 and EN 14214 standard and therefore, the biodiesel produced by *S. abundans* was used in automobiles (Knothe, 2012). This renewable energy candidate *S. abundans* also proved its nature in terms of biodiesel quality. Cetane number is very important among all biodiesel properties as it is highly influenced by SFA and MUFA profile and increases with the length of fatty acid chain. Higher cetane value indicates better combustion, best performance of the diesel engine enabling easier engine start-up and low nitrous oxide (NO_x) emissions into atmosphere. The CN values of methyl esters of *S. dimorphus* was 32.9 (Islam et al., 2013). The CN values from *S. abundans* obtained in current study were 44.47 and 46.34 under diurnal natural sunlight and diurnal simulated sunlight respectively in single stage medium scale PBR.

Table 6.8. Biodiesel composition and properties of *S. abundans* in single stage medium scale PBR at Diurnal natural sunlight (480 hr) and Diurnal simulated sunlight (480 hr).

FAME	Diurnal natural sunlight		Diurnal simulated sunlight	
	%FAME in DCW	%FAME in total FAME	%FAME in DCW	%FAME in total FAME
C14:0	0.16	0.29	0.25	0.36
C15:0	0.07	0.13	-	-
C15:1	0.11	0.21	0.11	0.17
C16:0	8.50	15.35	13.72	20.13
C16:1 trans	3.03	5.47	4.99	7.32
C16:2 cis	1.47	2.66	0.95	1.39
C16:2 trans	0.03	0.06	0.04	0.07
C16:3 cis	0.03	0.06	-	-
C16:3 trans	0.06	0.11	0.04	0.06
C17:0	0.34	0.63	0.25	0.37
C17:1	0.46	0.83	0.54	0.79
C17:2 cis	0.06	0.11	0.09	0.13
C17:2 trans	0.13	0.23	0.09	0.13
C18:0	2.22	4.01	2.52	3.69
C18:2 cis	9.40	17.00	14.19	20.82
C18:2 trans	29.17	52.71	30.32	44.48
C20:1	0.07	0.14	0.05	0.08
∑ C16-C18	53.91	97.43	66.77	97.96
SFA	11.29	20.41	16.74	24.55
MUFA	3.67	6.65	5.69	8.36
PUFA	40.35	72.94	45.72	67.08
FAME	55.31	100.00	68.15	99.99
Biodiesel property	***value***		***value***	
SV	194.56 mg KOH g^{-1} oil		195.40 mg KOH g^{-1} oil	
IV	132.77 g I_2 100 g^{-1} oil		123.93 g I_2 100 g^{-1} oil	
CN	44.47		46.34	
DU	152.53		142.53	
LCSF	3.54		3.85	
CFPP	-5.35 °C		-4.35 °C	
CP	3.08 °C		5.59 °C	
PP	-3.47 °C		-0.74 °C	
OSI	4.28 hrs		4.39 hrs	
HHV	39.63 MJ Kg^{-1}		39.63 MJ Kg^{-1}	
ρ (at 15 °C)	881 kg m^{-3}		880 kg m^{-3}	
v (at 40 °C)	3.89 mm^2 s^{-1}		3.92 mm^2 s^{-1}	
FP	439.34 °C		436.51 °C	

ASTM D6751-12 standard, SV < 500, CN ≥ 47, OSI ≥ 3

EN 14214 standard IV ≤ 120, HHV ≥ 35, 860 ≤ ρ ≤ 900, 3.5 ≤ v ≤ 5.0, FP ≥ 120, CP and PP - location and season dependent, CFPP - ≤ +5 (summer) or ≤ -20 (winter)

6.5. Conclusions

Test tube PBRs were customized and used for performing PBD, RSM, verification of multi-objective optimization experiments. Among 12 process variables in modified Chu-13 media, PBD determines urea, $CoCl_2.6H_2O$, $CuSO_4.5H_2O$ and $Na_2MoO_4.2H_2O$ as significant process variables influencing FAME content in DCW, FAME concentration, ASF and EPS concentration by *S. abundans*. The quadratic model equations of responses from RSM-CCD enhance single objective at a time. Therefore, these model equations from RSM-CCD are used with desirability approach for multi-objective optimization. The optimized multi-objective RSM media was formulated and used in medium scale PBR. The developed media produced 55% of FAME content in dry biomass, 1.79 g/l FAME, ASF of 1.83 within 1 hr, 290 mg/l EPS under diurnal natural sunlight. Thus, *S. abundans* could be used extensively for production of biodiesel and EPS under sunlight.

CHAPTER 7

Process development for immobilized enzyme based transesterification for biodiesel production from lipid enriched biomass of *S. abundans* by entrapment method

7.1. Background and uniqueness of the study

Microalgal biomass can be directly transesterified with methanol in presence of alkaline, acid or enzymatic catalysts to produce fatty acid methyl ester (FAME, biodiesel). The use of alkaline catalysts for transesterification is not suitable as it results in soap formation (Macías-Sánchez et al., 2015). Acid catalyzed biodiesel production is very slow due to water formation (Canakci & Van Gerpen, 2001). Lipases as enzyme catalyst has been employed as an alternative for transesterification process to overcome the problems of chemical catalysts (Guldhe et al., 2015). Lipase catalysis occurs at mild reaction conditions as compared to chemical catalysts. However, the recovery of free lipase enzyme after transesterification is difficult and require high process costs. Therefore, the concept of lipase immobilization by entrapment method was applied such that lipases could be reused for transesterification without significant loss in catalytic activity. Enzyme entrapment in porous matrices (alginate and acrylamide beads) is a rapid, nontoxic, inexpensive technique (Datta et al., 2013). This technique offers good mechanical strength as well as high porosity for substrate and product diffusion. Alginate is the most widely used polymer for enzyme entrapment (Zhang et al., 2013). Alginate is an anionic linear copolymer that is composed of 1,4-linked β-D-mannuronic acid and α-L-guluronic acid in different proportions and sequential arrangements. Porous calcium alginate beads are synthesized by crosslinking the carboxyl group of the α-L-guluronic

acid with a cationic crosslinker ($CaCl_2$) and used extensively due to its natural biocompatibility, ease of formation and mild physiological gelation conditions.

In calcium alginate matrices, the pore size of the beads and the amount of entrapped enzyme can be controlled by varying the concentration of sodium alginate. The capacity to retain enzyme inside the beads (i.e., to reduce leaching) increases with increasing concentration of sodium alginate. But, conversely, the activity of immobilized enzyme decreases. An increase in sodium alginate concentrations causes extensive cross networking of the matrix that results in reduced pore size of beads and causing reduced mass transfer or diffusion of substrate to the enzyme active site (Priyanka et al., 2019). The external mass transfer is inversely proportional to the thickness of boundary layer around the particle. Important parameters influencing internal mass transfer are particle size, pore size and the effective diffusion coefficient of the substrate within the pores of the enzyme (Won et al., 2005). Enzymes can lose their activity during storage due to denaturation of their tertiary structure and/or active site (Homaei et al., 2013). As far as our knowledge is concerned, very few studies reported immobilized lipase mediated direct transesterification of algal biomass using methanol as sole solvent to produce biodiesel via entrapment method.

Hence, the present work deals with free lipase and immobilized lipase mediated direct transesterification of *S. abundans* biomass in presence of methanol to produce biodiesel. Here, we have optimized reaction conditions for free lipase enzyme. Experiments with immobilized lipase via entrapment method were performed. Reaction kinetics of free lipase and immobilized lipase with microalgal biomass was investigated. Biodiesel composition and properties of *S. abundans* at optimized free lipase and immobilized lipase conditions was determined. Further, reusability and storage stability of immobilized lipase was examined.

7.2. Experiments for free lipase and immobilized lipase mediated transesterification

7.2.1. Experiments with free lipase

Steapsin lipase (specifications: appendices, Table A2) was used for enzyme based transesterification process. Different process variables such as mass ratio of methanol to algal biomass, mass ratio of lipase to algal biomass, temperature and pH were varied in 30 ml glass vials. One at a time variation was performed for all experiments. Methanol to biomass mass ratio experiment (4:1, 8:1, 12:1, 16:1, 20:1, 24:1, 28:1) was performed with 250 mg biomass, 4 ml methanol, 800 RPM using magnetic stirrer, 30 ºC reaction temperature and 8 hr reaction time by keeping constant enzyme concentration (50 mg/ml) to avoid dilution of enzyme. Lipase concentration variation (lipase to biomass mass ratio) was performed by varying lipase amounts with respect to biomass (0, 1, 5, 10, 15, 30, 50, 80%) with optimum methanol to biomass mass ratio and experimental conditions mentioned previously. Temperature variation experiment was performed by varying temperature (30 ºC, 40 ºC) with optimum methanol to biomass mass ratio, optimum lipase amounts with respect to biomass and experimental conditions mentioned previously. pH variation was performed by varying pH from 5 to 9 with optimum methanol to biomass mass ratio, optimum lipase amounts with respect to biomass, optimum reaction temperature and experimental conditions mentioned previously. In pH variation, control experiment was performed without adjusting pH and pH of control was 6.5 ± 0.1. All experiments in **Chapter 7** were performed in 30 ml glass vials (kept at airtight condition).

7.2.2. Experiments with immobilized lipase

Lipase immobilization by entrapment method was performing by mixing different loadings of lipase (50, 200, 500, 750, 1000 mg) separately with 3% sodium alginate in water (5 ml). The lipase-sodium alginate solution was mild heated at 30 ºC for mixing uniformly. The 5 ml reaction mixture was taken gently in 10 ml syringe and ejected into 0.2 M $CaCl_2.2H_2O$

solution (100 ml) in beaker. Hence, ~75 lipase-calcium alginate beads (3 mm diameter) are formed for each enzyme loading in the beaker and stored overnight at 4 ºC for stability. Enzyme loading of 0.66 mg lipase/bead, 2.66 mg lipase/bead, 6.66 mg lipase/bead, 10 mg lipase/bead, 13.33 mg lipase/bead were noted for 50 mg, 200 mg, 500 mg, 750 mg and 1000 mg lipase respectively. The beads with respective enzyme loadings are washed twice with water, collected separately and dried under fan for few minutes to avoid moisture. Experiment was performed with 10, 25 and 50 lipase beads of different enzyme loadings with 250 mg biomass, 4 ml methanol, 800 RPM, 30 ºC for 8 hrs in 30 ml glass vials.

7.2.3. Kinetic study experiments

Kinetic study was performed with the optimized free lipase and immobilized lipase conditions for microalgal biomass to find the residence time. Reaction mixture of 1 ml was collected in 5 ml centrifuge tube at time intervals of 0, 10, 60, 180, 300 and 480 min and FAMEs were extracted using 1 ml hexane. Water (1 ml) was added to remove aqueous impurities. The reaction mixture was centrifuged at 10000 RPM for 1 min. The top hexane layer containing FAME was collected in fresh 2 ml centrifuge tube and washed with water. Then, FAME in hexane layer was collected in 250 µl PCR tubes and 1 µl sample was injected in GC for FAME analysis. GC operating conditions and procedure were same as mentioned in the previous studies (Mahesh et al., 2019; Naira et al., 2019).

7.2.4. Reusability experiments with immobilized lipase in different buffers

The main aim of this study was reusing the enzyme to overcome biodiesel production cost. Enzyme loading of 750 mg (optimized enzyme loading from **Section 7.2.2**) was mixed with 3% sodium alginate in water (5 ml). The formation of 75 lipase-calcium alginate beads protocol was same as mentioned in **Section 7.2.2**. The beads were stored in 100 ml of 0.2 M $CaCl_2.2H_2O$ overnight at 4 ºC for stability. Thus, reusability experiments were performed with 250 mg biomass, 4 ml methanol, 25 beads of 750 mg enzyme i.e., lipase loading of 10

mg/alginate bead (62.5 mg/ml enzyme concentration) (optimized reaction condition from **Section 7.2.2**) at 800 RPM, 30 ºC for 8 hrs in 30 ml glass vials. The lipase-calcium alginate beads was stored in water overnight at 4 ºC after every cycle. Transesterification efficiency decreased drastically after 2 cycles. To overcome this problem, lipase-calcium alginate beads were prepared using 5% sodium alginate and used for reusability experiments. Lipase-calcium alginate beads were stored overnight at 4 ºC separately in water, 50 mM Tris-HCl buffer (pH 7 ± 0.2), 50 mM phosphate buffer (pH 7 ± 0.2), 50 mM citrate buffer (pH 7 ± 0.2) after every cycle for stability. Reusability experiments were also performed with 250 mg biomass, 4 ml methanol, 25 beads of 1500 mg enzyme i.e., lipase loading of 20 mg/alginate bead (125 mg/ml enzyme concentration) and 25 beads of 3000 mg enzyme i.e., lipase loading of 40 mg/alginate bead (250 mg/ml enzyme concentration) separately at 800 RPM, 30 ºC for 8 hrs in 30 ml glass vials (lipase-calcium alginate beads were prepared using 5% sodium alginate). Lipase-calcium alginate beads (25 beads of 1500 mg enzyme and 25 beads of 3000 mg enzyme) were stored separately in water overnight at 4 ºC after every cycle.

7.2.5. Storage stability experiments with immobilized lipase in water

For checking storage stability of lipase-calcium alginate beads (prepared using 5% sodium alginate), 25 beads of 750 mg enzyme and 25 beads of 1500 mg enzyme were prepared and stored in 100 ml of 0.2 M $CaCl_2.2H_2O$ overnight at 4 ºC for stability. The beads were washed twice with water and stored separately in 4 ml water in 30 ml glass vials at 4 ºC. After 24 hrs, 25 beads of 750 mg enzyme and 25 beads of 1500 mg enzyme were dried under fan for few minutes and used separately for 250 mg biomass, 4 ml methanol at 800 RPM, 30 ºC for 8 hrs in 30 ml glass vials. In another experiment, 25 lipase-calcium alginate beads of 1500 mg enzyme (prepared using 5% sodium alginate) were formed and stored in 100 ml of 0.2 M $CaCl_2.2H_2O$ overnight at 4 ºC for stability. The beads were washed twice with water and stored in 4 ml water in 30 ml glass vials at 4 ºC. After 48 hrs, 25 beads of 1500 mg enzyme were dried

under fan for few minutes and used for 250 mg biomass, 4 ml methanol at 800 RPM, 30 ºC for 8 hrs in 30 ml glass vials.

7.3. Results and Discussion

7.3.1. Free lipase mediated transesterification

In methanol to biomass mass ratio experiment, FAME content in DCW (45%) was observed with methanol to biomass mass ratio (16:1) (Fig. 7.1A). Increasing the methanol concentration increases the transesterification efficiency (%FAME in DCW). Note that enzyme concentration is constant (50 mg/ml) in methanol to biomass mass ratio experiment. Significant increment in FAME content in DCW was not observed in comparing methanol to biomass mass ratio of 16:1, 20:1, 24:1 and 28:1. Methanol to biomass mass ratio of 16:1 was optimal for extraction of lipids and provides good total surface area for reaction. Therefore, mass ratio of 16:1 was used for performing subsequent experiments. Note that %FAME in DCW was found to be 43% using optimized conventional (base followed by acid catalyst) method. Regarding lipase concentration variation experiment (lipase to biomass mass ratio), lipase amount with respect to biomass (80%) resulted in highest FAME content in DCW of 43% and hence used for subsequent experiments (Fig. 7.1B). In temperature variation experiment, reaction temperature of 30 ºC resulted in 43.45% FAME content in DCW whereas 40 ºC reaction temperature resulted in FAME content of 8.45% in DCW (Fig. 7.1C). Therefore, reaction temperature of 30 ºC was used for pH variation experiment. The decrease in FAME content when enzyme operated at 40 ºC suggests that higher temperature would cause significant loss of enzyme activity leading to its deactivation. Linsha et al. stated for free steapsin lipase, the optimal reaction temperature was 35 °C and showed a higher extent of deactivation at a temperature beyond 45 °C (Linsha et al., 2016). In pH variation experiment, free steapsin lipase works optimum without pH adjustments in current study. pH of control experiment was 6.5 ± 0.1. Control experiment (without adjusting pH) resulted in FAME

content of 43.45% in DCW (Fig. 7.1D). Linsha et al. reported optimal pH of 7 is desirable for outstanding enzymatic activity of free steapsin lipase (Linsha et al., 2016). The optimized conditions for free lipase were 16:1 methanol to biomass mass ratio, 80% lipase amount with respect to biomass, 30 ºC reaction temperature (room temperature) and works optimum without pH adjustments.

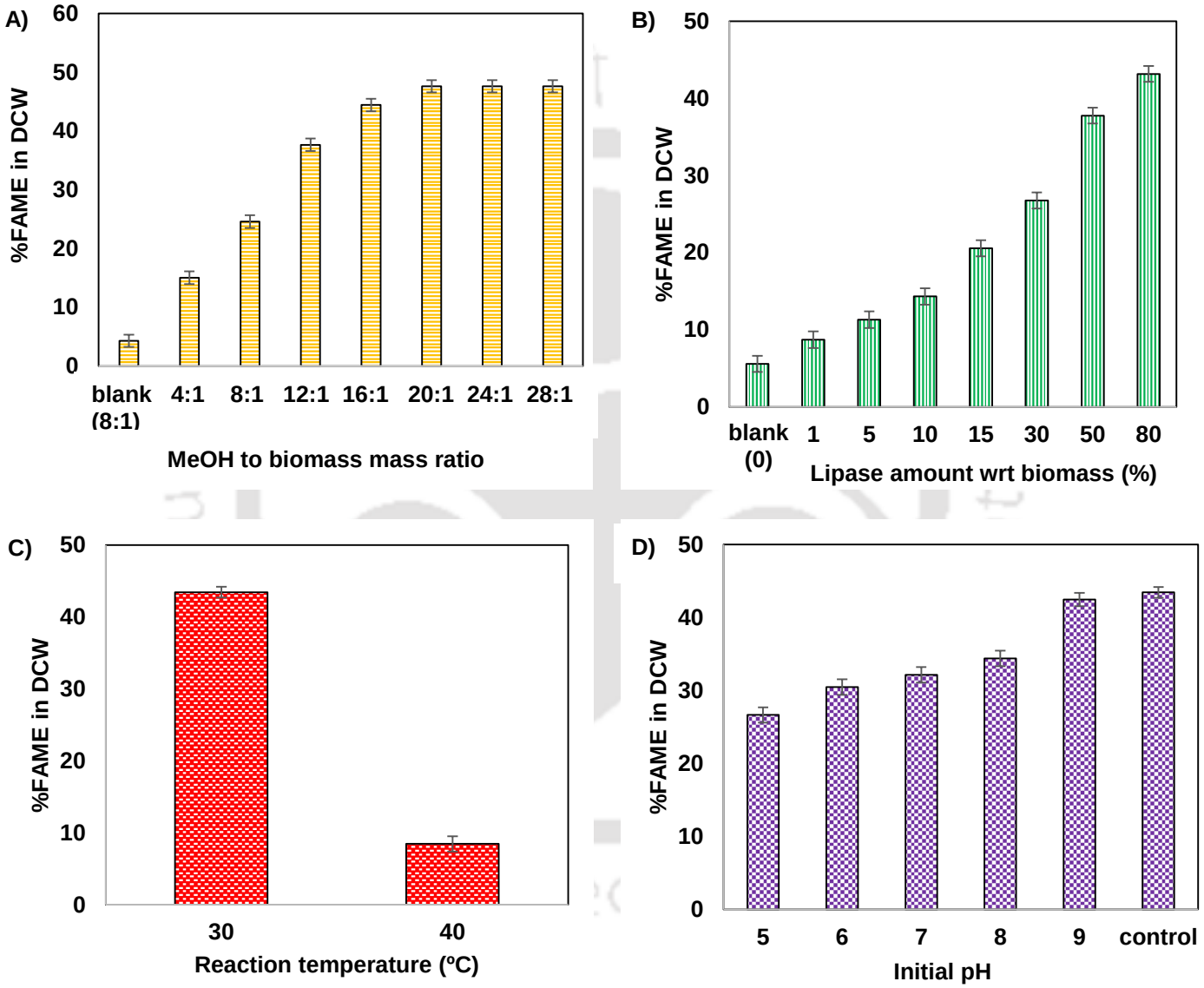

Fig. 7.1. Free lipase experiments. **A)** Methanol to biomass mass ratio, **B)** Lipase amount wrt to biomass, **C)** Temperature variation and **D)** Initial pH variation.

7.3.2. Immobilized lipase mediated transesterification

FAME content in DCW of 10, 25 and 50 lipase beads for different enzyme loadings is shown in Fig. 7.2. FAME content in DCW increases with increase in lipase loading for all

lipase beads 10, 25 and 50. Lipase loading of 10 mg/alginate bead (62.5 mg/ml lipase concentration) produced highest %FAME in DCW (44%) among different enzyme loadings (Fig. 7.2). Therefore, lipase loading of 10 mg/alginate bead (62.5 mg/ml lipase concentration) was used for reusability experiments.

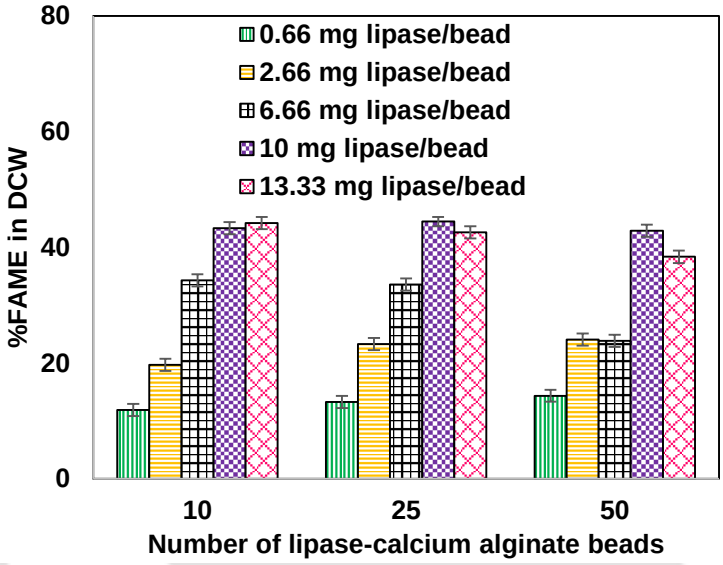

Fig. 7.2. Lipase immobilization experiment with different enzyme loadings.

7.3.3. Assessment of biodiesel quality

Biodiesel quantity and quality was estimated for *S. abundans* biomass at optimized free lipase and immobilized lipase conditions. The percentage of each FAME in DCW, each FAME in total FAME, % SFA, % MUFA, % PUFA composition were given in Table 7.1. FAME quantification by gas chromatography revealed abundance of methyl esters of palmitate, linoleate (trans and cis) as compared to other FAME that proves the capacity of *S. abundans*. Methyl esters of C_{16} and C_{18} fatty acids constitute 97% of total FAME. The SV, IV, CN, DU, LCSF, CFPP, CP, PP, OSI, HHV, Density, Kinematic viscosity and FP values of biodiesel were also given in Table 7.1 and were close to ASTM D6751-12 and EN 14214 standard indicating that the biodiesel produced by *S. abundans* could be effectively used in automobiles.

Table 7.1. Biodiesel composition and properties of *S. abundans* at optimized free lipase and immobilized lipase conditions.

FAME	Free lipase		Immobilized lipase	
	%FAME in DCW	%FAME in total FAME	%FAME in DCW	%FAME in total FAME
C12:0	0.02	0.05	0.02	0.05
C14:0	0.20	0.47	0.19	0.43
C15:0	0.08	0.18	0.06	0.14
C15:1	0.11	0.26	0.11	0.26
C16:0	8.68	20.23	9.76	22.23
C16:1 cis	0.01	0.02	-	-
C16:1 trans	2.66	6.19	2.32	5.29
C16:2 cis	0.66	1.54	0.59	1.34
C17:0	0.21	0.49	0.23	0.51
C17:1	0.12	0.28	0.11	0.25
C17:2 trans	0.54	1.25	0.37	0.85
C18:0	1.11	2.60	1.33	3.04
C18:1 cis	0.11	0.26	0.19	0.43
C18:2 cis	7.45	17.35	8.06	18.36
C18:2 trans	20.28	47.24	20.10	45.78
C18:3	0.64	1.50	0.42	0.94
C20:0	0.04	0.09	0.04	0.09
∑ C16-C18	41.60	96.93	42.77	97.41
SFA	10.34	24.11	11.63	26.49
MUFA	3.01	7.01	2.73	6.23
PUFA	29.57	68.88	29.54	67.27
FAME	42.92	100.00	43.90	99.99
Biodiesel property	***value***		***value***	
SV	195.48 ± 0.01 mg KOH g^{-1} oil		195.52 ± 0.02 mg KOH g^{-1} oil	
IV	127.12 ± 0.25 g I_2 100 g^{-1} oil		123.04 ± 0.24 g I_2 100 g^{-1} oil	
CN	45.61 ± 0.03		46.52 ± 0.04	
DU	144.77 ± 0.13		140.78 ± 0.11	
LCSF	3.40 ± 0.02		3.83 ± 0.01	
CFPP	-5.77 ± 0.01 °C		-4.42 ± 0.02 °C	
CP	5.64 ± 0.05 °C		6.70 ± 0.06 °C	
PP	-0.68 ± 0.02 °C		0.45 ± 0.01 °C	
OSI	4.37 ± 0.01 hrs		4.40 ± 0.02 hrs	
HHV	39.62 ± 0.01 MJ Kg^{-1}		39.62 ± 0.00 MJ Kg^{-1}	
ρ (at 15 °C)	880 ± 0.01 kg m^{-3}		880 ± 0.02 kg m^{-3}	
v (at 40 °C)	3.89 ± 0.01 mm^2 s^{-1}		3.92 ± 0.02 mm^2 s^{-1}	
FP	436.65 ± 0.02 °C		436.19 ± 0.01 °C	

ASTM D6751-12 standard, SV < 500, CN ≥ 47, OSI ≥ 3

EN 14214 standard IV ≤ 120, HHV ≥ 35, 860 ≤ ρ ≤ 900, 3.5 ≤ v ≤ 5.0, FP ≥ 120, CP and PP - location and season dependent, CFPP - ≤ +5 (summer) or ≤ -20 (winter)

7.3.4. Kinetic studies of free lipase and immobilized lipase

Kinetic study experiments was performed with free lipase and immobilized lipase to evaluate the optimal residence time. Transesterification efficiency increases with increase in reaction time for both free lipase and immobilized lipase with microalgal biomass (Fig. 7.3).

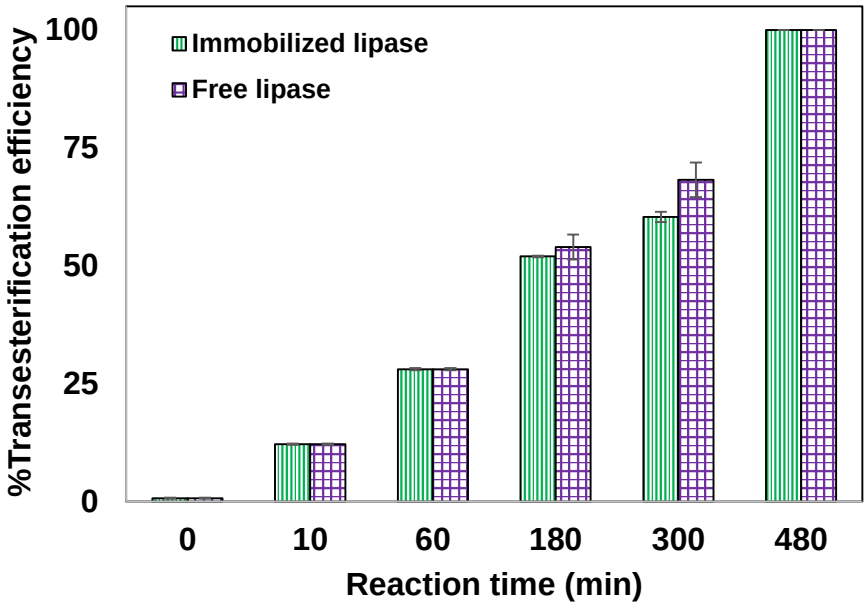

Fig. 7.3. Biomass transesterification efficiency analysis using free lipase and immobilized lipase.

7.3.5. Reusability of immobilized lipase in different buffers

Reusability experiment was performed as a preliminary study with 250 mg biomass, 4 ml methanol, 25 beads of 750 mg enzyme (prepared using 3% sodium alginate) at 800 RPM, 30 ºC for 8 hrs in 30 ml glass vials and storing lipase-calcium alginate beads in water overnight at 4 ºC after every cycle. Transesterification efficiency of immobilized steapsin lipase remained unaltered in first 2 cycles. Then, the catalytic performance of immobilized steapsin lipase decreased drastically with increase in cycle number (Fig. 7.4A). Hence, reusability of immobilized lipase was tested with 5% sodium alginate and storing lipase-calcium alginate beads overnight at 4 ºC separately in water, 50 mM Tris-HCl buffer (pH 7 ± 0.2), 50 mM phosphate buffer (pH 7 ± 0.2), 50 mM citrate buffer (pH 7 ± 0.2) after every cycle for stability

(other experimental conditions were same as mentioned previously). Phosphate and citrate chelate the calcium away from alginate, causing it to dissolve. Therefore, the stability and strength of lipase-calcium alginate beads is destroyed and is not possible for reusability experiments when stored in phosphate and citrate buffers (Fig. 7.4B). The major limitation of the use of calcium alginate as immobilization matrix is its sensitivity towards chelating compounds, such as phosphate, citrate and lactate or non-gelling cations such as sodium or magnesium ions (Thu et al., 1996). Transesterification efficiency was higher in every cycle when lipase calcium alginate beads are stored in water as compared to Tris-HCl buffer (Fig. 7.4B). This clearly indicates that water acts as a better storage medium than Tris-HCl buffer of pH 7 ± 0.2 for immobilized lipase and hence water was used for storing lipase-calcium alginate beads in subsequent experiments. Poppe et al. reported that Novozyme 435 (*Candida antarctica* lipase B immobilized in an acrylic resin) retained 70% of original enzyme activity after 8 reaction cycles, by performing a simple washing procedure with n-hexane between reaction batches (Poppe et al., 2013). Note that the cost of Novozyme 435 is high as compared to steapsin used in our study.

Reusability experiments was also performed with higher enzyme loadings (25 beads of 1500 mg lipase and 25 beads of 3000 mg lipase separately) and storing separately in water overnight at 4 ºC after every cycle. Transesterification efficiency and catalytic performance of immobilized lipase was better in every cycle for enzyme loading of 1500 mg lipase with 25 beads as compared to 750 mg lipase with 25 beads (Fig. 7.4C). Enzyme loading of 3000 mg lipase with 25 beads was not suitable for reusability as 5% sodium alginate failed to provide mechanical strength (Fig. 7.4C). Lipase-calcium alginate beads (3000 mg lipase with 25 beads) were fragile, flat in shape, broken into smaller pieces and became miscible with the reaction mixture due to agitation (800 RPM).

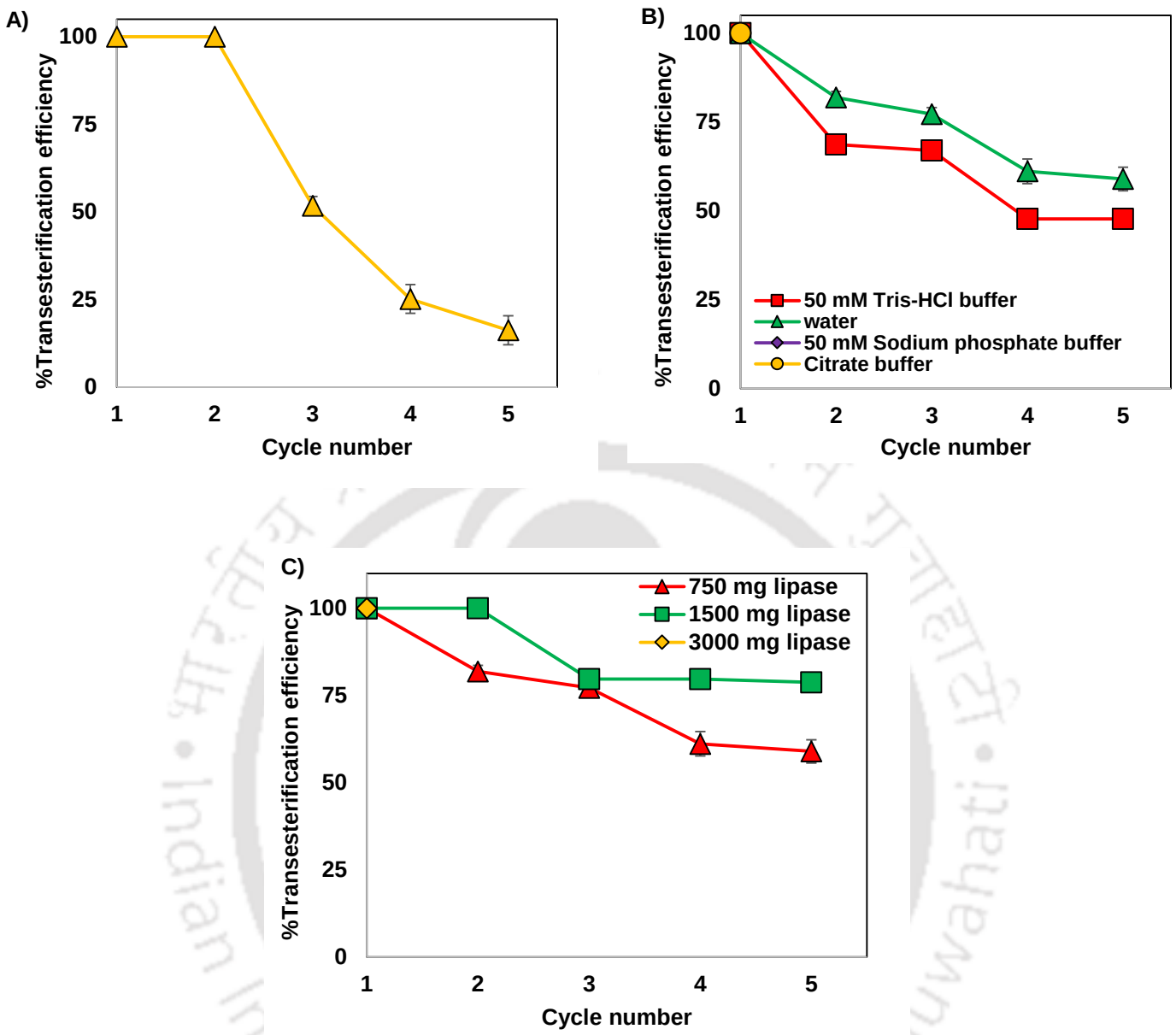

Fig. 7.4. Reusability of immobilized lipase in different buffers. **A)** 3% sodium alginate with water as storage medium, **B)** 5% sodium alginate with different buffers used for storage and **C)** different enzyme loadings with 5% sodium alginate and water as storage medium.

7.3.6. Storage stability of immobilized lipase in water

Storage stability of immobilized lipase 25 beads of 750 mg and 25 beads of 1500 mg lipase (prepared using 5% sodium alginate) was tested separately by storing in water at 4 ºC for 24 hr and then using stored lipase-calcium alginate beads (after drying under fan for few minutes) separately with 250 mg biomass, 4 ml methanol at 800 RPM, 30 ºC for 8 hrs in 30 ml glass vials. Enzyme loading of 750 mg resulted in 56% transesterification efficiency after

storing in water for 24 hr (Fig. 7.5). The decrease in transesterification efficiency was due to denaturation of tertiary structure and active site of enzyme. Homaei et al. stated that enzymes can lose their activity during storage due to denaturation of their tertiary structure and active site (Homaei et al., 2013). But, the loss of activity was not observed with 1500 mg lipase after storing in water for 24 hr (Fig. 7.5). Thus, 25 beads of 1500 mg enzyme (stored in water at 4 ºC for 48 hr) were dried under fan for few minutes and used for 250 mg biomass, 4 ml methanol at 800 RPM, 30 ºC for 8 hrs in 30 ml glass vials. This resulted in transesterification efficiency of 77% after storing in water for 48 hr and we can conclude that catalytic performance of immobilized steapsin lipase could be impaired under storage conditions (Fig. 7.5).

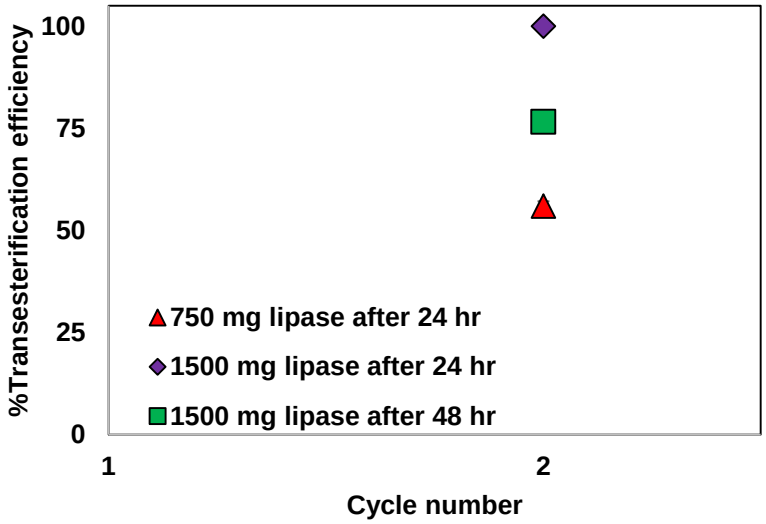

Fig. 7.5. Storage stability of immobilized lipase in water.

7.4. Conclusions

This study was performed to optimize reaction conditions for free lipase enzyme with microalgal biomass. Methanol was used as lipid extraction solvent, acyl acceptor and reaction medium. Immobilized lipase via entrapment method and reaction kinetics of free lipase and immobilized lipase with microalgal biomass was investigated. The optimized reaction conditions for free steapsin lipase were 16:1 methanol to biomass mass ratio, 80% lipase amount with respect to biomass, 30 ºC reaction temperature (room temperature) and works optimum without pH adjustments. Lipase loading of 10 mg/alginate bead (62.5 mg/ml enzyme concentration) produced highest FAME content in DCW (44%) among different enzyme loadings in immobilization experiments. The biodiesel property values at optimized free lipase and optimized immobilized lipase conditions were close to ASTM D6751-12 and EN 14214 standard that indicates the feasibility of using biodiesel produced by *S. abundans* in automobiles. Transesterification efficiency increases with increase in reaction time for both free lipase and immobilized lipase in kinetic study experiments. Water acts as a better storage medium as compared to buffers for immobilized lipase in reusability experiments. Lipase loading of 20 mg/alginate bead (125 mg/ml enzyme concentration) resulted in transesterification efficiency of 79% at 5^{th} cycle in reusability experiments. Higher lipase loading of 20 mg/alginate bead (125 mg/ml enzyme concentration) produced better transesterification efficiency as compared to lipase loading of 10 mg/alginate bead (62.5 mg/ml enzyme concentration) in storage stability experiments.

CHAPTER 8

Overall conclusions

Microalgae have the potential to produce high oil yield (L/ha) as compared to other energy crops. However, the commerciality of biodiesel production from algae has not been successful due to less biomass yield and low lipid content resulting in lower biodiesel productivity mainly derived from cultivation systems such as open raceway ponds and high cost photobioreactors (PBRs). Lack of efficient harvesting technology and undesirable transesterification process also led to infeasibility of biodiesel from algae. Moreover, in order to make biodiesel economically viable, there is a need to exploit other products such as exopolysaccharides (EPS) concomitantly apart from biodiesel and reduce downstream processing costs. Thus, present study focusses on developing a cost-effective medium scale flat panel photobioreactor with effective process design and media engineering to produce high biomass titer, high lipid and EPS yield under outdoor natural sunlight. Autoflocculation studies on microalgae for developing efficient harvesting technology and process development for immobilized enzyme based transesterification by entrapment method have also been carried out in the present study. Based upon major factors that influence microalgae growth and lipid production under natural sunlight, our study started with construction of mass transfer efficient flat panel PBR and engineering of optimized growth media for microalgae under high light intensity. Subsequently, process design to enhance biodiesel in single stage medium scale flat panel PBR under natural sunlight was explored. Also, multi-objective optimization of nutrients to enhance biodiesel, autosedimentation factor and EPS was studied using oleaginous microalgae *Scenedesmus abundans* in single stage medium scale flat panel PBR under diurnal

natural sunlight. Finally, free lipase and immobilized lipase mediated direct transesterification of algal biomass in presence of methanol as sole solvent were performed using entrapment method to produce biodiesel.

With respect to photobioreactor design, flat panel PBR technology was preferred due to its major advantages such as high surface area to volume ratio, large surface areas for illumination, lesser optical path length, less dark zone formation, low oxygen buildup. Medium scale bubble driven flat panel photobioreactor was constructed by installing customized mass transfer efficient membrane sparger. The medium scale flat panel PBR produced K_{La,CO_2} and t_m of 0.0125 s^{-1} and 8 sec respectively at 0.43 cm/s superficial gas velocity. Customized LED lighting system was designed to supply light energy for microalgae in laboratory experiments. Parallel mini flat panel PBR was developed and used for formulating optimized growth media. Maximum biomass titer of 6.9 g/l was achieved at end of growth phase using optimum growth media in medium scale flat panel PBR under LED light at 2162 µE/m^2/s, 1 VVM indoor condition. The productions were 1.53 g/l (22% of DCW) FAME with productivity of 67 mg/l/ day and 236 mg/l EPS with yield of 37 mg/g biomass under nitrogen starvation. *S. abundans* revealed its novelty by exhibiting no photoinhibition at 2162 µE/m^2/s high light intensity, capability of producing multi-products, cost effective natural autoflocculation based biomass harvesting and EPS purification can make the process sustainable.

From the perspective of process design to enhance biodiesel in medium scale flat panel PBR under natural sunlight, test tube PBRs were designed to find the effect of macronutrients and micronutrients in microalgal growth and lipid production photoautotrophically via a single stage. We have also studied the levels of micronutrient interaction on lipid production in microalgae. The optimized lipid media was formulated for enhancing lipid content in microalgae. The single stage produced 2.5 fold higher FAME content in DCW than two stage and economical as harvesting steps could be minimized. Single stage strategy improves the

lipid content in microalgae but it sacrifices the algal biomass concentration. The comparison of single and two stage cultivation strategy for lipid accumulation in *Scenedesmus* sp. was not explored extensively so far in literature. Biomass titer of 2.79 g/l with maximum FAME content of 46% was achieved using developed media in medium scale flat panel PBR under diurnal natural sunlight. FAME concentration, FAME productivity and maximum EPS concentration of 1.28 g/l, 27 mg/l/day and 155 mg/l were obtained under sunlight study. *S. abundans* could be a potential candidate for simultaneous production of biodiesel and exopolysaccharides with natural autoflocculation abilities. Therefore, the exploitation of *S. abundans* as a co-producer of biodiesel and EPS under sunlight could be a feasible approach. Though production capability of EPS and autoflocculation efficiency of *Scenedesmus* sp. have been explored for the cultivation system under LED light but these are not investigated earlier under outdoor natural sunlight.

This study also focusses on multi-objective optimization of nutrients to enhance biodiesel, autosedimentation factor and EPS using composite desirability approach under outdoor natural sunlight. As sunlight is diurnal by nature and has broad range (0 – 2000 $\mu E/m^2/s$) of continuous light intensity variations from dawn to dusk, diurnal simulated sunlight intensity was generated from pulse width modulation (PWM) and OPTO22 control system that controls LED light intensity ranging from 0 to 2200 $\mu E/m^2/s$ (capable of mimicking sunlight intensities in laboratory). Test tube PBRs were used for performing PBD, RSM and verification of multi-objective optimization experiments. PBD determines urea, $CoCl_2.6H_2O$, $CuSO_4.5H_2O$ and $Na_2MoO_4.2H_2O$ as significant process variables in modified Chu-13 media that influences FAME content in dry biomass, FAME concentration, ASF and EPS concentration by *S. abundans.* The quadratic model equations of responses from RSM-CCD enhance single objective at a time. Therefore, these model equations from RSM-CCD are used with composite desirability approach for formulating optimized multi-objective RSM media. The formulated

media produced 55% of FAME content in dry biomass, 1.79 g/l FAME, ASF of 1.83 within 1 hr, 290 mg/l EPS under diurnal natural sunlight. As per our knowledge is concerned, no studies have been performed using multi-response optimization to enhance FAME, ASF and EPS concomitantly in *S. abundans*.

Finally, free steapsin lipase mediated direct transesterification of microalgal biomass was performed to optimize reaction conditions. Methanol was used as lipid extraction solvent, acyl acceptor and reaction medium. The optimized reaction conditions for free steapsin lipase were 16:1 methanol to biomass mass ratio, 80% lipase amount with respect to biomass, 30 ºC reaction temperature (room temperature) and works optimum without pH adjustments. Experiments with immobilized lipase reveals that lipase loading of 10 mg/alginate bead (62.5 mg/ml enzyme concentration) produced highest FAME content in DCW (44%) among different enzyme loadings. The biodiesel property values at optimized free lipase and optimized immobilized lipase conditions satisfies the required limits of ASTM D6751-12 and EN 14214 standard that indicates the feasibility of using biodiesel produced by *S. abundans* in automobiles. Reaction kinetics of free lipase and immobilized lipase with biomass depicts that transesterification efficiency increases with increase in reaction time. Water behaves as better storage medium for lipase-calcium alginate beads in reusability experiments and lipase loading of 20 mg/alginate bead (125 mg/ml enzyme concentration) resulted in transesterification efficiency of 79% at 5^{th} cycle. Higher lipase loading of 20 mg/alginate bead (125 mg/ml enzyme concentration) produced better transesterification efficiency as compared to lipase loading of 10 mg/alginate bead (62.5 mg/ml enzyme concentration) in storage stability experiments. The use of immobilized lipase mediated direct transesterification of algal biomass using methanol as sole solvent to produce biodiesel via entrapment method is reported in very few studies in literature. Specific light availability per algal cell, mixing and mass transfer issues are major bottlenecks for scale-up studies in photobioreactors. Efficient sparger design

for good mixing and mass transfer, incorporation of tiny mixers that operate by bubble driven agitation (resolve mixing issues in photobioreactor), availability of specific light intensity per algal cell in the photobioreactor by using bubble driven mixers, studies on cheap harvesting technology, immobilization studies using industrial lipases are essential for scale-up process. The research findings from this study such as simultaneous production of biodiesel and exopolysaccharides from *S. abundans* in medium scale flat panel photobioreactor, modulation of macro and micronutrients to enhance lipid production by *S. abundans* via single stage cultivation under natural sunlight, enhancing multiproducts (biodiesel and EPS) by formulating optimized multi-objective RSM media under natural sunlight and performing direct transesterification of microalgal biomass for biodiesel production using steapsin lipase immobilization by entrapment method could be tested at larger scale to meet industrial applications. The biodiesel obtained in this study could be used in the automobile industries and engines with or without modifications. Exopolysaccharides produced in this study could be formulated and tested its efficacy in various electrical, food, cosmetic, pharmaceutical and textile industries.

Future Prospects

- ✓ The constructed medium scale flat panel photobioreactor with mass transfer efficient neoprene membrane sparger would be applicable for mass culturing of any microalgal strain under diurnal natural sunlight. Overall biomass titer of 6.9 g/l and biomass productivity of 1.2 g/l/day were attained at the end of growth phase (134 hr) using optimized growth media. In some cases, other than biodiesel production, e.g., bio-oil, the production and the extraction cost decreases with the increase in biomass density.

- ✓ High natural autoflocculating ability (90% cell recovery) was observed in 3 min when *S. abundans* biomass was around 1.5 g/l in optimized growth media. Harvesting operation cost would be significantly reduced upon using this strain in large scale cultivation.

- ✓ Extracellular metabolites (EPS) was produced during microalgal cultivation and purified after autoflocculation of *S. abundans*. This extracellular platform is highly beneficial in the perspective of downstream processing economics as they require less energy to recover. There is huge scope as EPS could be used in food (e.g. jelly, candy, sauce and beverages), pharmaceuticals (e.g. capsule covering and antitumor drugs), textiles (e.g. printing and dyeing), cosmetics (e.g. body lotion and emulsifier), detergents, adhesives, wastewater treatment, bioremediation, bioflocculants and oil recovery.

- ✓ The single stage strategy produced 2.5 fold higher FAME content than two stage strategy in this study. Single stage is economical as compared to two stage since an extra step where algal cell is harvested after high growth and re-suspension in a nutrient limiting media for promoting lipid could be neglected. Note that single stage strategy improves the lipid content in microalgae but it sacrifices the algal biomass concentration.

- ✓ Single stage cultivation of *S. abundans* using optimized multi-objective RSM media via composite desirability approach for enhancing production of biodiesel and EPS under natural sunlight is a feasible biorefinery approach. Concomitant synthesis of high intracellular and extracellular products would reduce the upstream, downstream processing costs, overall cost of their production and yield profits.

- ✓ Free steapsin lipase works optimum at room temperature and pH adjustments are not required. Immobilized steapsin lipase could be recovered and reused in direct transesterification of algal biomass.

- ✓ Higher steapsin lipase loadings in immobilization by calcium alginate entrapment method depicted better transesterification efficiency in reusability experiments. Industrial enzymes such as Novozyme 435 could retain good enzyme activity in reusability studies as compared to steapsin immobilization performed in our study. But, the cost of Novozyme 435 and other industrial enzymes are much higher than steapsin lipase. Therefore, low cost and good activity lipases could be explored and used in reusability studies by immobilization method.

References

Abdelaziz, A.E., Leite, G.B., Hallenbeck, P.C. 2013. Addressing the challenges for sustainable production of algal biofuels: II. Harvesting and conversion to biofuels. *Environmental technology*, **34**(13-14), 1807-1836.

Abdulla, R., Ravindra, P. 2013. Immobilized Burkholderia cepacia lipase for biodiesel production from crude Jatropha curcas L. oil. *Biomass and Bioenergy* **56**, 8-13.

Abu-Rezq, T.S., Al-Musallam, L., Al-Shimmari, J., Dias, P. 1999. Optimum production conditions for different high-quality marine algae. *Hydrobiologia*, **403**, 97-107.

Acién, F., Fernández, J., Magán, J., Molina, E. 2012. Production cost of a real microalgae production plant and strategies to reduce it. *Biotechnology advances*, **30**(6), 1344-1353.

Aguirre, A.M., Bassi, A. 2013. Investigation of biomass concentration, lipid production, and cellulose content in Chlorella vulgaris cultures using response surface methodology. *Biotechnology and bioengineering*, **110**(8), 2114-2122.

Alabi, A.O., Tampier, M., Bibeau, E. 2009. Microalgae technologies and processes for biofuels/bioenergy production in British Columbia: current technology, suitability and barriers to implementation: executive summary.

Al-Shatri, A.H.A., Ali, E., Al-Shorgani, N.K.N., Kalil, M.S. 2014. Growth of Scenedesmus dimorphus in different algal media and pH profile due to secreted metabolites. *African Journal of Biotechnology*, **13**(16).

Angelaalincy, M., Senthilkumar, N., Karpagam, R., Kumar, G.G., Ashokkumar, B., Varalakshmi, P. 2017. Enhanced extracellular polysaccharide production and self-sustainable electricity generation for PAMFCs by Scenedesmus sp. SB1. *ACS omega*, **2**(7), 3754-3765.

Anuradha, S., Thadikamala, S., Harish, B., Gayathri, G., Thulasidharan, D., Uppuluri, K.B. 2021. Open system for the autotrophic cultivation of Scenedesmus obliquus NCIM 5586: multiobjective optimization for the tradeoff between biomass and lipid. *Biomass Conversion and Biorefinery* 1-11.

Aransiola, E.F., Ojumu, T.V., Oyekola, O., Madzimbamuto, T., Ikhu-Omoregbe, D. 2014. A review of current technology for biodiesel production: State of the art. *Biomass and bioenergy*, **61**, 276-297.

Arias-Peñaranda, M.T., Cristiani-Urbina, E., Montes-Horcasitas, C., Esparza-García, F., Torzillo, G., Cañizares-Villanueva, R.O. 2013. Scenedesmus incrassatulus CLHE-Si01: a potential source of renewable lipid for high quality biodiesel production. *Bioresource technology*, **140**, 158-164.

Atabani, A., Badruddin, I.A., Mekhilef, S., Silitonga, A.S. 2011. A review on global fuel economy standards, labels and technologies in the transportation sector. *Renewable and Sustainable Energy Reviews*, **15**(9), 4586-4610.

Banerjee, S., Kaushik, S., Tomar, R.S. 2019. Global scenario of biofuel production: Past, present and future. *Prospects of Renewable Bioprocessing in Future Energy Systems*, 499-518.

Barabás, I., Todoruț, I.-A. 2011. Biodiesel quality, standards and properties. *Biodiesel-quality, emissions and by-products*, 3-28.

Barrow, C., Shahidi, F. 2007. *Marine nutraceuticals and functional foods*. CrC press.

Baweja, P., Sahoo, D. 2015. Classification of algae. in: *The algae world*, Springer, pp. 31-55.

Bhushan, I., Parshad, R., Qazi, G.N., Ingavle, G., Rajan, C., Ponrathnam, S., Gupta, V.K. 2008. Lipase enzyme immobilization on synthetic beaded macroporous copolymers for kinetic resolution of chiral drugs intermediates. *Process Biochemistry*, **43**(4), 321-330.

Bilanovic, D., Andargatchew, A., Kroeger, T., Shelef, G. 2009. Freshwater and marine microalgae sequestering of CO2 at different C and N concentrations–response surface methodology analysis. *Energy Conversion and Management*, **50**(2), 262-267.

Bišová, K., Zachleder, V. 2014. Cell-cycle regulation in green algae dividing by multiple fission. *Journal of experimental botany*, **65**(10), 2585-2602.

Brennan, L., Owende, P. 2010. Biofuels from microalgae—a review of technologies for production, processing, and extractions of biofuels and co-products. *Renewable and sustainable energy reviews*, **14**(2), 557-577.

Breuer, G., Lamers, P.P., Martens, D.E., Draaisma, R.B., Wijffels, R.H.J.B.t. 2013. Effect of light

intensity, pH, and temperature on triacylglycerol (TAG) accumulation induced by nitrogen starvation in Scenedesmus obliquus. *Bioresource technology*, **143**, 1-9.

Camp, P.J., Randall, D.D. 1985. Purification and characterization of the pea chloroplast pyruvate dehydrogenase complex: a source of acetyl-CoA and NADH for fatty acid biosynthesis. *Plant physiology*, **77**(3), 571-577.

Canakci, M., Van Gerpen, J. 2001. Biodiesel production from oils and fats with high free fatty acids. *Transactions of the ASAE*, **44**(6), 1429.

Cao, J., Yuan, H., Li, B., Yang, J. 2014. Significance evaluation of the effects of environmental factors on the lipid accumulation of Chlorella minutissima UTEX 2341 under low-nutrition heterotrophic condition. *Bioresource technology*, **152**, 177-184.

Carvalho, A.P., Malcata, F.X. 2001. Transfer of carbon dioxide within cultures of microalgae: plain bubbling versus hollow-fiber modules. *Biotechnology progress*, **17**(2), 265-272.

Chakraborty, T., Sen, A., Pal, R. 2015. Stress induced enhancement in exo-polysaccharide production in Spirulina subsalsa and its chemical characterization. *Journal of Algal Biomass Utilization*, **6**, 24-38.

Chen, B., You, W., Huang, J., Yu, Y., Chen, W. 2010. Isolation and antioxidant property of the extracellular polysaccharide from Rhodella reticulata. *World Journal of Microbiology and Biotechnology*, **26**(5), 833-840.

Chen, C.-Y., Yeh, K.-L., Chang, H.-Y., Chang, J.-S. 2014. Strategies to improve oil/lipid production of microalgae in outdoor cultivation using vertical tubular-type photobioreactors. *Energy Procedia*, **61**, 2755-2758.

Chen, Z., Chen, Y., Zhang, H., Qin, H., He, J., Zheng, Z., Zhao, L., Lei, A., Wang, J. 2022. Evaluation of Euglena gracilis 815 as a new candidate for biodiesel production. *Frontiers in Bioengineering and Biotechnology*, 441.

Cheng, J., Huang, R., Li, T., Zhou, J., Cen, K. 2015. Physicochemical characterization of wet microalgal cells disrupted with instant catapult steam explosion for lipid extraction. *Bioresource Technology*, **191**, 66-72.

Cheng, K.-C., Ren, M., Ogden, K.L. 2013. Statistical optimization of culture media for growth and lipid

production of Chlorella protothecoides UTEX 250. *Bioresource technology*, **128**, 44-48.

Cheng, L., Zhang, L., Chen, H., Gao, C. 2006. Carbon dioxide removal from air by microalgae cultured in a membrane-photobioreactor. *Separation and purification technology*, **50**(3), 324-329.

Chisti, Y. 2007. Biodiesel from microalgae. *Biotechnology advances*, **25**(3), 294-306.

Cho, H.U., Park, J.M. 2018. Biodiesel production by various oleaginous microorganisms from organic wastes. *Bioresource technology*, **256**, 502-508.

Choi, Y.-K., Kumaran, R.S., Jeon, H.J., Song, H.-J., Yang, Y.-H., Lee, S.H., Song, K.-G., Kim, K.J., Singh, V., Kim, H.J. 2015. LED light stress induced biomass and fatty acid production in microalgal biosystem, Acutodesmus obliquus. *Spectrochimica Acta Part A: Molecular and Biomolecular Spectroscopy*, **145**, 245-253.

Coates, J. 2000. Encyclopedia of analytical chemistry. *Interpretation of infrared spectra, a practical approach. Wiley, Chichester*, 10815-10837.

Collins, M., Knutti, R., Arblaster, J., Dufresne, J.-L., Fichefet, T., Friedlingstein, P., Gao, X., Gutowski, W.J., Johns, T., Krinner, G. 2013. Long-term climate change: projections, commitments and irreversibility. in: *Climate change 2013-The physical science basis: Contribution of working group I to the fifth assessment report of the intergovernmental panel on climate change*, Cambridge University Press, pp. 1029-1136.

Contreras, A., García, F., Molina, E., Merchuk, J. 1998. Interaction between CO2-mass transfer, light availability, and hydrodynamic stress in the growth of Phaeodactylum tricornutum in a concentric tube airlift photobioreactor. *Biotechnology and Bioengineering*, **60**(3), 317-325.

Converti, A., Casazza, A.A., Ortiz, E.Y., Perego, P., Del Borghi, M. 2009. Effect of temperature and nitrogen concentration on the growth and lipid content of Nannochloropsis oculata and Chlorella vulgaris for biodiesel production. *Chemical Engineering and Processing: Process Intensification*, **48**(6), 1146-1151.

Costa, J.A.V., Freitas, B.C.B., Santos, T.D., Mitchell, B.G., Morais, M.G. 2019. Open pond systems for microalgal culture. in: *Biofuels from Algae*, Elsevier, pp. 199-223.

Dahl, A. 1974. Biology of the Rhodophyta, JSTOR.

Datta, S., Christena, L.R., Rajaram, Y.R.S. 2013. Enzyme immobilization: an overview on techniques

and support materials. *3 Biotech*, **3**(1), 1-9.

de Jaeger, L., Verbeek, R.E., Draaisma, R.B., Martens, D.E., Springer, J., Eggink, G., Wijffels, R.H. 2014. Superior triacylglycerol (TAG) accumulation in starchless mutants of Scenedesmus obliquus:(I) mutant generation and characterization. *Biotechnology for biofuels*, **7**(1), 1-11.

Demirbas, A. 2009. Progress and recent trends in biodiesel fuels. *Energy conversion and management*, **50**(1), 14-34.

Derringer, G., Suich, R. 1980. Simultaneous optimization of several response variables. *Journal of quality technology*, **12**(4), 214-219.

Deshmukh, S., Bala, K., Kumar, R. 2019. Selection of microalgae species based on their lipid content, fatty acid profile and apparent fuel properties for biodiesel production. *Environmental Science and Pollution Research*, **26**, 24462-24473.

Dizge, N., Aydiner, C., Imer, D.Y., Bayramoglu, M., Tanriseven, A., Keskinler, B. 2009a. Biodiesel production from sunflower, soybean, and waste cooking oils by transesterification using lipase immobilized onto a novel microporous polymer. *Bioresource technology*, **100**(6), 1983-1991.

Dizge, N., Keskinler, B., Tanriseven, A. 2009b. Biodiesel production from canola oil by using lipase immobilized onto hydrophobic microporous styrene–divinylbenzene copolymer. *Biochemical Engineering Journal*, **44**(2-3), 220-225.

Doran, P.M. 1995. *Bioprocess engineering principles*. Elsevier.

Dou, X., Lu, X.-H., Lu, M.-Z., Yu, L.-S., Xue, R., Ji, J.-B. 2013. The effects of trace elements on the lipid productivity and fatty acid composition of Nannochloropis oculata. *Journal of Renewable Energy*, **2013**.

Ehimen, E., Sun, Z., Carrington, C. 2010. Variables affecting the in situ transesterification of microalgae lipids. *Fuel*, **89**(3), 677-684.

Esakkimuthu, S., Krishnamurthy, V., Govindarajan, R., Swaminathan, K. 2016. Augmentation and starvation of calcium, magnesium, phosphate on lipid production of Scenedesmus obliquus. *Biomass and Bioenergy* **88**, 126-134.

Fawzy, M.A. 2017. Fatty acid characterization and biodiesel production by the marine microalga Asteromonas gracilis: statistical optimization of medium for biomass and lipid enhancement.

Marine Biotechnology, **19**(3), 219-231.

Fawzy, M.A., Alharthi, S. 2021. Use of response surface methodology in optimization of biomass, lipid productivity and fatty acid profiles of marine microalga Dunaliella parva for biodiesel production. *Environmental Technology and Innovation*, **22**, 101485.

Fernandes, B.D., Mota, A., Ferreira, A., Dragone, G., Teixeira, J.A., Vicente, A.A. 2014. Characterization of split cylinder airlift photobioreactors for efficient microalgae cultivation. *Chemical Engineering Science*, **117**, 445-454.

Ferreira, G.F., Rios Pinto, L.F., Carvalho, P.O., Coelho, M.B., Eberlin, M.N., Maciel Filho, R., Fregolente, L.V. 2021. Biomass and lipid characterization of microalgae genera Botryococcus, Chlorella, and Desmodesmus aiming high-value fatty acid production. *Biomass Conversion and Biorefinery*, **11**, 1675-1689.

Francisco, E.C., Neves, D.B., Jacob-Lopes, E., Franco, T.T. 2010. Microalgae as feedstock for biodiesel production: carbon dioxide sequestration, lipid production and biofuel quality. *Journal of Chemical Technology and Biotechnology* **85**(3), 395-403.

Freire-Nordi, C.S., Vieira, A.A.H., Nascimento, O.R. 2005. The metal binding capacity of Anabaena spiroides extracellular polysaccharide: an EPR study. *Process Biochemistry*, **40**(6), 2215-2224.

Fritsch, F.E. 1935. *Structure and Reproduction of the Algae*.

Fuentes-Grünewald, C., Garcés, E., Alacid, E., Rossi, S., Camp, J. 2013. Biomass and lipid production of dinoflagellates and raphidophytes in indoor and outdoor photobioreactors. *Marine Biotechnology*, **15**(1), 37-47.

Garcia-Ochoa, F., Gomez, E. 2009. Bioreactor scale-up and oxygen transfer rate in microbial processes: an overview. *Biotechnology advances*, **27**(2), 153-176.

Gardner, R.D., Lohman, E., Gerlach, R., Cooksey, K.E., Peyton, B.M. 2013. Comparison of CO2 and bicarbonate as inorganic carbon sources for triacylglycerol and starch accumulation in Chlamydomonas reinhardtii. *Biotechnology and bioengineering*, **110**(1), 87-96.

Gavrilescu, M., Chisti, Y. 2005. Biotechnology—a sustainable alternative for chemical industry. *Biotechnology advances*, **23**(7-8), 471-499.

Gerbersdorf, S.U., Westrich, B., Paterson, D.M. 2009. Microbial extracellular polymeric substances

(EPS) in fresh water sediments. *Microbial ecology*, **58**(2), 334-349.

Giordano, M., Beardall, J., Raven, J.A. 2005. CO2 concentrating mechanisms in algae: mechanisms, environmental modulation, and evolution. *Annu. Rev. Plant Biol.*, **56**, 99-131.

Giordano, M., Wang, Q. 2018. Microalgae for industrial purposes. *Biomass and green chemistry: Building a renewable pathway*, 133-167.

González-Garcinuño, Á., Tabernero, A., Sánchez-Álvarez, J.M., Del Valle, E.M.M., Galán, M.A. 2014. Effect of nitrogen source on growth and lipid accumulation in Scenedesmus abundans and Chlorella ellipsoidea. *Bioresource technology*, **173**, 334-341.

Gorain, P.C., Bagchi, S.K., Mallick, N. 2013. Effects of calcium, magnesium and sodium chloride in enhancing lipid accumulation in two green microalgae. *Environmental technology*, **34**(13-14), 1887-1894.

Griffiths, M.J., Harrison, S.T. 2009. Lipid productivity as a key characteristic for choosing algal species for biodiesel production. *Journal of applied phycology*, **21**(5), 493-507.

Griggs, D., Stafford-Smith, M., Gaffney, O., Rockström, J., Öhman, M.C., Shyamsundar, P., Steffen, W., Glaser, G., Kanie, N., Noble, I. 2013. Sustainable development goals for people and planet. *Nature*, **495**(7441), 305-307.

Grima, E.M., Belarbi, E.-H., Fernández, F.A., Medina, A.R., Chisti, Y. 2003. Recovery of microalgal biomass and metabolites: process options and economics. *Biotechnology advances*, **20**(7-8), 491-515.

Grima, E.M., Pérez, J.S., Garc Camacho, F.Í., Medina, A.R. 1993. Gas-liquid transfer of atmospheric CO2 in microalgal cultures. *Journal of Chemical Technology and Biotechnology* **56**(4), 329-337.

Gualtieri, P., Barsanti, L. 2014. *Algae Anatomy, Biochemistry, and Biotechnology*. Taylor & Francis Group.

Guiry, M., GM, G. 2015. AlgaeBase. 2015 World-wide electronic publication, National University of Ireland, Galway.

Guldhe, A., Singh, B., Mutanda, T., Permaul, K., Bux, F. 2015. Advances in synthesis of biodiesel via enzyme catalysis: Novel and sustainable approaches. *Renewable and Sustainable Energy*

Reviews, **41**, 1447-1464.

Günerken, E., D'Hondt, E., Eppink, M., Garcia-Gonzalez, L., Elst, K., Wijffels, R.H. 2015. Cell disruption for microalgae biorefineries. *Biotechnology advances*, **33**(2), 243-260.

Gupta, R., Gupta, N., Rathi, P. 2004. Bacterial lipases: an overview of production, purification and biochemical properties. *Applied microbiology and biotechnology* **64**(6), 763-781.

Gupta, S., Pawar, S.B., Pandey, R. 2019. Current practices and challenges in using microalgae for treatment of nutrient rich wastewater from agro-based industries. *Science of the total environment*, **687**, 1107-1126.

Hallenbeck, P.C., Grogger, M., Mraz, M., Veverka, D. 2015. The use of Design of Experiments and Response Surface Methodology to optimize biomass and lipid production by the oleaginous marine green alga, Nannochloropsis gaditana in response to light intensity, inoculum size and CO2. *Bioresource technology*, **184**, 161-168.

Harris, G. 2012. *Phytoplankton ecology: structure, function and fluctuation*. Springer Science & Business Media.

He, Q., Yang, H., Xu, L., Xia, L., Hu, C. 2015. Sufficient utilization of natural fluctuating light intensity is an effective approach of promoting lipid productivity in oleaginous microalgal cultivation outdoors. *Bioresource technology*, **180**, 79-87.

Hegewald, E. 1997. Taxonomy and phylogeny of Scenedesmus. *Algae*, **12**(4), 235-46.

Hidalgo, P., Toro, C., Navia, R. 2013. Advances in direct transesterification of microalgal biomass for biodiesel production. *Reviews in Environmental Science and Bio/Technology*, **12**(2), 179-199.

Ho, S.-H., Chen, C.-Y., Chang, J.-S. 2012. Effect of light intensity and nitrogen starvation on CO2 fixation and lipid/carbohydrate production of an indigenous microalga Scenedesmus obliquus CNW-N. *Bioresource technology*, **113**, 244-252.

Hoekman, S.K., Broch, A., Robbins, C., Ceniceros, E., Natarajan, M. 2012. Review of biodiesel composition, properties, and specifications. *Renewable and sustainable energy reviews*, **16**(1), 143-169.

Homaei, A.A., Sariri, R., Vianello, F., Stevanato, R. 2013. Enzyme immobilization: an update. *Journal of chemical biology*, **6**(4), 185-205.

Hu, Q. 2004. Environmental effects on cell composition in Handbook of Microalgal Culture: Biotechnology and Applied Phycology (Richmond, A., ed.), Oxford: Blackwell Science Ltd.

Hussain, J., Wang, X., Sousa, L., Ali, R., Rittmann, B.E., Liao, W. 2020. Using non-metric multi-dimensional scaling analysis and multi-objective optimization to evaluate green algae for production of proteins, carbohydrates, lipids, and simultaneously fix carbon dioxide. *Biomass and Bioenergy* **141**, 105711.

Islam, M.A., Magnusson, M., Brown, R.J., Ayoko, G.A., Nabi, M.N., Heimann, K. 2013. Microalgal species selection for biodiesel production based on fuel properties derived from fatty acid profiles. *Energies*, **6**(11), 5676-5702.

Ismail, S.A.-e.A., Ali, R.F.M. 2015. Physico-chemical properties of biodiesel manufactured from waste frying oil using domestic adsorbents. *Science and Technology of Advanced Materials*.

Jago, C., Kennaway, G., Novarino, G., Jones, S. 2007. Size and settling velocity of suspended flocs during a Phaeocystis bloom in the tidally stirred Irish Sea, NW European shelf. *Marine Ecology Progress Series*, **345**, 51-62.

John, M.K. 1970. Colorimetric determination of phosphorus in soil and plant materials with ascorbic acid. *Soil Science*, **109**(4), 214-220.

Juneja, A., Ceballos, R.M., Murthy, G.S. 2013. Effects of environmental factors and nutrient availability on the biochemical composition of algae for biofuels production: a review. *Energies*, **6**(9), 4607-4638.

Katiyar, R., Gurjar, B.R., Biswas, S., Pruthi, V., Kumar, N., Kumar, P. 2017. Microalgae: an emerging source of energy based bio-products and a solution for environmental issues. *Renewable and Sustainable Energy Reviews*, **72**, 1083-1093.

Knezevic, Z., Milosavic, N., Bezbradica, D., Jakovljevic, Z., Prodanovic, R. 2006. Immobilization of lipase from Candida rugosa on Eupergit® C supports by covalent attachment. *Biochemical Engineering Journal*, **30**(3), 269-278.

Knothe, G. 2006. Analyzing biodiesel: standards and other methods. *Journal of the American Oil Chemists' Society*, **83**(10), 823-833.

Knothe, G. 2012. Fuel properties of highly polyunsaturated fatty acid methyl esters. Prediction of fuel

properties of algal biodiesel. *Energy & fuels*, **26**(8), 5265-5273.

Knothe, G., Sharp, C.A., Ryan, T.W. 2006. Exhaust emissions of biodiesel, petrodiesel, neat methyl esters, and alkanes in a new technology engine. *Energy & fuels*, **20**(1), 403-408.

Kunjapur, A.M., Eldridge, R.B. 2010. Photobioreactor design for commercial biofuel production from microalgae. *Industrial & engineering chemistry research*, **49**(8), 3516-3526.

Kusumaningtyas, P., Nurbaiti, S., Suantika, G., Amran, M.B., Nurachman, Z. 2017. Enhanced oil production by the tropical marine diatom Thalassiosira Sp. cultivated in outdoor photobioreactors. *Applied Biochemistry and Biotechnology* **182**(4), 1605-1618.

Lee, S.Y., Cho, J.M., Chang, Y.K., Oh, Y.-K. 2017. Cell disruption and lipid extraction for microalgal biorefineries: A review. *Bioresource technology*, **244**, 1317-1328.

Li, X., Přibyl, P., Bišová, K., Kawano, S., Cepák, V., Zachleder, V., Čížková, M., Brányiková, I., Vítová, M. 2013. The microalga Parachlorella kessleri—A novel highly efficient lipid producer. *Biotechnology and bioengineering*, **110**(1), 97-107.

Li, X., Xu, H., Wu, Q. 2007. Large-scale biodiesel production from microalga Chlorella protothecoides through heterotrophic cultivation in bioreactors. *Biotechnology and bioengineering*, **98**(4), 764-771.

Li, Y., Han, F., Xu, H., Mu, J., Chen, D., Feng, B., Zeng, H. 2014. Potential lipid accumulation and growth characteristic of the green alga Chlorella with combination cultivation mode of nitrogen (N) and phosphorus (P). *Bioresource technology*, **174**, 24-32.

Linsha, V., Aboo Shuhailath, K., Mahesh, K.V., Mohamed, A.A.P., Ananthakumar, S. 2016. Biocatalytic conversion efficiency of steapsin lipase immobilized on hierarchically porous biomorphic aerogel supports. *ACS Sustainable Chemistry & Engineering*, **4**(9), 4692-4703.

Liu, J., Yuan, C., Hu, G., Li, F. 2012a. Effects of light intensity on the growth and lipid accumulation of microalga Scenedesmus sp. 11-1 under nitrogen limitation. *Applied biochemistry and biotechnology* **166**(8), 2127-2137.

Liu, L., Pohnert, G., Wei, D. 2016. Extracellular metabolites from industrial microalgae and their biotechnological potential. *Marine drugs*, **14**(10), 191.

Looney, B., Dale, S. 2021. BP Statistical Review of World Energy 2021.

Lürling, M. 1999. *The smell of water: grazer-induced colony formation in Scenedesmus*. Wageningen University and Research.

Macías-Sánchez, M., Robles-Medina, A., Hita-Peña, E., Jiménez-Callejón, M., Estéban-Cerdán, L., González-Moreno, P., Molina-Grima, E. 2015. Biodiesel production from wet microalgal biomass by direct transesterification. *Fuel*, **150**, 14-20.

Madhubalaji, C., Sarat Chandra, T., Chauhan, V., Sarada, R., Mudliar, S.N. 2020. Chlorella vulgaris cultivation in airlift photobioreactor with transparent draft tube: effect of hydrodynamics, light and carbon dioxide on biochemical profile particularly ω-6/ω-3 fatty acid ratio. *Journal of food science and technology*, **57**, 866-876.

Magdalena, J.A., Ballesteros, M., González-Fernandez, C. 2018. Efficient anaerobic digestion of microalgae biomass: proteins as a key macromolecule. *Molecules*, **23**(5), 1098.

Mahesh, R., Naira, V.R., Maiti, S.K. 2019. Concomitant production of fatty acid methyl ester (biodiesel) and exopolysaccharides using efficient harvesting technology in flat panel photobioreactor with special sparging system via Scenedesmus abundans. *Bioresource technology*, **278**, 231-241.

Mahesh, R., Panda, S.K., Das, M., Yashavanth, P., Dhull, S., Negi, B.B., Jakhwal, P., Maiti, S.K. 2021. Advances in biotechnological tools for bioremediation of wastewater using bacterial–algal symbiotic system. in: *Wastewater Treatment*, Elsevier, pp. 385-411.

Mandal, M.K., Saikia, P., Chanu, N., Chaurasia, N. 2019. Modulation of lipid content and lipid profile by supplementation of iron, zinc, and molybdenum in indigenous microalgae. *Environmental Science and Pollution Research*, **26**(20), 20815-20828.

Mandotra, S., Kumar, P., Suseela, M., Nayaka, S., Ramteke, P. 2016. Evaluation of fatty acid profile and biodiesel properties of microalga Scenedesmus abundans under the influence of phosphorus, pH and light intensities. *Bioresource Technology*, **201**, 222-229.

Mandotra, S., Kumar, P., Suseela, M., Ramteke, P. 2014. Fresh water green microalga Scenedesmus abundans: a potential feedstock for high quality biodiesel production. *Bioresource Technology*, **156**, 42-47.

Manoylov, K.M. 2014. Taxonomic identification of algae (morphological and molecular): species

concepts, methodologies, and their implications for ecological bioassessment. *Journal of phycology*, **50**(3), 409-424.

Mata, T.M., Martins, A.A., Caetano, N.S. 2010. Microalgae for biodiesel production and other applications: a review. *Renewable and sustainable energy reviews*, **14**(1), 217-232.

Merchuk, J.C., Gluz, M., Mukmenev, I. 2000. Comparison of photobioreactors for cultivation of the red microalga Porphyridium sp. *Journal of Chemical Technology & Biotechnology: International Research in Process, Environmental & Clean Technology*, **75**(12), 1119-1126.

Miao, X., Wu, Q. 2006. Biodiesel production from heterotrophic microalgal oil. *Bioresource technology*, **97**(6), 841-846.

Mirón, A.S., García, M.-C.C., Camacho, F.G., Grima, E.M., Chisti, Y. 2004. Mixing in bubble column and airlift reactors. *Chemical Engineering Research and Design*, **82**(10), 1367-1374.

Moheimani, N.R. 2013. Inorganic carbon and pH effect on growth and lipid productivity of Tetraselmis suecica and Chlorella sp (Chlorophyta) grown outdoors in bag photobioreactors. *Journal of applied phycology*, **25**(2), 387-398.

Moheimani, N.R., Parlevliet, D. 2013. Sustainable solar energy conversion to chemical and electrical energy. *Renewable and Sustainable Energy Reviews*, **27**, 494-504.

Mohn, F. 1988. Harvesting of micro-algal biomass. *Micro-algal biotechnology*, 395-414.

Mona, S., Kaushik, A. 2015. Chromium and cobalt sequestration using exopolysaccharides produced by freshwater cyanobacterium Nostoc linckia. *Ecological Engineering*, **82**, 121-125.

Mondal, M., Khan, A.A., Halder, G. 2019. Estimation of biodiesel properties based on fatty acid profiles of Chlamydomonas sp. BTA 9032 and Chlorella sp. BTA 9031 obtained under mixotrophic cultivation conditions. *Biofuels*.

Moorthy, R.K., Premalatha, M., Arumugam, M. 2017. Batch sedimentation studies for freshwater green alga scenedesmus abundans using combination of flocculants. *Frontiers in chemistry*, **5**, 37.

Morweiser, M., Kruse, O., Hankamer, B., Posten, C. 2010. Developments and perspectives of photobioreactors for biofuel production. *Applied microbiology and biotechnology* **87**(4), 1291-1301.

Muñoz, C.F., Südfeld, C., Naduthodi, M.I., Weusthuis, R.A., Barbosa, M.J., Wijffels, R.H., D'Adamo,

S. 2021. Genetic engineering of microalgae for enhanced lipid production. *Biotechnology Advances*, **52**, 107836.

Nagle, N., Lemke, P. 1990. Production of methyl ester fuel from microalgae. *Applied Biochemistry and Biotechnology* **24**(1), 355-361.

Naira, V.R., Das, D., Maiti, S.K. 2019. Real time light intensity based carbon dioxide feeding for high cell-density microalgae cultivation and biodiesel production in a bubble column photobioreactor under outdoor natural sunlight. *Bioresource technology*, **284**, 43-55.

Naira, V.R., Mahesh, R., Panda, S.K., Maiti, S.K. 2020. Biorefinery Approaches for the Production of Fuels and Chemicals from Lignocellulosic and Algal Feedstocks. *Biorefinery of Alternative Resources: Targeting Green Fuels and Platform Chemicals*, Springer, 141-170.

Ndiaye, M., Gadoin, E., Gentric, C. 2018. CO2 gas–liquid mass transfer and kLa estimation: Numerical investigation in the context of airlift photobioreactor scale-up. *Chemical Engineering Research and Design*, **133**, 90-102.

Nelson, D.L., Lehninger, A.L., Cox, M.M. 2008. *Lehninger principles of biochemistry*. Macmillan.

Oswald, W.J. 1988. Large-scale algal culture systems (engineering aspects). *Micro-algal biotechnology*, 357-394.

Pal, D., Khozin-Goldberg, I., Cohen, Z., Boussiba, S. 2011. The effect of light, salinity, and nitrogen availability on lipid production by Nannochloropsis sp. *Applied microbiology and biotechnology* **90**(4), 1429-1441.

Park, J.-Y., Kim, D.-K., Lee, J.-P., Park, S.-C., Kim, Y.-J., Lee, J.-S. 2008. Blending effects of biodiesels on oxidation stability and low temperature flow properties. *Bioresource technology*, **99**(5), 1196-1203.

Pascher, A. 1931. *Systematische Übersicht über die mit Flagellaten in Zusammenhang stehenden Algenreihen und Versuch einer Einreihung dieser Algenstämme in die Stämme des Pflanzenreiches*. Verlag von C. Heinrich.

Philichi, T.L., Stenstrom, M.K. 1989. Effects of dissolved oxygen probe lag on oxygen transfer parameter estimation. *Journal of the water pollution control federation*, 83-86.

Plackett, R.L., Burman, J.P. 1946. The design of optimum multifactorial experiments. *Biometrika*,

33(4), 305-325.

Poppe, J.K., Garcia-Galan, C., Matte, C.R., Fernandez-Lafuente, R., Rodrigues, R.C., Ayub, M.A.Z. 2013. Optimization of synthesis of fatty acid methyl esters catalyzed by lipase B from Candida antarctica immobilized on hydrophobic supports. *Journal of Molecular Catalysis B: Enzymatic*, **94**, 51-56.

Posten, C. 2009. Design principles of photo-bioreactors for cultivation of microalgae. *Engineering in Life Sciences*, **9**(3), 165-177.

Priyanka, P., Kinsella, G.K., Henehan, G.T., Ryan, B.J. 2019. The Effect of Calcium Alginate Entrapment on the Stability of Novel Lipases from P. Reinekei and P. brenneri. *Trends in Peptide and Protein Sciences*, **4**, 1-10 (e7).

Pruvost, J., Van Vooren, G., Le Gouic, B., Couzinet-Mossion, A., Legrand, J. 2011. Systematic investigation of biomass and lipid productivity by microalgae in photobioreactors for biodiesel application. *Bioresource technology*, **102**(1), 150-158.

Quigg, A. 2016. Micronutrients. in: *The physiology of microalgae*, Springer, pp. 211-231.

Rai, M.P., Gupta, S. 2017. Effect of media composition and light supply on biomass, lipid content and FAME profile for quality biofuel production from Scenedesmus abundans. *Energy Conversion and Management*, **141**, 85-92.

Ramanna, L., Rawat, I., Bux, F. 2017. Light enhancement strategies improve microalgal biomass productivity. *Renewable and Sustainable Energy Reviews*, **80**, 765-773.

Ramírez-Verduzco, L.F., Rodríguez-Rodríguez, J.E., del Rayo Jaramillo-Jacob, A. 2012. Predicting cetane number, kinematic viscosity, density and higher heating value of biodiesel from its fatty acid methyl ester composition. *Fuel*, **91**(1), 102-111.

Ramos, M.J., Fernández, C.M., Casas, A., Rodríguez, L., Pérez, Á. 2009. Influence of fatty acid composition of raw materials on biodiesel properties. *Bioresource technology*, **100**(1), 261-268.

Ranganathan, S.V., Narasimhan, S.L., Muthukumar, K. 2008. An overview of enzymatic production of biodiesel. *Bioresource technology*, **99**(10), 3975-3981.

Raza, W., Yang, W., Jun, Y., Shakoor, F., Huang, Q., Shen, Q. 2012. Optimization and characterization of a polysaccharide produced by Pseudomonas fluorescens WR-1 and its antioxidant activity.

Carbohydrate Polymers, **90**(2), 921-929.

Rengel, R., Smith, R.T., Haslam, R.P., Sayanova, O., Vila, M., Leon, R. 2018. Overexpression of acetyl-CoA synthetase (ACS) enhances the biosynthesis of neutral lipids and starch in the green microalga Chlamydomonas reinhardtii. *Algal Research*, **31**, 183-193.

Rizwan, M., Mujtaba, G., Rashid, N., Lee, K. 2017. Enhancing lipid production of Dunaliella tertiolecta by manipulating the interactive effect of salinity and nitrogen. *Chemical and Biochemical Engineering Quarterly*, **31**(3), 199-207.

Rocha, D.N., Martins, M.A., Soares, J., Vaz, M.G.M.V., de Oliveira Leite, M., Covell, L., Mendes, L.B.B. 2019. Combination of trace elements and salt stress in different cultivation modes improves the lipid productivity of Scenedesmus spp. *Bioresource Technology*, **289**, 121644.

Rodionova, M.V., Poudyal, R.S., Tiwari, I., Voloshin, R.A., Zharmukhamedov, S.K., Nam, H.G., Zayadan, B.K., Bruce, B.D., Hou, H.J., Allakhverdiev, S.I. 2017. Biofuel production: challenges and opportunities. *International Journal of Hydrogen Energy*, **42**(12), 8450-8461.

Rodolfi, L., Chini Zittelli, G., Bassi, N., Padovani, G., Biondi, N., Bonini, G., Tredici, M.R. 2009. Microalgae for oil: Strain selection, induction of lipid synthesis and outdoor mass cultivation in a low-cost photobioreactor. *Biotechnology and bioengineering*, **102**(1), 100-112.

Rosenthal, H.L. 1955. Determination of urea in blood and urine with diacetyl monoxime. *Analytical chemistry*, **27**(12), 1980-1982.

Rossi, F., De Philippis, R. 2015. Role of cyanobacterial exopolysaccharides in phototrophic biofilms and in complex microbial mats. *Life*, **5**(2), 1218-1238.

Royon, D., Daz, M., Ellenrieder, G., Locatelli, S. 2007. Enzymatic production of biodiesel from cotton seed oil using t-butanol as a solvent. *Bioresource technology*, **98**(3), 648-653.

Sahay, S. 2021. *Handbook of Biofuels*. Academic Press.

Sajjadi, B., Chen, W.-Y., Raman, A.A.A., Ibrahim, S. 2018. Microalgae lipid and biomass for biofuel production: A comprehensive review on lipid enhancement strategies and their effects on fatty acid composition. *Renewable and Sustainable Energy Reviews*, **97**, 200-232.

Salim, S., Kosterink, N., Wacka, N.T., Vermuë, M., Wijffels, R. 2014. Mechanism behind autoflocculation of unicellular green microalgae Ettlia texensis. *Journal of biotechnology*, **174**,

34-38.

Salim, S., Shi, Z., Vermuë, M., Wijffels, R. 2013. Effect of growth phase on harvesting characteristics, autoflocculation and lipid content of Ettlia texensis for microalgal biodiesel production. *Bioresource technology*, **138**, 214-221.

Sarin, A., Arora, R., Singh, N., Sarin, R., Malhotra, R., Kundu, K. 2009. Effect of blends of Palm-Jatropha-Pongamia biodiesels on cloud point and pour point. *Energy*, **34**(11), 2016-2021.

Sawayama, S., Minowa, T., Yokoyama, S.-Y. 1999. Possibility of renewable energy production and CO2 mitigation by thermochemical liquefaction of microalgae. *Biomass and Bioenergy*, **17**(1), 33-39.

Saxena, P., Jawale, S., Joshipura, M.H. 2013. A review on prediction of properties of biodiesel and blends of biodiesel. *Procedia Engineering*, **51**, 395-402.

Schenk, P.M., Thomas-Hall, S.R., Stephens, E., Marx, U.C., Mussgnug, J.H., Posten, C., Kruse, O., Hankamer, B. 2008. Second generation biofuels: high-efficiency microalgae for biodiesel production. *Bioenergy research*, **1**(1), 20-43.

Scherholz, M.L., Curtis, W.R. 2013. Achieving pH control in microalgal cultures through fed-batch addition of stoichiometrically-balanced growth media. *BMC biotechnology*, **13**(1), 1-17.

Schlesinger, A., Eisenstadt, D., Bar-Gil, A., Carmely, H., Einbinder, S., Gressel, J. 2012. Inexpensive non-toxic flocculation of microalgae contradicts theories; overcoming a major hurdle to bulk algal production. *Biotechnology advances*, **30**(5), 1023-1030.

Scott, S.A., Davey, M.P., Dennis, J.S., Horst, I., Howe, C.J., Lea-Smith, D.J., Smith, A.G. 2010. Biodiesel from algae: challenges and prospects. *Current opinion in biotechnology*, **21**(3), 277-286.

Sebastião, F.d.A., Pilarski, F., Lemos, M.V.F. 2013. Composition of Extracellular Polymeric Substances (EPS) produced by Flavobacterium columnare isolated from tropical fish in Brazil. *Brazilian Journal of Microbiology*, **44**(3), 861-864.

Shafiei, S., Salim, R.A. 2014. Non-renewable and renewable energy consumption and CO2 emissions in OECD countries: a comparative analysis. *Energy policy*, **66**, 547-556.

Sharma, A.K., Sahoo, P.K., Singhal, S. 2016. Comparative evolution of biomass production and lipid

accumulation potential of Chlorella species grown in a bubble column photobioreactor. *Biofuels*, **7**(4), 389-399.

Sharma, K.K., Schuhmann, H., Schenk, P.M. 2012. High lipid induction in microalgae for biodiesel production. *Energies*, **5**(5), 1532-1553.

Shen, Y., Yuan, W., Pei, Z., Wu, Q., Mao, E. 2009. Microalgae mass production methods. *Transactions of the ASABE*, **52**(4), 1275-1287.

Shereena, K., Thangaraj, T. 2009. Biodiesel: An alternative fuel produced from vegetable oils by transesterification. *Electronic journal of biology*, **5**(3), 67-74.

Show, P.L., Tang, M.S., Nagarajan, D., Ling, T.C., Ooi, C.-W., Chang, J.-S. 2017. A holistic approach to managing microalgae for biofuel applications. *International journal of molecular sciences*, **18**(1), 215.

Sibi, G., Shetty, V., Mokashi, K. 2016. Enhanced lipid productivity approaches in microalgae as an alternate for fossil fuels–A review. *Journal of the Energy Institute*, **89**(3), 330-334.

Siddiki, S.Y.A., Mofijur, M., Kumar, P.S., Ahmed, S.F., Inayat, A., Kusumo, F., Badruddin, I.A., Khan, T.Y., Nghiem, L., Ong, H.C. 2022. Microalgae biomass as a sustainable source for biofuel, biochemical and biobased value-added products: An integrated biorefinery concept. *Fuel*, **307**, 121782.

Silverstein, R.M., Bassler, G.C. 1962. Spectrometric identification of organic compounds. *Journal of Chemical Education*, **39**(11), 546.

Singh, B., Guldhe, A., Rawat, I., Bux, F. 2014. Towards a sustainable approach for development of biodiesel from plant and microalgae. *Renewable and sustainable Energy reviews*, **29**, 216-245.

Singh, D., Sharma, D., Soni, S., Sharma, S., Sharma, P.K., Jhalani, A. 2020. A review on feedstocks, production processes, and yield for different generations of biodiesel. *Fuel*, **262**, 116553.

Singh, P., Kumari, S., Guldhe, A., Misra, R., Rawat, I., Bux, F. 2016. Trends and novel strategies for enhancing lipid accumulation and quality in microalgae. *Renewable and Sustainable Energy Reviews*, **55**, 1-16.

Solovchenko, A., Khozin-Goldberg, I., Didi-Cohen, S., Cohen, Z., Merzlyak, M. 2008. Effects of light intensity and nitrogen starvation on growth, total fatty acids and arachidonic acid in the green

microalga Parietochloris incisa. *Journal of applied Phycology*, **20**(3), 245-251.

Strickland, J., Parsons, T. 1968. A handbook of seawater analysis: pigment analysis. *Bulletin of Fisheries Research Board of Canada*, **167**.

Suali, E., Sarbatly, R. 2012. Conversion of microalgae to biofuel. *Renewable and Sustainable Energy Reviews*, **16**(6), 4316-4342.

Suganya, T., Varman, M., Masjuki, H., Renganathan, S. 2016. Macroalgae and microalgae as a potential source for commercial applications along with biofuels production: a biorefinery approach. *Renewable and Sustainable Energy Reviews*, **55**, 909-941.

Sun, X., Cao, Y., Xu, H., Liu, Y., Sun, J., Qiao, D., Cao, Y. 2014. Effect of nitrogen-starvation, light intensity and iron on triacylglyceride/carbohydrate production and fatty acid profile of Neochloris oleoabundans HK-129 by a two-stage process. *Bioresource Technology*, **155**, 204-212.

Takeshita, T., Ota, S., Yamazaki, T., Hirata, A., Zachleder, V., Kawano, S. 2014. Starch and lipid accumulation in eight strains of six Chlorella species under comparatively high light intensity and aeration culture conditions. *Bioresource Technology*, **158**, 127-134.

Tan, T., Lu, J., Nie, K., Deng, L., Wang, F. 2010. Biodiesel production with immobilized lipase: a review. *Biotechnology advances*, **28**(5), 628-634.

Thu, B., Smidsrod, O., Skjåk-Bræk, G. 1996. Alginate gels-Some structure-function correlations relevant to their use as immobilization matrix for cells. in: *Immobilization Cells: Basics and Applications*, Vol. 11, pp. 19-30.

Tian, C., Li, B., Liu, Z., Zhang, Y., Lu, H. 2014. Hydrothermal liquefaction for algal biorefinery: A critical review. *Renewable and Sustainable Energy Reviews*, **38**, 933-950.

Tornabene, T., Holzer, G., Lien, S., Burris, N. 1983. Lipid composition of the nitrogen starved green alga Neochloris oleoabundans. *Enzyme and Microbial Technology*, **5**(6), 435-440.

Udayan, A., Pandey, A.K., Sirohi, R., Sreekumar, N., Sang, B.-I., Sim, S.J., Kim, S.H., Pandey, A. 2022. Production of microalgae with high lipid content and their potential as sources of nutraceuticals. *Phytochemistry Reviews*, 1-28.

Uduman, N., Qi, Y., Danquah, M.K., Forde, G.M., Hoadley, A. 2010. Dewatering of microalgal

cultures: a major bottleneck to algae-based fuels. *Journal of renewable and sustainable energy*, **2**(1), 012701.

Ugwu, C., Aoyagi, H., Uchiyama, H. 2008. Photobioreactors for mass cultivation of algae. *Bioresource technology*, **99**(10), 4021-4028.

Vega-Estrada, J., Montes-Horcasitas, M., Domínguez-Bocanegra, A., Cañizares-Villanueva, R. 2005. Haematococcus pluvialis cultivation in split-cylinder internal-loop airlift photobioreactor under aeration conditions avoiding cell damage. *Applied microbiology and biotechnology*, **68**(1), 31-35.

Vijayaraghavan, K., Hemanathan, K. 2009. Biodiesel production from freshwater algae. *Energy & Fuels*, **23**(11), 5448-5453.

Vitova, M., Bisova, K., Kawano, S., Zachleder, V. 2015. Accumulation of energy reserves in algae: from cell cycles to biotechnological applications. *Biotechnology advances*, **33**(6), 1204-1218.

Wang, B., Lan, C.Q., Horsman, M. 2012. Closed photobioreactors for production of microalgal biomasses. *Biotechnology advances*, **30**(4), 904-912.

Wang, Z.T., Ullrich, N., Joo, S., Waffenschmidt, S., Goodenough, U. 2009. Algal lipid bodies: stress induction, purification, and biochemical characterization in wild-type and starchless Chlamydomonas reinhardtii. *Eukaryotic cell*, **8**(12), 1856-1868.

Weldy, C.S., Huesemann, M. 2007. Lipid production by Dunaliella salina in batch culture: effects of nitrogen limitation and light intensity. *Journal of Undergraduate Research*, **7**.

West, G. 1916. Algae (vol I) Botany handbooks. Cambridge, a treatise on the British fresh water algae, Cambridge University Press, London P. Baweja and D. Sahoo.

Widjaja, A., Chien, C.-C., Ju, Y.-H. 2009. Study of increasing lipid production from fresh water microalgae Chlorella vulgaris. *Journal of the Taiwan Institute of Chemical Engineers*, **40**(1), 13-20.

Williams, P.J.l.B., Laurens, L.M. 2010. Microalgae as biodiesel & biomass feedstocks: Review & analysis of the biochemistry, energetics & economics. *Energy & environmental science*, **3**(5), 554-590.

Wingender, J., Neu, T.R., Flemming, H.-C. 1999. What are bacterial extracellular polymeric

substances? in: *Microbial extracellular polymeric substances*, Springer, pp. 1-19.

Won, K., Kim, S., Kim, K.-J., Park, H.W., Moon, S.-J. 2005. Optimization of lipase entrapment in Ca-alginate gel beads. *Process biochemistry*, **40**(6), 2149-2154.

Wu, C., Xiao, Y., Lin, W., Li, J., Zhang, S., Zhu, J., Rong, J. 2017. Aqueous enzymatic process for cell wall degradation and lipid extraction from Nannochloropsis sp. *Bioresource Technology*, **223**, 312-316.

Wu, X., Ruan, R., Du, Z., Liu, Y. 2012. Current status and prospects of biodiesel production from microalgae. *Energies*, **5**(8), 2667-2682.

Xin, L., Hong-Ying, H., Yu-Ping, Z. 2011. Growth and lipid accumulation properties of a freshwater microalga Scenedesmus sp. under different cultivation temperature. *Bioresource technology*, **102**(3), 3098-3102.

Xiong, W., Gao, C., Yan, D., Wu, C., Wu, Q.J.B.t. 2010. Double CO2 fixation in photosynthesis–fermentation model enhances algal lipid synthesis for biodiesel production. *Bioresource technology*, **101**(7), 2287-2293.

Yadavalli, R., Ratnapuram, H., Motamarry, S., Reddy, C.N., Ashokkumar, V., Kuppam, C. 2020. Simultaneous production of flavonoids and lipids from Chlorella vulgaris and Chlorella pyrenoidosa. *Biomass Conversion and Biorefinery*, 1-9.

Yan, J., Cheng, R., Lin, X., You, S., Li, K., Rong, H., Ma, Y. 2013. Overexpression of acetyl-CoA synthetase increased the biomass and fatty acid proportion in microalga Schizochytrium. *Applied microbiology and biotechnology* **97**, 1933-1939.

Yang, F., Long, L., Sun, X., Wu, H., Li, T., Xiang, W. 2014. Optimization of medium using response surface methodology for lipid production by Scenedesmus sp. *Marine drugs*, **12**(3), 1245-1257.

Yeesang, C., Cheirsilp, B. 2011. Effect of nitrogen, salt, and iron content in the growth medium and light intensity on lipid production by microalgae isolated from freshwater sources in Thailand. *Bioresource technology*, **102**(3), 3034-3040.

Yeh, K.L., Chang, J.S. 2011. Nitrogen starvation strategies and photobioreactor design for enhancing lipid content and lipid production of a newly isolated microalga Chlorella vulgaris ESP-31: implications for biofuels. *Biotechnology Journal*, **6**(11), 1358-1366.

Yin, K., Wang, Q., Lv, M., Chen, L. 2019. Microorganism remediation strategies towards heavy metals. *Chemical Engineering Journal*, **360**, 1553-1563.

Yodsuwan, N., Sawayama, S., Sirisansaneeyakul, S. 2017. Effect of nitrogen concentration on growth, lipid production and fatty acid profiles of the marine diatom Phaeodactylum tricornutum. *Agriculture and Natural Resources*, **51**(3), 190-197.

You, Q., Yin, X., Zhao, Y., Zhang, Y. 2013. Biodiesel production from jatropha oil catalyzed by immobilized Burkholderia cepacia lipase on modified attapulgite. *Bioresource technology*, **148**, 202-207.

Yücel, S., Terzioğlu, P., Özçimen, D. 2012. Lipase applications in biodiesel production. *Biodiesel-Feedstocks, Production and Applications. InTech, Croatia*, 209-250.

Zhang, A., Tsang, V.L., Korke-Kshirsagar, R., Ryll, T. 2014. Effects of pH probe lag on bioreactor mixing time estimation. *Process Biochemistry*, **49**(6), 913-916.

Zhang, S., Shang, W., Yang, X., Zhang, S., Zhang, X., Chen, J. 2013. Immobilization of lipase using alginate hydrogel beads and enzymatic evaluation in hydrolysis of p-nitrophenol butyrate. *Bulletin of the Korean Chemical Society*, **34**(9), 2741-2746.

Zhao, G., Yu, J., Jiang, F., Zhang, X., Tan, T. 2012. The effect of different trophic modes on lipid accumulation of Scenedesmus quadricauda. *Bioresource technology*, **114**, 466-471.

Zhila, N., Kalacheva, G., Volova, T. 2005. Effect of nitrogen limitation on the growth and lipid composition of the green alga Botryococcus braunii Kutz IPPAS H-252. *Russian Journal of Plant Physiology*, **52**(3), 311-319.

Zhou, X., Xia, L., Ge, H., Zhang, D., Hu, C. 2013. Feasibility of biodiesel production by microalgae Chlorella sp.(FACHB-1748) under outdoor conditions. *Bioresource technology*, **138**, 131-135.

Zhu, L., Takala, J., Hiltunen, E., Wang, Z. 2013. Recycling harvest water to cultivate Chlorella zofingiensis under nutrient limitation for biodiesel production. *Bioresource technology*, **144**, 14-20.

Appendices

1. Procedure for calculation of biodiesel properties

The standard Supelco 37 component FAME mix (Sigma Aldrich, USA) was analysed by GC according to the method described in **Section 3.4.12**. For estimation of resulted FAME produced by microalgae, the peak areas of known concentrations of individual FAMEs from Supelco 37 component FAME mix (FAME standard) were taken as reference. Based on the resulted peak areas of run samples (FAME samples of microalgae), the unknown concentrations of individual FAMEs were calculated by extrapolating standard peak areas and presented in the Tables 4.1, 5.2, 6.8 and 7.1. Table A1 (Refer **Section 2**, appendices) was constructed from the data analysis of GC. Consequently, the biodiesel properties were calculated by using empirical equations 3.11 – 3.23 (Refer **Chapter 3**). An example of the calculation procedure of biodiesel properties for FAME data of Table A1 is given below.

For calculation of saponification value, equation 3.11, $SV = \sum \left[\frac{(560 \times F_i)}{M_i}\right]$ was solved by substituting percentage of individual FAME in total FAME (F_i) and molecular weight of individual FAME (M_i) of C14:0 – C20:1 FAMEs.

$$SV = \sum \left[\frac{(560 \times 0.29)}{242}\right] + \cdots + \left[\frac{(560 \times 15.35)}{270}\right] + \cdots + \left[\frac{(560 \times 0.14)}{324}\right]$$

$SV = 194.56$ mg KOH g^{-1} oil

For calculation of iodine value, equation 3.12, $IV = \sum \left[\frac{(254 \times F_i \times D_i)}{M_i}\right]$ was solved by substituting percentage of individual FAME in total FAME (F_i), number of double bonds in individual FAME (D_i) and molecular weight of individual FAME (M_i) of C14:0 – C20:1 FAMEs.

$$IV = \sum \left[\frac{(254 \times 0.29 \times 0)}{242}\right] + \cdots + \left[\frac{(254 \times 15.35 \times 0)}{270}\right] + \cdots + \left[\frac{(254 \times 0.14 \times 1)}{324}\right]$$

$IV = 132.77$ g I_2 100 g^{-1} oil

For calculation of cetane number, equation 3.13, $CN = \left[46.3 + \left(\frac{5458}{SV}\right)\right] - (0.225 \times IV)$ was solved by substituting SV and IV obtained from the previous equations 3.11 and 3.12 respectively

$CN = \left[46.3 + \left(\frac{5458}{194.56}\right)\right] - (0.225 \times 132.77)$

$CN = 44.47$

For calculation of degree of unsaturation, equation 3.14, $DU = \sum MUFA + [2 \times \sum PUFA]$ was solved by substituting MUFA and PUFA.

$DU = 6.65 + 2 \times 72.94$

$DU = 152.53$

For calculation of long chain saturation factor, equation 3.15, $LCSF = 0.1 \times F_{C16:0} + 0.5 \times F_{C18:0} + 1 \times F_{C20:0} + 1.5 \times F_{C22:0} + 2 \times F_{C24:0}$ was solved by substituting F_i of saturated FAME.

$LCSF = 0.1 \times 15.35 + 0.5 \times 4.01$

$LCSF = 3.54$

For calculation of cold filter plugging point, equation 3.16, $CFPP = 3.1417 \times LCSF - 16.477$ was solved by substituting LCSF.

$CFPP = 3.1417 \times 3.54 - 16.477$

$CFPP = -5.35$ °C

For calculation of cloud point, equation 3.17, $CP = 0.526 \times F_{C16:0} - 4.992$ was solved by substituting F_i of C16:0 FAME.

$CP = 0.526 \times 15.35 - 4.992$

$CP = 3.08$ °C

For calculation of pour point, equation 3.18, $PP = 0.571 \times F_{C16:0} - 12.24$ was solved by substituting F_i of C16:0 FAME.

$PP = 0.571 \times 15.35 - 12.24$

$PP = -3.47$ °C

For calculation of oxidation stability index, equation 3.19, $OSI = \left(\frac{117.9295}{(F_{C18:2} + F_{C18:3})}\right) + 2.5905$ was solved by substituting F_i of C18:2 and C18:3 FAMEs.

$OSI = \left(\frac{117.9295}{(17+52.71+0)}\right) + 2.5905$

$OSI = 4.28$ hrs

For calculation of higher heating value, equation 3.20, $HHV(MJ.Kg^{-1}) = \sum \left[\frac{(F_i \times \delta_i)}{100}\right]$ was solved by calculating F_i and δ_i where $\delta_i = 46.19 - \frac{1794}{M_i} - 0.21 \times D_i$

First, δ_i was calculated for all FAMEs i.e., C14:0 – C20:1

For example, $\delta_{C14:0} = 46.19 - \frac{1794}{242} - 0.21 \times 0$

= 38.78

$\delta_{C20:1} = 46.19 - \frac{1794}{324} - 0.21 \times 1$

= 40.45

$HHV = \sum \left[\frac{(0.29 \times 38.78)}{100}\right] + \cdots + \left[\frac{(0.14 \times 40.45)}{100}\right]$

= 39.63 MJ kg^{-1}

For calculation of kinematic viscosity, equation 3.21, $\nu(mm^2.s^{-1}) = e^{\Sigma\left[\frac{(F_i \times \ln(\nu_i))}{100}\right]}$ was solved by calculating F_i and $\ln(\nu_i)$ where $\ln(\nu_i) = -12.503 - (0.178 \times D_i) + 2.496 \times \ln M_i$

First, $\ln(\nu_i)$ was calculated for all FAMEs i.e., C14:0 – C20:1

For example, $\ln(\nu_{C14:0}) = -12.503 - (0.178 \times 0) + 2.496 \times \ln(242)$

= 1.20

$\ln(\nu_{C20:1}) = -12.503 - (0.178 \times 1) + 2.496 \times \ln(324)$

= 1.75

$\nu = e^{\Sigma\left[\frac{(F_i \times \ln(\nu_i))}{100}\right]}$

$= e^{\Sigma\left[\frac{(0.29 \times 1.20)}{100}\right] + \cdots + \left[\frac{(0.14 \times 1.75)}{100}\right]}$

= 3.89 mm^2 s^{-1}

For calculation of density, equation 3.22, $\rho\ (g.cm^{-3}) = \sum\left[\frac{(\rho_i \times F_i)}{100}\right]$ was solved by calculating F_i and ρ_i where $\rho_i = 0.8463 + \frac{4.9}{M_i} + 0.0118 \times D_i$

First, ρ_i was calculated for all FAMEs i.e., C14:0 – C20:1

For example, $\rho_{C14:0} = 0.8463 + \frac{4.9}{242} + 0.0118 \times 0$

= 0.866

$\rho_{C20:1} = 0.8463 + \frac{4.9}{324} + 0.0118 \times 1$

= 0.873

$\rho = \sum\left[\frac{(0.866 \times 0.29)}{100}\right] + \cdots + \left[\frac{(0.873 \times 0.14)}{100}\right]$

= 0.881 g cm^{-3}

= 881 kg m^{-3}

For calculation of flash point, equation 3.23, $FP = 23.362 \times \sum \left[\frac{(N_i \times F_i)}{100}\right] + 4.854 \times \sum \left[\frac{(D_i \times F_i)}{100}\right]$ was solved by substituting N_i (number of carbon atoms in individual FAME) , F_i and D_i of all FAMEs i.e., C14:0 – C20:1

$$FP = 23.362 \times \sum \left[\frac{(15 \times 0.29)}{100}\right] + \cdots + \left[\frac{(21 \times 0.14)}{100}\right] + 4.854 \times \sum \left[\frac{(0 \times 0.29)}{100}\right] + \cdots + \left[\frac{(1 \times 0.14)}{100}\right]$$

$FP = 439.34$ °C

2. Important tables

Table A1. Biodiesel composition of *S. abundans* in single stage medium scale PBR under Diurnal natural sunlight (480 hr).

FAME	M_i	D_i	N_i	%FAME in DCW (W_i)	%FAME in total FAME (F_i)
C14:0	242	0	15	0.16	0.29
C15:0	256	0	16	0.07	0.13
C15:1	254	1	16	0.11	0.21
C16:0	270	0	17	8.50	15.35
C16:1 trans	268	1	17	3.03	5.47
C16:2 cis	266	2	17	1.47	2.66
C16:2 trans	266	2	17	0.03	0.06
C16:3 cis	264	3	17	0.03	0.06
C16:3 trans	264	3	17	0.06	0.11
C17:0	284	0	18	0.34	0.63
C17:1	282	1	18	0.46	0.83
C17:2 cis	280	2	18	0.06	0.11
C17:2 trans	280	2	18	0.13	0.23
C18:0	298	0	19	2.22	4.01
C18:2 cis	294	2	19	9.40	17.00
C18:2 trans	294	2	19	29.17	52.71
C20:1	324	1	21	0.07	0.14
∑ C16-C18				53.91	97.43
SFA				11.29	20.41
MUFA				3.67	6.65
PUFA				40.35	72.94
FAME				55.31	100.00

Table A2. Specifications of analytical equipments used in the study.

Equipment/Software/Chemical	Company/Model/Specifications
Inverted microscope	Nikon Eclipse Ti8-E, Nikon Corporation, Japan
Visible spectrophotometer	Model 2305, Electronics India
High performance liquid chromatograph	Shimadzu Corporation, Japan
Aminex HPX 87H column for HPLC	Bio-Rad, USA
Fourier transform infrared spectrometer	IRAffinity-IS Model
Powder X-ray diffractometer	Model D8 Advance Bruker AXS
Differential scanning calorimeter/ Thermogravimetric analyser	Netzsch, Model: STA449F3A00
Design–Expert®, trial version 7.0.0	Stat–Ease Inc, USA
pH electrode	Erma Inc, Japan, Model: PE-03
Thermometer	Omsons, India
pH controller	Countronics, India, Model: 110pH-Tx
OPTO22 control system	OPTO22, USA
Zetasizer	Litesizer 500 Anton Paar
Omega cuvette for zeta potential	Mat. No. 155765
CP-Sil 8CB column for GC	30 m × 0.25 mm i.d., 0.25 µm film thickness, Agilent technologies, USA
Gas chromatograph	GC-FID, Varian 450, Netherlands
GC syringe	Hamilton, USA
Supelco 37 component FAME mix	Sigma Aldrich, USA
Acrylic sheet for flat panel PBR	Sun Acrylam Pvt. Ltd., India
Bolts for flat panel PBR	Size: M3, India
Constant current source regulator	Metravi Instruments Pvt. Ltd., India
Lux meter	Sigma Instruments, India
Dissolved O_2 probe	Suntronic Inc., India
PTFE filters	AXIVA, India
Manual air/CO_2 flow meter	CM flowmeters Pvt. Ltd., India
Pulse width modulation adapter	Mouser electronics, USA
Cool white LED cobs	100 W, 6500 K color temperature, Ebay.in
Silicone tubing (for sparger)	Himedia Laboratories Pvt. Ltd., India
Steapsin lipase	Sisco Research Laboratories Pvt. Ltd., India

Table A3. Comparison of biodiesel production (quantity and quality) using various microalgal strains cultivated in photobioreactors operated single stage photoautotrophically.

Strain name	Photobioreactor/ cultivation conditions	Biodiesel (g/l)/lipid content (%)	SV (mg KOH g^{-1} oil)	IV (g I_2 100 g^{-1} oil)	CN	DU	LCSF	CFPP (°C)	CP (°C)	PP (°C)	OSI (hrs)	HHV (MJ kg^{-1})	ρ (at 15 °C) (kg m^{-3})	ν (at 40 °C) (mm^2 s^{-1})	FP (°C)
Scenedesmus abundans (current study)	Optimized lipid media in medium scale flat panel PBR under outdoor natural sunlight	1.28	196.15	130.2	44.82	147.64	2.50	-8.59	4.27	-2.18	4.44	39.59	881	3.84	435.31
Scenedesmus abundans (current study)	Optimized lipid media in medium scale flat panel PBR at 2162 µE/m^2/s	2.01	195.17	128.81	45.28	147.99	2.98	-7.10	5.15	-1.22	4.31	39.62	880	3.89	437.51
Scenedesmus abundans (current study)	Multi-objective RSM media in medium scale flat panel PBR under diurnal natural sunlight	1.79	194.56	132.77	44.47	152.53	3.54	-5.35	3.08	-3.47	4.28	39.63	881	3.89	439.34
Scenedesmus abundans (current study)	Multi-objective RSM media in medium scale flat panel PBR at diurnal simulated sunlight	3.69	195.40	123.93	46.34	142.53	3.85	-4.35	5.59	-0.74	4.39	39.63	880	3.92	436.51
Chlorella sp. FC2 IITG (Naira et al., 2019)	BG-11 media in 10 l scale tubular PBR under diurnal natural sunlight	1.40	194.81	123.07	46.63	134.37	ND	1.88	5.00	-1.38	ND	38.60	860	3.64	395

Chlorella sp. (FACHB-1748) (Zhou et al., 2013)	BG-11 media in 5 L triangular flasks	0.98	196.04	98.65	51.94	ND	0.38	-15.30	ND	ND	ND	ND	ND	ND	ND
Chlorella (Deshmukh et al., 2019)	BG-11 media in Erlenmeyer flask	32.30	ND	141.27	50.07	ND	ND	-8.07	ND	ND	4.51	39.52	882	3.75	ND
Chlorococcum (Deshmukh et al., 2019)	BG-11 media in Erlenmeyer flask	28.80	ND	127.14	51.74	ND	ND	-8.76	ND	ND	4.77	39.58	880	3.89	ND
Chroococcus (Deshmukh et al., 2019)	BG-11 media in Erlenmeyer flask	21.19	ND	129.69	51.54	ND	ND	-8.43	ND	ND	4.82	39.63	881	3.93	ND
Nostoc (Deshmukh et al., 2019)	BG-11 media in Erlenmeyer flask	24.94	ND	109.99	53.64	ND	ND	-5.96	ND	ND	5.30	39.65	878	4.06	ND
L. putealis (Deshmukh et al., 2019)	BG-11 media in Erlenmeyer flask	10.54	ND	66.26	59.27	ND	ND	0.894	ND	ND	8.57	39.55	873	4.09	ND
Calothrix (Deshmukh et al., 2019)	BG-11 media in Erlenmeyer flask	19.14	ND	57.06	60.74	ND	ND	3.61	ND	ND	8.99	39.55	871	4.14	ND

ASTM D6751-12 standard, SV < 500, CN ≥ 47, OSI ≥ 3

EN 14214 standard IV ≤ 120, HHV ≥ 35, 860 ≤ ρ ≤ 900, 3.5 ≤ v ≤ 5.0, FP ≥ 120, CP and PP - location and season dependent, CFPP - ≤ +5 (summer) or ≤ -20 (winter)

Table A4. Cost analysis of biodiesel and EPS production from 20 days cultivation of *Scenedesmus abundans* in 10000 litre large scale flat panel photobioreactor (based on optimized multi-objective RSM media under Diurnal natural sunlight).

Source	Substrate	Concentration (mg/l)	Cost per kg (INR)	Cost for 10000 l reactor (INR)
	Media components			
IndiaMart	Urea	659.63	8	52.77
IndiaMart	K_2HPO_4	80	90	72
IndiaMart	$MgSO_4.7H_2O$	200	8	16
IndiaMart	$CaCl_2.2H_2O$	107	9.75	10.43
IndiaMart	Ferric citrate	20	240	48
IndiaMart	Citric acid	100	45	45
IndiaMart	$CoCl_2.6H_2O$	0.08	1000	0.8
IndiaMart	$ZnSO_4.7H_2O$	0.44	28	0.12
IndiaMart	$CuSO_4.5H_2O$	1.17	120	1.4
IndiaMart	$Na_2MoO_4.2H_2O$	0.03	450	0.14
IndiaMart	H_3BO_3	5.72	20	1.14
IndiaMart	$MnCl_2.4H_2O$	3.62	16	0.58
	*Water (reused)			0
	Natural sunlight			0
ehow.com	**Air flow rate (from air compressor)			990
	CO_2 (recovered from flue gas)			0
	Downstream process			
	Algal harvesting (natural autoflocculation)			0
	Algal drying (under sunlight)			0
	Substrate for transesterification	**Concentration (g/l)**		
	Algal biomass	3.26		
IndiaMart	***Methanol used		20	8260
IndiaMart	****Base catalyst (NaOH) used		30	300
IndiaMart	Biodiesel produced	1.79	125	2238
IndiaMart	Glycerol produced	0.20	600	1200
	Extracellular products from algae	**Concentration (mg/l)**		
Alibaba	EPS produced	155	3000	4650

***Water cost is considered to be negligible.
**Air compressor rating 3300 W operating for 3 hrs per day = 9.9 kWh per day (cost of 1 kWh = Rs. 5).
***Methanol used in transesterification = 413 kg (methanol to biomass mass ratio = 16:1).
****Base catalyst (NaOH) used in transesterification = 10 kg.

3. Important figures

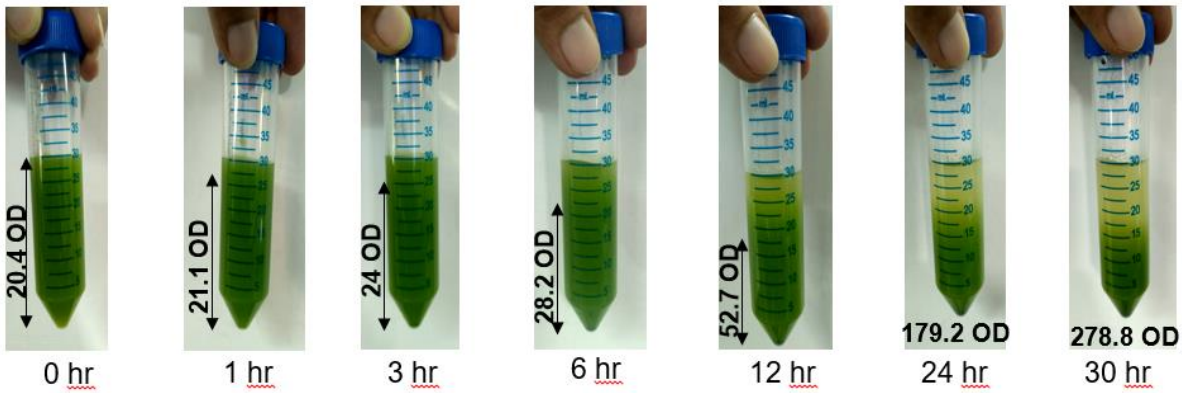

Fig. A1. Autoflocculation rate of microalgal culture under diurnal natural sunlight (720 hr).

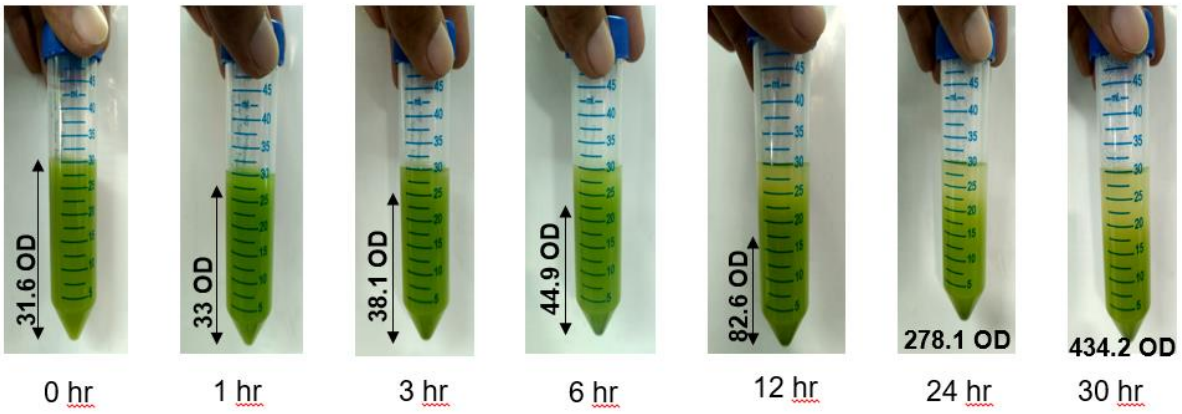

Fig. A2. Autoflocculation rate of microalgal culture at diurnal simulated sunlight (720 hr)

List of publications

Manuscripts

- **Mahesh, R.,** Naira, V.R., Maiti, S.K. 2019. Concomitant production of fatty acid methyl ester (biodiesel) and exopolysaccharides using efficient harvesting technology in flat panel photobioreactor with special sparging system via *Scenedesmus abundans*. *Bioresource technology*, 278, 231-241.

- **Mahesh, R.,** Yashavanth, P.R., Maiti, S.K. Modulation of macro and micronutrients to enhance lipid production by *Scenedesmus abundans* in a flat panel photobioreactor under outdoor natural sunlight. *Biofuels*, 1-16.

- **Mahesh, R.,** Maiti, S.K. Multi-objective optimization of nutrients to enhance biodiesel, autosedimentation factor and exopolysaccharides from *Scenedesmus abundans* in a single stage flat panel photobioreactor under diurnal natural sunlight (ready for submission).

Book chapter

- Naira, V.R., **Mahesh, R.,** Panda, S.K., Maiti, S.K. 2020. Biorefinery Approaches for the Production of Fuels and Chemicals from Lignocellulosic and Algal Feedstocks. in: *Biorefinery of Alternative Resources: Targeting Green Fuels and Platform Chemicals*, Springer, 141-170.

- **Mahesh, R.,** Panda, S.K., Das, M., Yashavanth, P.R., Dhull, S., Negi, B.B., Jakhwal, P., Maiti, S.K. 2021. Advances in Biotechnological Tools for Bioremediation of Wastewater Using Bacterial–Algal Symbiotic System. in: *Wastewater Treatment*, Elsevier, pp. 385-411.

Conferences

- **Mahesh R** and Soumen Kumar Maiti (2017). Presented poster on the topic entitled **'Media optimisation for the production of lipid rich high density microalgae, *Scenedesmus abundans* NCIM 2897 in flat panel photobioreactor'** in the 5th Bioprocessing India Conference held at IIT Guwahati, India during 9th Dec to 11th Dec, 2017.

- **Mahesh R** and Soumen Kumar Maiti (2018). Presented poster on the topic entitled **'Effect of nutrients on the growth of microalgae *Scenedesmus abundans* NCIM 2897 in flat panel photobioreactor'** in the Indo-Japan Bilateral Symposium on Future Perspective of Bioresource Utilization In North – East India (February 1 – 4, 2018). Jointly Organized by Indian Institute of Technology Guwahati, India and Gifu University, Japan held at IIT Guwahati.

- **Mahesh R** and Soumen Kumar Maiti (2018). Actively participated in Poster presentation at Research Conclave'18 organized by Students' Academic Board, Indian Institute of Technology Guwahati, India.

- **Mahesh R** and Soumen Kumar Maiti (2019). Presented poster on the topic entitled **'Simultaneous production of biodiesel and exopolysaccharides using autoflocculation harvesting technology in flat panel photobioreactor with membrane sparging system via *S. abundans*'** in the International Conference on Sustainable Environment and Energy (ICSEE' 19) organized by Hindustan Institute of Technology & Science, Chennai on 21st & 22nd February 2019.

- **Mahesh R** and Soumen Kumar Maiti (2019). Actively participated in Oral presentation at Research Conclave'19 organized by Students' Academic Board, Indian Institute of Technology Guwahati, India.

- **Mahesh R** and Soumen Kumar Maiti (2019). Actively participated in Poster presentation in the 1st Departmental Retreat (Biotech Express) organized by Department of Biosciences and Bioengineering (BSBE), Indian Institute of Technology Guwahati, held on 21st December 2019, Guwahati, Assam, India.

- **Mahesh R** and Soumen Kumar Maiti (2020). Presented poster on the topic entitled **'The effect of nutrients (urea, K_2HPO_4, macronutrients and micronutrients) to promote microalgal growth as well as lipid induction in micro photobioreactors'** in the International Conference on "Algae, Fungi and Plants: Systematics to Applications (AFPSA- 2020)" held on January 24-25, 2020 at CAS-VII, Department of Botany, University of Calcutta, Kolkata, India.

- **Mahesh R** and Soumen Kumar Maiti (2021). Delivered virtual oral presentation on the topic entitled **'Multi-objective optimization for the production of biodiesel and exopolysaccharides with high autoflocculation efficiency in photoautotrophic conditions via *Scenedesmus abundans* cell factory'** in 3rd International Conference on "Bioresource Technology for Bienergy, Bioproducts & Environmental Sustainability (BIORESTEC-2021)" organized by Elsevier held on 17th – 19th May 2021 at Riva del Garda, Italy.

- **Mahesh R** and Soumen Kumar Maiti (2021). Presented virtual poster on the topic entitled **'Simultaneous production of biodiesel and exopolysaccharides from *Scenedesmus abundans* cell factory in flat panel photobioreactor using cost effective harvesting strategy under diurnal natural sunlight'** in 10th International Conference on "Algal Biomass, Biofuels & Bioproducts (AlgalBBB-2021)" organized by Elsevier held on 14th – 16th June 2021 at Hawaii, USA.

- **Mahesh R** and Soumen Kumar Maiti (2022). Delivered oral presentation on the topic entitled **'Optimization of process variables for biodiesel production from oleaginous microalgae, *Scenedesmus abundans* NCIM 2897 using lipase enzyme'** in NERC 2022 held on 20th – 22nd May 2022 at IIT Guwahati.

Poster Award

- Awarded best poster presentation on the topic entitled **'Simultaneous production of biodiesel and exopolysaccharides using autoflocculation harvesting technology in flat panel photobioreactor with membrane sparging system via *S. abundans*'** in the International Conference on Sustainable Environment and Energy (ICSEE' 19) organized by Hindustan Institute of Technology & Science, Chennai on 21st & 22nd February 2019.

Vitae

The author was born on 18th August 1993 in Tirupati, Andhra Pradesh, India. He passed the Secondary School Examination conducted by Central Board of Secondary Education from Vivekananda Vidhyalaya, Chennai in 2010. He cleared the Higher Secondary School Examination conducted by Central Board of Secondary Education from Devi Academy, Chennai in 2012. He completed Bachelor of Technology in Industrial Biotechnology from Shri Mata Vaishno Devi University, Katra, Jammu and Kashmir in 2016. He was awarded Chancellor Gold Medal for securing highest CGPA among all students in Bachelor of Technology.

Mahesh R joined his PhD programme in July 2016 at Department of Biosciences and Bioengineering, Indian Institute of Technology Guwahati, Assam, India. He received junior and senior research fellowships under the scheme run by Ministry of Human Resource and Development (MHRD), India. He successfully completed course work with 9.33 Cumulative Point Index (CPI). He gave PhD Synopsis Seminar of his thesis work before Doctoral Committee on 8th July 2022 and his performance was satisfactory. He submitted his PhD thesis on 7th November 2022 for examination. He presented his PhD viva-voce examination on 5th July 2023.